

# SYNTHESIS OF 5- AND 6-DONOR SCHIFF BASE LIGANDS FOR THE SELECTIVE EXTRACTION AND TRANSPORT OF SELECTED BASE METALS IONS

by

Hezron Felix Odhiambo Ogutu



UNIVERSITEIT  
iYUNIVESITHI  
STELLENBOSCH  
UNIVERSITY

*A dissertation in fulfilment of the requirements for the degree of PhD in Chemistry at the department of chemistry and polymer science University of Stellenbosch*

1918 · 2018

Supervisor: Dr. Robert C. Luckay

Faculty of Science

Department of Chemistry and Polymer

Science

Co-supervisor: Dr: Rehana Malgas-Enus

Faculty of Science

Department of Chemistry and Polymer

Science

December 2018

i



## **Declaration**

By submitting this thesis/dissertation electronically, I declare that the entirety of the work contained therein is my own, original work, that I am the sole author thereof (save to the extent explicitly otherwise stated), that reproduction and publication thereof by Stellenbosch University will not infringe any third party rights and that I have not previously in its entirety or in part submitted it for obtaining any qualification.

Hezron Ogutu

Date: December 2018

Copyright© 2018 Stellenbosch, University of Stellenbosch

All rights reserved

*Dedicated to my father Mr. Timon Ogutu Owiti and my mother Mrs. Monica Auma Ogutu,  
your belief in me and your sacrifice has been a constant reminder and source of strength  
throughout my academic journey*

## Abstract

Schiff base ligands have various advantageous properties that can be employed for use in solvent extraction processes. They are relatively cheap to synthesize, stable, robust and can be modified to accommodate multiple donor groups. Schiff base ligands were therefore synthesized through a Schiff base condensation method using five aldehydes; *salicylaldehyde*, *para-methoxy salicylaldehyde*; *para-tertbutyl salicylaldehyde*, *para-nonyl salicylaldehyde* and *2-hydroxynaphthylaldehyde* with N-(2-aminoethyl)ethane-1,2-diamine, N-(3-aminopropyl)propane-1,3-diamine, N,N-bis(2-aminoethyl)ethane-1,2-diamine to make five pentadentate ligands with ethylalkyl spacers (class A ligands **L1-L5**). Five pentadentate ligands with propylalkyl spacer groups (class B ligands **L6-L10**) and five heptadentate tripodal with ethyl alkyl spacers (class C ligands **L11-L15**) with N-donor groups. 2-(2-Aminoethoxy) ethylamine and 2,2'-[ethane-1,2-diylbis(oxy)]diethanamine was then used to synthesise the pentadentate (class D ligands **L16-L20**) and hexadentate O-donor ligands (class E ligands **L21-L25**). All these ligands were obtained in good yield and were fully characterized by FTIR, <sup>1</sup>H NMR, and <sup>13</sup>C {H}NMR, ESI-MS, and CHN analysis.

The IR and NMR studies of the imine peak of the synthesized products show different shifts due to the different substituents. The analysis of the ligands on the IR showed a red shift for methoxy, tertbutyl and nonyl substituents in comparison to the unsubstituted salicylaldehyde. The naphthylaldehyde showed a blue shift in comparison to the unsubstituted salicylaldehyde. The analysis through the <sup>1</sup>H and <sup>13</sup>C {H} NMR of the imine peak also showed the same trend with the chemical shift indicating an upfield shift of the imine peak and downfield shift due to the naphthylaldehyde. The addition of the alkyl group in the spacer and the change of the different donor group from the N-donor to the O- donor group did not show a significant shift of the imine peaks.

The results obtained for the class B ligands with the naphthylaldehyde showed that the ligand exists in two *tautomeric* forms; the quaternary imine and the hydroxyl form. A study of the  $^1\text{H}$  NMR of class D ligands shows that these ligands undergo molecular dynamism caused by the symmetry and flexibility of these molecules. One of the class E ligands, ligand, **L22** containing the methoxy substituent was observed to undergo photochromic colour change that was attributed to tautomerism which is unusual behavior for Schiff base ligands. The colour change was studied using confocal microscopy showing fluorescence emission of the ligand in solid state with a wide band gap of between 611 nm - 407 nm.

Three of the class D ligands were studied using single crystal X-ray diffraction (SXRD). The ligand **L18** with the *naphthylaldehyde* was obtained showing the tautomeric form of the ligand with the proton shift of the OH proton to the imine N-atom with the phenolic oxygen stabilized by the aromatic system. The Schiff base ligand complexes were synthesized and fully characterized using ATIR, UV-Vis and ESI-MS analysis. Five crystal structures of **L1-Cu**, **L1Co**, **L4-Cu**, **L17-Cu**, **L18-Cu**, **L19-CuPb** were also obtained and analyzed using the SXRD. The complexes synthesized from the class A ligands **L1-Co** was obtained showing an octahedral coordinate complex around the Co metal, while the **L1-Cu**, **L4-Cu**, were obtained showing a metal induced hydrolyzed square planar geometry. The **L17-Cu**, **L18-Cu** complexes synthesized from class D ligands with the methoxy, and *naphthyl* groups respectively were observed to form metallocycles with Cu-metal. The geometry of the Cu-centre was observed to be four coordinate, forming a distorted square-planar geometry. **L19-CuPb** with the *tertbutyl* substituent was observed to form a bi-metallic Cu-Pb complex with four Cu-metallocycles coordinated to one Pb-metal in octahedral geometry.

All the ligands were subjected to solvent extraction studies. The results obtained showed that all the class A and class C ligands, except the nonyl based substituent, showed a high degree of bleeding into the aqueous phase. The ligands with the *nonyl*-containing substituents for class

A and class C were observed to selectively extract 83% and 86% of  $\text{Cu}^{2+}$ . The ligands that showed high degree of bleeding to the aqueous phase were subsequently used for synergistic solvent extraction studies using three different synergists. Synergist A (palmitic acid) was observed to synergistically promote selectivity of  $\text{Pb}^{2+}$ , synergist B (dodecylsulfonate) synergistically promoted selectivity of  $\text{Cu}^{2+}$  and  $\text{Pb}^{2+}$  while synergist C (dodecylbenzylsulfonate) was observed to extract both  $\text{Cu}^{2+}$  and  $\text{Pb}^{2+}$  slightly since it showed low selectivity.

The ligands that did not show bleeding into the aqueous phase (class B, D and E ligands) were observed to be very selective towards  $\text{Cu}^{2+}$  in accordance with the nature of stability of their complexes as shown by the Irving Williams series. The class D and E ligands containing the O-donor group showed excellent extraction and selectivity of  $\text{Cu}^{2+}$ . The highest extraction was observed for the non-substituted *salicylaldehyde* based ligand at 87% and 95% for the *naphthylaldehyde* based ligand for class D and class E ligands respectively. For all the O-donor based ligands, the % extraction of a secondary metal was less than 10% indicating exceptional selectivity of  $\text{Cu}^{2+}$ . These results were very good and showed that despite the increased organic nature of the alkyl chain substituent, the non-substituted ligand showed the highest extraction of  $\text{Cu}^{2+}$ . This high selectivity and extraction were correlated to the crystal structure obtained. This correlation showed that the nature of coordination of the ligand to the metal ion has a profound effect on the % extraction of the ligand in solvent extraction.

## Opsomming

Schiff-basis ligande besit 'n aantal voordelige eienskappe wat hulle doeltreffend maak in ekstraksie prosesse. Hulle is goedkoop om te sintetiseer, hulle is stabiel, veerkragtig en kan verander word om veelvuldige skenker groepe te akkomodeer. Schiff-basis ligande was dus gesintetiseer deur die Schiff-basis kondensasie metode met gebruik van vyf verskillende aldehiede: *salisielaldehyd*, *para-metoksie salisielaldehyd*, *para-butiel salisielaldehyd*, *para-noniel salisielaldehyd* en *2-hidroksienaftielaldehyd*. Die amiene was *N*-(2-aminoetiel)etaan-1,2-diamien, *N*-(3-aminopropiel)propaan-1,3-diamien, *N,N*-bis(2-aminoetiel)etaan-1,2-diamien. Vyf pentadentaat ligande met etielalkiel groepe (klas A ligande **L1 – L5**) en vyf pentadentaat ligande met propielalkiel groepe (klas B ligande **L6 – L10**) is gesintetiseer. Vyf heptadentate tripodiel ligande met etiel alkiel groepe (klas C ligande **L11 – L15**) is ook gesintetiseer. 2-(2-aminoetoksie) etielamien en 2,2'-[etaan-1,2-dielbis(oksie)]dietaanamien is dan gebruik om pentadentaat ligande (klas D ligande **L16 – L20**) en heksadentaat ligande (klas E ligande **L21 – L25**) te sintetiseer. Alle ligande se opbrengs was goed en hulle is volledig gekarakteriseer deur middel van FTIR, <sup>1</sup>H KMR, en <sup>13</sup>C {H}KMR, ESI-MS, en CHN analiese. Die IR en KMR studies van die imien piek van die gesintetiseerde produkte toon verskillende verskuiwings as gevolg van die verskillende substituentte. Die analise van die ligande op die IR het 'n rooi verskuiwing vir metoksie-, tert-butiel- en noniel-substituentte getoon in vergelyking met die ongesubstitueerde salisielaldehyd. Die naftielaldehyd het 'n blou verskuiwing vertoon in vergelyking met die ongesubstitueerde salisielaldehyd. Die analise deur die <sup>1</sup>H en <sup>13</sup>C {H} NMR van die imien piek het ook dieselfde tendens getoon met die chemiese verskuiwing wat 'n opwaartse verskuiwing van die imien piek en afwaartse verskuiwing weens die naftielaldehyd aandui. Die toevoeging van die alkielgroep in die brug en die verandering van die verskillende donor groep van die N-skenker na die O-donor groep het nie 'n beduidende verskuiwing van die imien pieke getoon nie.

Die resultate verkry vir die klas B ligande met die naftielaldehyd het getoon dat die ligand in twee tautomeriese vorms bestaan uit die kwaternêre imien en die hidroksielvorm. 'n Studie van die  $^1\text{H}$ -KMR van klas D ligande toon dat hierdie ligande molekulêre dinamiek ondervind deur simmetrie en die buigsaamheid van hierdie molekules te ondergaan. Een van die klas E ligande, ligand **L22** wat die metoksiesubstituent bevat, is waargeneem om fotochromiese kleurverandering te ondergaan wat toegeskryf word aan tautomerisme wat ongewone gedrag vir Schiff-basis ligande is. Die kleurverandering is bestudeer met behulp van konfokale mikroskopie wat fluoresensie-emissie van die ligand in vaste toestand toon met 'n wye band gaping tussen 611 nm - 407 nm.

Drie van die klas D ligande is bestudeer met behulp van enkel kristal X-straal diffraksie (SXRDR). Die ligand **L18** met die naftielaldehyd is verkry wat die tautomerise vorm van die ligand toon met die protonverskuiwing van die OH proton na die imien-N-atoom met die fenoliese suurstof wat deur die aromatiese stelsel gestabiliseer is. Die Schiff-basis komplekse is gesintetiseer en ten volle gekarakteriseer deur gebruik te maak van ATIR, UV-Vis en ESI-MS analise. Vyf kristalstrukture van **L1-Cu**, **L1-Co**, **L4-Cu**, **L17-Cu**, **L18-Cu**, **L19-CuPb** is ook verkry en geanaliseer met behulp van die SXRDR. Die komplekse gesintetiseer uit die klas A ligande **L1-Co** is verkry met 'n oktahedriese koördinaatkompleks rondom die Co-metaal, terwyl die **L1-Cu**, **L4-Cu** verkry is wat metaal veroorsaakde hidroliseerde vierkante vlak geometrie toon. Die **L17-Cu**, **L18-Cu** komplekse wat gesintetiseer uit onderskeidelik klas D ligande met die metoksiel- en naftielgroepe is waargeneem om metallosiklisse met Cu-metaal te vorm. Die geometrie van die Cu-sentrum is waargeneem om vier koördinaat te wees, wat 'n vervormde vierkantige geometrie vorm. **L19-CuPb** met die tertbutiel substituent is waargeneem om 'n bi-metaal Cu-Pb kompleks te vorm met vier Cu-metallosiklisse wat gekoördineer is tot een Pb-metaal in oktahedriese geometrie.

Al die ligande is onderworpe aan oplosmiddel ekstraksie studies. Die resultate wat verkry is, het getoon dat al die klas A- en klas C-ligande, behalwe die noniel-substituent, 'n hoë graad van loging toon. Die ligande met die noniel-bevattende substituent vir klas A en klas C is waargeneem om selektief 83% en 86%  $\text{Cu}^{2+}$  te onttrek. Die ligande wat 'n hoë graad van loging toon, is later gebruik vir sinergistiese oplosmiddel ekstraksie studies met behulp van drie verskillende sinergiste. Synergis A (palmitiensuur) is waargeneem om sinergisties die selektiwiteit van  $\text{Pb}^{2+}$  te bevorder, synergis B (dodesielsulfonaat) synergisties bevorder die selektiwiteit van  $\text{Cu}^{2+}$  en  $\text{Pb}^{2+}$  terwyl synergis C (dodesielbenzielsulfonaat) waargeneem is om al die metaalione met beide  $\text{Cu}^{2+}$  en  $\text{Pb}^{2+}$  effens hoër te onttrek in vergelyking met die ander metaalione.

Die ligande wat nie uitloging (klasse B, D en E ligande) toon nie, was baie selektief teenoor  $\text{Cu}^{2+}$  in ooreenstemming met die aard van stabiliteit van hul komplekse, soos aangedui deur die Irving Williams-reeks. Die klasse D- en E-ligande wat die O-skenkergroep bevat, het uitstekende ekstraksie en selektiwiteit van  $\text{Cu}^{2+}$  getoon. Die hoogste ekstraksie is waargeneem vir die nie-gesubstitueerde salisielaldehydebeseerde ligand by 87% en 95% vir die naftielaldehydebeseerde ligand van onderskeidelik klas D en klas E ligande. In al hierdie O-donor-geseerde ligande was die % ekstraksie van 'n sekondêre metaal minder as 10% wat uitsonderlike selektiwiteit van  $\text{Cu}^{2+}$  aandui. Hierdie resultate was baie goed en het getoon dat ondanks die verhoogde organiese aard van die alkielketting substituent, die nie-gesubstitueerde ligand die hoogste ekstraksie van  $\text{Cu}^{2+}$  getoon het. Hierdie hoë selektiwiteit en ekstraksie is gekorreleer met die kristalstruktuur wat verkry is. Hierdie korrelasie het getoon dat die aard van koördinasie van die ligand na die metaalioon 'n diepgaande uitwerking op die % ekstraksie van die ligand op die metaalioon het.

## Acknowledgment

Firstly, I would like to thank the almighty God for his love, his grace and covering over me throughout the duration of my stay and study at Stellenbosch University. It is the gift of life and chemistry that we converge in this work.

The greatest appreciation and thank you has to go to my supervisor Dr. Robert. C. Luckay whose leadership, patience and knowledge has been integral in the creation of this work. His open-door policy and ability to create time and space for all of his students is unparalleled.

The role of my co-supervisor Dr. Rehana Malgas-Enus through whom I secured my place at this university cannot go unmentioned, your guidance and friendship throughout my stay in South Africa has been one of ages. Your ability to listen and guide me throughout my postgraduate studies has always been positive and encouraging.

To my friends at the Department of Chemistry and Polymer Science, Mr. Cassiem Joseph, Mr. Jacquin October, Mr. Joshua Hensberg, Ms. Tsepiso Khutlane, Ms. Manana Moletsa, Ms. Nusrat Begum and my colleagues and former colleagues at the hydrometallurgy research group, Brendan Pearce, Elaine Barnard and Claire Ineza you have all helped me in various parts of my studies and your input and discussion has been essential to this work. Special thanks has to go to Dr. Waheed Saban who has been a tremendous blessing as a friend and a source of help during my study, your help in the development of the crystal structures at a time I was losing patience gave life to this work.

To the academic staff and the support staff at the Inorganic chemistry building and the entire Department of Chemistry and Polymer Science; Mrs. Peta Steyn, Mr. Jabu Lukhele, Mr. Ayanda Nxope, Mr. Kwezi Mbalo, Mrs. Chalon Van Reenen, Mr. Malcolm Mclean, Mr. Moebarick Bickerstaff and Mrs. Sylette May you have all been a source of help and friendship at the university and during my research particularly when chemicals were needed for the

various reactions. Your quick response and ability to go out of your way to help us attain our goals is greatly appreciated.

To the research assistants and the central analytical facility staff, I would like to pass my gratitude for your help, Mrs. Riana Rossouw at the ICP, Mrs Elsa Malherbe and Dr. Jacobus Brand of the NMR and the Professor Len Barbour supramolecular research group: Dr. Leigh Loots, Dr. Vincent Smith, Dr. Banele Vesta and Mr. Phumile Sikiiti. I would like to thank you all for your help even in those times I was a constant menace trying to use your instruments, your inputs and knowledge have helped me a lot in my analysis work.

Special thanks goes to My Pastor, Pastor Ben Kinnear, his wife Mrs. Tsitsi Kinnear and the entire Stellenbosch Potters House Christian fellowship church family for being my family here in Stellenbosch. Brother Quintone Ndala and Brother Manoj Pranshal and their families, brother Dumiso Sibanda my brother and fellow workers of God, sister Dorothy Diamond and her family, sister Joan and her family thank you all for welcoming me into your lives and being a source of joy and strength. Your warm friendship and love has kept me grounded in faith and understanding of the word of God.

I would also like to thank Maseno University Kenya for granting me the leave of absence to allow me to undertake my studies in South Africa. I would also like to thank the NRF and Stellenbosch University for the funding they gave me to enable me to undertake my studies here.

Finally, I would like to thank my family, my brothers Pervince Onyango, Fred C. Okoth, George B. Otieno and my sister Elizabeth B. Akinyi. You are a source of inspiration and your closeness and love reminds me that life is worth living, it keeps me going.

**TABLE OF CONTENT**

Declaration .....	Error! Bookmark not defined.
Abstract .....	iv
Acknowledgment .....	x
CHAPTER 1 .....	1
LITERATURE REVIEW.....	1
1.0 Introduction .....	2
1.1 Historical perspective and definition of solvent extraction.....	4
1.2 Principles of solvent extraction .....	6
1.2.1 The distribution law by Nernst .....	7
1.2.2 The distribution ratio.....	8
1.2.3. Separation factor.....	9
1.3 Application of solvent extraction.....	10
1.4 Challenges in solvent extraction.....	11
1.4.1 Solvent in solvent extraction.....	11
1.4.1.1 The aqueous solution .....	11
1.4.1.2 Metal ions in solution.....	11
1.5 Effect of pH.....	13
1.6 Choice of diluent.....	14
1.7 Organic extractants.....	15
1.7.1 Extractants in solvent extraction .....	16
1.7.2 Ion pair extractants .....	17
1.7.3 Chelating extractant .....	17
1.7.4 Neutral and solvating extractants .....	18

1.8 Choice of extractant in solvent extraction of base metals.....	19
1.8.1 Inner and outer sphere coordination.....	19
1.8.2 Solubility of the ligand and complex in the organic phase.....	19
1.8.3 Effect of donor groups of the ligands.....	20
1.8.4 Thermodynamics of complex formation and the chelate effect.....	21
1.8.4.1 Effect of multiple donor groups.....	22
1.9 Commercial extractants.....	22
1.9.1 Oxime and hydroxime ligands.....	23
1.10 Schiff base ligands.....	24
1.10.1 Reactivity and properties of schiff base ligands.....	24
1.10.2 Salen type ligands.....	25
1.11 Base metals ions.....	27
1.11.1 Competitive extraction of base metals.....	27
1.12 Metal ion transport.....	28
1.12.1 Liquid membranes.....	28
1.12.2 Emulsion membrane.....	28
1.12.3 Supported liquid membranes.....	29
1.12.4 Multistage three-phase extraction.....	29
1.12.5 Bulk liquid membrane.....	29
1.12.5.1 Mechanism of bulk liquid transport.....	30
1.12.5.2 Factors affecting transport.....	30
1.12.5.2.1 Effect of carrier structure on the cation transport.....	30
1.12.5.2.2 Receiving phase.....	31
1.12.5.2.3 Effect of organic solvent in the membrane phase.....	31
1.13 Problem statement.....	31
1.14 Justification.....	32

1.15 Aims and objectives.....	32
1.16 Thesis layout .....	33
CHAPTER 2 .....	34
SYNTHESIS OF N-DONOR SCHIFF BASE LIGANDS .....	34
2.0 Introduction.....	35
2.1 Condensation reaction.....	35
2.1.1 Mechanism of condensation reaction .....	35
2.1.1.1 Process of formation of carbinolamine .....	36
2.1.1.2 Dehydration of the carbinolamine.....	36
2.2 Template synthesis process .....	37
2.3 Stability of schiff base ligands .....	38
2.4 N-donor salen type ligands.....	38
2.5 Chapter objective .....	39
2.6 Chemicals and reagents .....	41
2.7 Instrumentation.....	42
2.7.1 IR spectroscopic analysis .....	42
2.7.2 Nuclear magnetic resonance analysis .....	43
2.7.3 Mass spectrometry and microanalysis .....	44
2.7.4 Melting point determination.....	44
2.8 Synthesis and characterization of aldehydes .....	44
2.8.1 Synthesis of the 5-tert butyl salicylaldehyde .....	44
2.8.2 Method 1: synthesis of 5-tert butyl salicylaldehyde .....	44
2.8.3 Results from method 1.....	45
2.9 Synthesis of Schiff base salen type N-donor ligands.....	46
2.9.1 Method 2: synthesis of (2, 2'-[iminobis[ethane-2,1-diylnitrilo(e) methylylidene]} diphenol) (ligand L1). .....	46

2.9.1.1 Results and discussion from method 2 .....	47
2.9.1.1.1 Discussion of the change of electronic and the steric effect in the synthesis results of method 2 ...	48
2.9.1.2 Discussion of the <sup>1</sup> H NMR results from method 1 .....	48
2.9.1.2.1 The effect of added substituent on the <sup>1</sup> H NMR .....	49
2.9.1.3 Discussion of the <sup>13</sup> C nmr for ligand L1 .....	50
2.9.2 Synthesis of class B ligands .....	51
2.9.2.1.1 Discussion of the electronic effect of class B results .....	51
2.9.3 Synthesis of ligands containing the 5-methoxy salicylaldehyde .....	52
2.9.3.1 Method 3: synthesis of ligand L2 and L7 .....	53
2.9.4 Synthesis of ligands containing the naphthyl aldehyde .....	54
2.9.5 Synthesis of ligand L8 .....	55
2.9.5.1 Method 4: synthesis of ligand L8 .....	59
2.9.6 Synthesis of tripodal ligands .....	59
2.9.6.1 Results from tripodal ligand synthesis .....	60
2.10 Shift of the electronic due to the different ligands .....	61
2.11 Mass spectrometry .....	63
2.12 Elemental analysis .....	65
2.13 Summary and conclusion .....	66
2.14. Characterization .....	67
2.14.1 Characterization of <i>p</i> -substituted salicylaldehyde .....	67
2.14.2 Synthesis and characterization class a ligands .....	67
2.14.3 Synthesis and characterization of class b ligands .....	70
2.14.4 Characterization of class c ligands .....	73
CHAPTER 3 .....	77
SYNTHESIS OF MULTIDONOR SCHIFF BASE LIGANDS CONTAINING O-DONOR GROUP .....	77

3.0 Introduction .....	78
3.1 Oxygen containing ligand systems .....	78
3.2 Problem statement .....	79
3.2.1 Justification of study .....	79
3.3 Chapter objective .....	80
3.4 Chemicals and reagents .....	80
3.5 Preparation of 2, 2-oxydiethylamine .....	81
3.6 Synthesis of class d ligands .....	81
3.6.1 Synthesis of ligand L16 .....	81
3.6.1.1 IR analysis results and discussions .....	82
3.6.2 <sup>1</sup> H nmr analysis discussions .....	83
3.6.2.1 Molecular dynamism studies .....	85
3.6.2.2 Effect of substituents on the <sup>1</sup> H NMR .....	87
3.6.2.3 <sup>13</sup> C { <sup>1</sup> H} NMR analysis .....	87
3.6.3 General discussion of the NMR results .....	89
3.7 Synthesis of hexadentate OCH <sub>2</sub> CH <sub>2</sub> O- ligands .....	90
3.8 Results and discussion .....	90
3.8.1 IR analysis .....	90
3.8.2 <sup>1</sup> H NMR analysis .....	91
3.8.2.1 Effect of added substituents .....	93
3.8.2.2 Discussion of the effect of the added donor groups .....	94
3.9 Photochromic effect studies .....	95
3.9.1 Solid state UV-vis analysis .....	96
3.9.2 Confocal microscopy .....	97
3.9.3 Discussion of the photochromic study .....	99

3.10 Mass spectrometry .....	100
3.11 Effect of the added donor group .....	101
3.12 Elemental analysis .....	101
3.13 Summary and conclusion .....	102
3.14 Experimental .....	103
3.14.1 characterization of class D ligands .....	103
3.14.2 synthesis of class E ligands .....	106
CHAPTER 4 .....	109
CRYSTAL STRUCTURE DETERMINATION AND FLOURESCENCE STUDIES .....	109
4.0 Introduction .....	110
4.1 ligand-metal interaction .....	110
4.1.1 Coordination in solution .....	111
4.1.2 Factors affecting coordination of extractant to metal ions .....	112
4.1.2.1 Jahn-teller distortion .....	112
4.1.2.2 Effect of hydrogen bonding in solution .....	113
4.1.3 Pre-organization and bite size .....	113
4.1.4 Coordination of salen type ligands .....	114
4.2 Problem statement .....	116
4.3 Chapter objective .....	116
4.4 Instrumentation .....	116
4.4.1 Single crystal X-ray diffraction .....	116
4.4.2 UV-vis study .....	117
4.5 Results and discussion .....	117
4.5.1 Single crystal X-ray diffraction (SXRD) analysis of the ligands .....	117
4.5.1 Formation of ligand crystals .....	117
4.5.1.1 Data collection .....	117

4.5.1.1 Measurement parameters .....	119
4.5.1.1.3 Discussion of crystal structure of ligand L17 .....	121
4.5.1.1.4 Discussion of crystal structure of ligand L18 .....	122
4.5.2 Summary of the study of crystal structure of the ligands alone .....	124
4.6 Determination of crystal structure of the complexes .....	124
4.6.1 Experimental .....	124
4.6.2 Synthesis of L17-Cu and L18-Cu and L19-Cu .....	125
4.6.2.1 Results .....	125
4.6.2.2 UV-vis spectroscopy .....	126
4.6.3 Determination of crystal structure .....	127
4.6.3.1 Discussion of crystal structures .....	127
4.6.3.1.1 L17-Cu and L18-Cu complexes .....	127
4.6.3.1.1.2 Discussion of the crystal structure of bi-metallic complex L19-Cu-Pb .....	135
4.6.3.1.2 For the N-donor group ligands .....	138
4.6.3.1.2.1 Discussion of the crystal structure of complex L1-Co .....	138
4.6.3.1.2.1 Discussion of crystal structure for complex L1-Cu and L4-Cu complex .....	139
4.6.3.1.2.1.1 Discussion of the crystal structure of hydrolysed L1-Cu complex .....	142
4.6.4.3 Discussion of the hydrolysed complex for L4-Cu .....	143
4.7 Fluorescence studies .....	144
4.7.1 Instrumentation .....	145
4.7.2 Experimental .....	145
4.7.2.1 Proposed mechanism of fluorescence of the ligands .....	146
4.7.3. Study of solvent effect in fluorescence .....	146
4.7.4 Metal ligand studies .....	147
4.7.4.1 Procedure .....	147
4.7.4.2 Results .....	148

4.7.5. Mechanism of metal induced fluorescence .....	150
4.8 Summary and conclusion .....	150
CHAPTER 5 .....	152
SOLVENT EXTRACTION OF THE N-DONOR SCHIFF BASE LIGANDS .....	152
5.0 Introduction .....	153
5.1 The donor group .....	153
5.1.1 N-donor group .....	153
5.1.1.1 Effect of added alkyl groups between the donor groups .....	154
5.2 Tetradentate N-containing ligands .....	155
5.3 Chapter objective .....	156
5.4 Solvent extraction studies .....	158
5.4.1 Reagents .....	159
5.4.2 Instrumentation .....	159
5.4.2.1 pH meter .....	159
5.4.2.2 Lab shaker .....	159
5.4.2.3 Inductively coupled plasma (ICP-OES) .....	160
5.5 Competitive solvent extraction.....	160
5.5.1 Results .....	161
5.5.1.1 Bleeding of the ligand .....	161
5.5.1.1 Discussion of competitive extraction results from class A ligands .....	162
5.6 Competitive solvent extraction of class B ligands .....	164
5.6.1 Discussion of extraction results from class B ligands .....	166
5.7 Competitive solvent extraction of class C ligands (Tripodal ligands) .....	168
5.7.1 Discussion of results from the competitive solvent extraction of the tripodal ligands.....	168
5.8 Discussion of leaching based on ICPResults .....	170
5.9 Summary of extraction results .....	172

5.10 Competitive bulk liquid membrane transport studies.....	172
5.10.1 Transport apparatus .....	173
5.10.2 Procedure .....	173
5.10.3 Results.....	174
5.10.4 Discussion of transport results .....	176
5.11 pH studies .....	176
5.11.2 Discussion of pH study effect .....	177
5.12 Summary and conclusion .....	178
<b>CHAPTER 6 .....</b>	<b>179</b>
<b>SYNERGISTIC EXTRACTION OF THE N-DONOR LIGANDS .....</b>	<b>179</b>
<b>6.0 Introduction .....</b>	<b>180</b>
6.1 Synergistic effect in solvent extraction .....	180
6.2 Mode of action of synergist.....	181
6.2.1 Classical metal ligand coordination .....	181
6.2.2 Supramolecular aggregates .....	184
6.2.3 Factors affecting aggregation .....	185
6.3 Type of synergist .....	185
6.4 Problem statement and justification .....	185
6.4.1 Choice of synergist .....	186
6.4.1.1 Alkyl sulfonates.....	186
6.4.1.2 Carboxylic acid.....	187
6.5 Chapter objective .....	187
6.6 Experimental.....	187
6.7 Results .....	187
6.7.1 Discussion of results from synergist extraction alone .....	187
6.8 Synergistic effects .....	189

6.8.1 Class A ligands .....	189
6.8.1.1 Experimental.....	190
6.8.1.2 Discussion of competitive synergistic extraction results for class A ligands .....	190
6.8.1.2.1 Effect of synergist on selectivity .....	192
6.8.2 Class C ligands .....	194
6.8.2.1 Discussion of competitive synergistic extraction results for class C ligands .....	196
6.8.3 Class B ligands: bis(3-aminopropyl)amine based ligands.....	199
6.8.3.1 Discussion of competitive synergistic extraction results for class B ligands .....	201
6.9 Summary of the synergistic action .....	201
6.10 Study of selectivity in synergistic transport.....	201
6.10.1 Experimental.....	202
6.10.2 Results from competitive transport study of ligand L11. ....	203
6.10.3 Discussion of the synergistic effect on transport studies .....	204
6.11 Summary and conclusion .....	205
<b>CHAPTER 7 .....</b>	<b>206</b>
<b>SOLVENT EXTRACTION OF THE SCHIFF BASE LIGANDS BEARING THE O-DONOR GROUPS.....</b>	<b>206</b>
7.0 Introduction .....	207
7.1 Oxygen containing ligand systems.....	207
7.1.2 Coordination of the oxygen donor group .....	208
7.2 Chapter objective .....	209
7.3 Competitive solvent extraction studies.....	210
7.4 Extraction results for pentadentate system L16-L20 .....	211
7.4.1 Discussion of results from class D ligands .....	211
7.4.2 Coordination structure in relation to extraction .....	213
7.5 Competitive solvent extraction of class E ligands .....	215

7.5.1 Discussion of results from class E ligands .....	217
7.6 Dilution studies.....	217
7.6.1 Procedure.....	219
7.6.2 Discussion on dilution studies .....	219
7.7 pH studies.....	219
7.7.1 pH Isotherms in extraction.....	221
7.7.1.2 Discussion of pH isotherms .....	222
7.8 Competitive bulk liquid transport studies .....	222
7.8.1 Experimental set up for transport studies for the O-donor ligands .....	223
7.8.2 Results and discussion .....	223
7.8.3 Discussion of transport results .....	224
7.8.3.1 Mechanism of transport.....	225
7.9 Summary and conclusion.....	225
<b>CHAPTER 8 .....</b>	<b>227</b>
<b>GENERAL DISCUSSION, CONCLUSION AND REFERENCES .....</b>	<b>227</b>
8:1 Summary.....	228
8.2 Conclusion.....	231
8.3 Future work .....	233
8.4 References .....	234
Appendices .....	250

## **LIST OF FIGURES**

Figure 1. 1 Common ores of copper -azurites ( $2\text{CuCO}_3 \cdot (\text{Cu}(\text{OH})_2)$ ), cuprite ( $\text{Cu}_2\text{O}$ ), chalcocopyrite ( $\text{CuFeS}_2$ ), malachite ( $\text{CuCO}_3 \cdot (\text{Cu}(\text{OH})_2)$ ), chalcocite ( $\text{CuS}$ ) .....	3
Figure 1. 2 Solvent extraction of an analyte using two immiscible solvents.....	4
Figure 1. 3 A Simple solvent extraction process using a separating funnel .....	6
Figure 1. 4 A Simple industrial design for the extraction system of platinum group metals .....	6

Figure 1. 5 An idealized representation of a flow sheet in the hydrometallurgical process.....	10
Figure 1. 6 Metal ions in aqueous solution .....	13
Figure 1. 7 1-Phenyl-3-methyl-4-benzoyl-5-pyrazolone (HPMBP) and (b) thenoyltrifluoroacetone (htta) ...	18
Figure 1. 8 Dibenzo-18-crown-6 ether (DB18C6).....	19
Figure 1. 9 Salicylimine based ligand with the coordinate metal ion .....	23
Figure 1. 10 Schiff base imine bond and the different substituents that can be modified. ....	25
Figure 1. 11 Schematic diagram of (a) salen ligand metal complex and (b) salen type ligand.....	26
Figure 1. 12 Mechanism of transport of metal cation through BLM containing phenylaza 15 crown 5 as Carrier .....	30
Figure 2. 1 Schematic representation of the N-donor ligands. Class A ligands represent the ethyl N-N-N, class B represents propyl N-N-N and class C represents tripodal N-N-N-N ligand systems.....	40
Figure 2. 2 Naphthyl based ligands L3, L8 and L13. ....	40
Figure 2. 3 Avatar ir (ATR) instrument with a ZnSe/Diamond crystal.....	43
Figure 2. 4 Stacked spectra of IR of 5-tert butyl and 5-nonyl salicylaldehyde .....	46
Figure 2. 5 The IR spectra of the unreacted salicylaldehyde, the diamine linker and the ligand L1.....	47
Figure 2. 6 The different functional groups on the salicylaldehyde group .....	48
Figure 2. 7 <sup>1</sup> H NMR spectrum of ligand L1 in CDCl <sub>3</sub> with the different protons numbered in relation to the ligand in the insert.....	49
Figure 2. 8 <sup>1</sup> H NMR spectra of ligand L1, L4 and L5 in CDCl <sub>3</sub> . ....	50
Figure 2. 9 <sup>13</sup> C { <sup>1</sup> H} NMR spectrum of ligand L1 in CDCl <sub>3</sub> with the different carbons numbered in relation to the spectrum.....	50
Figure 2. 10 (a) Schematic diagram of ligand L2 and (b) schematic diagram of ligand L7.....	52
Figure 2. 11 The black mass formed by unpurified ligand L2a and red viscous liquid of L7a.....	52
Figure 2. 12 The <sup>1</sup> H Nmr of unpurified ligand L2a in CDCl <sub>3</sub> .....	53
Figure 2. 13 The purified L2 and L7 products which were analysed in section 2.14.2.2 for L2 and 2.14.3.2 for L7.....	54
Figure 2. 14 Schematic diagram of ligand L3.....	54

Figure 2. 15 The coloured synthesized products from ligand L3 .....	54
Figure 2. 16 Schematic diagram of ligand L8.....	55
Figure 2. 17 The yellow solid product obtained for L8 (a) (Ho22a) and L8b orange (Ho22b). .....	55
figure 2. 18 The stacked $^1\text{H}$ NMR spectra of ligand L8a and L8b in $\text{CDCl}_3$ which are shown to look very similar .....	56
Figure 2. 19 The $^1\text{H}$ NMR of ligand L8a and L8b mixed together In a 1:10 ratio of orange to yellow product in $\text{CDCl}_3$ .....	56
Figure 2. 20 The stacked $^{13}\text{C}$ $\{^1\text{H}\}$ NMR spectra of ligand L8b in $\text{CDCl}_3$ and deuterated DMSO .....	58
Figure 2. 21 The $^1\text{H}$ NMR for ligand L11 in $\text{CDCl}_3$ .....	60
Figure 2. 22 The $^{13}\text{C}$ $\{^1\text{H}\}$ NMR for ligand L11 In $\text{CDCl}_3$ .....	61
Figure 2. 23 Ms Spectrum of ligand L5 with X- axis showing the m/z value and the Y-axis showing the % abundance of the different fragments (A) and (B) indicate the two ionizable masses formed. ....	63
Figure 2. 24 Proposed fragmentation pattern of ligand L5, (b) indicates the fragmented species while (a) represents the ionisable mass species M+H of the ligand (M=563.86g/Mol).....	63
Figure 2. 25 Ms spectrum of ligand L15 with X- axis showing the m/z value and the Y-axis showing the % abundance of the different fragments.....	65
Figure 2. 26 ligand L15 with the area under the circle labelled F1 for the ms analysis.....	65
Figure 2. 27 Schematic diagram of ligand L1 .....	67
Figure 2. 28 Schematic diagram of ligand L2.....	68
Figure 2. 29 Schematic diagram of ligand L3.....	68
Figure 2. 30 Schematic diagram of ligand L4.....	69
Figure 2. 31 Schematic diagram of ligand L5.....	70
Figure 2. 32 Schematic diagram of ligand L6.....	70
Figure 2. 33 Schematic diagram of ligand L7.....	71
Figure 2. 34 Schematic diagram of ligand L8a .....	71
Figure 2. 35 Schematic diagram of ligand L9.....	72
Figure 2. 36 Schematic diagram of ligand L10 .....	72

Figure 2. 37 Schematic diagram of ligand L11 .....	73
Figure 2. 38 Schematic diagram of ligand L12. ....	74
Figure 2. 39 Schematic diagram of ligand L13 .....	74
Figure 2. 40 Schematic diagram of ligand L14. ....	75
Figure 2. 41 Schematic diagram of ligand L15. ....	76
Figure 3. 1 Oligosalen complex showing the secondary coordinated metal .....	79
Figure 3. 2 Salen N-O-O-N donor ligand .....	79
Figure 3. 3 The five coordinate N-O-N ligand systems (pentadentate) and the six coordinate N-O-O-N schiff base ligands system (hexadentate) synthesized from five different aldehydes .....	80
Figure 3. 4 The pentadentate and hexadentate naphthyl containing O-donor salen type of ligands .....	80
Figure 3. 5 The ATR spectra of the schiff base products L16, L17, L18, L19 and L20 .....	82
Figure 3. 6 The $^1\text{H}$ NMR spectrum of ligand L16 in $\text{CDCl}_3$ with the different protons numbered by the position of the appearance of the carbon group it is attached to.....	83
Figure 3. 7 Representative ligands showing the explicit hydrogen of the spacer group where R is salicyl group, X=N or o for L1 and L16 respectively.....	84
Figure 3. 8 Stacked $^1\text{H}$ NMR spectra of L1 and L16 in $\text{CDCl}_3$ .....	85
Figure 3. 9 The stacked $^1\text{H}$ NMR spectra of ligand L16 in $\text{CDCl}_3$ at temperatures -25, -10, 0, 10 and 25 $^\circ\text{C}$ . 86	
Figure 3. 10 Superimposed $^1\text{H}$ NMR spectra of ligand L16 in $\text{CDCl}_3$ .....	86
Figure 3. 11 The $^1\text{H}$ NMR stacked spectra of ligand L16, L17, L18, L19 and L20 In $\text{CDCl}_3$ .....	87
Figure 3. 12 Shows the spectrum of $^{13}\text{C}$ $\{^1\text{H}\}$ NMR. for ligand L16 for purposes of this discussion in $\text{CDCl}_3$ .....	88
Figure 3. 13 The stacked spectra of $^{13}\text{C}$ $\{^1\text{H}\}$ NMR of class D ligands in $\text{CDCl}_3$ .....	88
Figure 3. 14 HSQC NMR results for ligand L16 in $\text{CDCl}_3$ .....	89
Figure 3. 15 Stacked IR spectra of class E ligands .....	90
Figure 3. 16 $^1\text{H}$ NMR for ligand L21 in $\text{CDCl}_3$ with explicit hydrogen atoms no observable third signal for the spacer protons.....	91
Figure 3. 17 The $^{13}\text{C}$ $\{^1\text{H}\}$ nmr for ligand L21 system in $\text{CDCl}_3$ . ....	92

Figure 3. 18 HSQC analysis of ligand L21 in CDCl <sub>3</sub> .....	93
figure 3. 19 The stacked <sup>1</sup> H NMR spectra of hexadentate schiff base ligands O-donor salen type ligand systems in CDCl <sub>3</sub> . ....	94
Figure 3. 20 Schematic of ligand L22.....	95
Figure 3. 21 ligand L22 and B the ligand L22 in direct sunlight.....	96
Figure 3. 22 Solid-state UV of ligand L22.....	96
Figure 3. 23 Confocal microscopy image of ligand L22.. ....	98
Figure 3. 24 The rich colour interplay due to transition emission of ligand L22 from 503 nm-639 nm. ....	99
Figure 3. 25 the fragmentation pattern of ligand L20, m represents the molecular mass of the ligand L20=563.86g/mol.....	100
Figure 3. 26 spectrum of ligand L20 showing the relative abundance with m/z value of the ligand. ....	101
Figure 3. 27 Schematic diagram of L16.....	103
Figure 3. 28 Schematic diagram of ligand L17.....	103
Figure 3. 29 Schematic diagram of ligand L18.....	104
Figure 3. 30 Schematic diagram of ligand L19.....	105
Figure 3. 31 Schematic diagram of ligand L20.....	105
Figure 3. 32 Schematic diagram of L21.....	106
Figure 3. 33 Schematic diagram of L22.....	106
Figure 3. 34 Schematic diagram L23.....	107
Figure 3. 35 Schematic diagram of L24.....	107
Figure 3. 36 Schematic diagram of L25.....	108
Figure 4. 1 The bite size of idealized cyclohexane (b) the ideal geometry for six membered ring and (c) idealized five membered ring.....	114
Figure 4. 2 Ortep diagram of L16 asymmetric molecule of the ligand.....	119
Figure 4. 3 The asymmetric unit cell of L16 ligand showing the packing of the unit molecules.....	120
Figure 4. 4 Ortep diagram of L16 ligand viewed from the spacer proton indicating the v-shaped bend of the ligand.....	120

Figure 4. 5 The two-unit molecules in the asymmetric unit of the crystal.....	121
Figure 4. 6 Packing diagram of ligand L17.....	122
Figure 4. 7 The structure of ligand L18 with the hydrogen atom bonded to the imine rather than the phenolic oxygen.....	123
Figure 4. 8 IR of ligand L17 alone and the L17-Cu complex.....	126
Figure 4. 9 L17-Cu UV-vis spectrum in CHCl <sub>3</sub> and L18-Cu UV-vis spectrum in CHCl <sub>3</sub> .....	127
Figure 4. 10 Schematic diagram of the tetrahedral L17-Cu complex drawn to represent the inversion mode of coordination of the Cu <sup>2+</sup> to the L17 ligand. ....	130
Figure 4. 11 Schematic diagram of the tetrahedral L18-Cu complex drawn to represent the inversion mode of coordination of the Cu <sup>2+</sup> to the L18 ligand.....	130
Figure 4. 12 Ortep diagram of ligand L17-Cu complex.....	131
Figure 4. 13 Ortep diagram of ligand L18-Cu complex.....	132
Figure 4. 14 Plane showing the slight twist of the bonds around the Cu-centre which are out of plane for L17.....	133
Figure 4. 15 Plane showing the slight twist of the bonds around the Cu-centre which are out of plane for L18.....	134
Figure 4. 16 Packing diagram indicating the solvent interaction in the L17-Cu.....	134
Figure 4. 17 Packing diagram of L18-Cu insert shows the two molecules perpendicular to each other and viewed from the top.....	135
Figure 4. 18 Schematic diagram of L19-CuPb bimetallic complex drawn to represent the inversion mode of coordination of the Pb <sup>2+</sup> and the Cu <sup>2+</sup> to the four L19 ligands.....	136
Figure 4. 19 Ortep diagram of disordered L19-CuPb complex with four copper L24 ligands and one Pb <sup>2+</sup> metal the ellipsoids are drawn at 10% displacement probability. some atoms have been deleted for picture clarity. ....	136
Figure 4. 20 Schematic diagram of L1-Co with DCM solvate.....	139
Figure 4. 21 Ortep diagram L1-Co with the DCM solvate.....	139
Figure 4. 22 Schematic diagram for hydrolysed L1-Cu with nitrate counter ion.....	140
Figure 4. 23 The Ortep diagram of hydrolysed L1-Cu structure.....	140
Figure 4. 24 The ortep diagram of the disordered crystal structure of hydrolysed L4-Cu.....	140

Figure 4. 25 Hydrolytic degradation of Schiff base ligand .....	141
Figure 4. 26 Coordination induced hydrolysis of salen type hexadentate ligand .....	142
Figure 4. 27 Schematic diagram of ligand L22 .....	144
Figure 4. 28 Schematic diagram of hexadentate O-donor salen type ligand .....	145
Figure 4. 29 The stacked spectra of the hexadentate O-donor salen type ligands .....	146
Figure 4. 30 Schematic diagrams of (a) L21 and (B) L23.....	147
Figure 4. 31 Fluorescence spectra of L21 and L23 using Me (Methanol), DMF (Dimethylformamide) and acetonitrile solvents .....	147
Figure 4. 32 Fluorescence spectra of different metal ions with L23 at ratio of 1:1 in DMF and H <sub>2</sub> O 1:1 solution at excitation at 360 nm at 25°C.....	148
Figure 4. 33 Fluorescence spectra of base metal ions with L25 at ratio of 1:1 In DMF and H <sub>2</sub> O 1:1 solution at excitation at 360 nm at 25°C.....	149
Figure 4. 34 Fluorescence spectra of base metals with ligand L8 at ratio of 1:1 In DMF and H <sub>2</sub> O 1:1 solution at excitation at 360 nm at 25°C .....	149
Figure 4. 35 Fluorescence spectra of base metals with ligand L10 at ratio of 1:1 in DMF and H <sub>2</sub> O 1:1 solution at excitation at 360 nm at 25°C .....	150
Figure 5. 1 Salen type ligands where R can be different alkyl groups and X being different donor groups..	154
Figure 5. 2 Class A ligands .....	157
Figure 5. 3 Class B ligands.....	157
Figure 5. 4 Class C ligands.....	158
Figure 5. 5 The thermo orion 420a+ pH meter with the two standard pH buffers besides it .....	159
Figure 5. 6 The SPL-Mp15 alcon linear platform shaker with the instrumental parameters shown .....	160
Figure 5. 7 The ligand L1 before and after the extraction process.....	161
Figure 5. 9 The ligand L2 before and after extraction .....	162
Figure 5. 8 Graphical representation of extraction results for class A ligands .....	164
Figure 5. 10 Showing the tautomerism of the schiff base product.....	167
Figure 5. 11 Extraction results of ligand L15 showing very high selectivity for Cu <sup>2+</sup> .....	170

Figure 5. 12 Examples of monotopic salen type ligands used for solvent extraction.....	170
Figure 5. 13 The crystal structure for ligand L1-Cu indicating water molecule coordinated to copper centre.....	171
Figure 5. 14 The disordered crystal structure of L4-Cu with the water molecules found at the centre of the molecule.....	172
Figure 5. 15 Schematic diagram of the concentric transport cell for bulk liquid membrane transport of metal ions. ....	173
Figure 5. 16 Graphical representation of bulk liquid membrane transport results.....	175
figure 5. 17 Graphical representation of the stripping study results.....	177
Figure 6. 1 Ortep diagram of Ni-complex drawn at 30% probability ellipsoids (b) Schematic diagram of the Ni-complex.....	183
Figure 6. 2 Example of reverse micelle made up from four TBP molecules TBP molecule shown on the side.....	184
Figure 6. 3 Acidic co-extractants used in the synergistic studies .....	186
Figure 6. 4 Graphical representation of extraction of synergist C .....	188
Figure 6. 5 Showing the schematic diagram of class A ligands .....	190
Figure 6. 6 Graphical representation of synergistic extraction results of ligand. ....	191
Figure 6. 7 Graphical representation of the trends of synergist extraction for Cu <sup>2+</sup> and Pb <sup>2+</sup> with synergist C.....	193
Figure 6. 8 Schematic diagrams of class C ligands used for synergistic solvent extraction .....	194
Figure 6. 9 Graphical representation of synergistic extraction of ligand L14.....	195
Figure 6. 10 Graphical representation of the trends of synergist extraction for Cu <sup>2+</sup> and Pb <sup>2+</sup> with synergist C .....	196
Figure 6. 11 <sup>1</sup> H NMR spectra of the ligand L1 indicating the spacer proton being tracked.....	197
Figure 6. 12 The induced shift of the spacer methylene signal in the <sup>1</sup> H NMR Spectrum of L1 on titration with different synergists in CDCl <sub>3</sub> .....	198
Figure 6. 13 Schematic diagram of the class B ligands used for synergistic solvent extraction studies. ....	199
Figure 6. 14 Graphical representation of synergistic extraction results of ligand L9 .....	200

Figure 6. 15 Ligands L11 used in synergistic transport study .....	202
Figure 6. 16 Transport cell containing the synergist and the ligand in the membrane phase and the metal mix in the source phase .....	202
Figure 6. 17 Synergist transport for synergist A-L11 .....	203
Figure 6. 18 Synergist transport for synergist C-L11 .....	204
Figure 7. 1 The pentadentate salen type ligands bearing the O-donor group class as D ligands.....	210
Figure 7. 2 The hexadentate salen type ligands bearing O-donor ligands as class E ligands. ....	210
Figure 7. 3 Graphical representation of extraction results for ligand L20 .....	213
Figure 7. 4 Ortep diagram of ligand L17-Cu complex with DCM solvate, ellipsoids drawn at 50% probability, .....	214
Figure 7. 5 Ortep diagram of ligand L18-Cu complex, ellipsoids drawn at 50% probability, insert shows the space filled model indicating existence of channels caused by resistance between the electron clouds of the naphthyl groups .....	214
Figure 7. 6 Ortep diagram of L19-CuPb complex showing the octahedral coordinated $Pb^{2+}$ centre surrounded by 4 planar copper complexes and monosolvate DMSO.. .....	215
Figure 7. 7 Graphical representations of extraction results for ligand L25 .....	217
Figure 7. 8 Graphical representation of dilution studies of L23 .....	218
Figure 7. 9 Graphical representations of competitive solvent extraction for ligand L23 and L25 pH 3. ....	220
Figure 7. 10 Graphical representations of competitive solvent extraction for ligand L23 and L25 at pH 1. ....	220
Figure 7. 11 pH isotherm of 5 metal ions for ArcogaP50 commercial extractant.....	221
Figure 7. 12 Graphical representation of the pH isotherms for the extraction of $Cu^{2+}$ ions under different pH.....	222
Figure 7. 13 Graphical representation of bulk liquid transport for ligand L23 .....	223
Figure 7. 14 Graphical representation of the transport results for ligand L24 for selected base metal ions. ....	224

## LIST OF TABLES

Table 2. 1 The aldehydes used .....	42
Table 2. 2 The diamines used .....	42

Table 2. 3 Summary of the IR and NMR spectra of the imine in different Schiff base products synthesized by the different linkers and aldehyde.....	62
Table 2. 4 Comprehensive CHN analysis table for all the ligands.....	66
Table 3. 1 The spectra showing the shift of the imine in the different substituents of the different O-donor salen type of ligands .....	95
Table 3. 2 EA analysis results.....	102
Table 4. 1 Crystal structure data for ligand L16, L17 And L18 .....	118
Table 4. 2 Selected bond lengths and angles for ligand L16 .....	121
Table 4. 3 Selected bond lengths and bond angles for ligand L17.....	122
Table 4. 4 FT-IR spectra for the imine stretching frequencies.....	126
Table 4. 5 For class D ligands complex.....	128
Table 4. 6 For class A ligands complex.....	129
Table 4. 7 Selected bond lengths for ligand L17-Cu and L18-Cu .....	132
Table 4. 8 Selected bond angle of L17 and L18.....	133
Table 4. 9 Selected bond lengths for L19-Cu-Pb.....	137
Table 4. 10 Selected bond angles for L19-Cu-Pb .....	137
Table 4. 11 Selected bond lengths and bond angle table of L1-Cu.....	143
Table 4. 12 Selected bond lengths for ligand L4-Cu. ....	143
Table 4. 13 Selected bond angles around the Cu Metal .....	144
Table 5. 1 The pKaH values of different alkyl groups to different amines .....	156
Table 5. 2 Summary of the % extraction of Cu <sup>2+</sup> with the different class a (n-donor ethyl) ligand systems. ....	164
Table 5. 3 The summary of the % extraction of the different base metal ions using the different class b (N-N-N propyl) ligand systems (Cu <sup>2+</sup> results are highlighted).....	166
Table 5. 4 The summary of the % extraction of Cu <sup>2+</sup> with the different class C, N- tripodal ligand systems .....	168

**LIST OF EQUATIONS**

Equation 1. 2 Definition of distribution law .....	7
Equation 1. 3 The distribution law in strongly solvate solution .....	8
Equation 1. 4 The distribution ratio of a specie m in organic and aqueous phase .....	8
Equation 1. 5 The % extraction in multiple extraction steps .....	9
Equation 1. 6 The % extraction relation to the distribution ratio for very dilute solution .....	9
Equation 1. 7 The relation between the separation factor and the distribution factor .....	9
Equation 1. 8 The hydrogen ion cycle for chelated extractant .....	17
Equation 1. 10 The formation of the neutral metal complex in the organic phase .....	18
Equation 1. 11 Extraction of uranium by a neutral extractant .....	18
Equation 1. 11 The stability constant.....	21
Equation 1. 12 Gibbs free energy of a ligand .....	21
Equation 1. 13 Relation between the free energy, enthalpy and entropy .....	21

**LIST OF SCHEMES**

Scheme 1. 1 Irving-williams series .....	27
Scheme 2. 1 The condensation reaction of a primary amine with carbonyl group incorporating the mechanistic arrows. ....	36
Scheme 2. 2 Hydrolysis of the carbinolamine .....	37
Scheme 2. 3 The template synthesis of Schiff base complexes.....	37
Scheme 2. 4 Reaction schematic of the synthesis of para-substituted-2-hydroxy benzaldehyde.....	45
Scheme 2. 5 Synthesis of ligand L1 through condensation reaction with salicylaldehyde.....	46
Scheme 2. 6 The tautomerism of a salen type ligand.....	57
Scheme 2. 7 Tautomerism of the schiff base product L8, (a) represents the hydroxyl tautomer product (yellow) and (b) represents the tautomer product (orange). ....	59

Scheme 4. 1 Dissociation and association mechanism of hydrated complex dissociation and association mechanism of hydrated complex redrawn.....	112
Scheme 4. 2 Common routes for the synthesis of salen type schiff base metal complexes .	115
Scheme 4. 3 Reaction scheme for the synthesis of the neutral schiff base copper complex for ligand L17 r= OCH <sub>3</sub> where the phenyl group is replaced by a naphthyl group .....	125
Scheme 6. 1 Possible mechanism of synergistic classical coordination.....	182



# **CHAPTER 1**

---

## **LITERATURE REVIEW**

---



## 1.0 INTRODUCTION

Base metals are part of the transitional and post transitional metals, which include metals like Nickel (Ni), Copper (Cu), Cobalt (Co), Cadmium (Cd), Zinc (Zn), Iron (Fe) and Lead (Pb). These metals have various properties such as good strength and stability. They are malleable, ductile and relatively resistance to oxidation. Because of these properties these metals have therefore found existential uses in various sectors of the economy [1-3]. For example, Cu metals has been used as coinage metals for centuries, Cu metal also has good electrical conductivity and has found applications in making of various electrical components in various electrical gadgets [3]. They are also used as pipes to replace the Pb pipes or the Fe pipes that preceded it for pumping water into homes. Ni metal are usually added to Fe to increase strength and resistance to rusting in make steel used in building and cars. Pb had been used for centuries for making water pipes and due to its high density, it is used in radiation control in the nuclear industry.

These metals are referred to as base metals because they oxidize or corrode easily and for purposes of solvent extraction the term base metals refer to the nonferrous transitional and post transitional metals. These metals are usually obtained as natural ores found in the earth's crust either as native or as mixed ores [1]. They are relatively endemic with occurrence and distribution in various continents. These metals are also obtained as by product of precious metal and platinum group metals (PGM) refinements. These metals are usually inexpensive with market value far less than those of precious metals or the platinum group metals (PGMs) [2].

The current demand and consumption for base metals has significantly increased [2]. For example, approximately 70% of the nickel produced in the world is now used in the production of stainless steel and related alloys. cobalt, zinc and copper are amongst the most important nonferrous metals with various application in hydrogen fuel storage, in sensors design and electrical conductivity [3]. There is more research that is being done on the use and application of these metals such as in nanotechnology and metal-organic frameworks (MOFs) for hydrogen storage, fuel cells, bio-inorganic research and applications where metals are used in various medicinal applications. With the high use and continuous applications of metals, the demand for metals will only get higher with greater demand to access metals easily and cheaply.

There are two principle techniques used in processing of base metals; pyrometallurgy or hydrometallurgy. Pyrometallurgy usually involves heating a mineral or a material with metal ions in a blast furnace at temperatures above 1500 °C to form a melt solution, or with a reducing agent such as coke or coal to form the metal or to form an intermediate product [4, 5]. Hydrometallurgy on the other hand is the process of separating of the mineral ore from its gangue material in biphasic medium [6].

Historically, base metals have been recovered from their primary sources mainly through pyrometallurgy techniques [4, 5]. Over the last 70 years there has been steady progress in the development of new mining processes and technology. However, most of the new technologies are still based on the improving the pyrometallurgy techniques [6]. Pyrometallurgy offers various advantages but it nonetheless also suffers some disadvantages which include its high cost of operation due to its continual use of fossil fuel and the release of dangerous greenhouse emission such as CO (carbon oxides) and the SO<sub>x</sub> gases (sulphur oxides). These emitted gases are usually the by-products of oxidation of the sulfide and carbonate ores shown by the example of copper ores in Figure 1.1.



Figure 1. 1 Common ores of Copper -Azurites ( $2\text{CuCO}_3 \cdot (\text{Cu}(\text{OH})_2)$ ), Cuprite ( $\text{Cu}_2\text{O}$ ), Chalcopyrite ( $\text{CuFeS}_2$ ), Malachite ( $\text{CuCO}_3 \cdot (\text{Cu}(\text{OH})_2)$ ), Chalcocite ( $\text{CuS}$ )

Currently there has been a steady push towards developments that promotes green technology in mineral exploration and recovery. This is mainly attributed to strict emission control laws and international agreements that restricts release of harmful emission [7]. Companies have therefore had to redesign their mining processes to recover or reduce this dangerous emission. This has subsequently led to both reduced output and high prices of metals produced by pyrometallurgy techniques. To maintain supplies of these critical metals, new technologies must be embraced. One of the method that has been adopted to cut costs, reduce emissions and lead to sustainable development is hydrometallurgy which is underpinned by solvent-solvent extraction.

## 1.1 Historical perspective and definition of solvent extraction

Solvent extraction (SX) or liquid-liquid extraction can be defined as the preferential transfer of one or more solutes between two immiscible or partly miscible liquid phases' as shown in Figure 1.2.

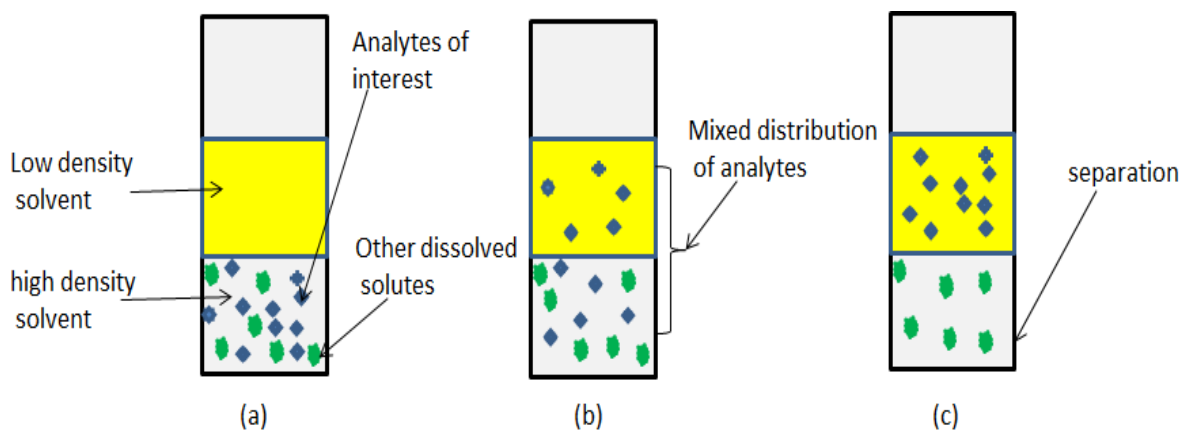


Figure 1. 2 Solvent extraction of an analyte using two immiscible solvents

Note (a) shows the dissolved solutes in high density solvent. (b) Indicates the distribution of the solute between the two phases. (c) Indicates the transfer of the analyte to the low-density solvent. (Note the solutes can be chalcopryite whereas the analyte is Cu while the other dissolved solutes include  $\text{Fe}(\text{NO}_3)_3$ ).

Solvent extraction(SX) has a long history dating back to the time of the alchemists when acids and alkalis became known and used [8]. Over the years there has been great progress in the development and use of this technique. One of the oldest known work in solvent extraction was done by Raimundus Lullus in the 15th century [9]. Nonetheless, the systematic investigations of solvent extraction can only be traced back to the beginning of the 18th century. This is shown by the earliest known reference by Bucholz in 1805 [10]. In this work Bucholz extracted uranium from a nitric acid solution into ethyl ether and back-extracted it into pure water [9].

The capacity offered by solvent extraction to purify and separate chemical elements from each other made solvent extraction an interesting field of research. From the time of Bucholz, to the beginning of the twentieth century, some basic scientific advances have taken place. For example French scientists, Jungfleisch and Berthelot described the distribution of several organic and inorganic compounds between diethyl ether or carbon disulphide and water [11]. In 1872, German scientist Nernst proposed that if a species has the same molecular formula in

the organic phase ( $A_{\text{org}}$ ) as in the aqueous phase ( $A_{\text{aq}}$ ), the final distribution will be dependent on total solute concentration. This law became known as the Nernst distribution law [12]. This is discussed in detail when dealing with principles of solvent extraction in section 1.3.1. The work by Nernst further led to the presentation of the extraction constant of mercury chloride in 1902 by Morse [13]. Since then there have been various other work on constant and distribution factor for different solvents and ions that have been developed [14].

Industrial solvent extraction technology can however only be traced back to the latter years of the 19th century when two major operations were discovered. The first was the cyanidation process of gold and silver and then the Bayer process for the treatment of bauxite into Alumina ( $\text{Al}_2\text{O}_3$ ) [8], both processes being discovered in 1887. Later, in the 1940s, a breakthrough came during the Manhattan Project in the United States (USA) [8, 15-17] where uranium was required for making nuclear bombs. The production of uranium for this purpose was principally done by the Bucholz method that had been developed 140 years before by extracting the uranium from an aqueous solution of uranyl nitrate into ethyl ether [10]. By 1942, the first industrial plant for hydrometallurgy had been developed by Mallinckrodt Chemical Co in St Louis USA for the production of tonnage amount of uranium [8]. The product had a 99.9% purity required for nuclear reactors [16, 17].

From these early days of solvent extraction, the primary pillars of the process have not changed. However, significant achievements have been made in developing of systems used in the process such as electrowinning and the design of metal selective extractants that are very selective for a specific metal [4, 18, 19]. This has consequently stimulated new methods and techniques used in the front end or back end of solvent extraction processes [20]. These include methods such as selective crystallization used in the removal of  $\text{PbCl}_2$  from *chlorometallates* as well as selective precipitation such as the addition of Fe to CoS and NiS mixture to selectively precipitate out one of the metals. Other methods include selective reduction for example cementation of Cu by addition of Fe-scrap to an aqueous Cu solution, selective adsorption of ions into a solid material such as the adsorption of cyano-gold into activated carbon and selective ion transfer into water immiscible phases such as the extraction of uranyl nitrate into tri-butyl phosphate [20].

SX technique has since become one of the most important separation processes in hydrometallurgy. It has found wide application in the hydrometallurgical processing of Cu, Ni, Co, Zn, U, Mo, W, V, Zr, Hf, Nb, Ta, rare earths elements, Ga, Ge, the PGMs. It is also the

principle method used for reprocessing of nuclear fuels, as well as in various other purification processes such as phosphoric acid and nitric acid recovery often obtained as by-products of the hydrometallurgy plant [21].

## 1.2 Principles of solvent extraction

To illustrate the principles of solvent extraction technique, the simplest representation can be shown through a simple setup of two immiscible solvents in a separating funnel [22] as shown in Figure 1.3. In an industrial setup however, the process usually involves various steps as shown in Figure 1.4.

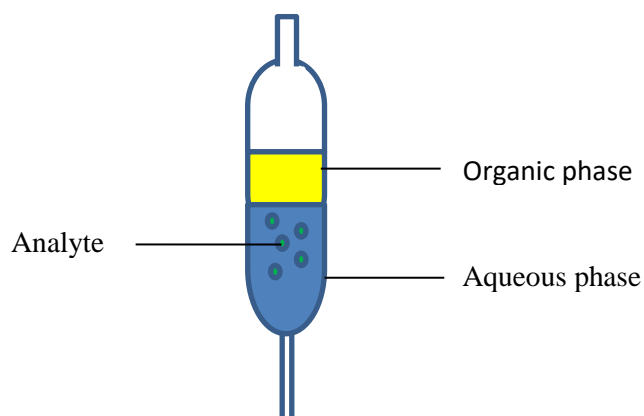


Figure 1. 3 A simple solvent extraction process using a separating funnel Redrawn courtesy of Jan Rydberg *et al.* [22]



Figure 1. 4 A simple industrial design for the extraction system of platinum group metals courtesy of the Matthey Rustenburg Refiners (UK) Limited, Royston, England [23]

From the simple set-up shown in Figure 1.3, it seems that the solvent extraction process looks easy, in practice, solvent extraction processes are much more complicated. Various factors such as hydrolysis, polymerization and complex formation in both phases, need to be taken into consideration [17]. To achieve good extraction in a batch system such as the one used in the laboratory, it is often difficult to make use of conventional mixer systems as opposed to the batch system used in the laboratory.

SX technique often involve various chemical species. These chemical species include the immiscible liquids and the targeted solute analyte of interest. For most SX techniques there are two principle analytes. The organic analyte which is the extractant and the solute material that is the metal [22]. The technique therefore uses the concept of unique solute distribution ratios between two immiscible solvents [24]. This distribution relation as had been mentioned is usually governed by the Nernst distribution law.

### 1.2.1 The distribution law by Nernst

Solvent extraction (SX) deals with the distribution of a solute or solutes between two immiscible liquid phases [16, 22]. The two immiscible solvents are usually in contact with each other as shown in Figure 1.2. It can therefore be deduced that there is a two-phase distribution that can be represented as shown by equation 1.1.



Equation 1. 1 A two phase distribution equilibrium

The two phases that are involved in SX are the aqueous phase (aq) and the organic phase (org). The distribution of the solute between the two solvents will therefore be given by the distribution constant  $K_D$  which is defined by the distribution law proposed by the Nernst equation 1.2 below

$$K_D = \frac{\text{concentration of species A in organic}}{\text{concentration of species A in aqueous}} = \frac{[A]_{org}}{[A]_{aq}}$$

Equation 1. 1 Definition of distribution law ([A] Refers to the concentration of the solute).

The application of the Nernst distribution law has been shown to be limited to pure solvents where there is no dissolution of the solvents. The reality of any solvent extraction system is that the solvents are always saturated with molecules of the other phases for example; a certain percentage of water will be dissolved in the organic phase or vice-versa. Also, the solutes of

interest may have different solubility in the two solvents. Because of this the Nernst distribution equation can only be considered valid only if the mutual solubility of the solvents is smaller than 1% and the activity factor of the system is constant [14].

For a system where the solute is strongly solvated or of high concentration (i.e. mole fraction is greater than 0.1), or if the ionic strength of the aqueous phase is larger than 0.1 M or changes, the Nernst equation must be corrected for deviations from ideal behaviour by the addition of the activity coefficient to the systems as indicated by equation 1.3. For such systems it would be more accurate to describe the distribution ratio of the systems in terms of activity coefficient as given below.

$$K_D^{\circ} = \frac{Y_{A'(org)}[A]_{(org)}}{Y_{A'(aq)}[A]_{(aq)}} = \frac{Y_{A'(org)}}{Y_{A'(aq)}} K_D$$

Equation 1. 2 The distribution law in strongly solvate solution

Note: Y is the activity coefficients, for a system with aqueous electrolytes, the activity factors will vary with the ionic strength of the solution.

### 1.2.2 The distribution ratio

The second principle that has to be considered in solvent extraction is the distribution ratio. The distribution ratio can be defined as the distribution of a mixed solute concentration between two phases. This distribution ratio differs from the distribution constant described above. The distribution constant above is limited to a single species whereas the distribution ratio is for all the species in the aqueous system. In most cases the aqueous solvent would be the pregnant leach solution containing a mixture of solutes, contaminants and acids dissolved in water. Often, in hydrometallurgy this is the product of the leaching process (acid or base leaching process). The organic phase on the other hand consists of the extractants dissolved in diluents or in some cases, a modifier and a synergistic agent. The distribution ratio therefore takes all this into consideration as shown by equation 1.4.

$$D = \frac{\text{concentration of all species containing M in organic phase}}{\text{concentration of all species containing M in aqueous phase}} = \frac{[M]_{t, org}}{[M]_{t, aq}}$$

Equation 1. 3 The distribution ratio of a specie M in organic and aqueous phase

Note:  $[M]_t$  refers to the sum of the concentrations of all metal M species in a given phase, i.e. M can be present in various forms or complexes in the aqueous phase and in the organic phase, and therefore the subscript (t) indicates the total of the M.

The distribution ratio D is dependent on the activity coefficients of the solute in each of the phases. Therefore, when the activity coefficients approach unity, (i.e. at low concentrations), D becomes constant. The distribution coefficient is determined by the percentage extraction, E, which uses multiple extraction steps and can be given as.

$$\%E = 100 D / [D + (V_{(aq)} / V_{(org)})]$$

Equation 1. 4 The % extraction in multiple extraction steps

The ratio of volumes of organic and aqueous phases are fixed to unity

$$\%E = 100D / (D + 1)$$

Equation 1. 5 The % extraction relation to the distribution ratio for very dilute solution

The effect of the various extraction steps is that it enhances better separation and purity. Consequently, it is the most ideal method for separating trace constituents from very large amounts of other substances [25].

### 1.2.3. Separation factor

The last consideration amongst the principles of solvent extraction is the separation factor. The separation factor is the parameter which measures the extent of separation of different species, for example two metals in identical physical condition. This factor is related to the distribution co-efficient also, where the difference between the distributions co-efficient gives the separation factor as shown in equation 1.7 below.

$$S.F = D1 / D2$$

Equation 1. 6 The relation between the separation factor and the distribution factor

D1 and D2 are the distribution co-efficient of the two metal ions under identical conditions. Therefore, species that have a high separation factor will achieve high extraction through a single extraction step.

### 1.3 Application of solvent extraction

Industrial solvent extraction process for processing base metals is principally divided into three main processes as shown by the Figure 1.5.

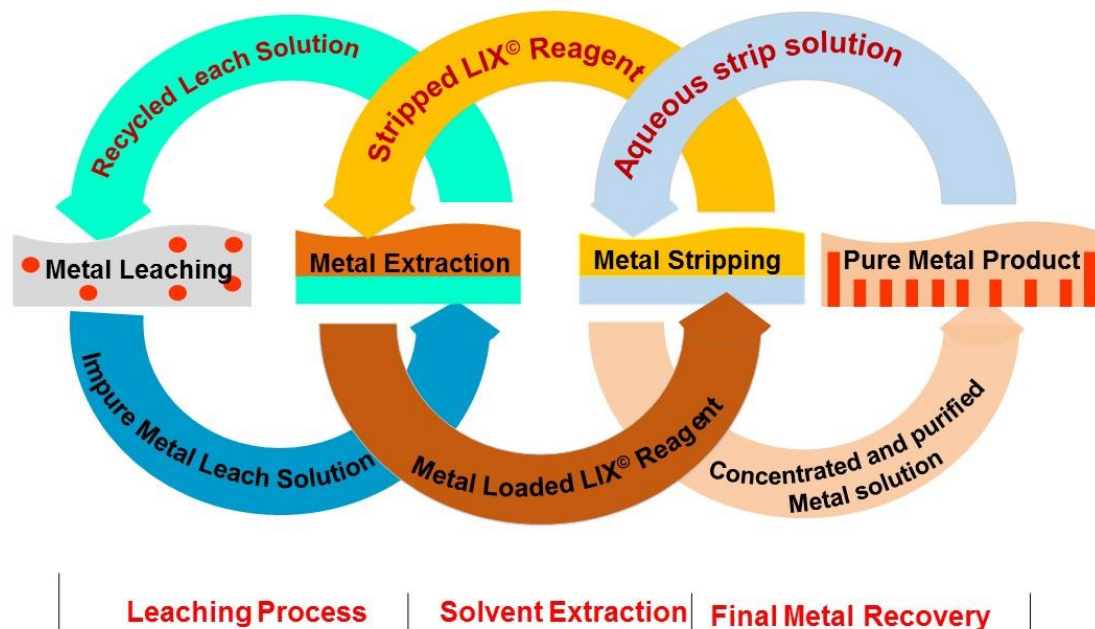


Figure 1. 5 An idealized representation of a flow sheet in the hydrometallurgical process picture courtesy of BASF company [26]).

The first step is the preparation of the pregnant leach solution containing the hydrolysed product of leaching. The leaching process can be non-selective using an acid or base or it can be selective through formation of *chlorometallates* that only dissolve in specific pH. The formation of chlorometallates finds most use in PGMs extraction. The secondary phase in the solvent extraction process of base metal would therefore be the organic phase composed of high boiling point and high flashpoint diluent [2, 27, 28]. The transfer of these metal ions or metal complex from the aqueous phase to the organic phase is therefore encouraged by organic molecules called extractants. The ability of the extractant which is usually an organic molecule with chelating or complexing ability to selectively extract a metal ion or metal complex from the aqueous phase to the organic phase; and later to be released; is the principle that governs solvent extraction. The last step in this process is the metal recovery process. This often involves various purification methods such as electrowinning and precipitation techniques. For purposes of this thesis the discussions will be restricted to the second step which is the solvent extraction process and stripping.

## 1.4 Challenges in solvent extraction

In the application of solvent extraction, there are various challenges that are met due to various chemical species involved in the process and how they interact. These species are discussed in detail as follows.

### 1.4.1 Solvent in solvent extraction

The nature of solvents used in hydrometallurgy usually affects the distribution of both the extractant and the metal ions. It is therefore important to know how the metal ion and the extractants interact in this solution. The study of such interaction also leads to further understanding of the mechanism of interaction of the metal and the extractant and how factors such as pH and temperature affect this process in a solution.

#### 1.4.1.1 The aqueous solution

In the hydrometallurgical SX technique water is one of the principal solvents used, therefore, the choice of the organic solvent (often called the diluent) should be carefully considered. The properties of water which include its density, viscosity, surface tension, vapour pressure; polarization and polarity are intrinsic to each solvent and can be exploited to play a critical role in the solvent extraction process. The role of the solvent is critical, and this can be shown by the solubility of the metal ions or complexes in solution.

#### 1.4.1.2 Metal ions in solution

There are various ways in which the metal ions, the water molecules and the anions or the extractants interact. The ability of the extractant or ligand to extract will depend on the nature of the metal specie in solution. These species can be metal ions or a charged metal complex. For base metal the predominant species in moderate pH (between 4-5) is the metal ions that are often associated with coordination behaviour described as follows. (Please not much lower pH in the presence of excess species such as  $\text{Cl}^-$  will often form the *chlorometallate*).

Metal ions in a solvent such as water are usually represented as  $\text{M}^{n+}$  ion which is not an accurate representation; this is because it shows metal ions as suspended ions in a structure less medium. The reality of metal ions in a solvent is that they are solvated complexes of water similar to complexes of other ligands [29]. The number of water molecules bound directly to the metal ions is similar to the number of donor atoms in a complex [29]. The effect of coordination and

complex formation on ligand-metal interaction in solution and in solid state is discussed in detail in Chapter 4.1.

The nature of coordination of the extractants to the metal ions can therefore either be through inner-sphere or outer sphere coordination [29]. For outer sphere coordination there is direct coordination of the water molecules to the metal ion and the subsequent coordination of the extractant to the formed solvated complex. This process usually involves direct coordination of the water oxygen atom to the metal ion, the O-atom acts as a good Lewis base to the metal ions. This means that the resultant anion or the extractant will have to coordinate to this coordinate water molecule. This type of coordination is often associated with ligands (extractants) or anions of sulfate functionality. For the nitrates and chlorides the nature of coordination involves the direct coordination of the anions or the extractant to the metal ion the nitrate anion coordinates directly to the metal ions this is subsequently called the inner-sphere coordination [22] as shown for nickel ion in Figure 1.6.

From Figure 1.6, the number of water molecules coordinated to the solvated metal ions and the final charge of the formed aggregate depends on the metal ion used (the radius of the metal ion and the electronic structure of the metal ion). The collection of these aggregate ions which include the solvate metal ions, the anions (e.g. nitrates), in the solution can therefore form an ordered region of dielectric constant that maintains the equilibrium of the solution [29]. The change of pH or the introduction of an extractant will therefore destabilize the equilibrium of this created dielectric constant. The process of solvent extraction from an aqueous phase into an organic phase can therefore be looked at as being due to conditions in which the water complex or the aggregate are replaced by aggregates of lower or net charge of zero. Or, they are modified in such a manner to reduce their compatibility with water by inferring to them a character of an organic compound [29]. This replacement therefore takes place in different ways and is affected by its environment and other factors discussed as follows.

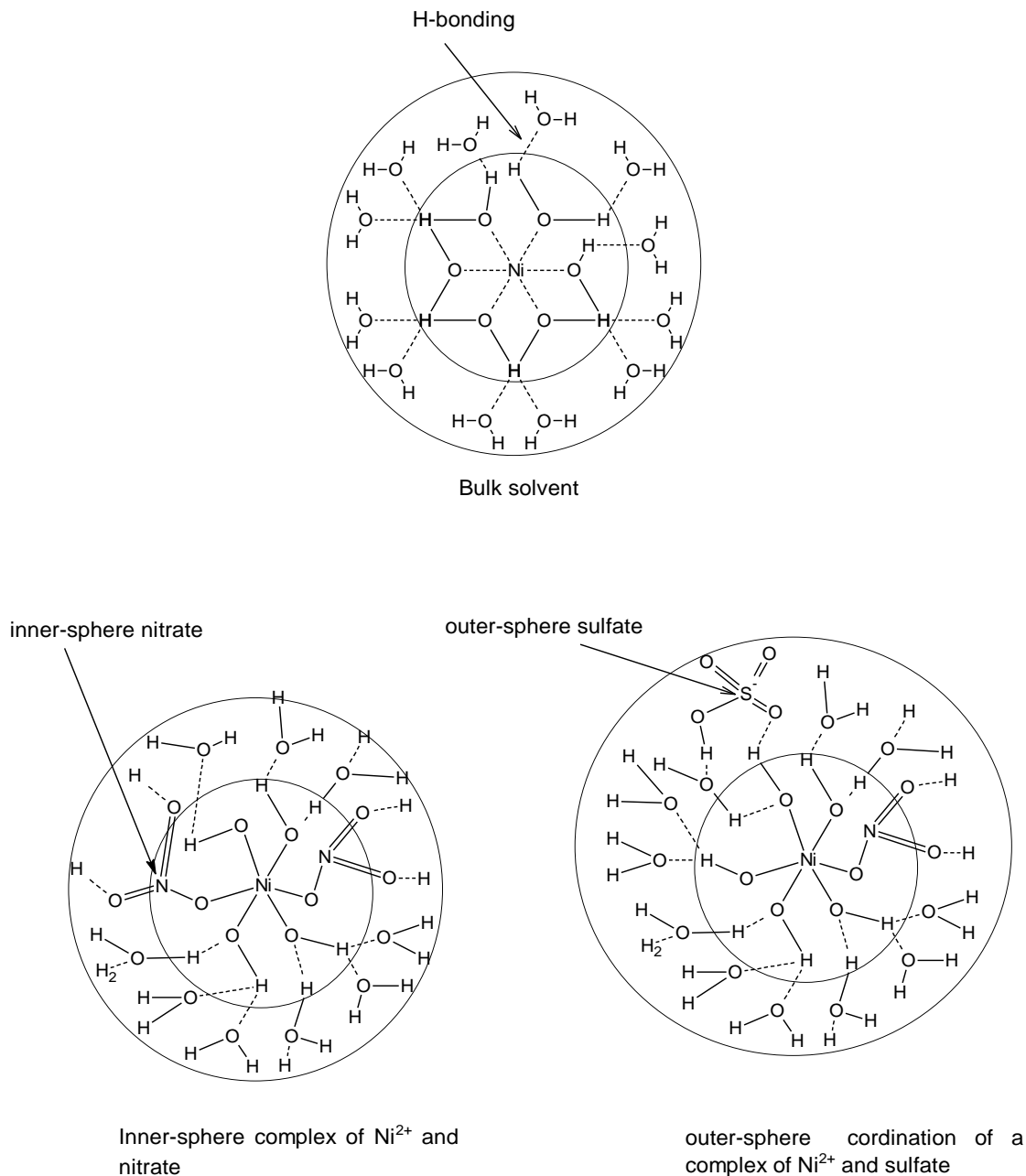


Figure 1. 6 Metal ions in aqueous solution redrawn courtesy of Martell *et al.* [29]

## 1.5 Effect of pH

The change of pH in a solution has three important effects. The first has to do with its ability to destabilize the equilibrium established between the metal ions and the water molecules as described previously. This equilibrium is often established by the ability of the  $\text{OH}^-$  and  $\text{H}_3\text{O}^+$  concentration which surround the metal ions and the anions. A change in pH will therefore lead to destabilization of the equilibrium of the system, equally by increasing the acidity for example by adding a solution of HCl into the solution, the distribution of the  $\text{H}^+$  and the  $\text{Cl}^-$  will destabilize the distribution of the  $\text{OH}^-$  and the  $\text{H}_3\text{O}^+$  ions in the system) [29]. This change in

the distribution of the ions in solution (change in the dielectric constant) means that for a system with metal ions with different coordination number, the distribution of this metal ion is dependent on the  $n^{\text{th}}$  power of the hydrogen-ion concentration (or OH concentration) [29] a change in the pH will lead to destabilization of this distribution.

The second effect also arises due to the already discussed reason which is the formation of the anionic metal complex specie. This occurs for example by changing the pH by adding HCl, this will lead to the formation of the different metal species such as chlorometallates for copper in HCl this is called speciation of the metal ions. (Speciation of metals is an important aspect in platinum group metals extraction). The formation of such species will also lead to change of solubility of the metal ions. Equally an increase in pH to higher pH (pH greater than 6) will lead to formation of hydroxide with base metals that are mostly insoluble.

The third effect caused by change of pH is towards the interaction of some ligand in the boundary layer. For ionic ligands, the reduction of pH (highly acidic medium) will lead to excess protons which in turn will lead to protonation of the selected extractant. The ability of the extractant to function will then be greatly compromised. The reverse of this process is also true where the increased pH will lead to deprotonating of the extractant to enable the coordination to occur. Because of this property, most hydrometallurgical studies of base metals make use of this principle by extracting the metal ions in moderately higher pH and then transferring the extracted solution to a secondary solution of lower pH to release the metal ions.

## **1.6 Choice of diluent**

It is often difficult to classify diluents (organic and inorganic solvents) due to their different physical and chemical properties [30]. Often broad classifications are used which often will lead to overlapping of definition of these solvents. A general classification of solvent can be based on the nature of chemical bonds that they form. For example, some solvents exist as molecular liquids with covalent bonds only, while some exist as ionic liquids composed of molten salts with ionic bonds only, or some will exist as atomic liquids composed of low-melting point metals like liquid mercury or liquid sodium with metallic bonds. Because of the existence of the various types of solvents there are numerous possible mixtures which can be obtained by mixing solvents of different classes leading to inexhaustible types of solvents [30].

The customary non-aqueous organic solvents belong to the group of molecular liquids with covalent bonds which can further be classified into aliphatic or aromatic hydrocarbons. These

can further be grouped into their halogen and nitro derivatives or they can be aliphatic or aromatic alcohols, carboxylic acids, esters, ethers, ketones, aldehydes, amines, nitriles, amides, sulfoxides, sulfones etc [30]. This simpler classification of solvents according to chemical constitution allows certain qualitative predictions, for example whether a compound will dissolve easily in a solvent possessing related functional groups or not. The solubility of the solvent is therefore based on their polarity in which water and perfluorohydrocarbons occupy two extreme positions on empirical solvent polarity scales. Water being the most polar solvent and perfluorohydrocarbons being among the least polar of solvents. A proper choice of solvent, based on the knowledge of its chemical reactivity, helps to avoid undesired reactions between solute and solvent.

In hydrometallurgy, any solvent at ambient pressures and temperatures can be used. However, the choice of the right diluent depends on certain factors such as solubility with the extractants, solubility of the extracted metal complex and coordinating ability of the diluent and miscibility of the diluent with water. With improvement of technology, the range of solvents that can be used in SX has also greatly increased. This is because various known gases can also be used as diluent through high pressure systems. An example of a liquefied gas used in solvent extraction is CO<sub>2</sub>.

The use of these pressurized systems has the benefit of exploiting the various properties of these liquefied gases. This is often done by fine-tuning the pressure and temperature to separate metal ions that are impossible to separate under normal atmospheric conditions [25, 31]. There are various advantages to using these compressed gases, this include good selectivity, they are comparatively faster than using the simple atmospheric based conditions, they have low surface tension, they are inert, they have low energy consumption compared to pyrometallurgy. They are relatively low cost, the compressed gases are nontoxic and are easily recycled by reducing the pressure and temperature to return it to normal gas state [31]. The drawback to industrial application of these liquids is the high pressure and temperature required which requires expensive equipment with high running cost [25].

## **1.7 Organic extractants**

There are various types of extractants that are used in solvent extraction processes. In most cases the commercial extractants used usually contain different organic molecules such as modifiers which are surface active reagents, synergists which are used to enhance the extraction

properties of the extractant and the main ligands which are used as extractants. All these organic reagents are important and serve specific function in the extraction process. For purposes of this chapter, the discussions will be limited to the extractants only. The other organic reagents such as modifiers and synergists are discussed in Chapter 6.

In principle most coordinating organic molecules can be used as extractants in a solvent extraction process [32, 33]. For a ligand to coordinate, it must have different functional groups brought about by the different donor atoms. The donor atom has to have a free electron pair on one or more of the donor atoms. Equally the orbital system of the central metal atom ( $M^{n+}$ ) must also be of the right energy and should be capable of accepting an electron pair from the ligand to form a coordinate covalent bond between itself and the ligand (L). The maximum number of donor atoms that coordinate directly to the central metal ion ( $M^{n+}$ ) is called the *coordination number*. The coordination numbers of 2, 4, 5, 6 and 8 are the most common and useful. Ligands that can coordinate through only one donor atom are called *monodentate* ligands [32] while ligands that coordinate through two or more donor atoms at the same time are called *polydentate* ligands.

While coordination number and donor properties are very important, a good extractant has to have certain basic characteristics to be considered for use in the SX process. These properties include good selectivity towards the metal ion, metal salt or the complex of choice. For purposes of this thesis the reference ions will be metal ion. A good extractant therefore has to be able to meet the metal coordination number by forming a neutral complex; the extractant has to have good extraction kinetics in the formation of the neutral complex. The formed metal-extractant complex should be relatively stable so as to be able to be transferred into the organic phase [34].

### 1.7.1 Extractants in solvent extraction

There are various types of extractants used in solvent extraction processes. They range from those used in leaching to those used in the final extraction process. Sudderth *et al.* [35] classified the different types of extractants used in solvent extraction into four main classes based on structure, extraction and stripping chemistry and the type of metal species extracted. These classes include: ion pair extractants, neutral or solvating extractants, organic acid extractants and chelating agents which are discussed as follows.

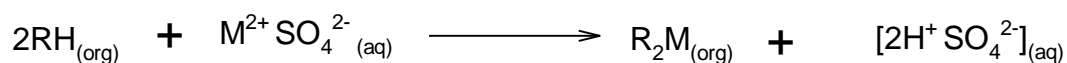
### 1.7.2 Ion pair extractants

Under high concentration of anion in aqueous phase, soluble metal ions remain in their ionic state. These metal ions can then be transferred into organic phase by the formation of ion pair with ionic extractant. These ionic extractants usually have different mechanism of extraction that can be shown in two ways; first, they convert ionic metals into electrically neutral species which becomes free from ion-dipole interactions and secondly, the presence of long chain alkyl groups or highly organic substituents in these molecules helps them to get solvated via organic interaction. These include the amine- and the phosphine-based ligands.

Some of the advantages are that they can be used for acidic to near-neutral solutions with varied pH range depending on the specific system. They are usually very selective with rapid kinetics of extraction and stripping. In most cases these extractants are usually used in conjunction with a synergist or modifiers. The modifiers used are long chain alcohols that can be added to the hydrocarbon diluent to prevent the formation of precipitates. Most of these extractants are either amine or phosphate based. The quaternary and tertiary amines are usually more selective than secondary or primary amines. Commercial examples include Adogen-464 [36].

### 1.7.3 Chelating extractant

Chelating extractants are well known and are usually characterized by their polydentate donor groups with ability to meet the metal's co-ordination number. These extractant's mechanism of extraction or mode of action involve the coordination of the metal ion and the reduction of the charge of the metal ions rendering it electrically neutral [35]. These extractants are relatively similar to the ionic extractants. However, the existence of the multiple donor groups allows the chelating agent to form metal chelates that are highly organic and can be transferred to the organic phase. These extractants usually operate on a hydrogen ion cycle [25] as shown by equation 1.8.



Equation 1. 7 The hydrogen ion cycle for chelated extractant

These extractants are some of the most popular extractants containing a polydentate system with multiple coordination sites. They have good phase separation with the ability to operate well with both acid and ammonia leach solutions to effect phase separation. They are more selective than either ion-pair or organic acid extractants. However, they tend to coordinate

much slower (kinetically slower) than organic acid and ion-pair extractants. These extractants are often more difficult to produce [25]. Examples include 1-phenyl-3-methyl-4-benzoyl-5-pyrazolone (HPMBP) [37] (shown in Figure 1.7a), 3-Phenyl-4-Benzoyl-5-isoxazolone (HPBI) [38], thenoyltrifluoroacetone (HTTA) [39] (shown in Figure 1.7b), 1-benzoyl acetone (bzac) [40], 2-hydroxy-5-nonylbenzophenone oxime [41] tetrabutylmalonamide [42]. The nature of coordination of chelates is discussed further in section 1.7.4 when considering the thermodynamics of complex formation.

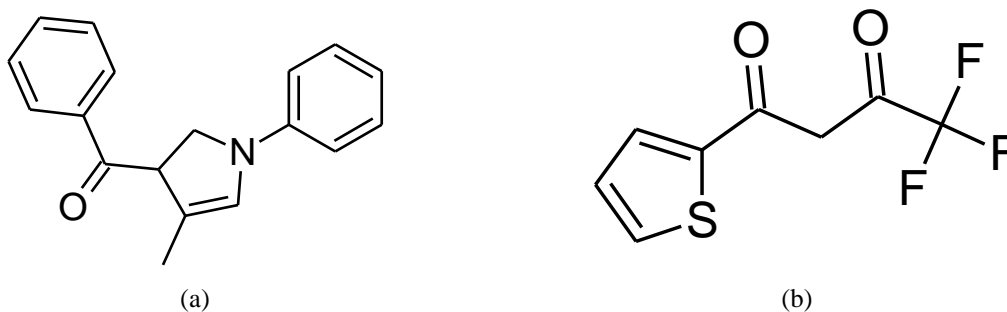
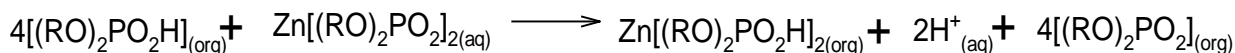


Figure 1. 7 1-phenyl-3-methyl-4-benzoyl-5-pyrazolone (HPMBP) and (b) Thenoyltrifluoroacetone (HTTA)

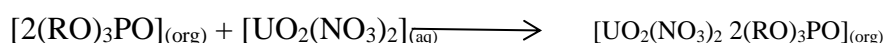
#### 1.7.4 Neutral and solvating extractants

Neutral extractants usually provide an organic centre where the electrically neutral metal compounds can be transferred to the non-polar organic diluents. These extractants operate on a hydrogen ion cycle like the chelated extractants as represented by Equation 1.9.



Equation 1. 8 The formation of the neutral metal complex in the organic phase

Neutral or solvating extractants [25] normally exhibit fast extraction and stripping kinetics and can be used to extract neutral metal complexes. They are generally not very selective. However, in combination with other extractants they can act as synergists, antagonists, or phase modifiers. Examples of these ligands include the well-known crown ethers (DC18C6, DB18C6,) as shown in Figure 1.8 [43] and trialkyl phosphine oxide ( $R_3P = O$ , where R can be n-octyl, n-butyl, phenyl) [44]. Their reaction in the extraction of uranium is given in Equation 1.10.



Equation 1. 9 Extraction of uranium by a neutral extractant

Please note that the strength of selectivity changes as  $R_3PO > (RO)_3PO > R_2CO > ROH > R_2O$  (Trialkylphosphine oxides > trialkylphosphates > ketones > alcohols > ethers).

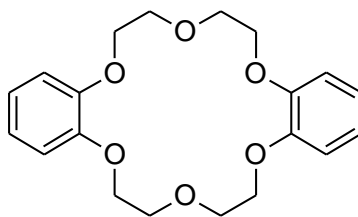


Figure 1. 8 Dibenzo-18-Crown-6 ether (DB18C6)

## 1.8 Choice of extractant in solvent extraction of base metals

Since there are a plethora of extractants, the choice of an extractant for use in the solvent extraction of a particular metal ion will depend on the properties of the metal ion and the character of the ligand as mentioned in section 1.7. The use of a particular ligand will therefore depend on the ligand solubility in the organic phase (insoluble in aqueous phase), its coordination preference to the metal ion and the type of donor group in the ligand. For any ligand to coordinate to the metal ions in solution, it should be able to overcome the coordinated water molecules as explained in section 1.4.1 by forming either inner sphere coordinate bonds.

### 1.8.1 Inner and outer sphere coordination

From the discussion in section 1.4.1, the ability of the extractants to extract the metal ions depends on the ability of the ligand to displace the water molecules or the coordinate anions such as nitrates from the metal ion to form a charge neutral metal complex. The type of complex formed can therefore be between the ligand and the metal, the ligand and the metal salt (metal and anion) or the ligand and the solvent molecules. While most organic extractants can easily displace the coordinate water molecules, the formation of the inner or outer sphere complex is greatly influenced by the nature of anion present in the pregnant leach solution [29]. This is more so for anions such as sulfates and chlorides which are not easily displaced from the metal ions and therefore will tend towards outer sphere coordination as shown earlier by Figure 1.6

### 1.8.2 Solubility of the ligand and complex in the organic phase

The second consideration in ligand design is the solubility of the neutral coordinated compound formed into the organic phase. It is very important that the extractant and its metal complexes have a very low solubility in water and a high solubility in the water-immiscible (non-aqueous) phase. Most organic solvents used are usually high boiling point hydrocarbons, chosen on the grounds of safety and cost. The low polarity of these hydrocarbon diluents favours the formation of H-bonds and other forms of secondary bonding between the neutral complex and the solution. These interactions in the organic phase contribute significantly to the strength and

selectivity of an extractant. The lack of these interactions usually leads to the solubility of the formed complex into the aqueous phase which is called the bleeding of the ligand. In most cases the solubility effect is usually used in relation to more conventional aspects of ligand design to develop reagents which can resist the ligand leaching effect in solvent extraction processes [29].

### 1.8.3 Effect of donor groups of the ligands

The type of donor atom in the ligand is perhaps the most significant consideration. This is because various extractants have different donor groups or functional groups. The effect of donor groups tends to be much more pronounced in extractants due to the donor atoms preference in coordinating to different metal ions. The ability of these donor groups to coordinate is greatly influenced by the inductive or steric influence around the donor group. Examples of common donor groups used in extractants include nitrogen containing groups for example in amines, imine, amides, and nitriles; and oxygen containing groups for example carboxylic, hydroxyl, phenolic, ether and carbonyl. Phosphate containing groups for example alkylphosphate and the sulfur containing groups such as in thiols, thiocarbamates and thioethers are also commonly used. The most popular commercial extractants for the divalent base metal ions such as  $\text{Cu}^{2+}$  and  $\text{Ni}^{2+}$  are the N-donor and O-donor containing ligands [34].

The ability of the different donor groups to coordinate to different metal ions has been extensively studied. In 1963 Pearson [45, 46] classified different ligands in relation to the ease of coordination to different metal ions.. This became known as Hard Soft Acid Base classification (HSAB). Over the years this classification has been expanded to include various ligands and donor groups. This classification mainly focuses on the stability of the complexes formed between the different donor groups and the metal ions. This stability usually depends on the favourable Lewis acid-Lewis base interactions and the chelate effects. Stereotypically hard Lewis acids, such as metal cations with high oxidation states, can easily form complexes with hard Lewis bases like hydroxyl-containing ligands and *vice versa* [47] as shown in Table 1.1.

From Table 1.1, various commercial extractants have since been synthesized either as monodentate derivatives or polydentate products bearing different donor groups. The different alkyl groups attached to the donor groups have the effect of altering the steric effect and the inductive effect around the main donor group. This will subsequently influence the ability of

the donor group to coordinate to the different metal ions. This usually forms the basis on which the different ligands are designed. The design of a single extractant with a given donor group should be able to be used for the extraction of a particular metal ion, however this is also affected by external factors such as pH and temperature which can influence the ability of the given ligand or extractant to extract another metal ion.

Table 1.1 Pearson's Hard Soft Acid Base classification (HSAB)

Hard	Soft	borderline
H <sup>+</sup> , Mn <sup>+</sup> , Li <sup>+</sup> , Cr <sup>+</sup> , Na <sup>+</sup> , Al <sup>3+</sup> , Co <sup>3+</sup> , K <sup>+</sup> , Ga <sup>3+</sup> , Fe <sup>3+</sup> , Mg <sup>2+</sup> , Ca <sup>2+</sup> , Ti <sup>3+</sup>	Cu <sup>+</sup> , Pt <sup>2+</sup> , Pt <sup>4+</sup> , Au <sup>+</sup> , Ti <sup>+</sup> , Hg <sup>2+</sup> , Cd <sup>2+</sup> , Pb <sup>2+</sup>	Fe <sup>2+</sup> , Ni <sup>2+</sup> , Zn <sup>2+</sup> , Co <sup>2+</sup> , Cu <sup>2+</sup>
H <sub>2</sub> O, CO <sub>3</sub> <sup>2-</sup> , NH <sub>3</sub> , OH <sup>-</sup> , NO <sub>3</sub> <sup>-</sup> , RNH <sub>3</sub> , CH <sub>3</sub> CO <sup>2-</sup> , ROH, N <sub>2</sub> H <sub>4</sub> , PO <sub>4</sub> <sup>3-</sup> , R <sub>2</sub> O, RO·ROPO <sub>3</sub> <sup>2-</sup> , (RO) <sub>2</sub> PO <sup>2-</sup> , Cl <sup>-</sup>	R <sub>2</sub> S, R <sub>3</sub> P, RS <sup>-</sup> , CN <sup>-</sup> , RSH, RNC, (RS) <sub>2</sub> PO <sup>2-</sup> , (RO) <sub>2</sub> P(O)S <sup>-</sup> , SCN <sup>-</sup> , CO, H <sup>-</sup>	NO <sup>2-</sup> , SO <sub>3</sub> <sup>2-</sup> , Br <sup>-</sup> , N <sub>3</sub> <sup>-</sup>

#### 1.8.4 Thermodynamics of complex formation and the Chelate effect

The stability of coordinate complexes can be described by the following thermodynamic functions. When a ligand forms a complex from metal ion with A<sub>n</sub>-donor (M<sup>n+</sup> + A<sup>n-</sup> → MA<sub>n</sub>), the stability constant (β<sub>n</sub>) can be given as equation 1.11;

$$\beta_n = \frac{(\text{MA})}{(\text{M})(\text{A})^n}$$

Equation 1. 10 The stability constant

The ligand free energy, ΔG<sub>n</sub>, can therefore be given as shown in Equation 1.12 below.

$$\Delta G_n = -RT \ln \beta_n.$$

Equation 1. 11 Gibbs free energy of a ligand

Since the free energy ΔG is usually attributed to the changes in enthalpy, ΔH<sub>n</sub> and entropy, ΔS<sub>n</sub> as shown in by Equation 1.13 below;

$$\Delta G_n = \Delta H_n - T\Delta S_n$$

Equation 1. 12 Relation between the free energy, enthalpy and entropy

The enthalpy change (ΔH) will therefore describe the energy changes due to bonding, while TΔS describes energy changes related to the number of independent species such as the effect of solvation [48].

For the formation of metal ligand complexes with highly charged polydentate ligands, the main contribution to stability is charge neutralization which leads to an increase in entropy [48]. For uncharged ligands such as polyamines, the stability is achieved by the decrease in enthalpy. The balance between enthalpy changes ( $\Delta H_n$ ) and entropy ( $\Delta S_n$ ) is that the enthalpy change (due to bonding) is restricted by the high dielectric constant of water which efficiently screens the electrostatic forces [48] as had been explained in Section 1.5.

Apart from this there are also other factors that play a critical role in thermodynamic stability of the complex formed. This includes the interplay of factors such as number of donor groups discussed below, the mutual repulsive forces between these donor groups and the entropy contribution due to conformational changes during complex formation. For repulsive forces or conformational change, the change of enthalpy  $\Delta H$  counteract the entropy requirements to stability as the ring size increases [48].

#### **1.8.4.1 Effect of multiple donor groups (chelate effect)**

As has been shown in the HSAB classification, the different donor groups preferentially coordinate to different metal ions. Most ligands usually contain two or more donor groups. The special arrangement of these donor groups may result in coordination with the metal ion forming a cyclic complex (termed a chelate) [49], and the ligand referred to as a chelating agent [32]. In multidentate ligands, coordination to a metal ion ( $M^{n+}$ ) results in multiple bonding. The formation of this chelate ring greatly increases the stability of the complex over that of an analogous non-chelating complex. The term chelate effect was coined by Schwarzenbach [49], in order to denote this increase in stability [32]. The introduction of one extra ring may increase the stability constant ( $\beta$ ) by a factor up to  $10^4$  (i.e. complexes of the type  $MA_n$  vs  $MA_{n+1}$ ).

The other consideration to effectively increase the ( $\beta$ ) value (stability constant) is by change of the donor group, for example, a change of "N" to "S" can increase  $\beta$  value by approximately 4 orders of magnitude for complexes with soft metals. This is very important to this work in which ligands with different donor groups and different alkyl chainlength between the donor groups are considered.

### **1.9 Commercial extractants**

In solvent extraction studies, the ability to design an extractant with strong selectivity and good extraction kinetics for a relevant or specific chemical species is usually the main desire of the coordination chemist. Commercially, most ligands used as extractants are usually singly

charged monodentate or bidentate ligands such as oximes, carboxylic acids or phosphoric acids [33]. The ability of these extractants to effect separation usually depends on two main properties i) the difference in the formation constant between the extractant and the metal ions of choice, ii) The distribution coefficient of the extracted metal species in the bi-phasic system in SX. Because only the uncharged (neutral) species are typically extracted into the organic phase, the use of double or triple charged ligands would therefore enhance the kinetic and stability of polyvalent metal ions [33, 50].

### 1.9.1 Oxime and hydroxime ligands

One of the most prominent ligands used in solvent extraction are the *oxime*-based ligands. These ligands are analogous to Schiff base ligands containing an imine with hydroxyl group next to it (C=NOH) [17]. These oxime based ligands have found successful use in extraction of copper as monodentate extractant known commercially as either LIX reagents (BASF) or as Arcorga® reagent [51]. The use of this reagent in hydrometallurgy has been extensively studied. It shows good extraction properties with the ability to be used in different pH conditions [52]. There have been various derivatives of this ligand that have been synthesized. One of the most commonly used ligands are the *hydroxime* ligands. These ligands are imine based ligands which contain a salicylaldehyde group and an imine [17] as shown in Figure 1.9.

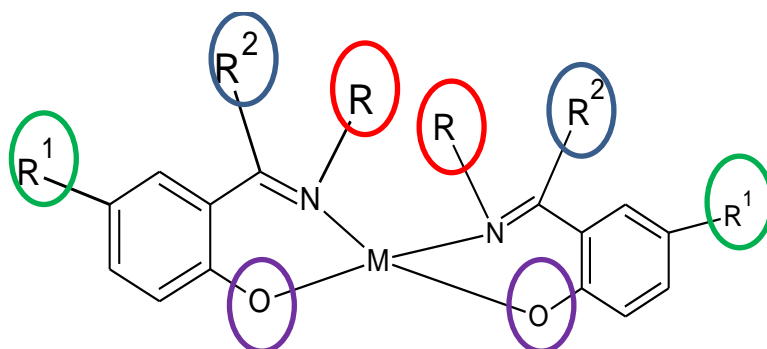


Figure 1. 9 Salicylimine based ligand with the coordinate metal ion. For oxime ligands R is OH and R<sup>1</sup> can be long chain alkyl group or aromatic groups for R<sup>2</sup> = H this are called aldoxime while if R<sup>2</sup> = alkyl group it is called ketoxime

The advantages of using the *oxime*- and the *hydroxime*-based ligands is the existence of the O, N O donor groups and the various modifications that can be obtained by the changes of the ancillary groups R, R<sup>1</sup> and R<sup>2</sup> as shown in Figure 1.9. Studies based on modification of the ancillary R<sup>1</sup> group are often associated with various changes in extraction potential. For example, the *oxime* based ligands (R = OH) shown in Figure 1.9 when the R<sup>2</sup> is a CH<sub>3</sub> or C<sub>6</sub>H<sub>5</sub>

are called *ketoximes*. This has the effect of allowing the ligand to exhibit moderate strength allowing the ligands to be used at pH above 1.6 [52]. This type of extractant is associated with good physical performance, excellent phase separation and low entrainment of the raffinate [52]. They are also known to not promote excessive crude product formation. However when the R<sup>2</sup> group is a H (*salicylaldoxime*), the ligand will then exhibit very strong extraction of copper with rapid transfer kinetics, and high extractive strength [52]. This ligand is however less stable than *ketoxime* due to the lack of the alkyl group. They are also not able to be stripped of the metal in low acidic conditions. Because of these reasons the development of complimentary ligands having the *bis-imine* and hydroxo functional groups would be a more appropriate approach to try and improve on the property of these ligands. One prominent ligand that also bares similar structural characteristics are the inexpensive salen-type Schiff base ligands.

### 1.10 Schiff base ligands

Schiff base ligands are imine based ligands, they are nitrogen analogues of an aldehyde or a ketone in which the carbonyl group (CO) has been replaced by an imine group (C=N) [53, 54]. These ligands were first reported by Hugo Schiff in 1864 [55]. These ligands are a popular class of ligands [56, 57] and have been extensively studied. These ligands can be used in making dyes and pigments, used in biological and medicinal application, used in catalysis, used in the making of polymers and can be used in hydrometallurgy as extractants [58]. These ligands are usually relatively easy to synthesize [59]. They are also easy to modify, offering various donor groups [58].

#### 1.10.1 Reactivity and properties of Schiff base ligands

The uses of Schiff base ligands are usually derived from the existence of the imine bond with the general formula R<sup>1</sup>R<sup>2</sup>C=NR<sup>3</sup> as shown in Figure 1.10. The imine bond with the R<sup>2</sup> as a hydrogen group is usually referred to as *azomethine* bond [60]. The polarity of the C=N bond with the carbon centre is partially positively charged. The nitrogen is partially negatively charged which allows for the reactivity of this sensitive system [60].

The effective reaction of the imine centre is based on the substituents attached to the imine centre R, R<sup>1</sup> and R<sup>2</sup> which can be any substituent such as alkyl, aryl or aromatic or heterocyclic groups having a variety of functionalities. The presence of alkyl groups usually stabilizes the

imine and makes them very efficient ligand systems. The presence of the cyclic aryl group leads to effective conjugation making them even more stable [17].

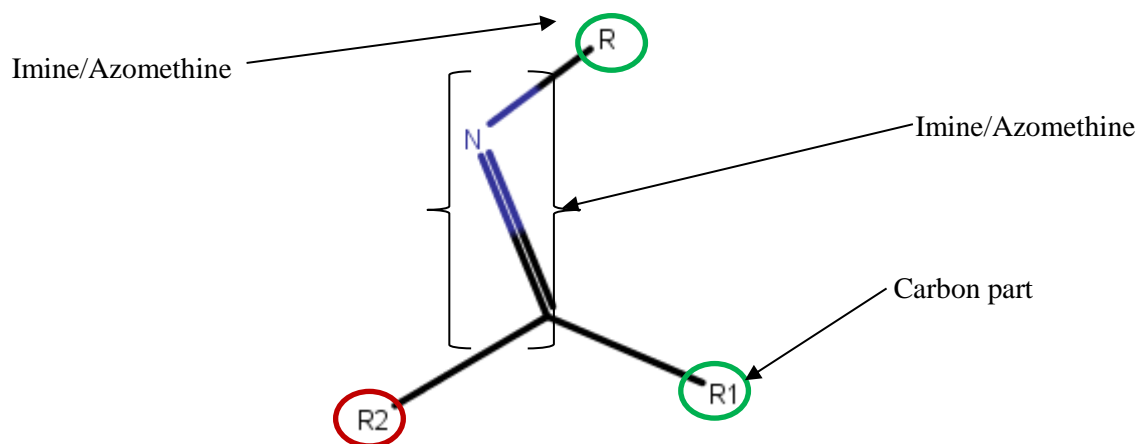


Figure 1. 10 Schiff base imine bond and the different substituents that can be modified[60].

There are various modifications that can be made to these ligand systems. One of the significant methods used to achieve this is through the addition of various donor groups in the ancillary R groups (i.e. R, R<sup>1</sup> or R<sup>2</sup>) [61]. The manipulation of these backbones will often lead to sophisticated systems capable of multiple coordination sites for these ligands. The most common functionalized groups are the systems containing nitrogen (N), oxygen (O), sulphur (S) and phosphorus (P) groups in the ligand backbone [17].

From literature, it has been shown that these ligands can coordinate to various transitional metal ions and post transitional metal ions with different oxidative states [62]. The product of such reactions are stable complexes [62]. The formed stable complexes have been subsequently studied in the catalysis of diverse processes, such as in oxygen and atom transfer, *enantioselective epoxidation* and *aziridination*, mediating organic *redox reactions* and as mediators in other *oxidation processes*. It is however important to note that very little is known about the formation equilibria of these ligands with transitional metals in solution [62, 63] and the use of these complexes as carriers in ion-selective electrodes [62, 64].

### 1.10.2 Salen type ligands

There are various types of Schiff base ligands that have been synthesized due to the various modifications. These ligands can be divided into two groups; the symmetric group for example the salen and salophen and the asymmetric Schiff base ligands for example hydrazones [62]. The symmetrical salen ligands are a prominent class of Schiff base ligands. These ligands are

synthesized from a salicylaldehyde and ethylenediamine to form the condensation product 2,2'-{ethane-1,2-diylbis[nitrilo(*E*)methylidene]}diphenol known commonly as salen ligand [62].

The reaction of these ligands to transitional and post transitional metal ions is through the imine centre and the OH group. The resultant complex forms a square pyramidal or octahedral coordination geometry [62] as shown in Figure 1.9. Because of the flexibility of these ligands due to the presence of the ethyl group and their oxygen binding activity, this makes these ligands a versatile class of ligands [58].

There are various modifications of the salen ligands that have been studied; this modification includes the synthesis of this class of ligands using various *salicylaldehydes substituents or derivatives* and various modifications of the diamines resulting in various symmetrical ligands. The product of these symmetrical diamines and the *salicylaldehydes* are therefore referred to as salen type of ligands which generally represents O, N, N, O ligands [65, 66] as shown in Figure 1.11b. These ligands therefore allow for various modifications and various donor groups forming relatively stable complexes.

Structurally these ligands are analogous to the *oxime* ligands however these salen type ligands have the advantage of having a *bis-imine* Schiff base system in place of the OH group, therefore offers better stability as complexing agents than their *monodentate* or *bidentate* analogues [67, 68]. These ligands can also be fine-tuned by varying the electronic and steric effects [69] and by the addition of another donor group, X, as shown previously in Figure 1.11.

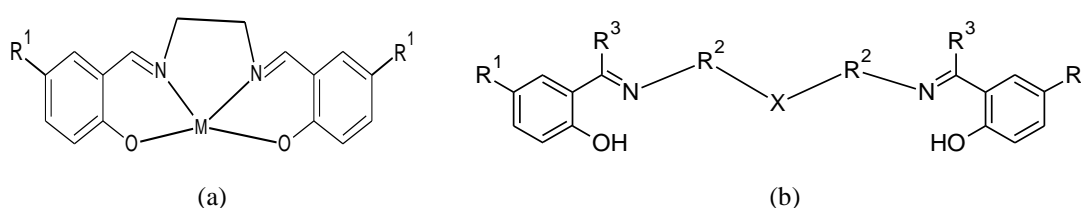


Figure 1. 11 Schematic diagram of (a) Salen ligand metal complex and (b) Salen type ligand

NOTE: R<sup>1</sup> = alkyl group, phenyl or substituted phenyl and even H, R<sup>2</sup> = alkyl group, R<sup>3</sup> = H, and X = any donor group such as N, O, S etc.

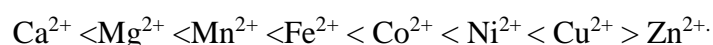
The reactivity of these ligands and their subsequent use in hydrometallurgy has a broad appeal and is usually as a consequence of the activity of the imine centre and the various donor groups. The added donor group, X, can therefore act as potential secondary coordinating centre for these ligands which can allow these ligands to make excellent chelating agents for the different base metals.

## 1.11 Base metals ions

The last three decades has seen a significant increase in the use of solvent extraction for the commercial recovery of base metals [70]. There are various base metals that are actively extracted through solvent extraction processes. For example approximately 30% of all copper (Cu) are now being extracted by solvent extraction process using the oxime based extractant, or phosphate based extractants [7, 71]. Nickel (Ni) and zinc (Zn) have also been extracted by solvent extraction; however, the general usage of this process is far less than that of Cu. For any metal to be extracted it must be soluble in the lixivants (aqueous phase) to form the pregnant leach solution. The lixivants can contain sulphuric acid, ammonia or cyanide. The metal therefore has to be able to be recovered from this concentrated leach solution. The extraction process for any metal consequently deals with the selective preference of the extractant to the metal ion in a competitive environment from the pregnant leach solution.

### 1.11.1 Competitive extraction of base metals

To effect separation of base metals in a solvent extraction process, the behaviour of metal ions towards the ligands is very important. There are various studies that have been undertaken to give a clear understanding of the competitive nature of the metal ions in the presence of an extractant. One such prominent work is by Irving, Rossotti and Williams [72-75] and J. Stary [76] in 1956. This work gives the order of stability of the formed complexes of divalent metal ions. This order of stability can therefore be used to indicate the preference of an extractant in solvent extraction for various divalent metal ions [17] as shown in Scheme 1.1.



Scheme 1. 1 Irving-Williams series [72]

This series therefore shows that the preference to coordination will start from  $\text{Ca}^{2+}$  to  $\text{Cu}^{2+}$  indicating that the selectivity is driven by the physical and chemical characteristics of both the metal ions as well as the donor groups on the ligands [48]. This order is therefore brought about due to ligand field effects and the atomic or ionic radius as indicated in the series. The preference to coordination of the  $\text{Cu}^{2+}$  over the  $\text{Zn}^{2+}$  is due to the Jahn-Teller effect that is discussed in Chapter 4.1.2.1.

## **1.12 Metal ion transport**

Solvent extraction processes offer various advantages, such as good selectivity, high purity and cost effectiveness. They however have some drawbacks such as the third phase formation, solvent degradation, crud product formation and high and excessive use of solvents. To overcome such limitations, the use of transport systems to effect separation has become an option [77]. Metal ion transport can therefore be defined as using chemical reagents to extract and separate the metal ions from a solution through a membrane. It therefore involves uptake, transport of the ions across the membrane and the stripping process. The use of the membrane offers a second factor to be considered in effecting selectivity of the extraction system as discussed in Chapter 5. The use of membranes offers greater advantages over liquid-liquid extraction. This includes the ability to overcome the above-mentioned limitations, while also offering various other advantages. By combining the extraction and stripping operations together the organic loading limitations of solvent extraction can be circumvented by this technique [78], which also reduces the levels of expensive complexing agents employed in liquid membranes [79].

### **1.12.1 Liquid membranes**

The first modern use of membranes in separation technology was by Li in 1968 [80]. Since then there have been great strides in the development of liquid membranes [77]. In recent years, a notable increase in the applications of liquid membrane techniques has been observed [79, 81-84]. Liquid membranes can be classified as Emulsion Liquid Membranes (ELM), supported liquid membranes (SLM), multi-stage three phase extraction and bulk liquid membranes (BLM).

### **1.12.2 Emulsion membrane**

This usually involves the formation of water-in-oil or oil-in-water emulsions by the organic solvent and surfactant-stabilized water. This water-oil barrier acts as the membrane through which the mass transfer occurs between the bulk and the immiscible membrane phase. This membrane is therefore usually formed by stirring the oil/water into the aqueous-oil feed solution. The biggest draw-back to this method is essentially in the preparation stage which requires several unit operations [85]. However, emulsion liquid membranes have shown great potential especially in cases where solute concentrations are comparatively low and other techniques cannot be efficiently applied [85-88].

### **1.12.3 Supported liquid membranes**

The supported liquid membranes usually make use of an organic liquid that is absorbed into small pores of a silica support or polymer support and is kept there by capillary forces. The support membrane separation has gained a lot of ground particularly in purification of drinking water where natural supports such as zeolites are used to support the membrane. This technique is normally restricted to selective separation, purification, and concentration of toxic wastes and valuable metals in aqueous solutions [89-92]. The main disadvantage of supported liquid membranes is the low productivity and problems associated with implementation in an industrial scale.

### **1.12.4 Multistage three-phase extraction**

This technique combines bulk and supported liquid membrane techniques and extraction is achieved in multiple stages (three-stages) of mass-transfer system. Each stage consists of two chambers, one extraction chamber (has the feed stream or donor phase) and one stripping chamber [85]. The liquid membrane therefore acts as the mass-transfer medium, since it is in contact with the donor and acceptor phase in the closed circuit where it flows through all the stages in counter current mode. The extraction therefore occurs in these chambers in multiple stages with forced circulation of the membrane phase.

### **1.12.5 Bulk liquid membrane**

Bulk liquid membranes (BLM) is one of the most used techniques and usually consists of an aqueous feed phase and stripping phase which are separated by a water-immiscible liquid membrane phase [85, 93]. The liquid membrane hosts the extracting agent and is in contact with two other aqueous liquids, the feed phase and the receiving phase. Transport occurs due to difference in potential across the different aqueous phases. BLM have various advantages such as its simplicity, its relatively low costs and its ability to be scaled up or down, depending on whether it is in a laboratory set up [79, 85] or an industrial or commercial process.

Among these technologies, BLM represents the techniques in which the liquid mobile carrier has the greatest effect in the efficacy and selectivity of the membrane transport. It also offers greater advantages in understanding the effect of the extracting agent, for example studies of competitive bulk liquid membrane (BLM) are very important because it offers such a powerful tool for environmental sample analyses where often the results that are achieved from a competitive system cannot be obtained from a single cation system [94, 95]. There are a lot of novel carriers that have been explored to create selective separation systems [79].

### 1.12.5.1 Mechanism of bulk liquid transport

The metal ion transport through the bulk liquid membrane usually occurs in two areas; the membrane interface between the source phase and the membrane interface; and the receiving phase. The process occurs through two simple steps, the extraction step and the stripping step is shown in Figure 1.12.

The first step is the extraction step which occurs at the source-membrane interface, where the cationic metal ions are coordinated to the ligands to form an uncharged complex. This occurs normally at high pH [79]. The second step is the metal stripping stage where the formed complex diffuses across the membrane at the membrane-receiving phase interface; this occurs through the decomposition of the metal ligand complex, where the metal ions are released into the receiving phase. This is associated with the gain in proton by the carrier from the receiving phase and the subsequent diffusion of the free carrier back across the membrane towards the donor/membrane interface where the cycle is repeated [79].

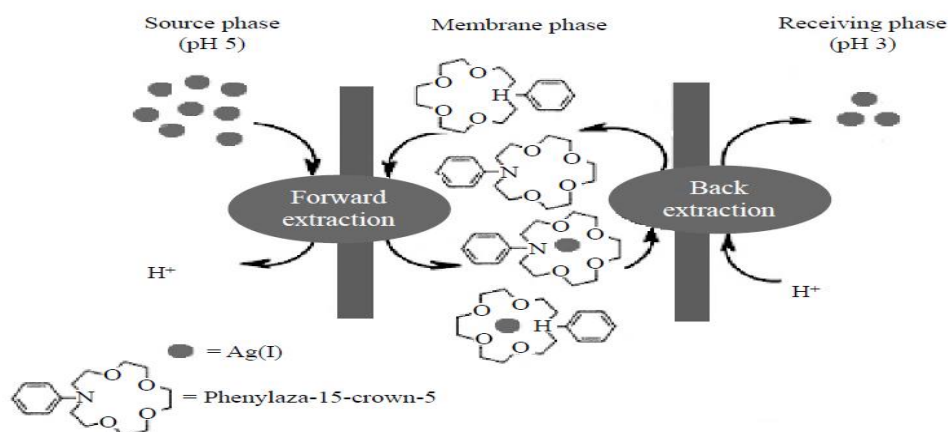


Figure 1. 12 Mechanism of transport of metal cation through BLM containing Phenylaza 15 crown 5 as carrier picture courtesy of Tarahomi et al. [79].(note the H in the azacrown ether indicates protonate N atom (NH+))

### 1.12.5.2 Factors affecting transport

#### 1.12.5.2.1 Effect of carrier structure on the cation transport

The first important factor to be considered in BLM transport is the nature and type of extractant or the carrier. This is because the extractant plays the role of phase transfer catalyst. It forms an extractable complex which diffuses in the membrane in the organic phase as described in the mechanism in Figure 1.12. This factor is well described in ligand design in any extraction system.

#### **1.12.5.2.2 Receiving phase**

The second factor involves the nature and concentration of the receiving phase. The concentration of the receiving phase has a great influence on the kinetics and efficiency of the systems. This is because it determines the rate at which the equilibrium will be reached. The nature of the receiving phase is partly determined by the nature of extractant used in the membrane phase and the type of mineral acid used in the receiving phase. The receiving phase has to be able to protonate the extractant to release the metal ions and the same time has to be able to maintain the concentration gradient of the hydrogen ion between both sides of the membrane [96]. Transport through the membrane is therefore controlled by the potential difference created by the difference in pH.

#### **1.12.5.2.3 Effect of organic solvent in the membrane phase**

There are various parameters which depend on the type of solvent used in transport just as it is equally important in extraction [14, 32]. The solvent has the direct effect of formation of the unstirred boundary layers in the membrane interface. The thickness of this unstirred boundary layer determines the diffusion coefficients of all mobile species in the system, the thickness of this boundary is also known as the diffusion path length. The composition of the boundary layers is a function of the mutual partial solvent solubility (for example water-chloroform solubility) and is determined by the physical and chemical properties of the solvents [79].

### **1.13 Problem statement**

For an efficient separation process, the development of extractants with a strong preference for relevant chemical species is important [50]. In the last 30 years there has been an increased interest in research towards the design of ligands that are capable of extracting in the front-end and back-end of a hydrometallurgy process. An example of this ligand system is the hydroxime ligands that are capable of coordinating to metal ions such as  $\text{Cu}^{2+}$ . These bidentate ligands are capable of coordinating to the metal ion such as  $\text{Cu}^{2+}$  in 1:2 ratio to form neutral metal complexes. This means for a 1:1 mole ratio, the extraction achieved by these ligands cannot be more than 50%. The use of Schiff base ligands that are relatively inexpensive due to their ease of synthesis, ease of modification and ability to encompass multiple donor groups, enables these ligands to complex metal ions in a 1:1 ratio offering better prospects as extractants in solvent extraction.

### 1.14 Justification

The mining industry is very important to the social wellbeing of the society, currently metals and various mixed metal material are used in every facet of the society. To meet the current demand for high grade metals, the mining industry has had to find a cost-efficient method for processing of the ores and the recovery of the metals. This has led to the development of the hydrometallurgical process.

In hydrometallurgy, achieving an optimal extraction of valuable mineral components is an extremely important goal. The process of solvent extraction is a major method of processing minerals under biphasic conditions. The success of this process is ascribed to the ability of the extractant to form neutral stable coordination complexes with metal ions in the aqueous solution [32]. The ability of these extractants to form these complexes is attributed to the various donor groups and the different alkyl substituents on the extractant. The interplay between the electronics of these donor groups and the alkyl groups often leads to selectivity and efficiency of the extraction system.

### 1.15 Aims and objectives

The aim of this research was to study multidentate salen type Schiff base ligands bearing N- and O- donor groups as potential extractants in solvent extraction processes. The work therefore is divided into synthesis and characterization, coordination studies, solvent extraction studies and transport studies as follows:

#### a) Synthesis and characterization

- Synthesis and characterization of ten *pentadentate* ligands with N-donor groups in their backbone, five of which have an ethyl group between the donor spacer backbone and five with a propyl group between the donor groups in the spacer backbone.
- Synthesis and characterization of five *tripodal heptadentate* N-donor ligands with ethyl groups in the spacer backbone.
- Synthesis and characterization of five *pentadentate* ligands with one O-donors and five *hexadentate* with two O-donor groups with ethyl groups between the donors in their spacer backbone.
- To study the spectroscopic and electronic effects of the addition of the various substituents on the salen type ligands.

**b) Coordination studies**

- To synthesize and characterize some selected Schiff base metal complexes.
- To study the coordination of the different ligands using different analytical techniques.
- To determine the crystal structures of some of the synthesized ligands and the crystal structures of some of the synthesized complexes through single crystal X-ray diffraction.
- To study the fluorescence behaviour of selected ligands in the presence of the different solvents and base metals.

**c) Solvent extraction studies**

- Competitive solvent extraction study of all the synthesized ligands for selectivity of the selected divalent metal ions such as  $\text{Cu}^{2+}$ ,  $\text{Cd}^{2+}$ ,  $\text{Co}^{2+}$ ,  $\text{Pb}^{2+}$ ,  $\text{Ni}^{2+}$  and  $\text{Zn}^{2+}$ .
- Competitive transport studies of selected ligands towards the selected base metals.
- Competitive dilution studies of selected ligands towards the selected base metals.
- To determine selectivity through pH differences in scrubbing studies of the selected divalent metals using the selected ligands.
- pH isotherm studies for selected ligands and base metals.

**d) Synergistic studies**

- Competitive synergistic solvent extraction studies of selected ligands towards the selected base metals.

**1.16 Thesis Layout**

The different classification and the sub objectives are dealt with in different chapters as follows. Chapter 2 and Chapter 3 will deal with the entire section (a). Chapter 2 will therefore only focus on the N-donor ligands. Chapter 3 will focus on the O-donor ligands. Chapter 4 will focus on the entire coordination studies. Chapter 5, Chapter 6 and Chapter 7 will deal with solvent extraction studies where; Chapter 5 only focuses on the N-donor ligands and Chapter 7 on the O-donor ligands. Chapter 6 will therefore focus on the synergistic studies in section (d) above. Chapter 8 will be the summary, conclusion and future work.

# **CHAPTER 2**

---

## **SYNTHESIS OF N-DONOR SCHIFF BASE LIGANDS**

---

## 2.0 Introduction

There are various methods that have been developed for the synthesis of Schiff base ligands. In this chapter, two of these methods are discussed, their advantages and their disadvantages. There are different approaches that are used in the synthesis of the N-donor type ligands. Special consideration is given to the inductive and steric effects caused by adding different substituents on the phenyl ring and the effect of increasing the spacer group (adding alkyl groups between the donor groups). Finally, the different analytical techniques and instruments used in the characterization of these ligands are also discussed.

## 2.1 Condensation reaction

Schiff base ligands (SBs) have many desirable properties as discussed in the literature review. One of the properties mentioned is the relative ease of synthesis [97]. The most popular methods for the synthesis of these ligands is the condensation method. This is a well-known method for the synthesis of the Schiff base ligands. This method usually involves simple self-condensation of suitable aldehyde or ketones and a primary amine precursor. This reaction was initially assumed to be a one-step reaction to give the imine group, (-C=N-) [98, 99]. However, in 1953 Braun, Stein and Snell [100, 101] proposed that the process had more than one step but rather two steps as discussed below.

### 2.1.1 Mechanism of condensation reaction

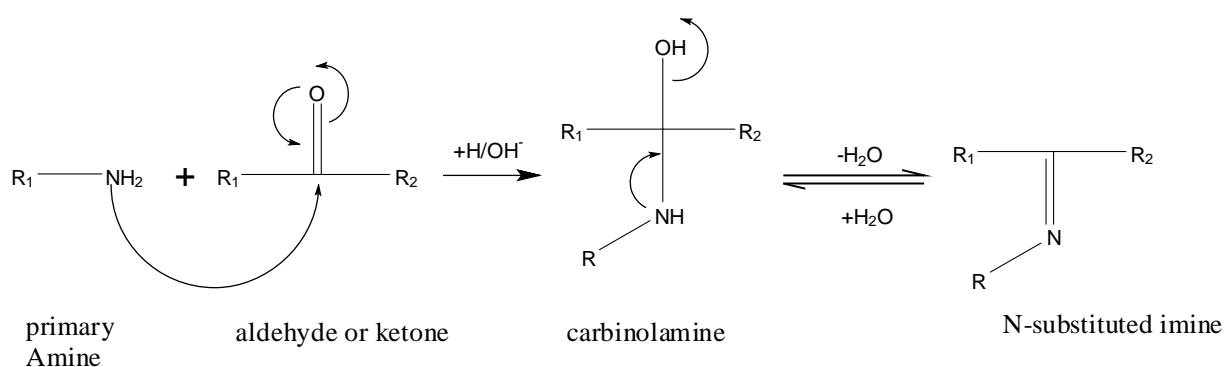
For a long time the mechanism of Schiff base formation was never known until the three biochemists Braun, Stein and Snell [100, 101] proposed the accepted mechanism for this reaction. The first step they proposed was that the process leads to the formation of an intermediate called the *carbinolamine*. This *carbinolamine* is composed of the amine and an intermediate hydroxyl group. The second step is the process of elimination of this hydroxyl group as water. This process is illustrated by Scheme 2.1 [102]. The forward direction for the formation of the product is driven by the removal of these water molecules or the separation of the product or both [17].

Although these two processes mentioned above are well accepted mechanism for the formation of these Schiff base ligands. It was however observed that these two steps usually over simplify this reaction. For synthesis of molecules with stereogenic centres there are various additional products that indicates that the formation of the *carbinolamine* and the dehydration processes are accompanied by other processes. These additional processes can be proton transfer,

hydrolysis and *carbinolamine* elimination processes [102]. Such reactions will often be accompanied by formation of polymeric products [102]. For this thesis the discussion will be restricted to the discussion of the *carbinolamine* formation and the dehydration process.

### 2.1.1.1 Process of formation of carbinolamine

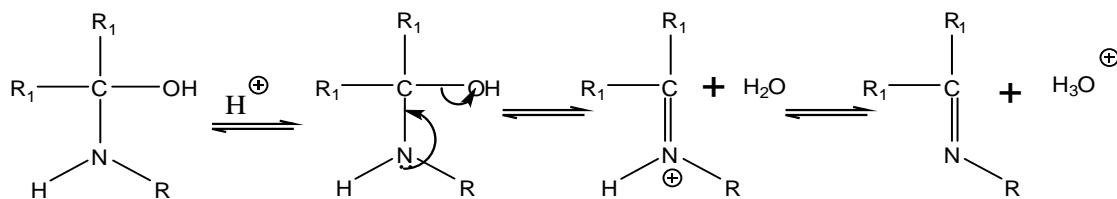
The formation of the Schiff base product through the condensation method usually takes place by means of nucleophilic addition of a primary amine to a carbonyl group. The primary amine in this case acts as the nucleophile, while the carbonyl carbon acts as an electrophile. The nucleophile therefore attacks the carbonyl carbon to give an unstable addition compound called the carbinolamine [17], this process is therefore shown by Scheme 2.1.



Scheme 2. 1 The condensation reaction of a primary amine with carbonyl group incorporating the mechanistic arrows. (Redrawn courtesy of Zoubi *et. al* [17].)

### 2.1.1.2 Dehydration of the carbinolamine

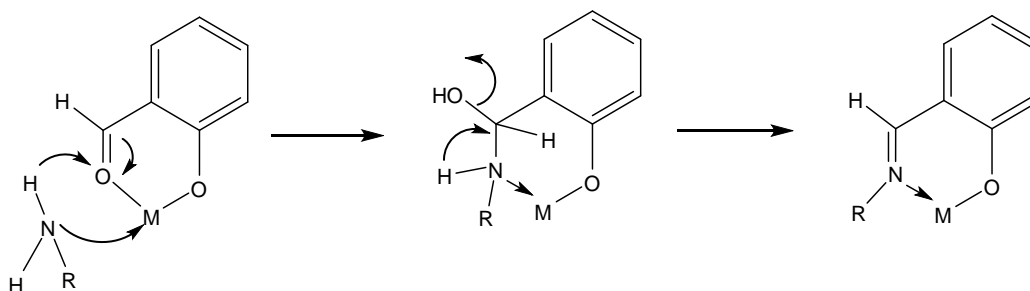
The dehydration of the *carbinolamine* is the second step and is usually the rate-determining step in the formation of the Schiff base product. The loss of the water molecule in this reaction can either be through acid or base catalyzed pathways. The *carbinolamine* formed above is an alcohol and therefore will likely undergo acid catalyzed dehydration as shown in Scheme 2.2. It should however be noted that the acid concentration should not be very high. This is because imines are basic compounds. If the formed imine is protonated in an acidic medium and becomes non-nucleophilic, equilibrium is going to be pulled to the left and carbinolamine formation will not occur. Therefore, many Schiff base syntheses can only be carried out at mildly acidic pH [17].



Scheme 2. 2 Hydrolysis of the carbinolamine (redrawn courtesy of W. A. Zoubi *et al* [17].)

## 2.2 Template synthesis process

This is the second method for the synthesis of Schiff base ligands. According to El-Sheriff *et al.* [103], there is no distinct definition of a template synthesis method. This is because the method involves using different templates. The template can be a metal ion, or any other centre that has a definite stereochemistry and electronic state which can serve as a mould or pattern for the formation of the desired ligand [103] as shown by Scheme 2.3. Once the moulded complex is formed, the template can then be removed.



Scheme 2. 3 The template synthesis of Schiff base complexes (redrawn courtesy of El-Sheriff *et al* [103]).

For the preparation of complexes or by use of mould containing metal templates, the metal can be replaced through transmetallation reactions to form the desired complex [103], or the metal can be reduced to remove it from the template leading to the desired product in high yield and in high purity [99].

There are various advantages that this method offers over the condensation method; this includes; suppression of secondary reactions such as polymerization that usually accompany Schiff base imines with stereogenic centres. Secondly the desired complex can be obtained directly, particularly for the inaccessible complexes [103]. Despite these advantages offered by this method the disadvantages outweigh its advantages since the yield is sensitive to a number of factors. These factors include the order and timing of reagent addition, the type of anion in the metal salts, the solvent used and even temperature. It has been hypothesized that either the

organic intermediate or the product ligand must be formed prior to the point where the mould (metal salt) is removed [103].

The work in this thesis will be limited to using the condensation methods of a primary amine and an aldehyde to form the Schiff base product. Therefore, the discussion of the synthesis method will be restricted to the method used and the various modifications done to obtain the Schiff base ligands.

### **2.3 Stability of Schiff base ligands**

The imine bonds are relatively stable bonds however, they are also very reactive. In most cases Schiff base condensation reactions are easily reversed in the presence of a highly acidic or basic medium during synthesis. Therefore, caution is usually taken during synthesis and even purification procedures. This means that use of untreated silica columns for separation is often avoided since they can easily hydrolyze the Schiff base ligands due to the acidic nature of the untreated silica column.

The other properties of the Schiff base ligands which have already been discussed is that they decompose or polymerize rapidly unless there is at least one aryl group bonded to nitrogen or carbon of the  $>C=N<$  double bond [104]. The presence of the aryl group serves to stabilize the bond through the effective conjugation and therefore the products are more stable and readily synthesized as opposed to the alkyl substituents which are relatively unstable and readily polymerizable [105-108].

Many aromatic Schiff base ligands usually have a secondary functional group such as an OH, NH or SH near the imine functional group. The proximity of these functional groups permits the formation of five or six membered chelate rings when coordinated to metal ions [17] as discussed in Chapter 1. When such products undergo aromaticity they usually undergo colour changes. This will be discussed further in Chapter 3 under photometric and fluorescence studies.

### **2.4 N-donor salen type ligands**

There are various donor groups that can be attached to the imine centre, the diversity of the groups that can be attached to this system leads to the various modifications that make these ligands adaptable for various applications. For salen type ligands, the changes are usually attributed to the added donor groups between the *bis-imine* centres. The reactivity of this added

donor group leads to an additional reactivity centre or change of property that is associated with these changes in the ligand series.

The N-containing Schiff base ligand systems are some of the most pervasive ligand systems in nature. This is because the nitrogen-containing units of these molecules play integral roles in biological activities, in coordination chemistry and also in hydrometallurgy [109]. The coordination ability of the N-containing group is directly related to the property of the N-atom. The N-atom is a relatively soft donor as discussed in Chapter 1. It therefore has the tendency to coordinate easily with most transitional metal ions such as  $\text{Co}^{2+}$ ,  $\text{Ni}^{2+}$ ,  $\text{Cu}^{2+}$ ,  $\text{Zn}^{2+}$ ,  $\text{Cd}^{2+}$  and  $\text{Pb}^{2+}$ .

The ability of the N atoms to coordinate in a multidentate system therefore depends on two reasons; the first is the size of the spacer (alkyl groups) between the two donor atoms. The second reason is due to the added substituent group on the phenyl system. The ability of this N-donor to react therefore enables these ligands to exhibit interesting ionophoric properties towards heavy metal ions.

This chapter will only focus on the synthesis of these ligands, and the electronic effects due to the change of the different substituents on the phenyl ring and the effect of the added alkyl group between the donor groups.

## 2.5 Chapter objective

In this chapter the synthesis and characterization of 15 different salen type Schiff base ligands bearing the N-donor system in their backbone are discussed. These ligands are shown in Figure 2.1 and 2.2. The electronic and the steric effects caused by the change of the substituents on the phenyl ring and the addition of alkyl groups between the donor groups will also be discussed.

The 15 ligands have been divided into three distinct classes based on the type of spacer group used in the backbone. Class A, is the diethylenetriamine based (ethyl system), class B is bis(3-aminopropyl)amine based (propyl system) and class C is the N,N-bis(2-aminoethyl)ethane-1,2-diamine based (*tripodal* ligands). These ligands are shown below in Figure 2.1 and Figure 2.2.

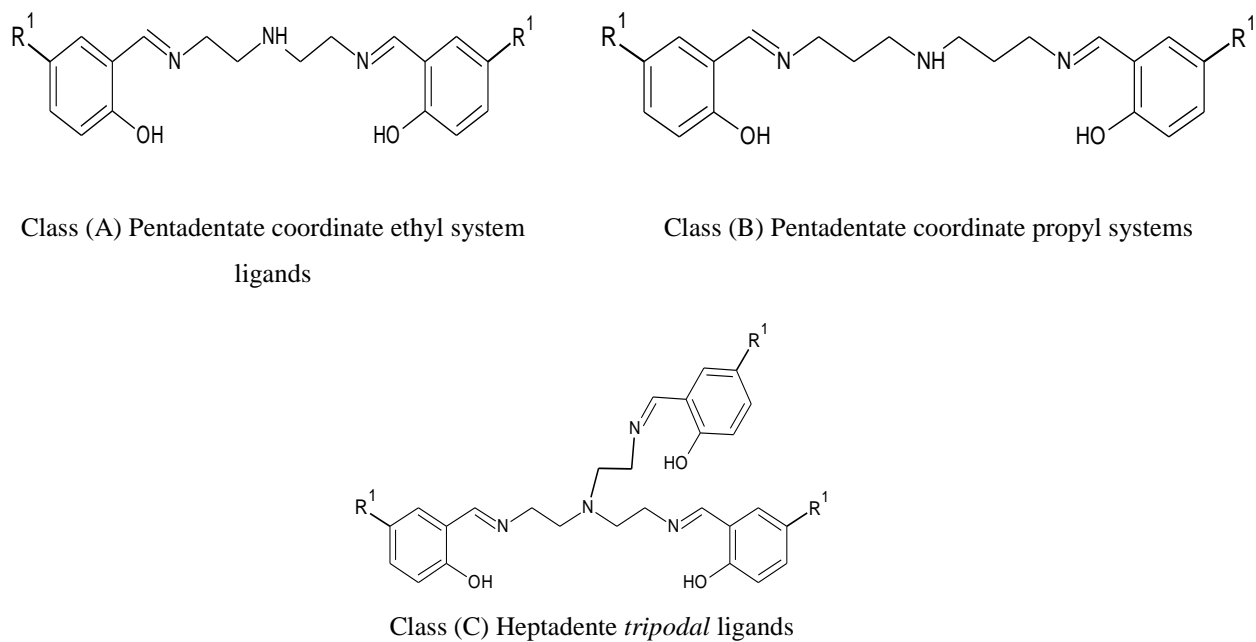


Figure 2. 1 Schematic representation of the N-donor ligands. Class A ligands represent the ethyl N-N-N, class B represents propyl N-N-N and class C represents tripodal N-N-N-N ligand systems.

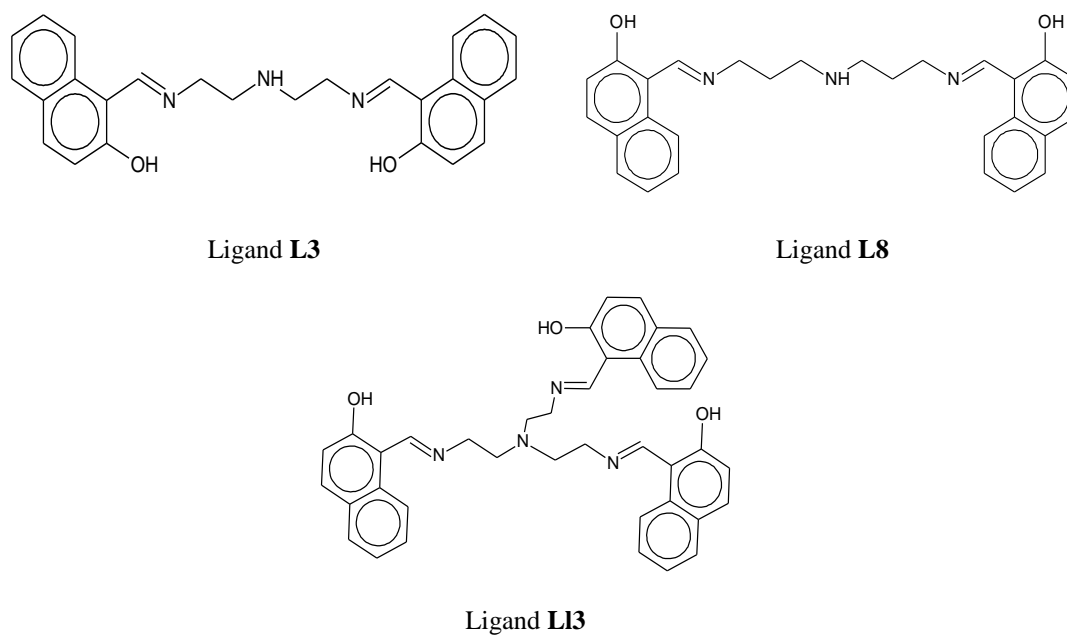


Figure 2. 2 Naphthyl based ligands **L3**, **L8** and **L13**.

Table 2. 1 The N-N-N ligand systems and their labels

Class A pentadentate ethyl	Class B pentadentate propyl	Class C heptadentate <i>tripodal</i>
L1: R <sup>1</sup> =H	L6: R <sup>1</sup> =H	L11: R <sup>1</sup> =H
L2: R <sup>1</sup> =Methoxy	L7: R <sup>1</sup> =Methoxy	L12: R <sup>1</sup> =Methoxy
L4: R <sup>1</sup> = <i>Tert</i> -butyl	L9: R <sup>1</sup> = <i>Tert</i> -butyl	L14: R <sup>1</sup> = <i>Tert</i> butyl
L5: R <sup>1</sup> = <i>Nonyl</i>	L10: R <sup>1</sup> = <i>Nonyl</i>	L15: R <sup>1</sup> = <i>Nonyl</i>

The ligands labelled **L3**, **L8** and **L13** were also synthesized using *naphthylaldehyde* and are shown in Figure 2.2. All the above ligands were therefore synthesized and characterized as described below.

## 2.6 Chemicals and reagents

The following chemicals and reagents were used in the synthesis and characterization procedure and include; 5-methoxy-2-hydroxyphenylaldehyde (5-methoxysalicylaldehyde), 2-hydroxy phenylaldehyde (*salicylaldehyde*) and 2-hydroxy *naphthylaldehyde* which were all purchased from Sigma Aldrich. The 5-*tert* butyl-2-hydroxy phenylaldehyde and 5-nonyl-2-hydroxy phenylaldehyde were synthesized according to method 2.1 from two corresponding alcohols 4-*tert* butyl-phenol and 4-*nonyl*-phenol together with formaldehyde all of which were purchased from Sigma Aldrich. All the aldehydes used are therefore shown in Table 2.2. The magnesium turnings used was purchased from Merck Schuchardt OHG. The toluene solvent, sulfuric acid (H<sub>2</sub>SO<sub>4</sub>) and nitric acid (HNO<sub>3</sub>) were bought from Merck laboratory supplies. All these reagents were used without further purification.

The corresponding three diamines bearing the added N-donor group; N-(2-aminoethyl)ethane-1,2-diamine, N-(3-aminopropyl)propane-1,3-diamine and N,N-bis(2-aminoethyl)ethane-1,2-diamine were bought from Sigma Aldrich and used without further purification. These three diamines are shown in Table 2.2.

The D-chloroform and D<sup>6</sup>DMSO used for NMR studies were bought from Sigma Aldrich. The ethanol solution and methanol solution were bought from B & M Scientific and were used after dry distillation. The cold ethanol was obtained by placing the dried ethanol (in a sealed 250 ml volumetric flask) in an ice bath for 24 hours. All aqueous solutions were prepared using double distilled deionized water from an econoPure16 reverse osmosis system.

Table 2. 1 The aldehydes used

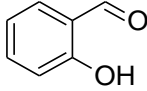
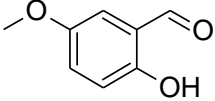
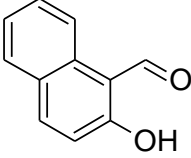
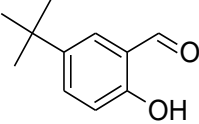
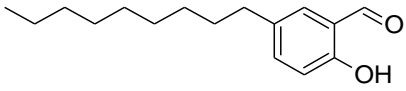
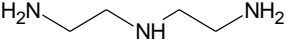
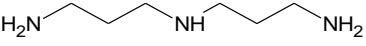
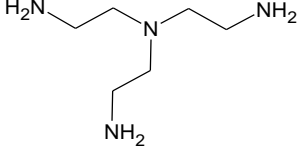
Name	Common name	diagram
2 hydroxy phenylaldehyde	Salicylaldehyde	
5-methoxy-2 hydroxy phenylaldehyde	5-methoxy salicylaldehyde	
2 hydroxy <i>naphthyl</i> aldehyde	2-hydroxy <i>naphthyl</i> -aldehyde	
5- <i>tert</i> butyl-2 hydroxy phenylaldehyde	5- <i>tert</i> butyl salicylaldehyde	
5-nonyl-2 hydroxy phenylaldehyde	5-nonyl salicylaldehyde	

Table 2. 2 The diamines used

Name	Common name	diagram
N-(2-aminoethyl)ethane-1,2-diamine	Diethylenetriamine	
N-(3-aminopropyl)propane-1,3-diamine	bis(3-aminopropyl)amine	
N,N-bis(2-aminoethyl)ethane-1,2-diamine	N,N-bis(2-aminoethyl)ethane-1,2-diamine	

## 2.7 Instrumentation

### 2.7.1 IR spectroscopic analysis

The IR analysis was the first characterization technique to be carried out on the synthesized ligands. There are two main reasons for this; the first general reason was due to the simplicity

of the analytical procedure. A Nicolet Avatar 330 FT-IR instrument with ATR accessory with a ZnSe/Diamond crystal was used. The analysis was carried out in transmission mode with 32 scans at a range between 4000-400  $\text{cm}^{-1}$ .



Figure 2. 3 Avatar IR (ATR) instrument with a ZnSe/Diamond crystal

For the solid samples and the very viscous liquids the freshly prepared samples were transferred using a spatula. For the less viscous liquid samples a disposable glass Pasteur pipette was used to transfer the samples onto the sample head as shown in Figure 2.3. The sample head was closed and the product analysed.

The second and more important reason for use of the IR spectroscopic analysis is due to its ability to detect the formation of the different functional groups due to dipole moments (polarity). The degree of the dipole moments and the ability of the bonds to stretch and vibrate determine the intensity of the spectra. From our work, our starting reagents and the final product have different functional groups with different dipole moments. This analytical technique can therefore be used to confirm the formation of the Schiff base product.

### 2.7.2 Nuclear magnetic resonance analysis

The second spectroscopic method used in characterizing the synthesized product was the  $^1\text{H}$  NMR and the  $^{13}\text{C}$   $\{^1\text{H}\}$  NMR. The spectra of all the ligands were all analysed using the Varian Unity Inova 300 Liquid State NMR Spectrometer, Varian Unity Inova 400 Liquid State NMR Spectrometer and the higher magnitude NMR Varian Unity Inova 600 Liquid State NMR Spectrometer which was used only when necessary to obtain better resolution of the spectra. Approximately 20 mg of the synthesized samples were weighed into an NMR tube and  $\text{CDCl}_3$  or  $\text{D}^6$  DMSO depending on the sample was then added and analysed on the above instruments. The  $^1\text{H}$  nuclei and  $^{13}\text{C}$  give rise to different chemical shifts when in different chemical environments under high magnetic frequency. This shift enables elucidation of the structure of the synthesized products.

### 2.7.3 Mass spectrometry and Microanalysis

The mass spectral analysis and CHN analysis were undertaken to further give evidence of the formation of the products. The mass analysis was therefore carried out on a Waters Synapt G2 High Resolution Mass Spectrometer, with a cone voltage of 15V. The analysis was done on a TOF (Time of flight) positive and negative electrospray ionisation (ESI+) and (ESI-). The ESI probe was injected into a stream of acetonitrile or ethanol and all signals recorded as a mass over charge ( $m/z$ ) ratio with the molecular ion typically observed as a  $(M+H)^+$  ion. These analyses were carried out at the central analytical facility (CAF) of Stellenbosch University. The CHN analysis on the other had was carried out using a Perkin-Elmer CHNS elemental analyser model 2400 at the school of chemistry at the University of KwaZulu-Natal.

### 2.7.4 Melting point determination

For the samples that were obtained as crystalline samples or powder samples these were analysed for melting points on a Stuart Scientific Melting Point apparatus SMP30.

## 2.8 Synthesis and characterization of aldehydes

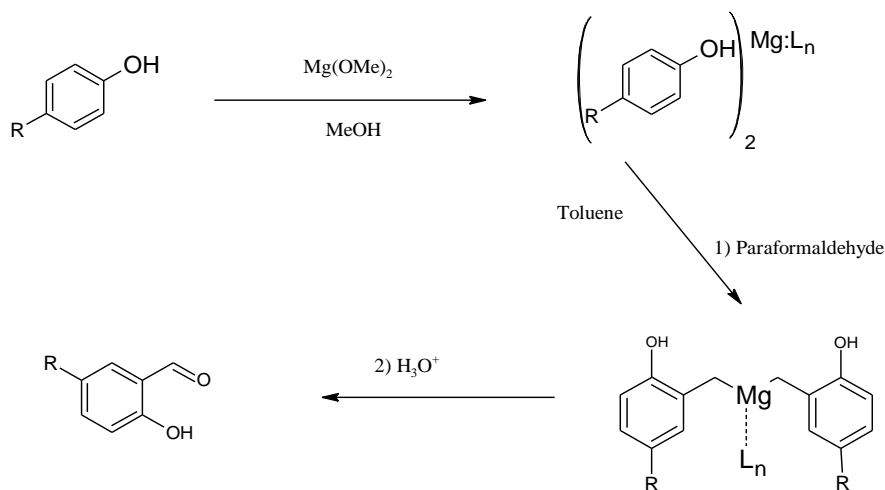
### 2.8.1 Synthesis of the 5-tert butyl salicylaldehyde

The 5-*tert* butyl *salicylaldehyde* and the 5-nonyl *salicylaldehyde* were prepared from modified magnesium-mediated *ortho*-specific formylation of phenols process using a modified literature method by Aldred *et al.* [110]. In this procedure the *para*-substituted phenol is reacted with formaldehyde to obtain *ortho*-substituted aldehyde functionality. This process was therefore carried out as follows.

### 2.8.2 Method 1: Synthesis of 5-tert butyl *salicylaldehyde*

High volumes of this starting product were required therefore 37.56 g (0.2500 moles) of 4-*tert* butylphenol was weighed and added to a solution containing 3.64 g, 0.147 mol of magnesium and 300 ml dry methanol (MeOH) in a two neck 500 ml round bottom flask with a magnetic stirrer bar. The mixture was refluxed until the solution appeared light brown. It was then refluxed for a further 90 minutes to ensure the formation of  $Mg(OMe)_2$  species. Since methanol was used in excess, approximately 200 ml of MeOH was then distilled off after which 200 ml of toluene was then added to the mixture under reflux for 1 hour. The addition of the toluene to the solution forms an azeotropic mixture of toluene and methanol. 200 ml of the azeotropic mixture was then distilled off. The remaining reaction solution forms a white precipitate. At

this stage paraformaldehyde 23.1 g, (0.770 mol) dissolved in 50 ml toluene was then added to the mixture resulting in the formation of a bright yellow colour indicating the formation of the Mg-phenyl aldehyde intermediate as shown by Scheme 2.4.



Scheme 2. 4 Reaction schematic of the synthesis of para-substituted-2-hydroxy benzaldehyde (redrawn courtesy of Aldred *et. al.* [110]).

The magnesium was then removed from this intermediate through the addition of 200 ml of 10 %  $\text{H}_2\text{SO}_4$  in water. The immiscible solution containing the organic toluene layer and the aqueous  $\text{H}_2\text{SO}_4$  layer is then separated and washed with 100 ml deionized water (x2). The final volume containing the organic layer was further reduced by distillation and rotary evaporator to remove the toluene. The final pale yellow viscous solution is removed and further purified using the short tube Kugelrohr apparatus to produce less viscous pale-yellow oil with a yield of 72 %.

The 5-Nonyl salicylaldehyde product was also synthesized through the same procedure with the replacement of 4-*tert* butyl phenol by 4-nonyl phenol. The yield in this case was much greater at 84 %.

### 2.8.3 Results from method 1

From the above reaction the desired product was obtained and analysed by the IR. The desired product was confirmed to contain the presence of the aldehyde as shown by the stacked spectra in Figure 2.4 vibrational band at  $1650\text{ cm}^{-1}$  and  $1652\text{ cm}^{-1}$  while the aliphatic C-H stretching bands were observed by weak bands at  $2866\text{ cm}^{-1}$  and  $2871\text{ cm}^{-1}$  for the 5-*tert* butyl and 5-Nonyl salicylaldehyde derivatives respectively. The medium bands between  $1600\text{-}1500\text{ cm}^{-1}$  were attributed to the C=C stretch of the benzene ring while the phenolic  $\text{C}_\text{Ar}\text{-O}$  stretch was

observed at between 1250-1290  $\text{cm}^{-1}$  as shown by the stacked spectra in Figure 2.4. These *salicylaldehydes* were also analysed with  $^1\text{H}$  NMR and  $^{13}\text{C}$  NMR and all the results are given in the experimental section 2.14.1.

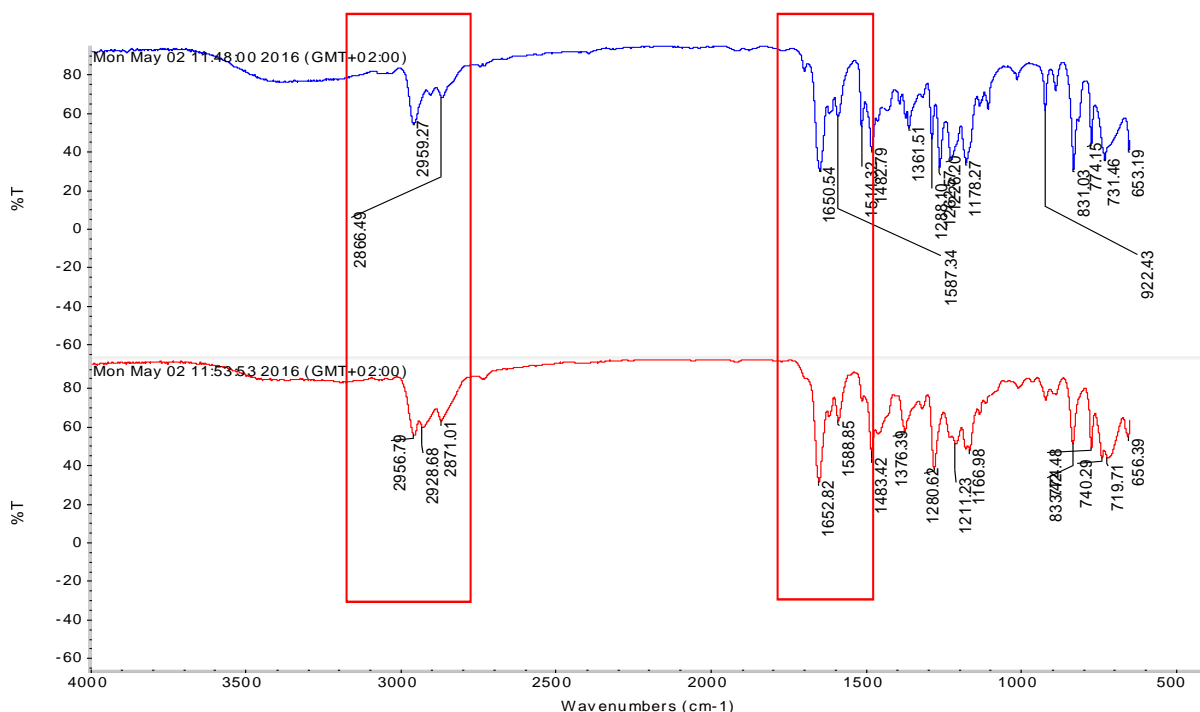
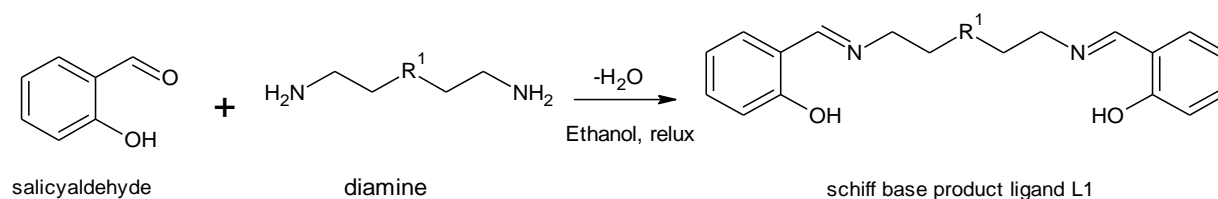


Figure 2. 4 Stacked spectra of IR of 5-tert butyl and 5-Nonyl salicylaldehyde

## 2.9 Synthesis of Schiff base salen type N-donor ligands

### 2.9.1 Method 2: Synthesis of (2, 2'-{iminobis[ethane-2,1-diyl]nitrido(e) methylidene}) diphenol (ligand L1).

This method was used for the synthesis of ligands made from salicylaldehyde, 5-*tert* butylsalicylaldehyde and 5-nonylsalicylaldehyde, ligands **L1**, **L4**, **L5** for class **A** and **L6**, **L9**, **L10** for class **B** ligands. For **L1**, 2.44 g (0.0200 moles) of *salicylaldehyde* was weighed and dissolved in 40 ml ethanol under reflux and 1.03g (0.0100 moles) of *diethylenetriamine* was weighed and immediately dissolved in 20 ml ethanol. This was added slowly to the reaction solution and then allowed to reflux for 24 hours, as shown by Scheme 2.5 below.



Scheme 2. 5 Synthesis of ligand **L1** through condensation reaction with salicylaldehyde

The reflux products were then allowed to cool down and the solvent removed via rotary evaporation. The yellow viscous liquid was then obtained by distilling from a diethyl ether solution and dried using a vacuum pump for 5 hours. The obtained product was kept under vacuum desiccator and then analysed through different analytical techniques.

The characterization data are indicated in the experimental section of the various ligands. The ligands synthesized from the methoxy groups ligand **L2** and **L6** and those containing the *naphthylaldehyde* group ligands **L3** and **L8** were synthesized from the modified methods discussed in section 2.9.1 and 2.9.4 respectively.

### 2.9.1.1 Results and discussion from method 2

From the IR analysis spectra shown in Figure 2.5, the presence of the Schiff base product was confirmed by the formation of the imine peak vibrational bands at  $1627\text{cm}^{-1}$  for ligand **L1**,  $1633\text{cm}^{-1}$  for ligand **L4** and  $1632\text{cm}^{-1}$  for ligand **L5**. The appearance of this peak together with the disappearance of the aldehyde peaks confirmed the presence of the imine product. The observance of peaks between  $2800\text{cm}^{-1}$  and  $2900\text{cm}^{-1}$  was assigned to the C-H stretching frequency as shown in Figure 2.5 for ligand **L1**.

The Figure 2.5 shows the stacked spectra of the starting materials *salicylaldehyde* and the *diethylenetriamine* spacer together with the final Schiff base product **L1**. The above spectrum of ligand **L1** was chosen as a representative ligand since ligands **L2**, **L4** and **L5** are analogues to ligand **L1** bearing different substituents.

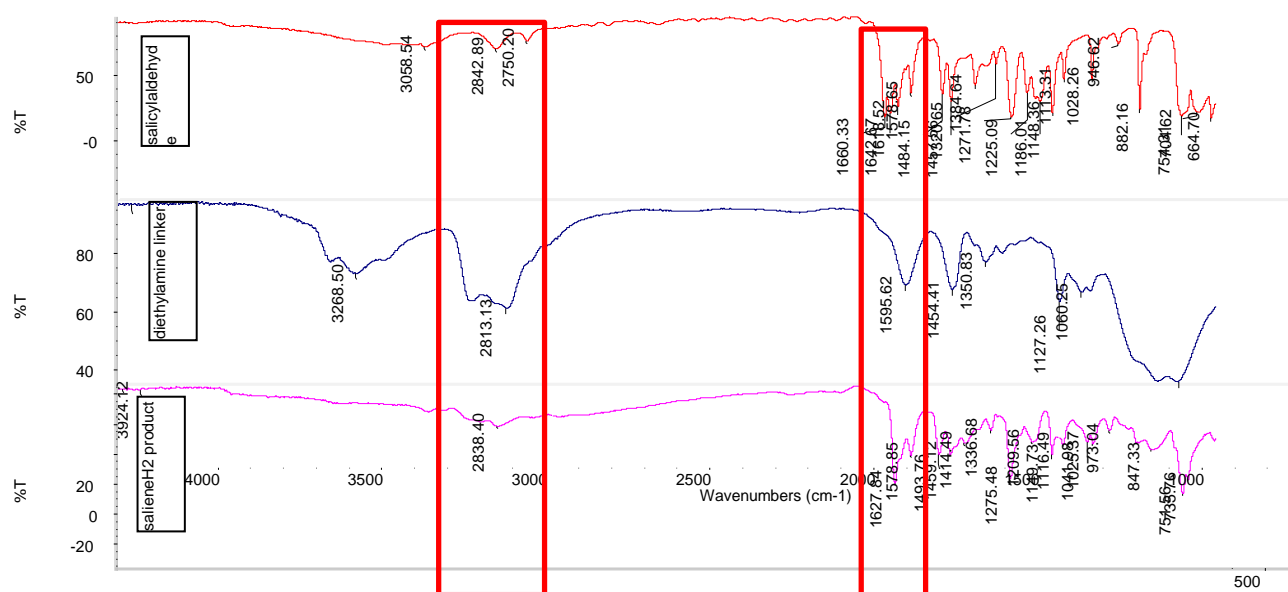


Figure 2. 5 The IR spectra of the unreacted salicylaldehyde, the diamine linker and the ligand **L1**

### 2.9.1.1.1 Discussion of the change of electronic and the steric effect in the synthesis results of method 2

The electronic effect of the different substitutions can therefore be observed as comparable to the change of property of the Schiff base *salicylaldehyde* ligand **L1**. This effect can in principle be followed by monitoring the shift of the imine proton and the phenolic proton on both the IR and the NMR spectra as shown in Figure 2.6. Unfortunately for this work, the phenolic proton was not always discernible in all the spectra obtained. The discussion of the changes of electronic effects due to the various substituents on the phenyl ring will be followed by observing the shift of the imine proton peak for  $^1\text{H}$  NMR and for the  $^{13}\text{C}$   $\{^1\text{H}\}$  NMR.

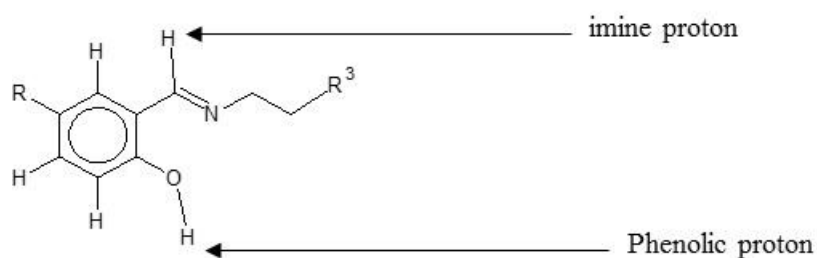


Figure 2. 6 The different functional groups on the salicylaldehyde group

R is H for the unsubstituted group while the R<sup>3</sup> implies the other asymmetric unit of the salen type ligand. The hydroxyl proton and the imine protons are also shown.

### 2.9.1.2 Discussion of the $^1\text{H}$ NMR results from method 1

The  $^1\text{H}$  NMR analyses were obtained for the different ligands as shown by the representation spectrum of ligand **L1** as shown in Figure 2.7.

From the spectrum shown in Figure 2.7, the two signals between 2.99-3.70 ppm were assigned to the spacer hydrogen proton indicated by s C13H, C14H and C10H, C11H. Each of these integrates to four equivalent protons. The proton signals indicated by the peak at 2.99 ppm were assigned to the four hydrogen protons on C11H and C13H while the four hydrogen protons on C10H and C14H were assigned to the peak at 3.70 ppm. The signals between 6.83 ppm and 7.30 ppm were assigned to the aromatic protons of the phenyl group. The signal at 8.34 ppm was assigned to the imine protons, which confirms the presence of the Schiff base products. The very weak broad peak between 13-14 ppm indicates the presence of the hydroxyl protons OH.

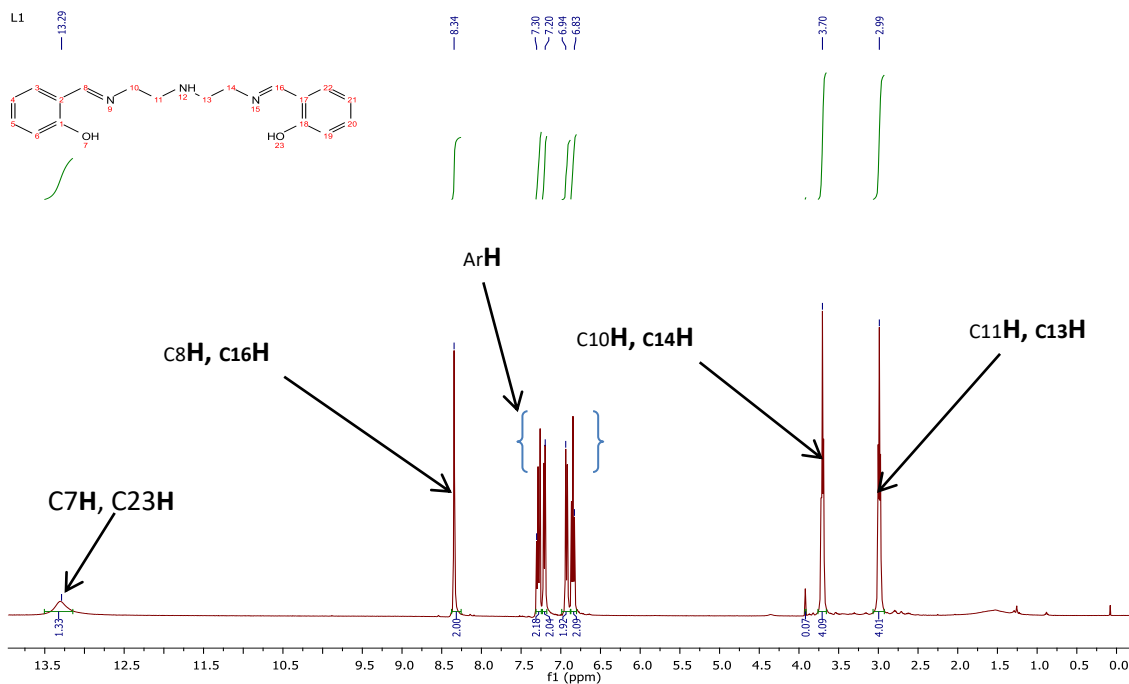


Figure 2.7  $^1\text{H}$  NMR spectrum of ligand L1 in  $\text{CDCl}_3$  with the different protons numbered in relation to the ligand in the insert

It is important to note that the  $\text{NH}_{12}$  proton on the linker is usually very difficult to observe due to the high shielding effect of the N-donor group. The lack of the carbonyl proton peak between 9–11 ppm for the aldehydes and the lack of any extraneous peaks indicates good purity of the product. These products were further analysed by MS and CHN analysis which will be discussed in section 2.11 and 2.12.

### 2.9.1.2.1 The effect of added substituent on the $^1\text{H}$ NMR

The introduction of substituents on the phenyl ring in ligand **L4** and **L5** shows the chemical shifts of the imine proton on the  $^1\text{H}$  NMR obtained when compared to the **L1** ligand. This effect is mainly due to the inductive effect caused by the electron donating group of the *tert*-butyl and *nonyl*-substituent for **L4** and **L5** respectively. Both of these ligands show a downfield shift of the imine signal as compared to ligand **L1** as shown in comprehensive analysis Table 2.4 which will be discussed later. The stacked spectra of the above ligands are shown in Figure 2.8.

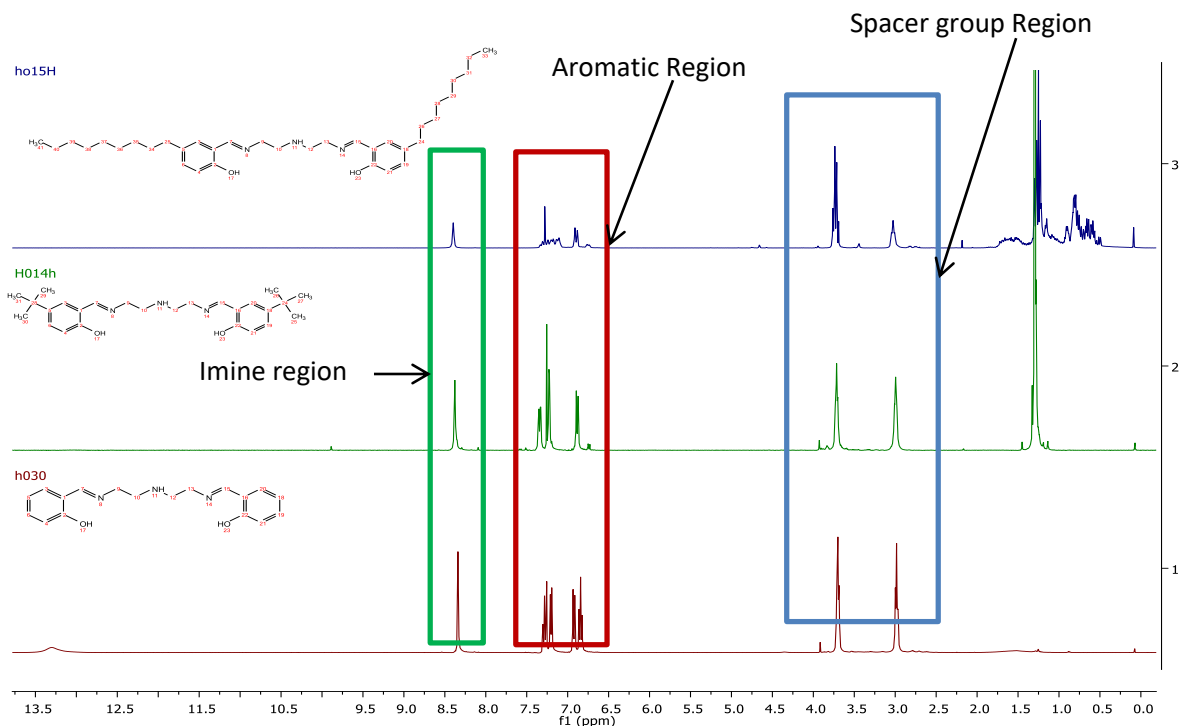


Figure 2. 8  $^1\text{H}$  NMR spectra of ligand L1, L4 and L5 in  $\text{CDCl}_3$ .

### 2.9.1.3 Discussion of the $^{13}\text{C}$ NMR for ligand L1

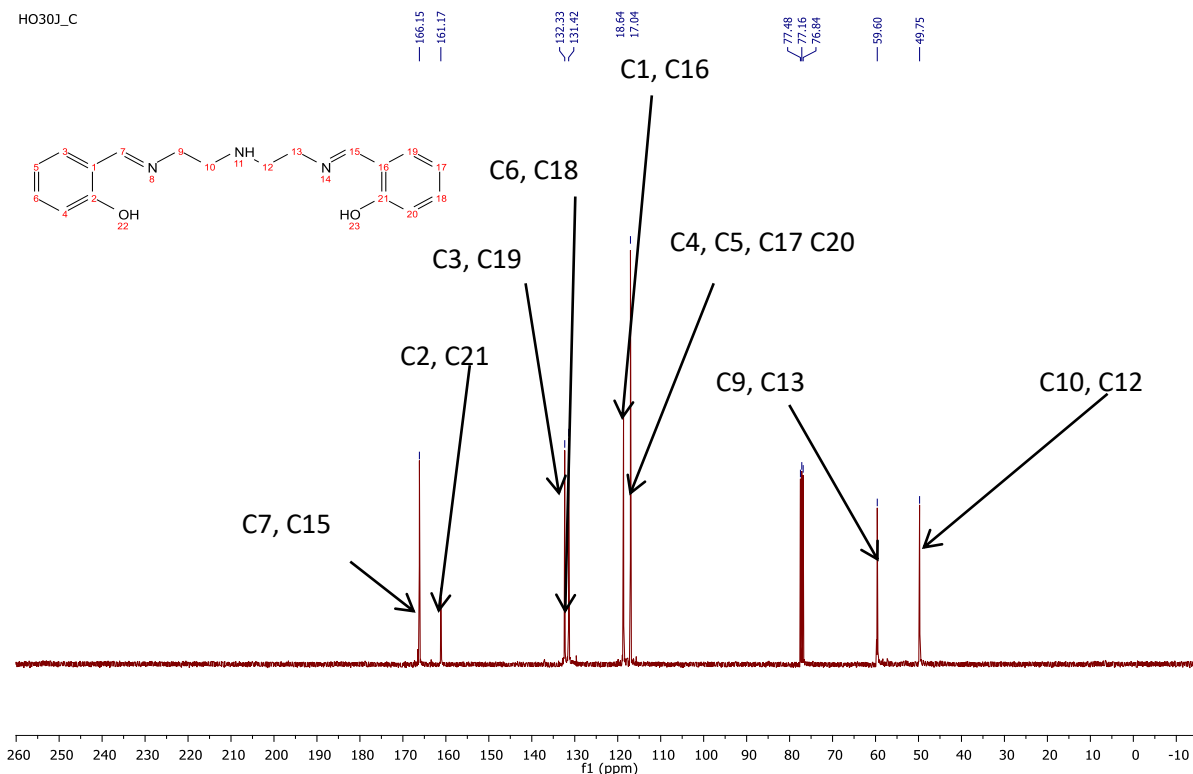


Figure 2. 9  $^{13}\text{C}$   $\{^1\text{H}\}$  NMR spectrum of ligand L1 in  $\text{CDCl}_3$  with the different carbons numbered in relation to the spectrum

The  $^{13}\text{C}$   $\{^1\text{H}\}$  NMR Spectra were also obtained for the different ligands that were synthesized using method 2.9.1.1. The  $^{13}\text{C}$   $\{^1\text{H}\}$  NMR spectrum of ligand **L1** as a representative ligand is shown in Figure 2.9. For these Schiff base ligands, the formation of the imine ( $\text{HC}=\text{N}$ ) bond is indicated by carbon 7 and 15 as shown in Figure 2.9. This peak appears as a strong signal at 166.15 ppm on the spectrum. The signals between 116 ppm to 162 ppm are assigned to the aromatic carbons with C4 and C5 observed to overlap. The amine spacer alkyl group signals appear as two signals at 59.60 ppm and at 49.75 ppm. The lack of any signal above the 190-ppm range which is usually indicative of the presence of the starting aldehyde carbon confirms the synthesis of the product **L1**. The lack of any other signals in this case also indicated the formation of the pure Schiff base product.

## 2.9.2 Synthesis of class B ligands

### 2.9.2.1 Synthesis of ligands L6, L9 and L10

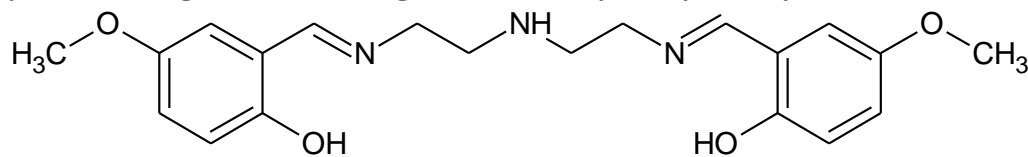
The three ligands **L6**, **L9** and **L10** were synthesized based on method 2 above with the replacement of the *diethylenetriamine* spacer with *bis(3-aminopropyl)amine*. The spectral results and the subsequent characterization results are discussed below.

#### 2.9.2.1.1 Discussion of the electronic effect of class B results

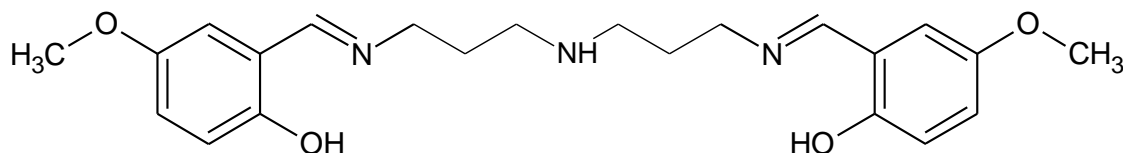
The results obtained for the Class B products were relatively similar to the results of the previously synthesized class A ligands. From the results the change of the spacer from ethyl group to a propyl group had minimal effect in the shift of the imine on the IR,  $^1\text{H}$  NMR and  $^{13}\text{C}$   $\{^1\text{H}\}$  NMR spectra, when compared to the shift that occurred due to the change of the different substituents on the phenolic group.

There is usually a limited inductive effect that is observed with the increase of the number of the alkyl groups between the donor groups. This is due to the higher inductive effect of the donor group. This inductive effect is subsequently referred to as the hidden inductive effect [29]. The comparative results of the shift of the imine on the IR,  $^1\text{H}$  NMR and  $^{13}\text{C}$   $\{^1\text{H}\}$  NMR for all 15 ligands are in Table 2.4 on the summary of electronic studies of the ligand N-donor ligands.

### 2.9.3 Synthesis of ligands containing the 5-methoxy salicylaldehyde



(a) L2



(b) L7

Figure 2. 10 (a) Schematic diagram of Ligand **L2** and (b) Schematic diagram of Ligand **L7**

The synthesis of ligands **L2** and **L7** containing the 5-methoxy *salicylaldehyde* were initially attempted through method 2.9.1 above. However, upon analysis of the obtained product the results showed inconsistent results with various unexpected peaks followed by colour change, this was also the case for ligands **L3** and **L8** discussed in the next section. For the ligands **L2** and **L7**, despite several attempts to obtain the desired product in good yield the product obtained consistently contained the undesired side products. This unpurified products are shown in Figure 2.11. For ligands **L2** the product obtained was initially yellow lumps which when left to dry quickly turned into a dark lump. Ligand **L7** on the other hand eventually formed a dark red viscous liquid as shown by Figure 2.11.



Ligand L2a



Ligand L7a

Figure 2. 11 The black mass formed by unpurified ligand **L2a** and red viscous liquid of **L7a**

From the analysis of the  $^1\text{H}$  NMR results, the formation of the Schiff base product in both cases could be confirmed. This was however also accompanied with other side products of incomplete reactions such as aldehydes and unreacted imine as shown in Figure 2.12 for ligand

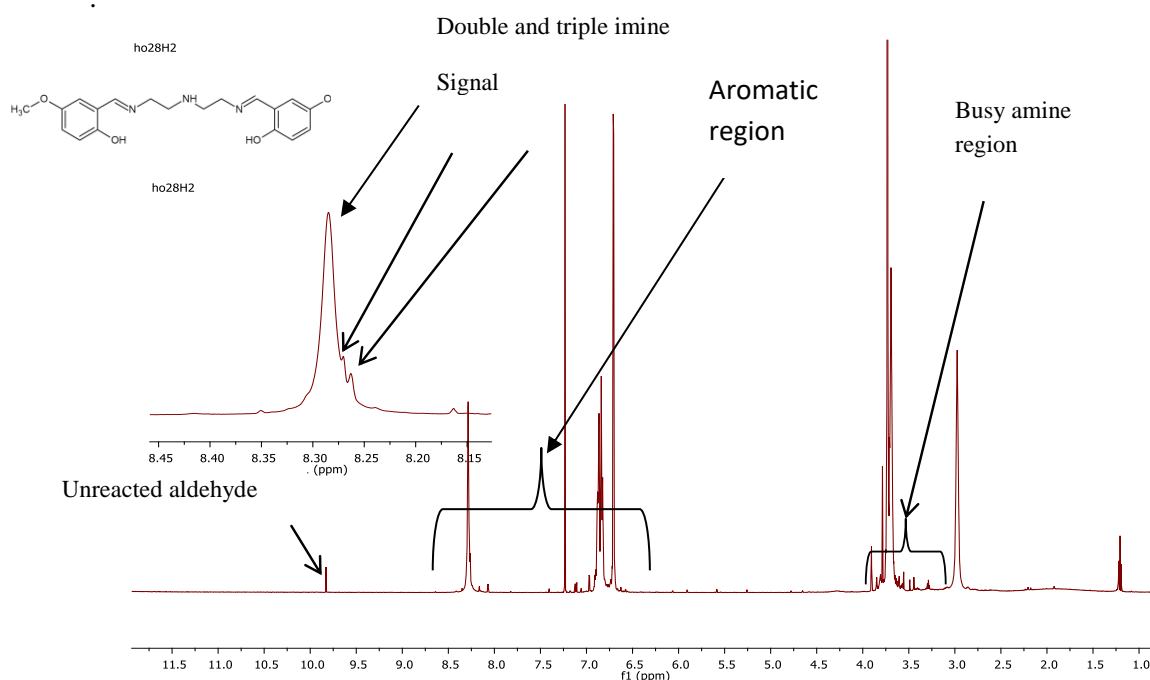


Figure 2. 12 The  $^1\text{H}$  NMR of unpetrified ligand L2a in  $\text{CDCl}_3$

The results show that the imine formed contained a triple signal as shown in Figure 2.12. The effect due to this is explained further in Section 2.9.5 when dealing with tautomerism. The results obtained for the ligand **L7** also contained impurities. While Schiff base condensation reactions tend to not react completely, this reaction however showed unexpected low product yield. This is even after leaving it to reflux for 48 hours and trying to use various techniques to clean the products. Since water is a by-product of this reaction as shown by Scheme 2.1, it can also catalyse the reverse reaction. To separate the water from the products, chloroform was used. The modified synthesis procedure is therefore discussed below.

### 2.9.3.1 Method 3: Synthesis of ligand L2 and L7

This method involved the change of solvent. For ligand **L2** therefore 1.52 g (0.0100 moles) of 4-methoxy salicylaldehyde dissolved in 40 ml of chloroform in a 250 ml round bottom flask 0.543 g (0.00526 moles) of the amine was added to 10 ml of methanol which was then slowly added to the chloroform solution and allowed to reflux for 24 hrs. The reaction solvent was evaporated using a rotary evaporator and the desired yellow oil was obtained, which when left in the desiccator slowly solidifies to a reddish-yellow solid as shown in Figure 2.13. The same method was used for the synthesis of ligand **L7**. The two products were subsequently analysed using the various analytical techniques and the results are shown in section 2.14.2.2 for **L2** and 2.14.3.2 for **L7**.



Ligand L2b



Ligand L7b

Figure 2. 13 The purified **L2** and **L7** products which were analysed in section 2.14.2.2 for **L2** and 2.14.3.2 for **L7**

## 2.9.4 Synthesis of ligands containing the naphthyl aldehyde

### 2.9.4.1 Synthesis of ligands L3

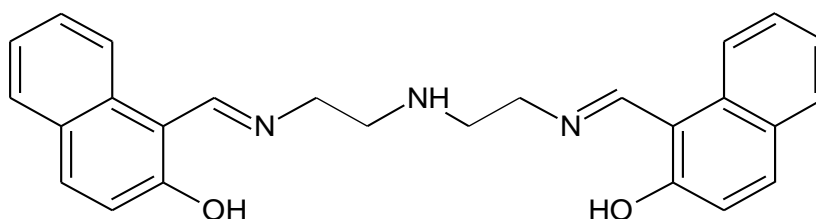


Figure 2. 14 Schematic diagram of ligand **L3**

The initial synthesis of ligand **L3**, using method 2, formed a yellow solution which upon filtration resulted in a red solution and a yellow solid as shown in Figure 2.15. The yellow residue was washed with cold ethanol and products dried. For the filtrate the product was obtained and dried in a vacuum pump and a final dark red product was therefore obtained. The two products were subsequently analysed as follows.



Yellow product



Red filtrate



Two products after drying

Figure 2. 15 The coloured synthesized products from ligand **L3**

The final products were analysed using IR and  $^1\text{H}$  NMR the results showed that the dark red product contained impurities with various other peaks which could not be accounted for. The yellow product was therefore confirmed as the desired product for ligand **L3** and was washed with cold ethanol and characterized through the various analytical techniques in section 2.14.2.3.

### 2.9.5 Synthesis of ligand **L8**

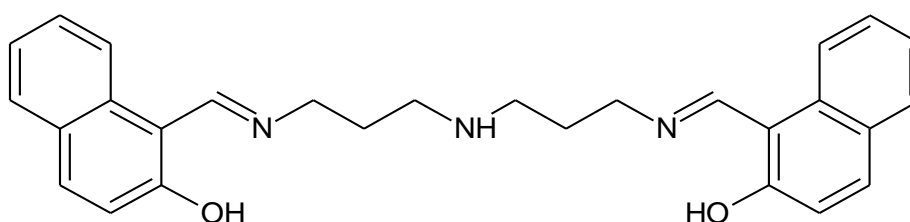


Figure 2. 16 Schematic diagram of ligand **L8**

For ligand **L8**, the initial method for synthesis of **L3** above produced a red solution with the yellow solid at the base. On filtration and washing with cold ethanol, the final product was obtained as an orange product in a yield of 78 % as shown in Figure 2.17.

The analysis of the two products via IR and  $^1\text{H}$  NMR spectroscopy indicated the formation of the desired product. The  $^1\text{H}$  NMR spectrum obtained showed identical signals as shown in Figure 2.18. This ligand is known however none of the literature analysis indicates the formation of these two products. The aim of the synthesis in our case is to use it for the solvent extraction process which is a new approach in its use.

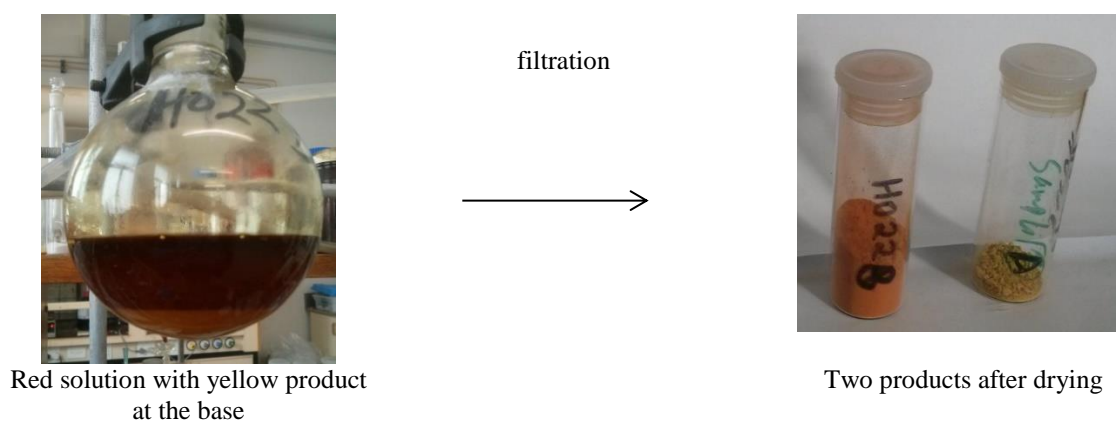


Figure 2. 17 The yellow solid product obtained for L8 a (HO22A) and L8b orange (HO22B).

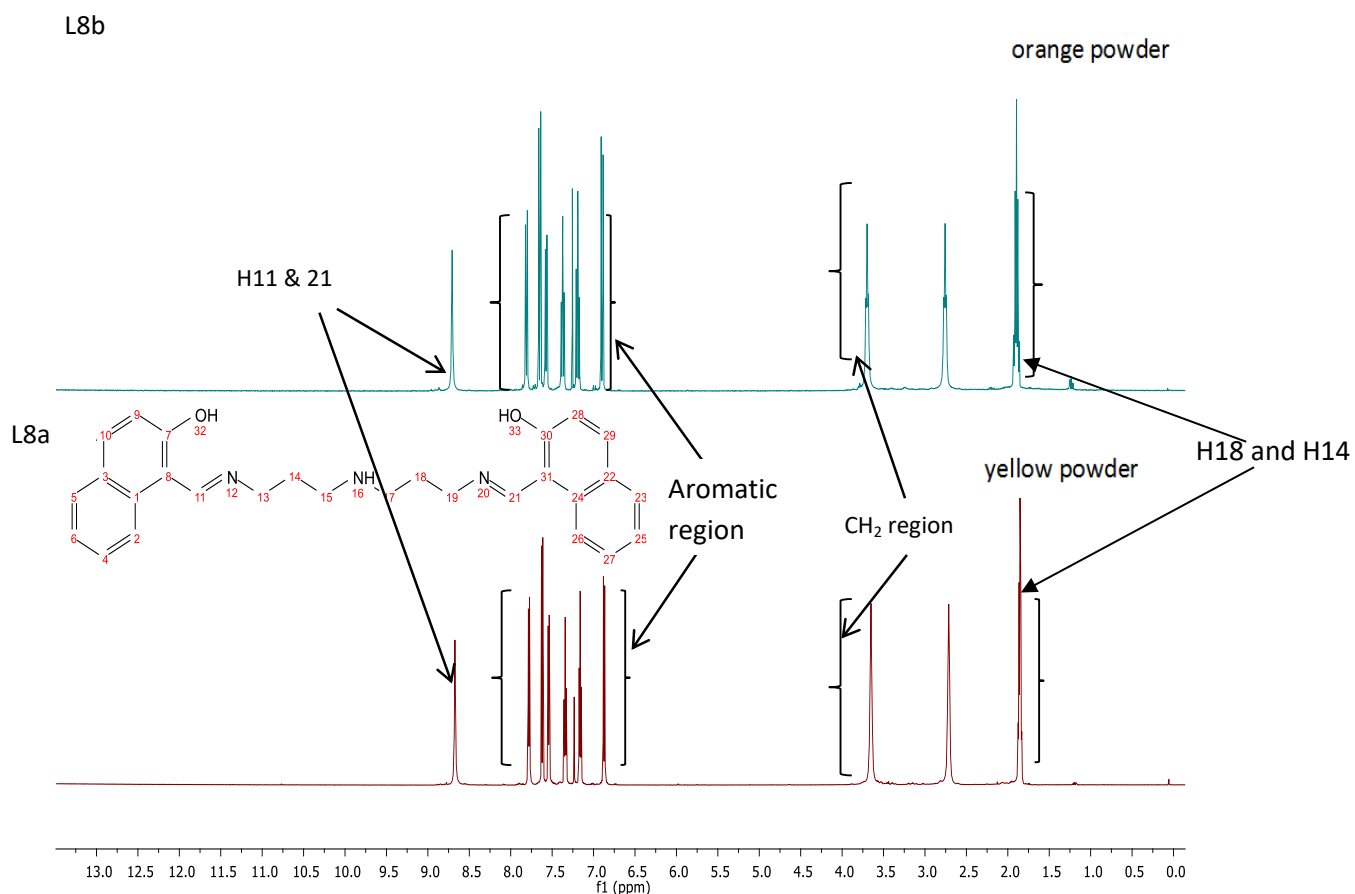


Figure 2. 18 The stacked <sup>1</sup>H NMR spectra of Ligand **L8a** and L8b in CDCl<sub>3</sub> which are shown to look very similar

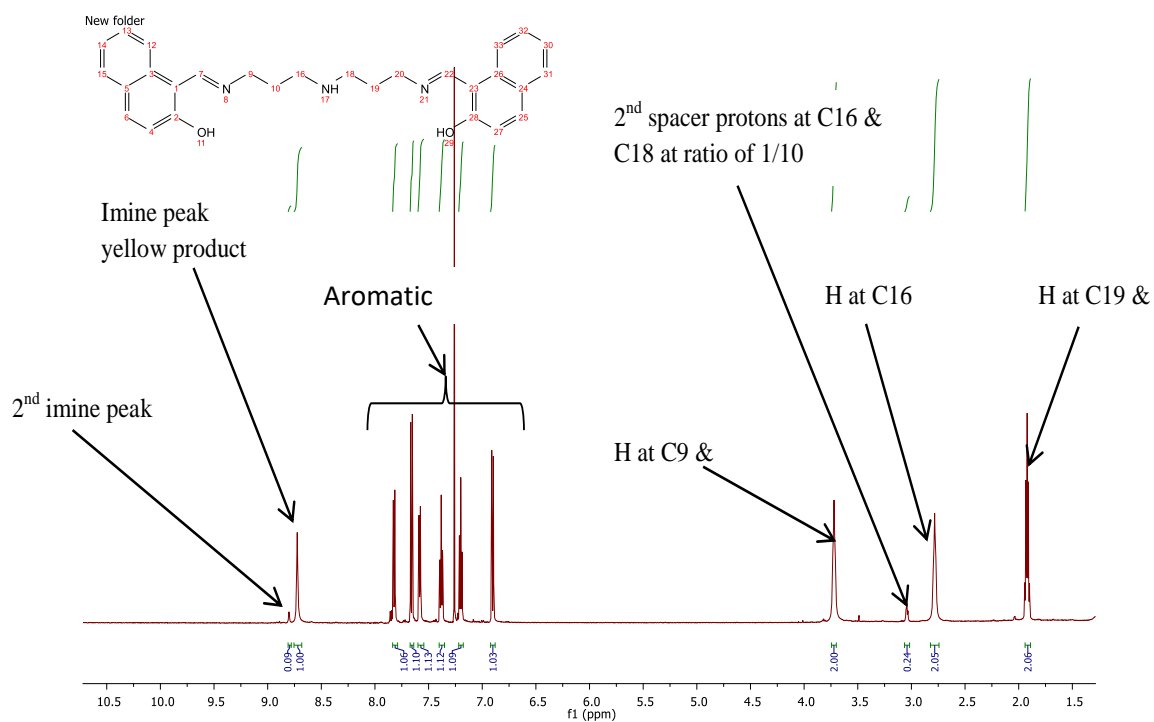
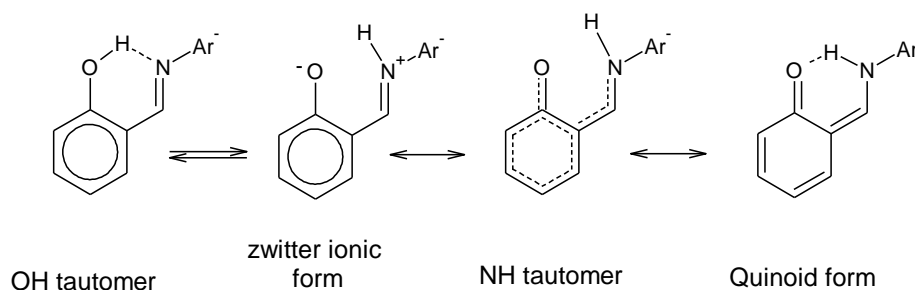


Figure 2. 19 The <sup>1</sup>H NMR of ligand **L8a** and **L8b** mixed together in a 1:10 ratio of orange to yellow product in CDCl<sub>3</sub>

This sample was then analysed by mixture of these two samples at a ratio of 1:10 for the orange to yellow respectively in the same NMR tube. This indicated a slight difference in the spectra shown by a shift of some of the protons as shown in Figure 2.19. This spectrum indicated second and a third peak of imine. The difference in the existence of the two imine signals in Figure 2.19 can be explained by inferring from literature. For example Julija *et al.* [111] characterized an analogous Schiff base ligand showing *tautomerism* of the hydroxyl proton between the imine (NH) and the hydroxyl (OH) group as shown in Scheme 2.6.



Scheme 2. 6 The tautomerism of a salen type ligand redrawn courtesy of Julija *et al.*[111]

From the  $^1\text{H}$  NMR results in Figure 2.18 it was not possible to show if indeed there is *tautomerism* in these ligands. However, the mixed ligands  $^1\text{H}$  NMR in Figure 2.19 can be used to show the existence of very similar compounds having different properties. From this it was therefore hypothesized that there is *tautomerism* of this ligand. If there is existence of this tautomerism between the hydroxyl oxygen proton and the imine, then this should be able to be observed in the  $^{13}\text{C}$   $\{^1\text{H}\}$  NMR. The two products were then analysed by  $^{13}\text{C}$   $\{^1\text{H}\}$  NMR. The results from the  $^{13}\text{C}$   $\{^1\text{H}\}$  NMR in deuterated DMSO were observed to show that sample **L8b** indicated the existence of an extra peak which could be assigned to the carbonyl carbon group as shown in Figure 2.20. This signal was not observed for the yellow sample **L8a**.

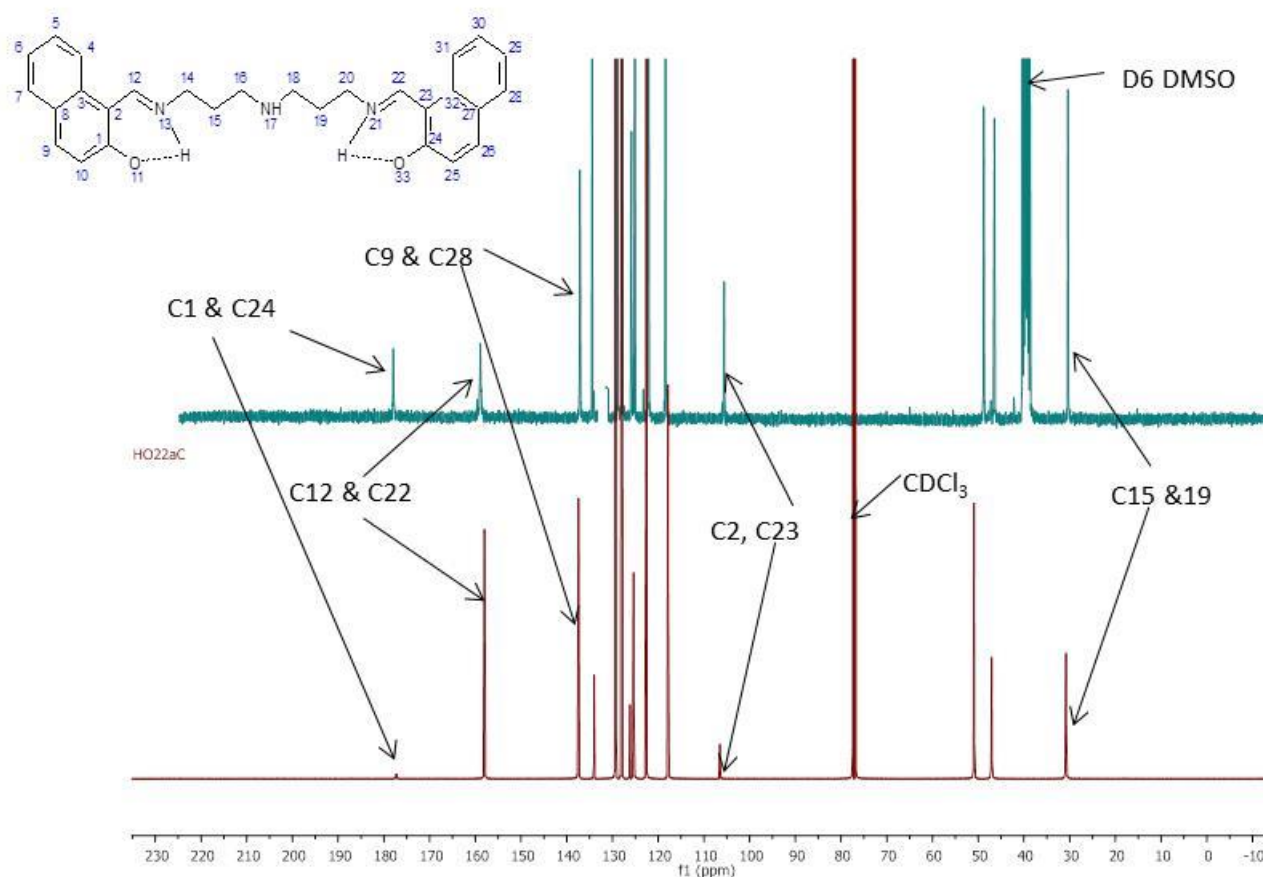
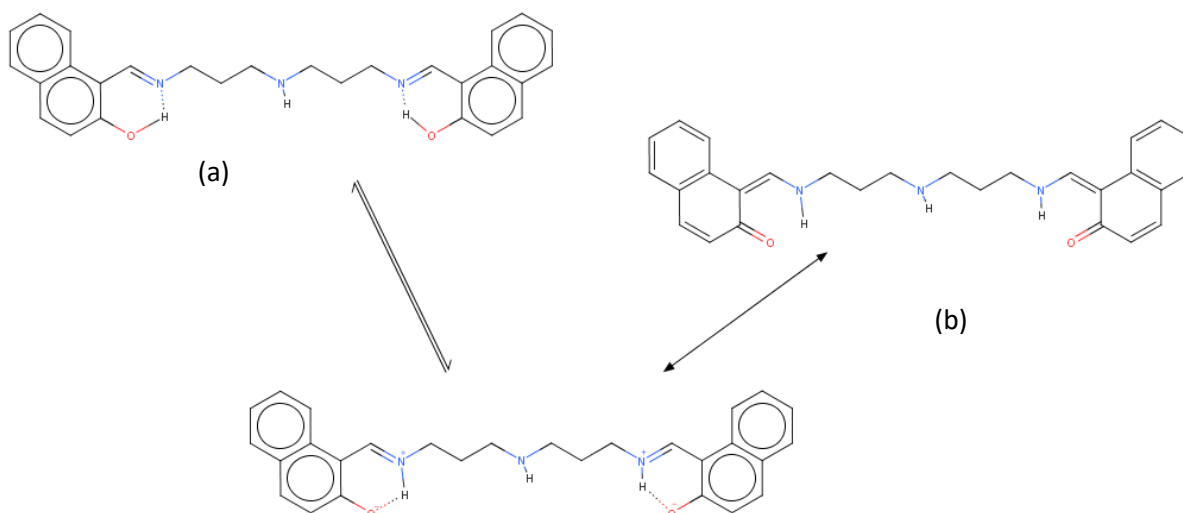


Figure 2. 20 The stacked  $^{13}\text{C} \{^1\text{H}\}$  NMR spectra of Ligand L8b in  $\text{CDCl}_3$  and deuterated DMSO

The above results therefore confirmed the existence of tautomeric behaviour of this ligand. From Figure 2.19 the second imine signal can be attributed to tautomer (b) as shown in Scheme 2.7. Scheme 2.7 gives the possible mechanism for the formation of the two *tautomers*'. This tautomeric effect occurs through the formation of H-bond between the phenolic hydrogen and the imine N-atom first. This later results in complete shift of the H-atom from the phenolic group to the imine as shown in scheme 2.6 and Scheme 2.7 The existence of the carbonyl product (N-H tautomer) is further supported by other literature evidence of Schiff base ligands undergoing this proton shift. For example R.M. Claramunt *et al.*[112], Abdullah *et al.* [113] and Marija Zbacnik *et al.* [114] all indicate the existence of the N-H tautomer. It is important to mention that this was the first time the existence of this *tautomerisim* is reported for these asymmetric salen-type Schiff base ligands.



Scheme 2. 7 Tautomerism of the Schiff base product **L8**, (a) represents the hydroxyl tautomer product (yellow) and (b) represents the tautomer product (orange).

The conclusion from this study therefore indicates that the two products of ligand **L8** contained the two tautomeric products were stable and could be isolated. The yellow product contained the phenolic proton species (a), while the orange product had species (b) as shown by Scheme 2.7. From the cited literature by Julija *et al.* [111], the transition between the tautomer can either be thermochromically initiated or photochromically initiated. The ligand **L8** was therefore resynthesized factoring in the above discussion by using a modified method 4 below.

#### 2.9.5.1 Method 4: Synthesis of ligand **L8**

This method involved the removal of heat and light during synthesis where 2.66 g (0.0149 moles) of *naphthylaldehyde* was dissolved in 50 ml of chloroform in a 250 ml round bottom flask covered by aluminium foil. 1.02 g (0.00775 moles) of the amine in 5 ml of ethanol was then added to this solution slowly and allowed to stir for 48 hrs. Chloroform in this case provided two important objectives. The first advantage as discussed in section 2.9.3 above in separating the product from the water. The second advantage is that it increases the solubility of the *naphthylaldehyde* since the *naphthylaldehyde* has relatively low solubility in cold ethanol. The product obtained in this case was the yellow product in 86 % yield. The product was then characterized, and the results presented in the experimental section 2.14.3.3.

#### 2.9.6 Synthesis of tripodal ligands (Class C)

For the *tripodal* ligand series ligand **L11** with the unsubstituted *salicylaldehyde* group was chosen as the representative ligand to show the method of synthesis. Therefore 3.78 g (0.0310

moles) of the *salicylaldehyde* was weighed and dissolved in 40 ml of chloroform, 1.52 g (0.0104 moles) of *2-N,N-bis(2-aminoethyl)ethane-1,2-diamine* was weighed and immediately dissolved into 10 ml of methanol. The synthesis set up and procedure was similar to the procedure used in method 3 above (section 2.9.3.1). The product ligand **L11** was obtained in 89.4 % yield as a yellow crystalline solid. The obtained results are discussed below.

### 2.9.6.1 Results from tripodal ligand synthesis

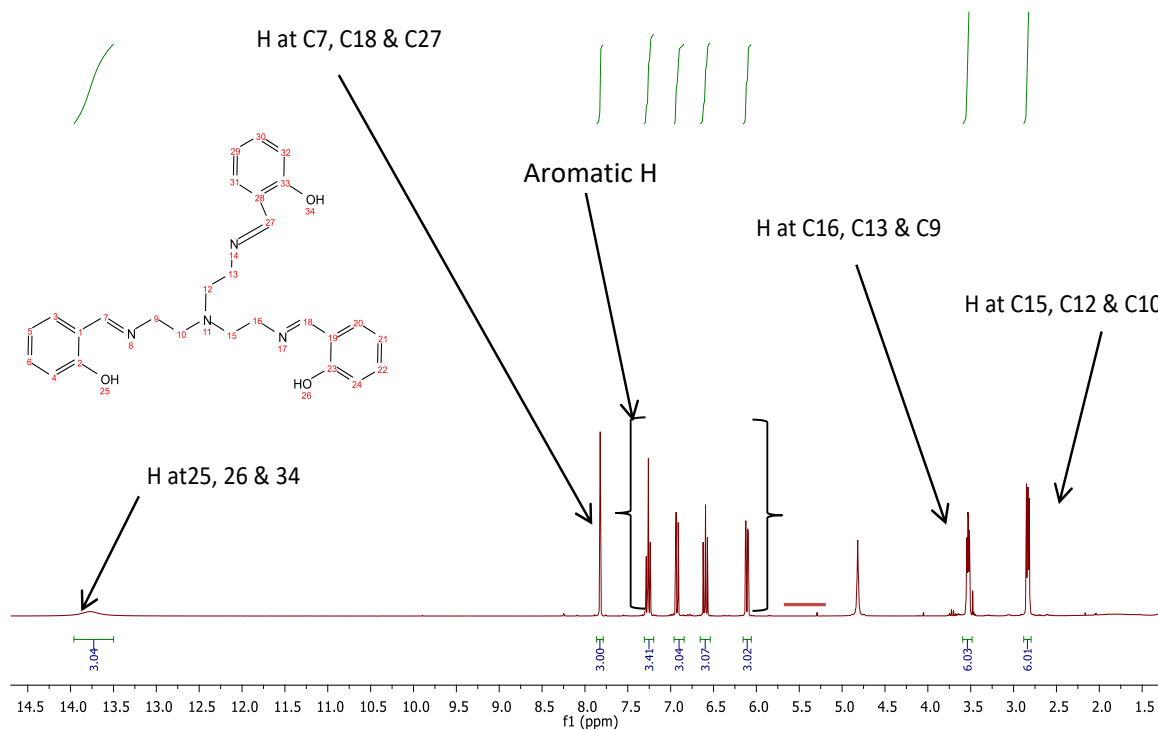


Figure 2. 21 The  $^1\text{H}$  NMR for ligand **L11** in  $\text{CDCl}_3$

The analysis of ligand **L11** on the IR confirmed the presence of the imine peak at  $1630\text{ cm}^{-1}$  while the aliphatic C-H stretches were observed at  $2937\text{ cm}^{-1}$ . The use of the aldehydes with different substituents on the phenolic ring resulted in a shift of the imine peak as was the case in the previous analysis. The NMR results are shown in Figure 2.21 and Figure 2.22 for the  $^1\text{H}$  NMR and  $^{13}\text{C}$   $\{^1\text{H}\}$  NMR respectively.

From these results, the observed signals were as expected and have been labelled as indicated. The spectra showed lack of impurities. The other ligands in the same class showed similar results for the  $^1\text{H}$  NMR and  $^{13}\text{C}$  NMR analysis. All the ligands were fully characterized as shown in section 2.14.4.

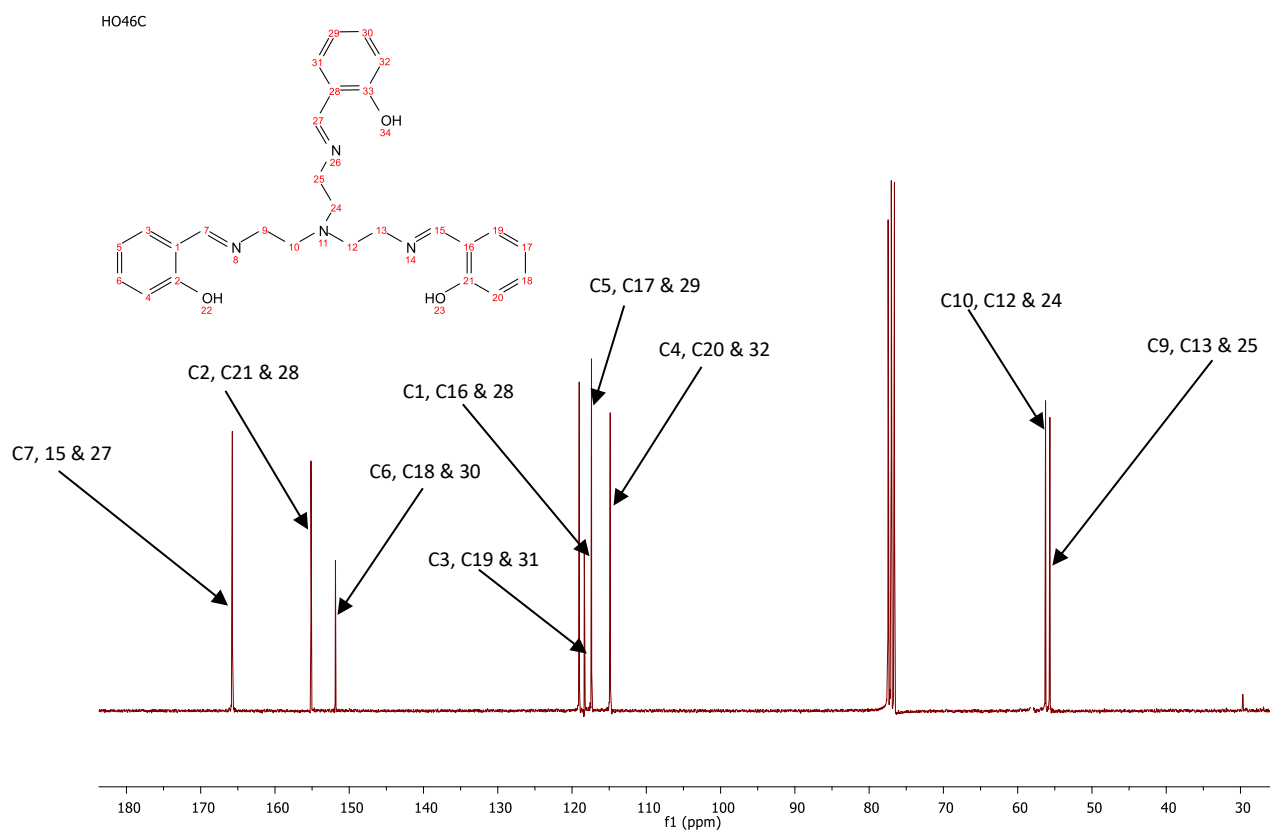
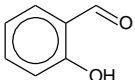
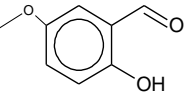
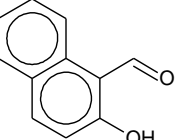
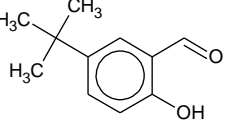
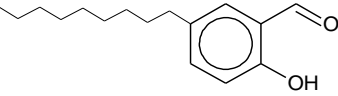


Figure 2. 22 The  $^{13}\text{C}$   $\{^1\text{H}\}$  NMR for ligand **L11** in  $\text{CDCl}_3$ .

## 2.10 Shift of the electronic due to the different ligands

From the analysis of the asymmetric N-donor Schiff base ligands, the shift of the imine was observed to be due to the different substituents and the different alkyl groups. These results are summarised in Table 2.4. The results show that the greatest shift occurs within each class due to the added substituent on the phenolic group. The change of the spacer group was observed to have minimal shifts, as had been discussed in the literature introduction of this chapter.

Table 2. 3 Summary of the IR and NMR spectra of the imine in different Schiff base products synthesized by the different linkers and aldehyde

Substituted Aldehyde	Schiff base product synthesized by using Diethylenetriamine linker			Schiff base product synthesized by using bis(3-aminopropyl)amine Linker			Schiff base product synthesized by using 2- <i>N,N</i> -bis(2-aminoethyl)ethane-1,2-diamine					
	IR cm <sup>-1</sup>	HNMR (in CDCl <sub>3</sub> ) ppm	<sup>13</sup> C{ <sup>1</sup> H}NMR (in CDCl <sub>3</sub> ) Ppm	IR cm <sup>-1</sup>	HNMR (in CDCl <sub>3</sub> ) ppm	<sup>13</sup> C{ <sup>1</sup> H}NMR (in CDCl <sub>3</sub> ) ppm	IR cm <sup>-1</sup>	HNMR (in CDCl <sub>3</sub> ) ppm	<sup>13</sup> C{ <sup>1</sup> H}NMR (in CDCl <sub>3</sub> ) ppm			
	<b>L1</b>	1627	8.34	166.15	<b>L6</b>	1628	8.33	165.04	<b>L11</b>	1630	7.82	166.27
	<b>L2</b>	1631	8.31	165.90	<b>L7</b>	1634	8.27	165.15	<b>L12</b>	1633	7.91	165.88
	<b>L3</b>	1610	8.79	178.51	<b>L8</b>	1614	8.76	176.14	<b>L13</b>	1620	8.72	158.93
	<b>L4</b>	1633	8.37	166.58	<b>L9</b>	1635	8.33	165.88	<b>L14</b>	1631	8.35	166.34
	<b>L5</b>	1632	8.35	165.67	<b>L10</b>	1634	8.32	165.58	<b>L15</b>	1631	8.35	166.46

## 2.11 Mass spectrometry

### 2.11.1 Discussion of Class A ligands

For purposes of this discussion, the spectrum of ligand **L5** is used to show the fragmentation pattern in this class of ligands. The Schiff base product **L5** was chosen as a representative ligand for class A due to its high molecular weight. The mass spectra showed that there are 2 main ionizable fragments as shown in Figure 2.23.

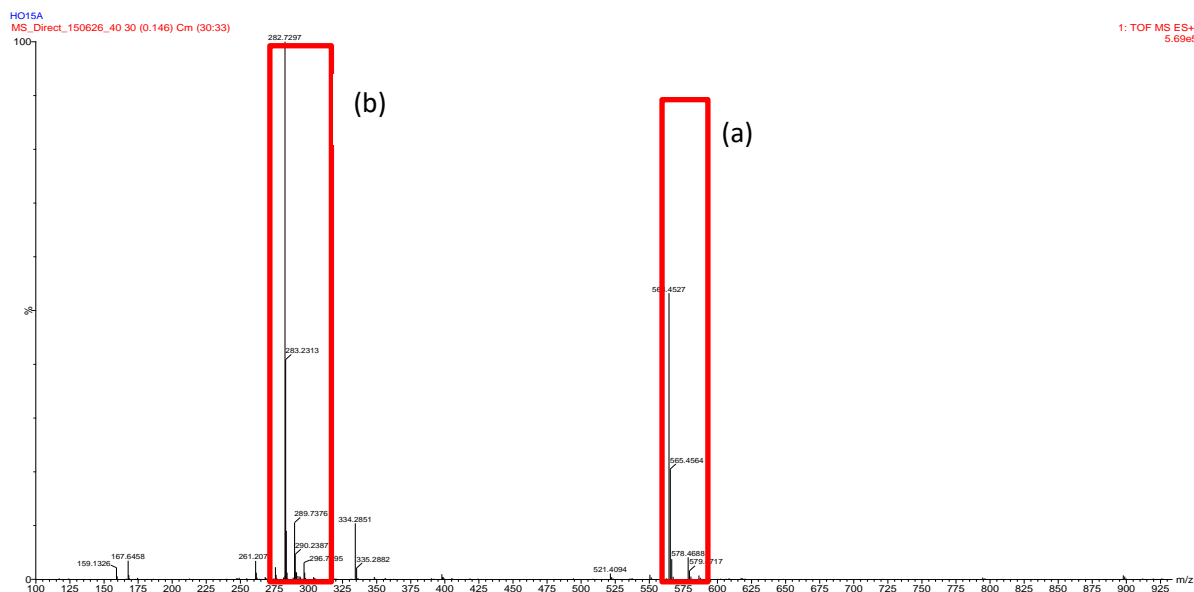


Figure 2. 23 MS Spectrum of ligand **L5** with x- axis showing the m/z value and the y-axis showing the % abundance of the different fragments. (a) and (b) indicate the two ionizable masses formed.

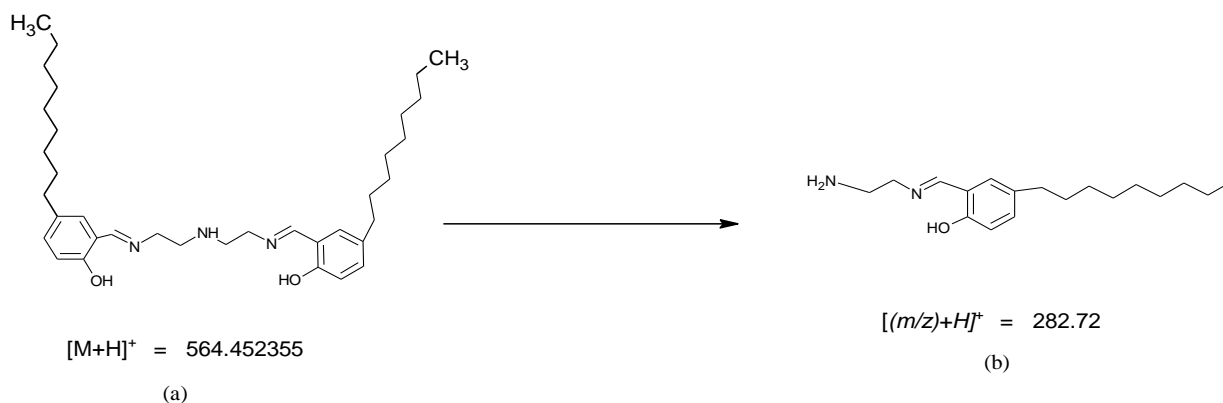


Figure 2. 24 Proposed fragmentation pattern of ligand **L5**, (b) indicates the fragmented species while (a) represents the ionisable mass species  $M+H$  of the ligand ( $M=563.86\text{g/mol}$ ).

### 2.11.1.1 Discussion of spectrum and the effect of added substituent on % abundanc.

The proposed fragmentation of **L5** Figure 2.24 shows that the m/z value with two fragments. Fragment (b) was proposed to represent the base peak at 100 % abundance, this is the specie  $[(M/2) + H]^+$ . Species (a) on the other hand is proposed to represent the ionizable mass species  $[M+H]$  ions at 50 % relative abundance. The nature of fragmentation of the other ligands did not differ greatly from this one proposed in Figure 2.24. However, the obtained spectra from the other ligands in this class showed only slight variance in which specie was formed in abundance. For ligand **L4**, this had the species (a) and (b) but the base peak in this case was the species (a)  $[M+H]$  at 100 % relative abundance while the species (b)  $[(M/2) + H]$  was at 25 % relative abundance. For ligands **L3-L1** these only showed the fragmented species (a) at 100 % relative abundance. This indicates that for these ligands only the ionisable  $[M+H]$  species is observed for each ligand. The general trend observed in these results showed that the addition of bulky alkyl substituents on the phenolic ring has the effect of increasing the bulkiness of the Schiff base product and this leads to stabilization of the ionisable species (b). The use of the less bulky ligands **L1**, **L2** and **L3** does not form the ionizable fragment (b). This trend in the distribution of mass spectra was also observed for the class B ligands.

### 2.11.1.2 The effect of added alkyl groups on the % abundance

As indicated above, the MS obtained for class A and class B ligands had the same distribution of the % abundant species, however for the class C ligands containing the *tripodal* ligand systems this was observed to contain other fragments as shown by Figure 2.25 for ligand **L15**.

The MS spectra obtained for the *tripodal* ligand **L15** as illustrated in Figure 2.25 showed that the ligand has four ionisable fragments. These are proposed to contain different species as discussed. The specie (c) is proposed to be the base peak at 100 % relative abundance representing  $[M-C_{27}H_{42}N_2O_{1.5}]^+$  or the  $[(M/2) + H]^+$  species. Species (a) would represents the ionizable mass fragment at 25 % relative abundance. The fragmented species (b) represents the ionisable  $[M-F^1]^+$  species. Where the specie F is shown by Figure 2.26. The species (d) represents the species  $[M-C_{36}H_{39}N_3]^+$  or  $[(M-F^1)/2]$  at 60 % abundance. It is important to remember that all these species are only present in the ionisable environment and are not products of the synthesis.

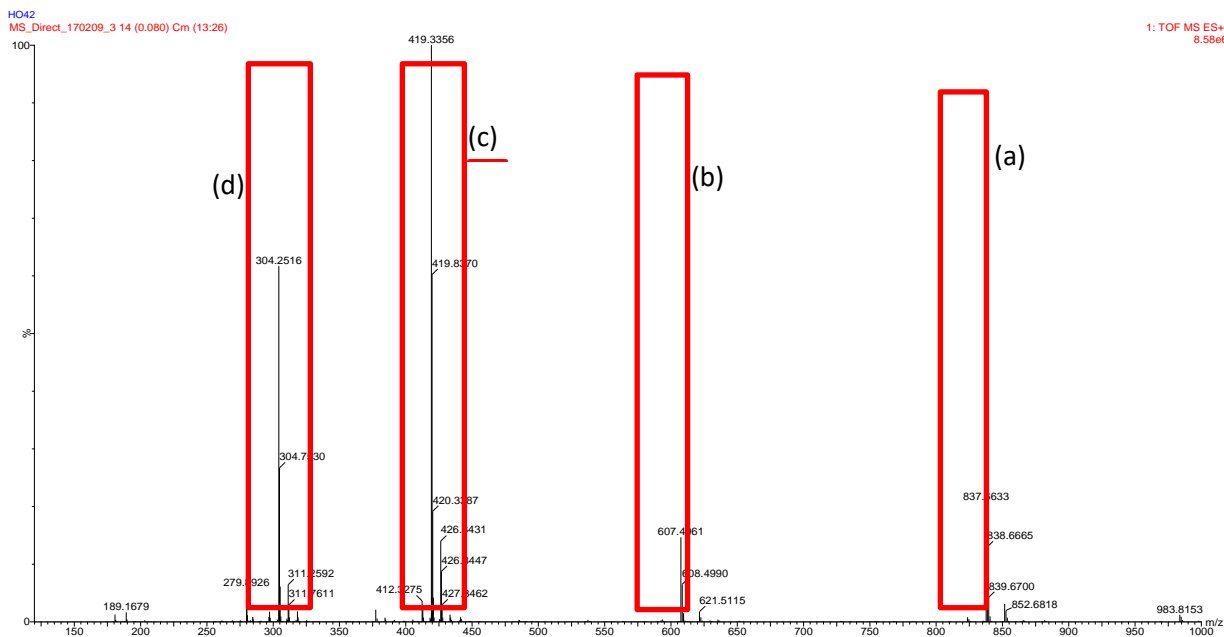


Figure 2. 25 MS Spectrum of ligand **L15** with x-axis showing the m/z value and the y-axis showing the % abundance of the different fragments.

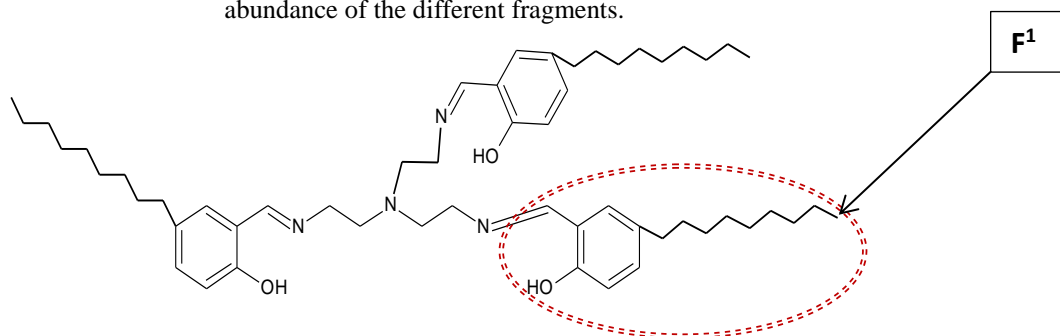


Figure 2. 26 Ligand **L15** with the area under the circle labelled **F1** for the MS analysis

## 2.12 Elemental analysis

All the ligands analysed were subsequently analysed and confirmed to contain the Schiff base product in high purity through the CHN analysis. It is also important to note that ligands **L2**, **L8**, **L12** and **L14** could not be dried completely so they contained some reaction solvents such as methanol and ethanol. This was also the case for the crystals obtained for the class C ligands. The results from CHN analysis are therefore summarized in Table 2.5 below.

Table 2. 4 Comprehensive CHN analysis table for all the ligands

	FORMULA	%CALCULATED			%OBTAINED		
		C	H	N	C	H	N
L1	C <sub>18</sub> H <sub>21</sub> N <sub>3</sub> O <sub>2</sub>	69.43	6.80	13.49	69.27	6.62	13.48
L2	C <sub>20</sub> H <sub>25</sub> N <sub>3</sub> O <sub>4</sub> (H <sub>2</sub> O)	61.68	6.94	10.79	61.82	6.59	10.11
L3	C <sub>26</sub> H <sub>25</sub> N <sub>3</sub> O <sub>2</sub>	75.89	6.12	10.21	75.07	6.32	10.06
L4	C <sub>26</sub> H <sub>37</sub> N <sub>3</sub> O <sub>2</sub>	73.72	8.80	9.92	73.91	8.44	9.80
L5	C <sub>36</sub> H <sub>57</sub> N <sub>3</sub> O <sub>2</sub>	76.68	10.19	7.45	76.14	10.08	7.62
L6	C <sub>20</sub> H <sub>25</sub> N <sub>3</sub> O <sub>2</sub>	70.77	7.42	12.38	70.29	7.26	12.38
L7	C <sub>22</sub> H <sub>29</sub> N <sub>3</sub> O <sub>4</sub>	66.14	7.32	10.52	66.17	7.03	10.13
L8	C <sub>28</sub> H <sub>29</sub> N <sub>3</sub> O <sub>2</sub> (C <sub>2</sub> H <sub>5</sub> OH)	74.20	6.65	8.65	74.07	6.14	9.07
L9	C <sub>28</sub> H <sub>41</sub> N <sub>3</sub> O <sub>2</sub>	74.46	9.15	9.30	74.23	9.11	9.42
L10	C <sub>38</sub> H <sub>61</sub> N <sub>3</sub> O <sub>2</sub>	77.11	10.39	7.10	77.89	10.34	7.95
L11	C <sub>27</sub> H <sub>30</sub> N <sub>4</sub> O <sub>2</sub>	70.72	6.59	12.22	70.86	6.61	11.70
L12	C <sub>30</sub> H <sub>36</sub> N <sub>4</sub> O <sub>6</sub> (C <sub>2</sub> H <sub>5</sub> OH)	64.63	7.12	9.42	64.79	6.57	9.85
L13	C <sub>39</sub> H <sub>36</sub> N <sub>4</sub> O <sub>3</sub> .2H <sub>2</sub> O	73.68	6.18	8.81	73.77	6.38	9.23
L14	C <sub>39</sub> H <sub>54</sub> N <sub>4</sub> O <sub>3</sub> (C <sub>2</sub> H <sub>5</sub> OH)	73.18	8.99	8.33	73.29	8.51	8.33
L15	C <sub>54</sub> H <sub>84</sub> N <sub>4</sub> O <sub>3</sub>	77.46	10.11	6.69	77.43	10.09	6.07

### 2.13 Summary and Conclusion

Fifteen different multidentate Schiff base ligands were synthesized containing the N-donor groups. They were comprehensively analyzed through different analytical techniques. The ligands **L1**, **L4**, **L5**, **L6**, **L9** and **L10** were all synthesized with the Schiff base condensation method 2, while ligands bearing the methoxy substituent **L2** and **L7** were synthesized using a modified method 3. Ligand with *naphthylaldehyde* **L3** with the ethyl spacer was also synthesized using method 3 while that containing the *naphthylaldehyde* with propyl spacer group **L8** was synthesized using method 4 and the products obtained were confirmed to undergo tautomerism.

The synthesized ligands were further studied for the electronic and steric effects due to the addition of the different substituents on the phenyl ring and the effect of adding the alkyl group between the donor groups. The results indicated that the addition of the substituent on the phenyl group had a much greater effect on the shift of the imine on both the IR analysis and the NMR analysis. The effect of adding the alkyl groups between the donor atoms was on the

other hand observed to have minimal shift of the imine. The heptadentate *tripodal* ligands showed a much greater shift of the imine due to the increased number of donor group and the increased bulkiness of these ligands.

All these ligands are evaluated in solvent extraction studies and will be discussed in Chapters 5 and 6.

## 2.14. Characterization

### 2.14.1 Characterization of p-substituted salicylaldehyde

#### 2.14.1.1 Characterization of the 5-tert butyl aldehyde

A pale yellow oil, yield 72 %,  $^1\text{H}$  NMR (400MHz,  $\text{CDCl}_3$ )  $\delta$  ppm 11.05 (1 H, s, OH); 9,95 (1H, s, CHO), 7.50 – 7.58 (2H, dd,  $J$  2.49 Hz, ArH), 6.9 - 6.95 (1H, d,  $J$  2.28 Hz, ArH), 0.8 -1.3 (9H, s,  $\text{C}(\text{CH}_3)_3$ ):  $^{13}\text{C}$   $\{^1\text{H}\}$  NMR. (400 MHz,  $\text{CDCl}_3$ )  $\delta$  C ppm ;192.40 ( $\text{C}_{\text{Ar}}\text{CHO}$ ), 162.40 ( $\text{C}_{\text{Ar}}\text{OH}$ ), 142.94 ( $\text{C}_{\text{Ar}}\text{C}(\text{CH}_3)_3$ ), 134.21 ( $\text{C}_{\text{Ar}}\text{H}$ ), 123.30 ( $\text{C}_{\text{Ar}}\text{H}$ ), 118.13 ( $\text{C}_{\text{Ar}}\text{H}$ ), 34.60 ( $\text{C}(\text{CH}_3)_3$ ), 31.08 ( $\text{C}(\text{CH}_3)_3$ ), IR (neat); 2952(m, C-H), 2863 (m, C-H); 1653 (s, C=O); 1588 (s, C=C); 1490 (m, C-H).

#### 2.14.1.2 Characterization of the 5-nonyl aldehyde

A pale greenish yellow oil, yield 84 %  $^1\text{H}$  NMR (300 MHz,  $\text{CDCl}_3$ )  $\delta$  H ppm 10.88 (1 H, s, OH), 9.89 (1 H, s, CHO), 7.46 (1 H, s, ArH), 6.94-6.92 (2 H, s, ArH), 1.31-0.58 (18 H, s).  $^{13}\text{C}$   $\{^1\text{H}\}$  NMR. (300 MHz,  $\text{CDCl}_3$ )  $\delta$  C ppm; 197.03 (CHO), 159.43 ( $\text{C}_{\text{Ar}}\text{H}$ ), 135.41 ( $\text{C}_{\text{Ar}}\text{H}$ ), 117.11 ( $\text{C}_{\text{Ar}}\text{H}$ ), 30.14 ( $\text{C}_9\text{H}_{19}$ ). IR (neat); 2956 (m, C-H), 2863 (m, CH); 1652 (s, C=O); 1588 (m, C=C); 1483 (s, C-H).

### 2.14.2 Synthesis and characterization class A ligands

#### 2.14.2.1 Characterization of (2, 2'-{iminobis[ethane-2,1-diyl]nitro(E) methylidene} diphenol) (Ligand L1)

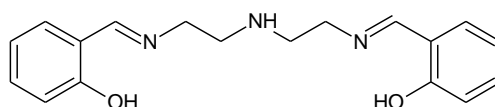


Figure 2. 27 Schematic diagram of ligand L1

A 2.44g (0.0200 moles) of *salicylaldehyde* and 1.03g (0.0100 moles) of *diethylenetriamine* was used. Reddish yellow oil that slowly solidified into a red mass was obtained. Yield obtained was 83 %. For  $\text{C}_{18}\text{H}_{21}\text{N}_3\text{O}_2$ : EA calculated (%) C (69.43), H (6.80), N (13.49) % EA Found (%); C (69.27), H (6.62), N (13.48).  $^1\text{H}$  NMR (400 MHz,  $\text{CDCl}_3$ )  $\delta$  H ppm; 8.34 (2 H, s, NCH),

7.28 (2 H, dd,  $J$  13.1 Hz, 4.8 Hz, ArH), 7.21 (2 H, dd,  $J$  7.6 Hz, 1.1, ArH), 6.93 (2 H, d,  $J$  8.3 Hz, ArH), 6.85 (2 H, t,  $J$  7.4 Hz, ArH), 3.70 (4 H, t,  $J$  5.8 Hz, (NCH<sub>2</sub>CH<sub>2</sub>)), 2.99 (4 H, t,  $J$  5.9 Hz, (NCH<sub>2</sub>CH<sub>2</sub>)). <sup>13</sup>C {<sup>1</sup>H} NMR. (101 MHz, CDCl<sub>3</sub>) δ<sub>c</sub> ppm 166.15 (NCH), 161.17 (C<sub>Ar</sub>OH), 132.33 (C<sub>Ar</sub>H), 131.42 (C<sub>Ar</sub>H), 118.64 (C<sub>Ar</sub>H), 117.04 (C<sub>Ar</sub>CN), 59.60 (NCH<sub>2</sub>CH<sub>2</sub>), 49.75 (NCH<sub>2</sub>CH<sub>2</sub>). IR (ATR, neat, cm<sup>-1</sup>); 2923(m, C-H), 2845 (m, C-H); 1628 (s, C=N); 1494 (m, C-H); 1276cm<sup>-1</sup> (m, C<sub>Ar</sub>-O); ESI-MS (ES<sup>+</sup>); Expected m/z (%) 312.2, obtained m/z (%) 312.6 (100) [M+H]<sup>+</sup>.

#### 2.14.2.2 Characterization of 2, 2'-{iminobis[ethane-2,1-diylnitrilo(E) methylidene]} di-(4-methoxy phenol) (Ligand L2)

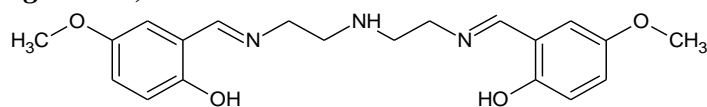


Figure 2. 28 Schematic diagram of ligand L2

A 1.52 g (0.0100 moles) of 4-methoxy *salicylaldehyde* and 0.543 g (0.00526 moles) of *diethylenetriamine* was used as indicated above. Yellow solid mass was obtained MP= 74.9-75.6 °C yield 84 %, Anal. Calc. For C<sub>20</sub>H<sub>25</sub>N<sub>3</sub>O<sub>4</sub> (H<sub>2</sub>O) EA calculated (%) C (61.68), H (6.99), N (10.79). EA Found (%); C (61.68), H (6.59), N (10.59); <sup>1</sup>H NMR (400 MHz, CDCl<sub>3</sub>) δ<sub>H</sub> ppm; 8.31 (2 H, s, NCH), 6.93 – 6.84 (4 H, m, ArH), 6.74 (2 H, d,  $J$  2.7 Hz, ArH), 3.76 (6 H, s, O(CH<sub>3</sub>)), 3.71 (4 H, t,  $J$  5.7 Hz, NCH<sub>2</sub>CH<sub>2</sub>), 2.99 (6 H, s, NCH<sub>2</sub>CH<sub>2</sub>). <sup>13</sup>C {<sup>1</sup>H} NMR. (400 MHz, CDCl<sub>3</sub>) δ<sub>c</sub> ppm; 165.90 (NCH); 155.29 (C<sub>Ar</sub>OH), 152.09 (C<sub>Ar</sub>OCH<sub>3</sub>), 119.44 (C<sub>Ar</sub>H), 118.44 (C<sub>Ar</sub>H), 117.78 (C<sub>Ar</sub>H), 114.97 (C<sub>Ar</sub>H), 59.87 (OCH<sub>3</sub>), 56.03 (NCH<sub>2</sub>CH<sub>2</sub>), 49.82 (NCH<sub>2</sub>CH<sub>2</sub>). IR (ATR, neat, cm<sup>-1</sup>); 2926, 2842 (m, CH); 1631(m, C=N); 1587(s, C=C), 1488 (m, CH), 1267cm<sup>-1</sup> (m, C<sub>Ar</sub>-O); ESI-MS (ES<sup>+</sup>); Expected m/z (%) 372.4 Obtained m/z (%) 372.2 (100) [M+H]<sup>+</sup>.

#### 2.14.2.3 Characterization of 1, 1'-{iminobis[ethane-2,1-diylnitrilo(E) methylidene]} di-2-hydroxy naphthalene) (Ligand L3)

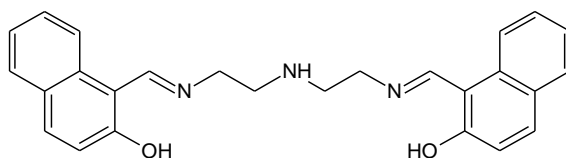


Figure 2. 29 Schematic diagram of ligand L3

A 5.29 g (0.0307 moles) of 2-hydroxy *naphthalene* and 1.63 g (0.0158 moles) of *diethylenetriamine* were used. Reddish yellow dry lumps were obtained MP=159-160 °C yield 69 %, For Anal. For C<sub>26</sub>H<sub>25</sub>N<sub>3</sub>O<sub>2</sub>, EA calculated (%) C (75.89) H (6.12%) N (10.21%),

EA Found (%): C (76.07%) H (6.32) N (10.06),  $^{13}\text{C}$   $\{^1\text{H}\}$  NMR. (300 MHz,  $\text{CDCl}_3$ )  $\delta_{\text{H}}$  ppm; 8.79 (2 H, s NCH), 7.84 (2 H, d,  $J$  8.4 ArH), 7.84 (2 H, d,  $J$  8.4 ArH) 7.65 (2 H, d,  $J$  9.3 ArH) 7.38 (2 H, ddd,  $J$  8.4 Hz, 7.1Hz, 1.4Hz, ArH), 7.25 – 7.15 (2 H, m, ArH), 6.90 (2 H, d,  $J$  9.3 Hz, ArH), 3.71 (4 H, t,  $J$  5.8Hz,  $\text{NCH}_2\text{CH}_2$ ), 3.08 – 2.98 (4 H, m,  $\text{NCH}_2\text{CH}_2$ ).  $^{13}\text{C}$  NMR (300 MHz, DMSO)  $\delta_{\text{C}}$  ppm; 165.96(NCH), 159.13 ( $\text{C}_{\text{Ar}}\text{OH}$ ), 134.45 ( $\text{C}_{\text{Ar}}\text{CN}$ ), 128.79( $\text{C}_{\text{Ar}}\text{H}$ ), 127.78 ( $\text{C}_{\text{Ar}}\text{H}$ ), 125.82 ( $\text{C}_{\text{Ar}}\text{H}$ ), 125.03 ( $\text{C}_{\text{Ar}}\text{H}$ ), 121.94 ( $\text{C}_{\text{Ar}}\text{H}$ ), 118.38 ( $\text{C}_{\text{Ar}}\text{H}$ ), 50.76 ( $\text{NCH}_2\text{CH}_2$ ), 48.98 ( $\text{NCH}_2\text{CH}_2$ ), IR (ATR, neat,  $\text{cm}^{-1}$ ); 2844 (m, C-H); 1610 (s, C=N); 1538 (s, C=C); 1488 (m, C-H); 1258  $\text{cm}^{-1}$  (m,  $\text{C}_{\text{Ar}}\text{-O}$ ); ESI-MS (ES+); Expected  $m/z$  (%) 412.5 Obtained  $m/z$ (%) 412.2 (100)  $[\text{M-H}]^+$ .

#### 2.14.2.4 Characterization of 2, 2'-{iminobis[ethane-2,1-diyl]nitrido(E) methylidene}di-(4-tert butylphenol) (Ligand L4)

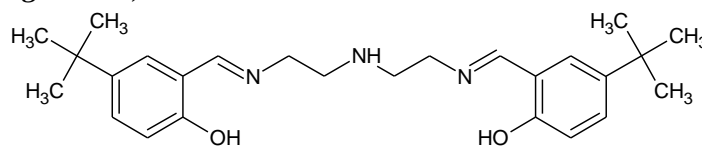


Figure 2. 30 Schematic diagram of ligand L4

A 4.33 g (0.0242 moles) of 4-*tert* butyl salicylaldehyde and 1.30 g (0.0126 moles) of diethylenetriamine was used. Yellowish orange viscous oil that slowly solidified slowly MP 64.9-66.2 °C, yield 88 %, For  $\text{C}_{26}\text{H}_{37}\text{N}_3\text{O}_2$ : EA calculated (%) C (73.72%) H (8.80%) N (9.92%), EA Found (%); C (73.91%), H (8.44) ,N(9.80);  $^1\text{H}$  NMR (300 MHz,  $\text{CDCl}_3$ )  $\delta_{\text{H}}$  ppm; 8.37 (2 H, s, NCH), 7.39 – 6.79 (6 H, m, ArH), 3.76 – 3.66 (4 H, m, ( $\text{NCH}_2\text{CH}_2$ )), 3.01 (4 H, d,  $J$  5.4 Hz, ( $\text{NCH}_2\text{CH}_2$ )), 1.30 (18 H, s,  $\text{C}(\text{CH}_3)_3$ ).  $^{13}\text{C}$   $\{^1\text{H}\}$  NMR. (300 MHz,  $\text{CDCl}_3$ )  $\delta_{\text{C}}$  ppm 166.58 (NCH), 159.97 ( $\text{C}_{\text{Ar}}\text{OH}$ ), 141.15 ( $\text{C}_{\text{Ar}}\text{H}$ ), 129.77 ( $\text{C}_{\text{Ar}}\text{H}$ ), 127.88 ( $\text{C}_{\text{Ar}}\text{H}$ ), 118.06 ( $\text{C}_{\text{Ar}}\text{CN}$ ), 116.41 ( $\text{C}_{\text{Ar}}\text{H}$ ), 59.73 ( $\text{NCH}_2\text{CH}_2$ ), 49.97 ( $\text{NCH}_2\text{CH}_2$ ), 31.87 ( $\text{C}(\text{CH}_3)_3$ ), 31.54 ( $\text{CH}_3$ )<sub>3</sub>. IR (ATR, neat,  $\text{cm}^{-1}$ ); 2865 (m, C-H); 1633 (s, C=N); 1589 (m, C=C); 1491 (m, C-H); 1266  $\text{cm}^{-1}$  (s,  $\text{C}_{\text{Ar}}\text{-O}$ ); ESI-MS (ES+); Expected  $m/z$  (%) 424.3, Obtained  $m/z$ (%) 212.65 (25%),  $[(\text{M}/2)+\text{H}]^+$ , 424.3 (100)  $[\text{M}+\text{H}]^+$ .

### 2.14.2.5 Characterization of (2, 2'-{iminobis[ethane-2,1-diyl]nitrido(E) methylidene}}di-(4-nonylphenol) (Ligand L5)

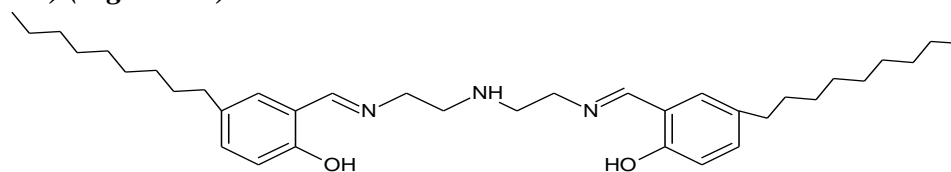


Figure 2. 31 Schematic diagram of ligand L5

A 5.81 g (0.0234 moles) of 4-nonyl *salicylaldehyde* and 1.13g (0.0109 moles) of *diethylenetriamine* was used. Orange viscous oil was obtained, yield 87 %, For  $C_{36}H_{57}N_3O_2$  EA calculated (%); (76.68%) H (10.19%) N (7.45%), EA Found (%): C (76.14%) H (9.08) N (7.62);  $^1H$  NMR (300 MHz,  $CDCl_3$ )  $\delta_H$  ppm; 13.04 (2 H, s, OH), 8.35 (2 H, s, NCH), 7.39 – 7.01 (4 H, m, ArH), 6.88 (2 H, d,  $J$  8.6 Hz, ArH), 3.87 – 3.50 (4 H, m,  $NCH_2CH_2$ ), 3.00 (4 H, t,  $J$  5.9 Hz,  $NCH_2CH_2$ ), 1.61 – 0.33 (36 H, m,  $(CH_2)_8CH_3$ ).  $^{13}C$   $\{^1H\}$  NMR. (300 MHz,  $CDCl_3$ )  $\delta_C$  ppm; 166.67 (NCH), 158.71 ( $C_{Ar}OH$ ), 138.16 ( $C_{Ar}C_9H_{19}$ ), 130.24 ( $C_{Ar}H$ ), 117.99 ( $C_{Ar}CN$ ), 116.42 ( $C_{Ar}H$ ), 59.90 ( $NCH_2CH_2$ ), 50.10 ( $NCH_2CH_2$ ), 41.56- 8.75 ( $C_9H_{19}$ ). IR (ATR, neat,  $cm^{-1}$ ); 2955 (m, C-H), 2870 (m, C-H); 1632 (s, C=N); 1588 (m, C=C); 1490 (m, C-H); 1280 $cm^{-1}$  (m,  $C_{Ar}-O$ ); ESI-MS (ES+); Expected  $m/z$ (%) 564.5 Obtained  $m/z$ (%) 282.7 (100)  $[(M/2)+H]^{2+}$ , 564.5 (50)  $[M+H]^+$ .

### 2.14.3 Synthesis and characterization of class B ligands

#### 2.14.3.1 Characterization of 2, 2'-{iminobis[propane-3,1-diyl]nitrido(E)methylidene}}diphenol (Ligand L6)

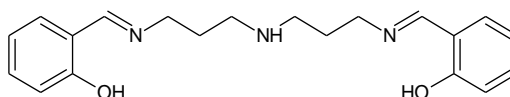


Figure 2. 32 Schematic diagram of ligand L6

A 2.44g (0.0200 moles) of *salicylaldehyde* and 1.33g (0.0101 moles) of *bis(3-aminopropyl)amine* was used. Yellow viscous oil was obtained that slowly solidified into a yellowish-red mass, yield 82%, Anal. Calc. For  $C_{20}H_{25}N_3O_2$ : EA calculated (%) C (70.77), H (7.42), N (12.38). EA Found (%); C (70.29), H (7.26), N (12.38).  $^1H$  NMR 600 MHz,  $CDCl_3$ )  $\delta_H$  ppm; 8.33 (2 H, s, NCH), 7.29 (2 H, t,  $J$  6.6 Hz, ArH), 7.22 (2 H, d,  $J$  6.5 Hz, ArH), 6.94 (2 H, d,  $J$  7.5 Hz, ArH), 6.85 (2 H, t,  $J$  7.2 Hz, ArH), 3.65 (4 H, s,  $NCH_2CH_2CH_2$ ), 2.72 (4 H, s,  $J$  106.9 Hz,  $NCH_2CH_2CH_2$ ), 1.91 – 1.84 (4 H, m,  $NCH_2CH_2CH_2$ ).  $^{13}C$   $\{^1H\}$  NMR. (400 MHz,  $CDCl_3$ )  $\delta_C$  ppm; 165.04 (NCH), 161.36 ( $C_{Ar}OH$ ), 132.23 ( $C_{Ar}H$ ), 131.28 ( $C_{Ar}H$ ), 118.59 ( $C_{Ar}H$ ), 117.10 ( $C_{Ar}CN$ ), 57.54 ( $NCH_2CH_2CH_2$ ), 47.63 ( $NCH_2CH_2CH_2$ ), 31.36 ( $NCH_2CH_2CH_2$ ). IR (ATR, neat,  $cm^{-1}$ ); 2923(m, C-H), 2845 (m, CH); 1628 (s, C=N); 1574 (s,

C=C); 1494 (m, CH); 1276  $\text{cm}^{-1}$  (s,  $\text{C}_{\text{Ar}}\text{-O}$ ); ESI-MS (ES+); Expected  $m/z$  (%) 340.20, obtained:  $m/z$  (%)170.60 (50)  $[(M/2)+\text{H}]^+$  and 340.20 (100)  $[\text{M}+\text{H}]^+$ .

### 2.14.3.2 Characterization of 2,2'-[iminobis[propane-3,1-diylnitro(*E*)methylylidene]] di-(4-methoxyphenol) (Ligand L7)

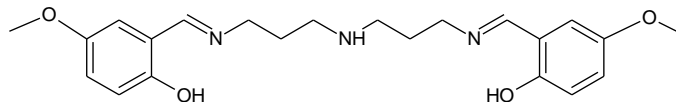


Figure 2. 33 Schematic diagram of ligand L7

A 1.90 g (0.0124 moles) of 4-methoxy -2 hydroxyl aldehyde and 0.864 g (0.00658 moles) of *bis*(3-aminopropyl)amine. Dark reddish yellow oil lumps, that slowly solidifies into yellow lumps was obtained yield 96 %. Anal. Calc. For  $\text{C}_{22}\text{H}_{29}\text{N}_3\text{O}_4$ , EA calculated (%); C 66.14, H 7.32, N 10.52. EA Found (%); C 66.17, H 7.03, N 10.13;  $^1\text{H}$  NMR (300 MHz,  $\text{CDCl}_3$ )  $\delta_{\text{H}}$  ppm; 8.27 (2 H, s, NCH), 6.86 (4 H, s, ArH), 6.72 (2 H, d,  $J$  2.1, ArH), 3.75 (6 H, s,  $\text{OCH}_3$ ), 2.86 – 2.72 (4 H, m,  $\text{NCH}_2\text{CH}_2\text{CH}_2$ ), 1.94 (4 H, d,  $J$  5.1 Hz,  $\text{NCH}_2\text{CH}_2\text{CH}_2$ ).  $^{13}\text{C}$   $\{^1\text{H}\}$  NMR. (75 MHz,  $\text{CDCl}_3$ )  $\delta_{\text{C}}$  ppm; 165.15 (NCH), 152.05 ( $\text{C}_{\text{Ar}}\text{-OH}$ ), 125.34 ( $\text{C}_{\text{Ar}}\text{OCH}_3$ ), 119.38 ( $\text{C}_{\text{Ar}}\text{H}$ ), 118.71 ( $\text{C}_{\text{Ar}}\text{CN}$ ), 117.70 ( $\text{C}_{\text{Ar}}\text{H}$ ), 114.86 ( $\text{C}_{\text{Ar}}\text{H}$ ), 57.34 ( $\text{OCH}_3$ ), 55.98 ( $\text{NCH}_2\text{CH}_2\text{CH}_2$ ), 47.17 ( $\text{NCH}_2\text{CH}_2\text{CH}_2$ ), 30.05  $\text{NCH}_2\text{CH}_2\text{CH}_2$ . IR (ATR, neat,  $\text{cm}^{-1}$ ); 2936 (m, CH), 2832 (m, CH); 1634 (s, C=N); 1589 (s, C=C); 1490 (m, C-H); 1266 $\text{cm}^{-1}$  (m,  $\text{C}_{\text{Ar}}\text{-O}$ ); ESI-MS (ES-); Expected  $m/z$ (%) 398.48  $m/z$ (%) Obtained 167.04(75)  $[\text{M}-\text{C}_{12}\text{H}_{20}\text{N}_2\text{O}_3]^+$  252.13(100)  $[\text{M}-\text{C}_8\text{H}_7\text{NO}_3]^+$ , 398.17 (100)  $[\text{M}-\text{H}]^+$ .

### 2.14.3.3 Characterization of 2,2'-[iminobis[propane-3,1-diylnitro(*E*)methyl idene]]di-2-hydroxy naphthalene) (ligand L8a)

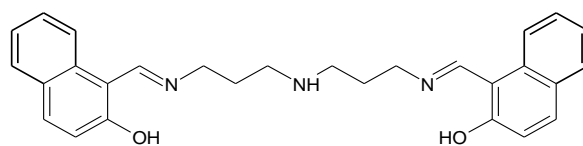


Figure 2. 34 Schematic diagram of ligand L8a

A 2.66 g (0.0150 moles) of 2-hydroxy naphthylene and 1.02 g (0.00800 moles) of *bis*(3-aminopropyl)amine was used, Yellow dry lumps were obtained MP 215-217 °C yield 86%, For Anal. Calc. For  $\text{C}_{28}\text{H}_{29}\text{N}_3\text{O}_2(\text{C}_2\text{H}_5\text{OH})$  EA calculated (%) C (74.20) H (6.65%) N (8.65%), EA Found (%): C (74.07) H (6.14) N (10.07);  $^1\text{H}$ NMR (400 MHz,  $\text{CDCl}_3$ )  $\delta_{\text{H}}$  ppm; 8.76 (2 H, s, NCH), 7.83 (2 H, d,  $J$  8.3 NCH), 7.64 (2 H, d,  $J$  9.3 Hz, ArH), 7.57 (2 H, d,  $J$  7.9 Hz, ArH), 7.38 (2 H, dd,  $J$  6.8 Hz, 1.1 Hz, ArH), 7.20 (2 H, ddd,  $J$  8.0 Hz, 7.1 Hz, 1.0 Hz, ArH), 6.89 (2 H, d,  $J$  9.3 Hz, ArH), 3.67 (4 H, t,  $J$  5.9 Hz,  $\text{NCH}_2\text{CH}_2\text{CH}_2$ ), 2.99 (4 H, t,  $J$  5.8 Hz,

NCH<sub>2</sub>CH<sub>2</sub>CH<sub>2</sub>), 1.23 (4 H, t, *J* 7.0 Hz, (NCH<sub>2</sub>CH<sub>2</sub>CH<sub>2</sub>)). <sup>13</sup>C {<sup>1</sup>H} NMR. (75 MHz, CDCl<sub>3</sub>) δ<sub>c</sub> ppm; 176.14(C<sub>Ar</sub>OH), 158.35(NCH) 137.30 (C<sub>Ar</sub>CN), 133.84 (C<sub>Ar</sub>H, 129.29 (C<sub>Ar</sub>H), 128.08 (C<sub>Ar</sub>H), 122.87 (C<sub>Ar</sub>H), 106.92 (C<sub>Ar</sub>H), 53.83 (NCH<sub>2</sub>CH<sub>2</sub>CH<sub>2</sub>), 49.50 (NCH<sub>2</sub>CH<sub>2</sub>CH<sub>2</sub>), 29.90 (NCH<sub>2</sub>CH<sub>2</sub>CH<sub>2</sub>), IR (ATR, neat, cm<sup>-1</sup>); 2955 (m, C-H), 2738 (m, C-H); 1614 (m, C=N); 1541 (s, C=C); 1491 (m, CH); 1273cm<sup>-1</sup> (m, C<sub>Ar</sub>-O); ESI-MS (ES+); Expected m/z(%) 440.54, obtained m/z(%) 440.23 (100) [M+H]<sup>+</sup>.

#### 2.14.3.4 Characterization of 2, 2'-{fiminobis [propane-3,1-diylnitriolo(E)methylylidene]} di-(4-tert butylphenol) (ligand L9)

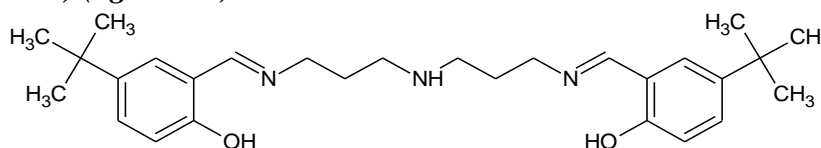


Figure 2. 35 Schematic diagram of ligand L9

A 5.59g (0.0313 moles) of 4-*tert* butyl-2 hydroxyl aldehyde and 2.10g (0.0160 moles) of *bis*(3-*aminopropyl*)*amine*, orange moderate viscous oil was obtained, yield 84%, For Anal Calc. For C<sub>28</sub>H<sub>41</sub>N<sub>3</sub>O<sub>2</sub>; EA calculated (%); C (74.46%) H (9.15%) N (9.30%), EA Found (%); C (74.23%) H (9.11) N (9.42); <sup>1</sup>H NMR (300 MHz, CDCl<sub>3</sub>) δ<sub>H</sub> ppm; 8.33 (2 H, s, NCH), 7.33 – 7.27 (2 H, m, ArH), 7.19 (2 H, d, *J* 2.2 Hz, ArH), 6.85 (2 H, d, *J* 8.6 Hz, ArH), 3.56 (4 H, t, *J* 33.5 Hz, NCH<sub>2</sub>CH<sub>2</sub>CH<sub>2</sub>), 2.68 (4 H, d, *J* 6.8 Hz, NCH<sub>2</sub>CH<sub>2</sub>CH<sub>2</sub>), 1.88 – 1.82 (4 H, m, NCH<sub>2</sub>CH<sub>2</sub>CH<sub>2</sub>), 1.30 – 1.21 (18 H, s, C(CH<sub>3</sub>)<sub>3</sub>). <sup>13</sup>C {<sup>1</sup>H} NMR. (75 MHz, CDCl<sub>3</sub>) δ<sub>c</sub> ppm; 165.88 (NCH); 158.71 (C<sub>Ar</sub>OH), 142.03 (C<sub>Ar</sub>C(CH<sub>3</sub>)<sub>3</sub>), 126.23 (C<sub>Ar</sub>H), 116.52 (C<sub>Ar</sub>H), 115.03 (C<sub>Ar</sub>H), 57.12 (NCH<sub>2</sub>CH<sub>2</sub>CH<sub>2</sub>), 48.22 (NCH<sub>2</sub>CH<sub>2</sub>CH<sub>2</sub>), 40.46 (NCH<sub>2</sub>CH<sub>2</sub>CH<sub>2</sub>), 31.49 (C(CH<sub>3</sub>)<sub>3</sub>). IR (ATR, neat, cm<sup>-1</sup>); 2960(m, C-H), 28649 (m, C-H); 1635 (s, C=N); 1590 (m, C=C); 1493 (m, CH); 1281 cm<sup>-1</sup> (m, C<sub>Ar</sub>-O); ESI-MS (ES+); Expected m/z(%) 452.3 Obtained m/z (%) 452.3 (100) [M+H]<sup>+</sup>.

#### 2.14.3.5 Characterization of 2,2'-{fiminobis[propane-3,1-diylnitriolo(E)methylylidene]} di-(4-nonylphenol) (Ligand L10)

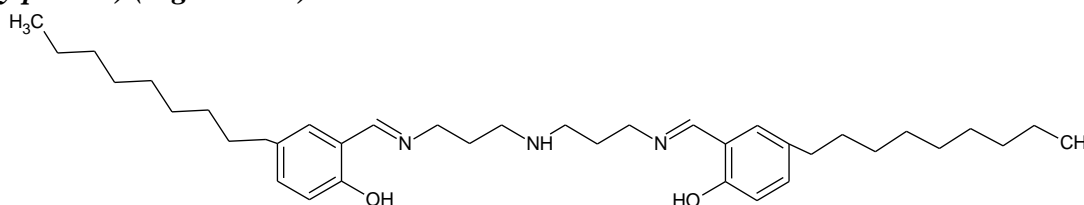


Figure 2. 36 Schematic diagram of ligand L10

A 7.52 g (0.0303 moles) of 4-nonyl *salicylaldehyde* and 1.98 g (0.0151 moles) of *bis*(3-*aminopropyl*)*amine*, dark reddish-yellow viscous oil, yield 87%, For Anal. Calc. For

$C_{38}H_{61}N_3O_2$ : EA calculated (%) C (77.11%) H (10.39%) N (7.10%), EA Found (%); C (77.89%) H (11.34) N (7.95);  $^1H$ NMR (400 MHz,  $CDCl_3$ )  $\delta_H$  ppm; 8.32 (2 H, s, NCH), 7.07 (2 H, d,  $J$  7.2 Hz, ArH), 6.87 (2 H, d,  $J$  8.3 Hz, ArH), 6.70 (2 H, d,  $J$  8.6 Hz, ArH), 3.60 (4 H, s,  $NCH_2CH_2CH_2$ ), 2.72 (4 H, d,  $NCH_2CH_2CH_2$ ), 1.85 (4 H, d,  $J$  6.0 Hz,  $NCH_2CH_2CH_2$ ), 1.72 – 0.45 (38H, m,  $C_9H_{19}$ ).  $^{13}C$  { $^1H$ } NMR. (151 MHz,  $CDCl_3$ )  $\delta_C$  ppm; 165.58 (NCH), 158.53 ( $C_{Ar}OH$ ), 116.49 ( $C_{Ar}CH_2$ ), 116.41 ( $C_{Ar}H$ ), 57.66 ( $NCH_2CH_2CH_2$ ), 47.78 ( $NCH_2CH_2CH_2$ ), 43.52 ( $NCH_2CH_2CH_2$ ), 37.41-8.77 ( $C_9H_{19}$ ). IR (ATR, neat,  $cm^{-1}$ ); 2956(w, C-H); 2871 (w, C-H); 1634 (s, C=N); 1589 (s, C=C); 1492 (m, C-H); 1283 $cm^{-1}$  (m,  $C_{Ar}-O$ ); ESI-MS (ES+); Expected  $m/z$ (%) 592.5 Obtained : $m/z$  (%) 592.8 (100)  $[M+H]^+$ .

## 2.14.4 Characterization of Class C ligands

### 2.14.4.1 Characterization of 2, 2, 2-Nitrilotris (ethane-2, 1-diyl) tris(azan-1-yl-1-ylidene)tris(methan-1-yl-1-ylidene)triphenol (Ligand L11)

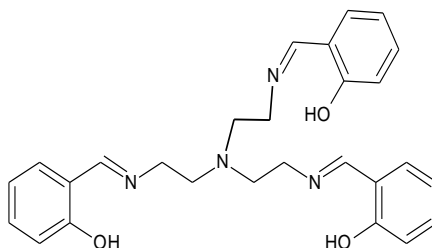


Figure 2. 37 Schematic diagram of ligand L11

A 3.78 (0.0310 moles) of 2-hydroxyl aldehyde and 1.52g (0.0104 moles) of 2-*N,N*-bis(2-aminoethyl)ethane-1,2-diamine. Product obtained is a yellow crystalline solid (3.136 g) yield 89.4% FM  $C_{27}H_{30}N_4O_3$  % EA calculated (%) C (70.72) H (6.59) N (12.22) EA Found C (70.87), H (6.61), N (11.70):  $^1H$  NMR (300 MHz,  $CDCl_3$ )  $\delta_H$  ppm; 13.77. (3H, S, OH), 7.82 (3 H, s, NCH), 7.31 – 7.23 (3 H, m, ArH), 6.95 – 6.89 (3 H, m, ArH), 6.59 (3 H, td,  $J$  7.5 Hz, 1.1 Hz, ArH), 6.11 (3 H, dd,  $J$  7.7 Hz, 1.7, ArH), 4.82 (3 H, s), 3.59 – 3.46 (6 H, m,  $NCH_2CH_2$ ), 2.83 (6 H, dd,  $J$  5.9Hz, 4.4 Hz,  $NCH_2CH_2$ ).  $^{13}C$  { $^1H$ } NMR. (75 MHz,  $CDCl_3$ )  $\delta$ ; 166.27 (NCH), 161.27 ( $C_{Ar}OH$ ), 132.05 ( $C_{Ar}H$ ), 131.89 ( $C_{Ar}H$ ), 118.72 ( $C_{Ar}H$ ), 118.65 ( $C_{Ar}CN$ ), 116.90 ( $C_{Ar}H$ ), 58.08 ( $NCH_2CH_2$ ), 56.03 (s,  $NCH_2CH_2$ ). IR (ATR, neat,  $cm^{-1}$ ); 2990(m, CH), 2815 (m, CH); 1631 (m, C=N); 1578 (m, C=C); 1496 (m, C-H); 1275  $cm^{-1}$  (m,  $C_{Ar}-O$ ); ESI-MS (ES+); Expected  $m/z$ (%) 459.55, Obtained  $m/z$ (%) 230.12(100)  $[(M/2) +H]^+$ , 355.21(30)  $[M-C_7H_4O_2]^+$ , 459.23(30)  $[M+H]^+$ .

#### 2.14.4.2 Characterization of 2,2, 2-Nitrilotris(ethane-2,1-diyl)tris(azan-1-yl-1-ylidene)tris(methan-1-yl-1-ylidene) tri-4- methoxyphenol) (Ligand L12)

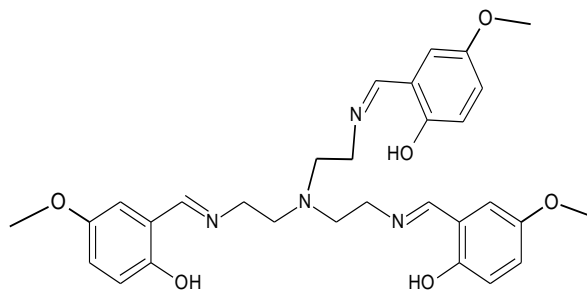


Figure 2. 38 Schematic diagram of ligand **L12**.

A 1.92 g (0.0126 moles) of 5-methoxy-2 hydroxyl aldehyde *salicylaldehyde* and 0.628 g (0.00429 moles) of 2-*N,N*-bis(2-aminoethyl)ethane-1,2-diamine; Product obtained yellow brown crystalline solid (yield 89.2 % FM  $C_{30}H_{36}N_4O_6(C_2H_5OH)$ , EA calculated (%) C (64.63), H (7.12), N (9.42) EA Found (%) C (64.79), H (6.57), N (9.85);  $^1H$  NMR (300 MHz,  $CDCl_3$ )  $\delta_H$  ppm, 7.91 (3 H, s, NCH), 6.96 – 6.79 (6 H, m, ArH), 6.05 (3 H, dd,  $J$  2.2 Hz, 1.0, ArH), 3.62 (9 H, s,  $OCH_3$ ), 3.58 – 3.50 (6 H, m,  $NCH_2CH_2$ ), 2.96 – 2.71 (6 H, m,  $NCH_2CH_2$ ).  $^{13}C$  { $^1H$ } NMR. (75 MHz,  $CDCl_3$ )  $\delta_C$  ppm; 165.88 (NCH), 155.30 ( $C_{Ar}OH$ ), 152.00 ( $C_{Ar}OCH_3$ ), 119.18 ( $C_{Ar}H$ ), 118.50 ( $C_{Ar}H$ ), 117.53 ( $C_{Ar}CN$ ), 115.00 ( $C_{Ar}H$ ), 58.15 ( $OCH_3$ ), 56.39 ( $NCH_2CH_2$ ), 55.81 ( $NCH_2CH_2$ ). IR (ATR, neat,  $cm^{-1}$ ); 2901(m, C-H), 2816 (m, C-H), 1633 (s, C=N), 1588 (m, C=C), 1488 (m, C-H), 1263  $cm^{-1}$  (m,  $C_{Ar}-O$ ): ESI-MS (ES+); Expected m/z(%) 549.63, Obtained m/z (%) 208.1(50) [ $M - C_{19}H_{20}N_4O_4$ ], 275.1 (100) [ $(M/2)+H$ ] $^+$ , 415.2 (25) [ $M - C_8H_8O_3$ ] $^+$ , 549.3 (25) [ $M+H$ ] $^+$ .

#### 2.14.4.3 Characterization of (2,2, 2-Nitrilotris(ethane-2,1-diyl)tris(azan-1-yl-1-ylidene)tris(methan-1-yl-1-ylidene)trinaphthalene-2-ol) (Ligand L13)

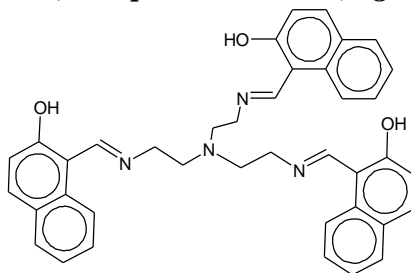


Figure 2. 39 Schematic diagram of ligand **L13**

A 2.34 g (0.0136 moles) of 2 hydroxyl naphthylaldehyde and 0.674 g (0.00461 moles) of 2-*N,N*-bis(2-aminoethyl)ethane-1,2-diamine. The product obtained was a yellowish green powder, yield 86.7 %, FM  $(C_{27}H_{30}N_4O_3)_3 \cdot 2H_2O$ , EA calculated (%) C (73.68), H (6.18), N (8.81) EA Found C(73.77), H (6.38), N (9.23)  $^1H$  NMR (300 MHz,  $CDCl_3$ )  $\delta_H$  ppm; 8.72 (3

H, s, NCH), 7.65 (3 H, d,  $J$  8.2 Hz, ArH), 7.39 (6 H, dt, 11.5Hz, 9.8 Hz, ArH), 7.12 (6 H, dtd,  $J$  14.6Hz, 7.1Hz, 1.3 Hz, ArH), 6.75 (3 H, t,  $J$  10.0 Hz, ArH), 3.69 (6 H, t,  $J$  5.5, NCH<sub>2</sub>CH<sub>2</sub>), 3.09 – 2.91 (6 H, m, NCH<sub>2</sub>CH<sub>2</sub>). <sup>13</sup>C {<sup>1</sup>H} NMR. (300 MHz, CDCl<sub>3</sub>) δ<sub>c</sub> ppm; 159.05 (NCH), 137.25 (C<sub>Ar</sub>OH), 133.76 (C<sub>Ar</sub>CN), 128.98 (C<sub>Ar</sub>C), 127.84 (C<sub>Ar</sub>H), 126.09 (C<sub>Ar</sub>H), 124.64 (C<sub>Ar</sub>C), 122.59 (C<sub>Ar</sub>H), 118.39 (C<sub>Ar</sub>H), 106.86 (C<sub>Ar</sub>H), 56.62 (NCH<sub>2</sub>CH<sub>2</sub>), 52.29 (NCH<sub>2</sub>CH<sub>2</sub>); IR (ATR, neat, cm<sup>-1</sup>); 3043 (w, OH); 2815, (m, CH); 1620 (m, C=N); 1541 (s, C=C); 1489 (m, CH); 1261 cm<sup>-1</sup> (m, C<sub>Ar</sub>-O); ESI-MS (ES+); Expected m/z(%) 609.3 obtained m/z(%) 305.1(100) [(M/2) +H]<sup>+</sup>, 609.3 (30) [M+H]<sup>+</sup>.

#### 2.14.4.4 Characterization of (2,2, 2-Nitrilotris(ethane-2,1-diyl)tris(azan-1-yl-1-ylidene)tris(methan-1-yl-1-ylidene) tri-4- tert butyl phenol (Ligand L14)

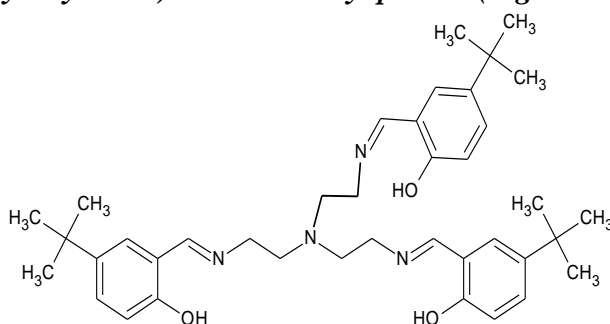


Figure 2. 40 Schematic diagram of ligand **L14**.

A 2.97 g (0.0167 moles) of 4-tert butyl salicylaldehyde and 0.821 g (0.00561 moles) of 2-N,N-bis(2-aminoethyl)ethane-1,2-diamine. The product obtained as yellow oil, yield 84.2 %. For C<sub>39</sub>H<sub>36</sub>N<sub>4</sub>O<sub>3</sub>(C<sub>2</sub>H<sub>5</sub>O), EA calculated (%) ; C (73.18), H (8.99), N (8.33) EA Found (%); C (73.29), H (8.51) N (8.33) <sup>1</sup>H NMR (600 MHz, CDCl<sub>3</sub>) δ<sub>H</sub> ppm; 8.36 (3 H, s, NCH), 8.28 (3 H, s, NCH), 7.33 (3 H, dd,  $J$  8.6 Hz, 2.5Hz, ArH), 7.18 (3 H, d,  $J$  2.5 Hz, ArH), 6.88 (3 H, d,  $J$  8.7 Hz, ArH), 3.65 (6 H, s, NCH<sub>2</sub>CH<sub>2</sub>), 2.92 (6 H, d,  $J$  6.4 Hz, NCH<sub>2</sub>CH<sub>2</sub>), 1.28 (27 H, s CH<sub>3</sub>). <sup>13</sup>C {<sup>1</sup>H} NMR. (151 MHz, CDCl<sub>3</sub>) δ<sub>c</sub> ppm 166.34 (NCH) 159.02 (C<sub>Ar</sub>OH), 141.28 (C<sub>Ar</sub>CN), 129.63 (C<sub>Ar</sub>CH<sub>2</sub>), 127.87, 118.20 (C<sub>Ar</sub>H), 116.61 (C<sub>Ar</sub>H), 58.48 (NCH<sub>2</sub>CH<sub>2</sub>), 56.06 (NCH<sub>2</sub>CH<sub>2</sub>), 34.09 (C(CH<sub>3</sub>)<sub>3</sub>) 31.59 (CH<sub>3</sub>)<sub>3</sub>. IR (ATR, neat, cm<sup>-1</sup>); 2952 (m, C-H), 2862, (m, C-H), 1631 (m, C=N); 1587 (s, C=C); 1489 (m, CH); 1265 cm<sup>-1</sup> (m, C<sub>Ar</sub>-O); ESI-MS (ES+); Expected m/z(%) 627.4 obtained m/z(%) 243.2 (35) [M-(C<sub>13</sub>H<sub>17</sub>NO)<sub>2</sub>]<sup>+</sup>, 314.2(100) [(M/2)+H]<sup>+</sup>, 627.4 (30) [M+H]<sup>+</sup>.

#### 2.14.4.5 Characterization of 5-nonyl salicylaldehyde and 2,2'-[ethane-1,2-diylbis(oxy)] diethanamine (ligand L15)

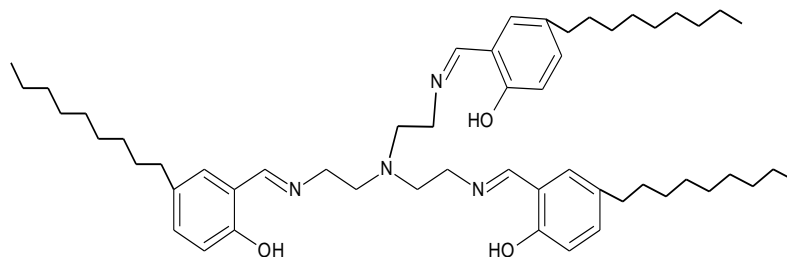


Figure 2. 41 Schematic diagram of ligand **L15**.

A 6.37 g (0.0256 moles) of *salicylaldehyde* and 1.26 g (0.00862 moles) of 2-*N,N*-bis(2-aminoethyl)ethane-1,2-diamine Product obtained yellow viscous oil, yield 87.3 %, FM  $C_{54}H_{84}N_4O_3$ , EA calculated (%) C (77.46) H (10.11) N (6.69) EA Found (%) C (77.43) H (10.09) N (6.07),  $^1H$  NMR (600 MHz,  $CDCl_3$ )  $\delta_H$  ppm; 8.28 (3 H, s, NCH), 7.15 (3 H, t,  $J$  13.3,  $C_{Ar}H$ ), 7.10 (3 H, d,  $J$  17.0,  $C_{Ar}H$ ), 6.88 (3 H, d,  $J$  8.4,  $C_{Ar}H$ ), 3.67 (6 H, d,  $J$  14.5Hz,  $NCH_2CH_2$ ), 2.94 (6 H, s,  $NCH_2CH_2$ ), 1.75 – 0.52 (57 H, m,  $(C_9H_{19})_3$ ):  $^{13}C$   $\{^1H\}$  NMR. (151 MHz,  $CDCl_3$ )  $\delta_C$  ppm; 166.46 (NCH), 158.77 ( $C_{Ar}OH$ ), 138.41 ( $C_{Ar}CN$ ), 130.35 ( $C_{Ar}CH_2$ ), 118.12 ( $C_{Ar}H$ ), 116.49 ( $C_{Ar}H$ ), 116.42 ( $C_{Ar}H$ ), 58.64( $NCH_2CH_2$ ), 56.14 ( $NCH_2CH_2$ ), 41.57-14.23 ( $C_9H_{19}$ ): **IR** (ATR, neat,  $cm^{-1}$ ); 2969(m, C-H), 2864 (m, C-H), 1631 (m, C=N). 1587 (s, C=C), 1490 (m, CH), 1279  $cm^{-1}$  (m,  $C_{Ar}-O$ ): ESI-MS (ES+); Expected  $m/z$ (%) 837.6, Obtained  $m/z$  (%) 304.3(65) ( $[(M-C_{16}H_{26}O)]/2$ ) $^+$ , 419.3 (100)  $[(M/2)+H]^+$ , 607.5 (15)  $[M-C_{16}H_{26}O]^+$ , 837.7 (15)  $[M+H]^+$ .

# **CHAPTER 3**

---

## **SYNTHESIS OF MULTIDONOR SCHIFF BASE LIGANDS CONTAINING O-DONOR GROUP**

---

### 3.0 INTRODUCTION

In this chapter, the synthesis of *pentadentate* and *hexadentate* Schiff base system with an O-donor in their spacer and their full characterization is discussed. The aim is to study the electronic changes due to the various substituents and the effect of the added O-donor groups.

#### 3.1 Oxygen containing ligand systems

The O-donor based ligands, such as the ethereal containing crown ether type ligands, have the ability to encapsulate metal ions. This complete casing of the metal ion usually occurs through coordination of the multidentate O-donor atoms in the crown ether. For a long time these crown ether type ligands have dominated various studies and applications of the O-donor ligands [115]. Over the years, various studies on uses of these ligands have been undertaken resulting in the synthesis of various crown ether and crown ether type ligands. These crown ether type ligands have therefore found uses in various sectors. These include uses in drug delivery systems, in hydrogen storage technology and in hydrometallurgy [116-118]. Despite all these advantages these crown ether type ligands remain privileged ligands because they are very difficult and expensive to synthesize.

There are analogues crown ether type ligands that have also attracted considerable interest. For example, *oligo salen* type ligands shown in Figure 3.1a. These ligands have the ethereal moiety associated with the crown ether ligand. They also possess side chains which have unique cation binding properties unmatched by the parent crown ether ligand [119-121]. These lariat crown ether type ligands possess various properties such as rapid, strong and three-dimensional cation binding sites that mimic the properties of naturally occurring ionophores [121, 122]. Because of these properties, Schiff base adducts of these lariat Schiff bases have become predominant and have been studied as *oligo salen* type ligands shown in Figure 3.1.

The introduction of the Schiff base adducts therefore introduces these crown ether type ligands to the activity of the Schiff base ligand centres. The extra O-donor groups act as the backbone of the salen type ligand that is a derivative of the hydroxime ligands commonly used in solvent extraction. Therefore, studies of these *oligo salen* type ligands shows that they have various advantages that include relative ease of synthesis and ability to be modified by either increasing or reducing the number of ethereal groups in the system. The increased number of these ethereal systems can lead to various properties that include ability to encapsulate secondary metal ion as indicated by **G** in Figure 3.1.

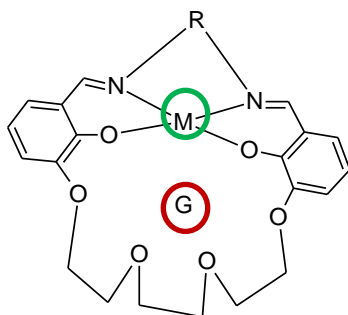


Figure 3. 1 Oligosalen complex showing the secondary coordinated metal G.

### 3.2 Problem statement

Schiff base ligands have two important advantages over other ligand systems such as crown ethers, they are inexpensive since they are relatively easy to synthesize, and they have various active centres due to the Schiff base centre and the various donor groups. These properties therefore allow these ligands to have a broad range of applications [123]. There has been a concerted effort to combine these Schiff base containing groups to be adopted into the crown ether type ligands such as in *oligo salen* type of ligands. The problem is that the macrocyclic systems are usually very expensive, therefore the *salen* type ligands with two imine and various donor groups allow for these ligand systems to be designed with an ethereal moiety to function like the macrocyclic upon coordination with metals as shown in Figure 3.2.

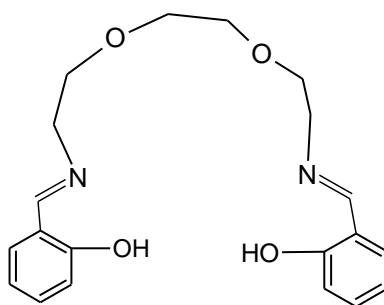


Figure 3. 2 Salen N-O-O-N donor ligand

#### 3.2.1 Justification of study

From the discussion in Chapter 2, the effect of adding the alkyl groups in these Schiff base ligands is discussed. The introduction of various O-donor groups in the salen type ligand backbone has the desired effect of altering the properties of these Schiff base ligands since the O-donor has higher electronegativity than the N-atom used in the previous chapter. This chapter therefore aims to study the effect of the increased O-donor groups and the electronic property of these ligand systems.

### 3.3 Chapter objective

The objective of this chapter is to synthesise 10 ligands. Five of these ligands will be *pentadentate Schiff base ligands with O-donor* in their spacer (class D) and the other five will be *hexadentate Schiff base ligands with two O-donor* in their spacer (class E). These ligands will be fully characterized and subsequently evaluated and discussed in Chapters 4 and 7. The ligands which were synthesized are therefore represented in Figure 3.3.

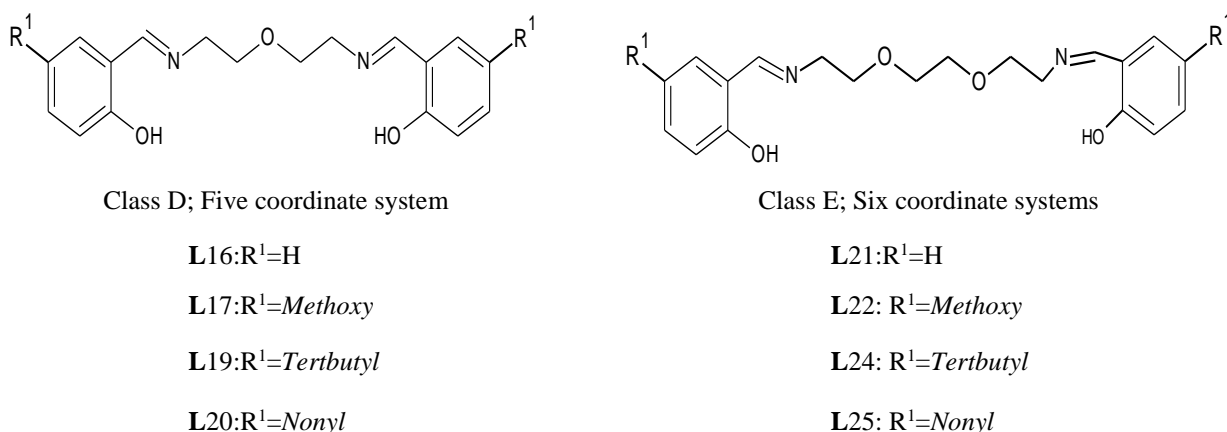


Figure 3. 3 The five coordinate N-O-N ligand systems (pentadentate) and the six coordinate N-O-O-N Schiff base ligands system (hexadentate) synthesized from five different aldehydes

There are two ligands which were synthesized bearing the *naphthyl* group as shown in Figure 3.4.

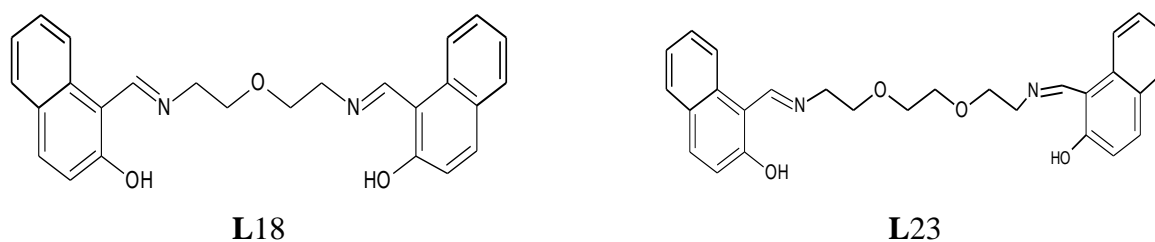


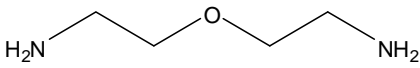
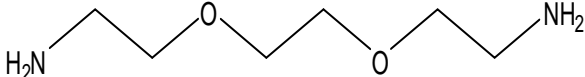
Figure 3. 4 The pentadentate and hexadentate naphthyl containing O-donor salen type of ligands

### 3.4 Chemicals and reagents

The list of chemicals and instrumentation used are similar to the ones used in Chapter 2 and include solutions and reagents such as the aldehydes and reaction solvents. The following two amines were used in this case 2, 2-dioxy ethylamine dihydrochloride and 2,2-[ethane-1, 2-diy]bis(oxy)]diethanamine which were bought from Sigma Aldrich and Alfa Aesar Co.

respectively. The 2, 2-dioxy ethylamine dihydrochloride was used after processing as shown in procedure 3.6.1 below to obtain the 2, 2-dioxy ethylamine shown in Table 3.1.

Table 3. 1 The diamine used

Name	Common name	Diagram
2-(2-Aminoethoxy) ethylamine	2, 2-oxydiethylamine	
2,2'-[ethane-1,2-diylbis(oxy)]diethanamine	1, 8-Diamino-3,6-dioxaoctane	

### 3.5 Preparation of 2, 2-oxydiethylamine

Sodium metal (1.04 g (0.0452 moles)) was dissolved in 20 ml dry absolute ethanol to form sodium ethoxide in a 100 ml round bottom flask. 2.66 g, (0.0150 mol) of 2,2-oxydiethylamine dihydrochloride was then added. The solution was then allowed to stir for 4 hours. The solution formed a faint yellow solution with white precipitate (sodium chloride). The resulting precipitate was then removed through filtration and the filtrate collected in a 100 ml volumetric flask and topped to the mark with dry ethanol to make 0.015 M solution of the diamine. The same ratio of sodium and the 2,2-oxydiethylamine dihydrochloride was maintained for successive preparation of 2,2-oxydiethylamine.

### 3.6 Synthesis of class D ligands

#### 3.6.1 Synthesis of ligand L16

These ligands were synthesized using the modified condensation method 2.9.1.1. The unsubstituted *salicylaldehyde* based ligand **L16** is used to illustrate the synthesis and characterization.

The ligand **L16** bearing the unsubstituted *salicylaldehyde* was synthesized as follows. 1.22g (0.0100 moles) of the *salicylaldehyde* was weighed and dissolved in 40 ml methanol under reflux and 0.0405 moles (30 ml) of the 2, 2-oxydiethylamine prepared above was measured and immediately dissolved in 20 ml ethanol. This was added slowly to the reaction solution over 30 minutes and then allowed to reflux for 24 hours. The reflux products were allowed to cool and the solvent removed via rotary evaporation. The yellow crystalline powder was obtained and dissolved in chloroform and washed 3 times with 10 ml water portions to remove

excess amine. The chloroform layer was dried with anhydrous sodium sulfate which was filtered off and the remaining chloroform layer removed using a rotary evaporator. The final yellow powder was recrystallized using ethanol which gave a yellow crystalline solid which was characterized as given in the experimental section 3.14.1. The results obtained are discussed below.

### 3.6.1.1 IR analysis results and discussions

The IR spectroscopy was therefore used in identifying the formation of the Schiff base product through the loss of the carbonyl peaks and the formation of the imine signal. For ligand **L16**, the *salicylaldehyde* starting material had the carbonyl functional group observed at  $1660\text{ cm}^{-1}$ . Upon formation of the Schiff base ligand **L16**, the imine (C=N) peak was observed with a relatively strong peak at  $1633\text{ cm}^{-1}$  as shown in Figure 3.5. The IR band at  $2855\text{ cm}^{-1}$  was attributed to the C-H stretching bands while the peaks at  $1283\text{ cm}^{-1}$  attributed to the C<sub>Ar</sub>-O stretching band. This result compares favourably to those of our previous produced N-containing ligands in Chapter 2. The other ligands in the same class were synthesized in the same manner. They were subsequently analysed using the FT-IR as shown in the stacked spectra in Figure 3.5.

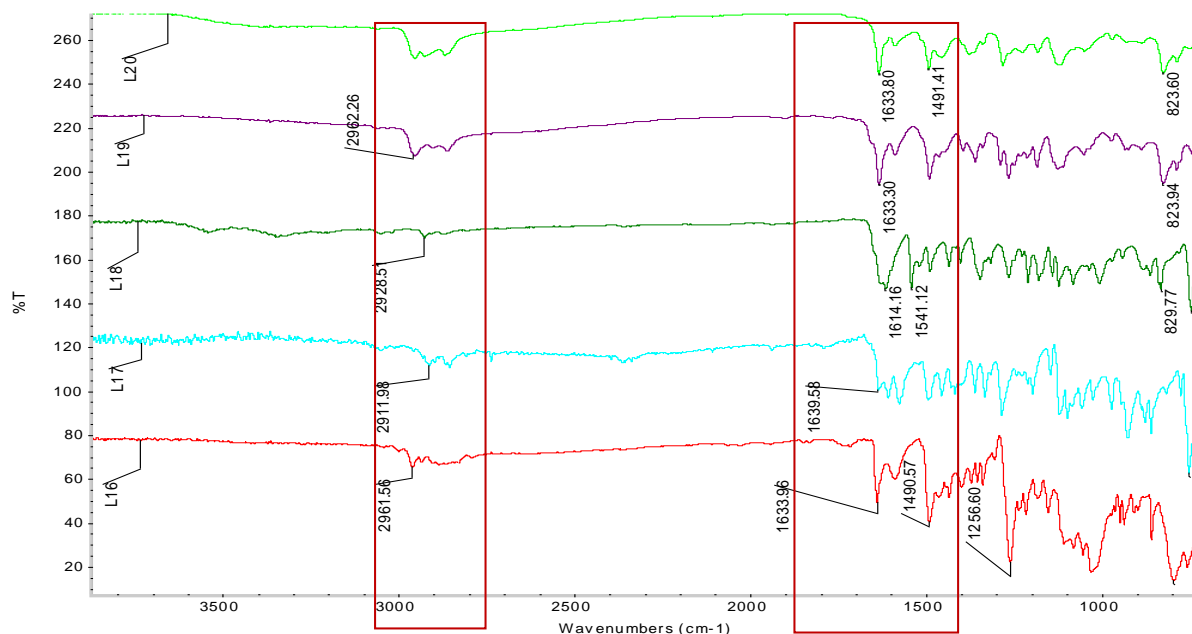


Figure 3. 5 The ATR spectra of the Schiff base products **L16**, **L17**, **L18**, **L19** and **L20**

From the spectra; the formation of the imine bond was observed from  $1639\text{ cm}^{-1}$  for the electron withdrawing *methoxy* substituent to  $1614\text{ cm}^{-1}$  for the *naphthylaldehyde* group. The IR spectra shows higher shift of the imine due to the *methoxy* group at  $1639\text{ cm}^{-1}$  indicating that

introduction of the *methoxy*-substituents into the phenyl rings of these ligands causes noticeable changes in electronic properties [124]. For the corresponding electron donating groups, the bulky *tert-butyl* group and the straight chain *nonyl* group both showed relatively small shift of the imine at  $1633.30\text{ cm}^{-1}$  and  $1633.80\text{ cm}^{-1}$  respectively. The difference in the shift of the imine peak in the series can be attributed to the difference in inductive effect of the different substituents [61, 124, 125].

### 3.6.2 $^1\text{H}$ NMR analysis discussions

The synthesized samples were then analyzed through the  $^1\text{H}$  NMR and  $^{13}\text{C}$  NMR using the 400 MHz instrument. The procedure for analysis was similar to that used in Chapter 2.7.2. The representative spectrum of ligand **L16** is shown in Figure 3.6.

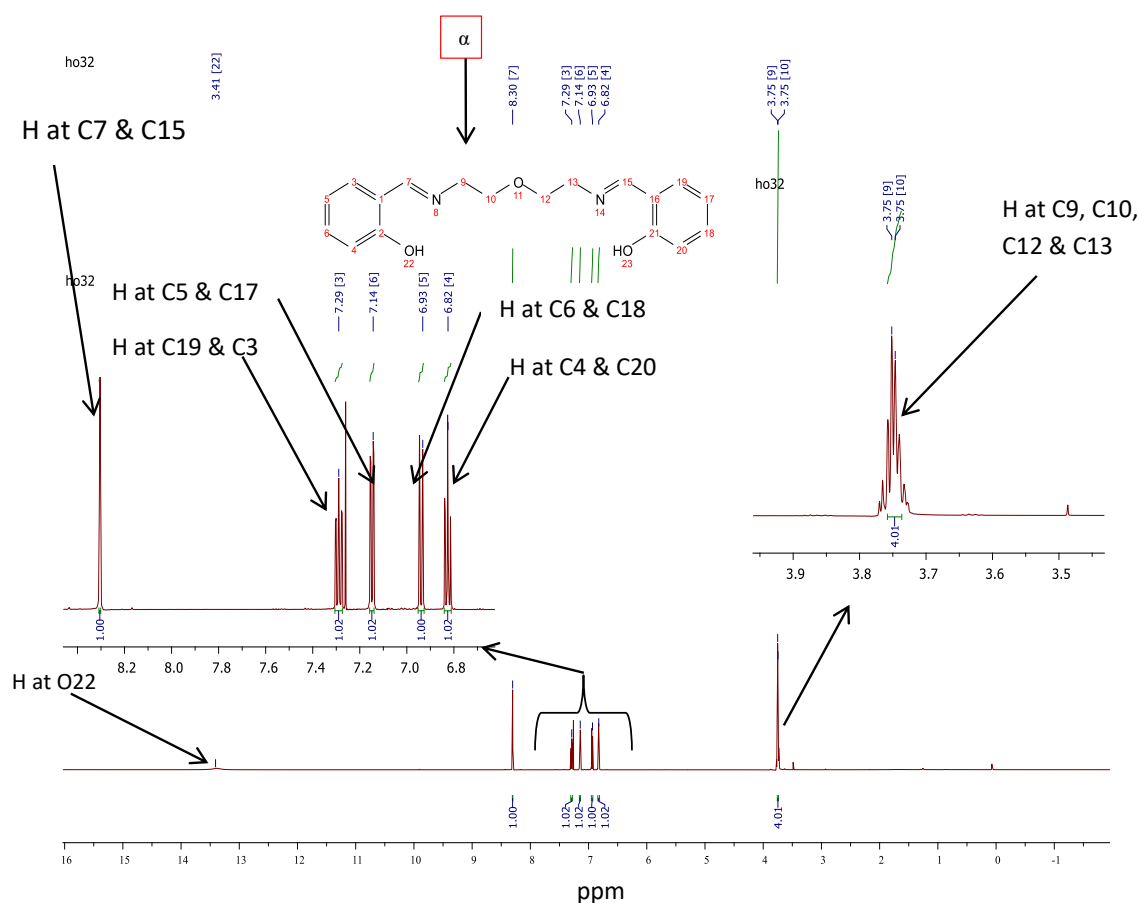


Figure 3. 6 The  $^1\text{H}$  NMR spectrum of ligand **L16** in  $\text{CDCl}_3$  with the different protons numbered by the position of the appearance of the carbon group it is attached to. (The insert shows the higher magnification of the aromatic region and the alkyl region expanded).

From the obtained results in Figure 3.6 for ligand **L16**, the  $^1\text{H}$  NMR spectrum showed the formation of the expected condensation products with the shift of the different proton signals



flexibility or symmetry of the ligand solution. The samples were therefore analysed under variable temperature  $^1\text{H}$  NMR analysis from temperature range of  $-25\text{ }^\circ\text{C}$  to  $25\text{ }^\circ\text{C}$ . The results are shown in Figure 3.9.

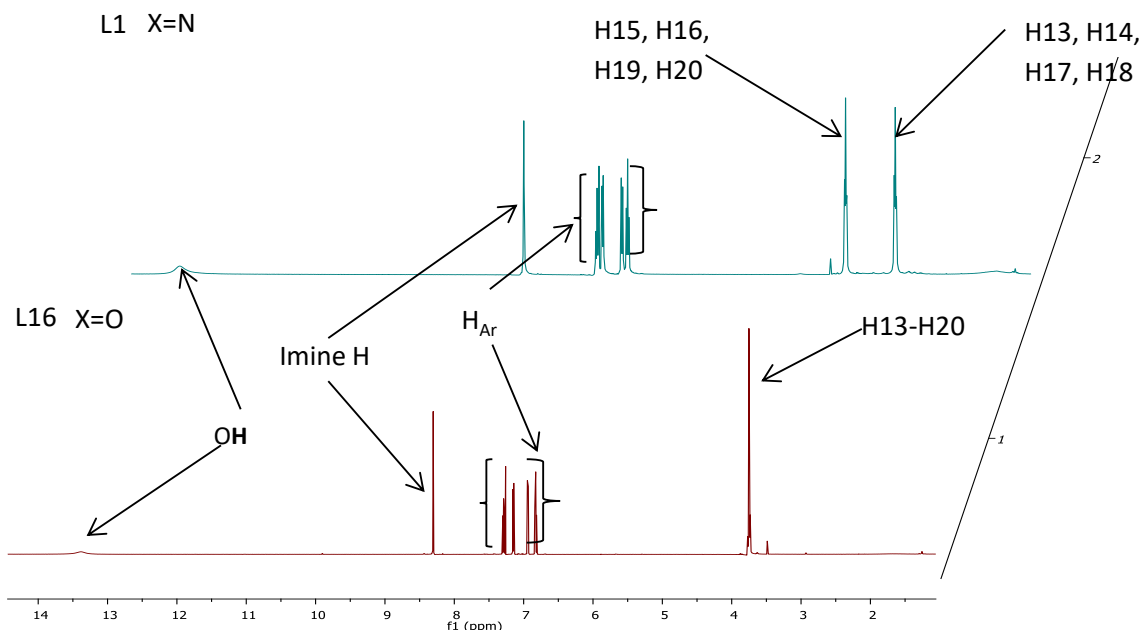


Figure 3. 8 Stacked  $^1\text{H}$  NMR spectra of **L1** and **L16** in  $\text{CDCl}_3$  (The two spectra are stacked at  $15^\circ$  angle to show the differences in the effect of the change of donor group X on the proton signal peaks).

### 3.6.2.1 Molecular dynamism studies

The variable temperature  $^1\text{H}$  NMR analysis did not show any resolution of the peaks under different temperatures, however a small shift of the OH peak at 13 ppm was observed as shown by Figure 3.10. These results highlighted the fact that by reducing the temperature to  $-25\text{ }^\circ\text{C}$  the OH signal becomes much more pronounced. From these results it can be postulated that the spacer protons of the *pentadentate* O-donor are chemically equivalent. The shift of the OH proton can be attributed to the presence of hydrogen bonded tautomer [61]. The shift of this signal and the strength of this signal can therefore be explained due to the stability of the H-proton of the hydroxyl group on the phenolic O-atom. The shift of this proton had already been discussed in Chapter 2.8.3.6 and this result can therefore be used as a confirmation of the tautomeric behaviour of the hydroxyl proton. Further analysis on this class of ligand is shown by the crystal structure of these ligands in Chapter 4.

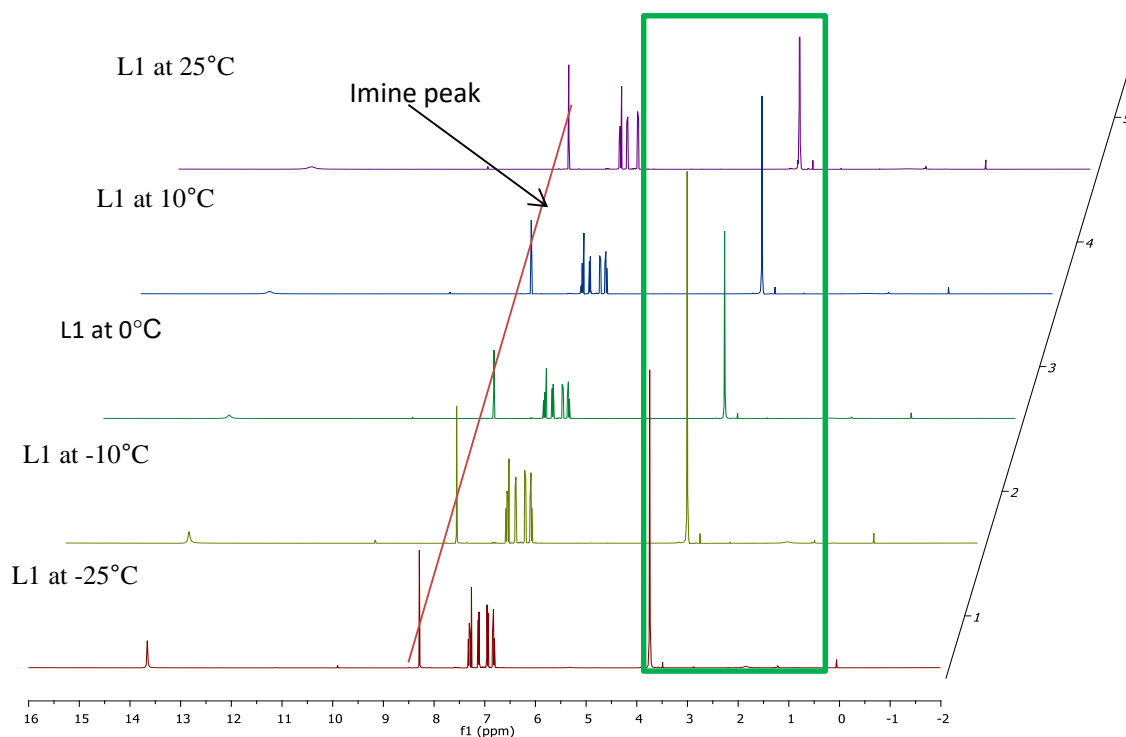


Figure 3. 9 The stacked  $^1\text{H}$  NMR spectra of ligand **L16** in  $\text{CDCl}_3$  at temperatures  $-25$ ,  $-10$ ,  $0$ ,  $10$  and  $25$  °C. (The spectra are stacked at  $15^\circ$  angle to show the differences in the effect of the temperature on the signal peaks).

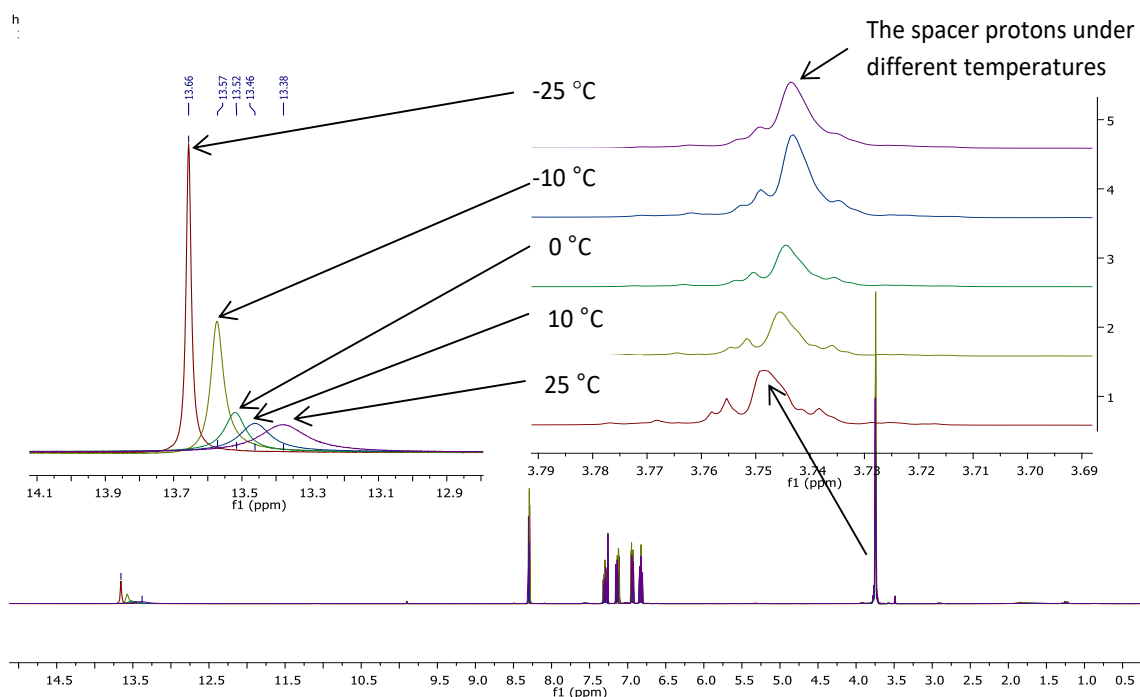


Figure 3. 10 Superimposed  $^1\text{H}$  NMR spectra of ligand **L16** in  $\text{CDCl}_3$  at temperature  $-25$  °C,  $-10$  °C,  $0$  °C,  $10$  °C and  $25$  °C (The insert shows the magnified shift of the OH proton at different temperatures, and the magnified stacked spectra of the spacer protons also at different temperatures).

### 3.6.2.2 Effect of substituents on the $^1\text{H}$ NMR

The results from the analysis of the *pentadentate* ligands bearing the different substituents on the phenyl ring and the *naphthylaldehyde* did not differ much from the above spectra. All the signals were accounted for as shown in Figure 3.11. The results also show that the spacer protons discussed above are chemically equivalent.

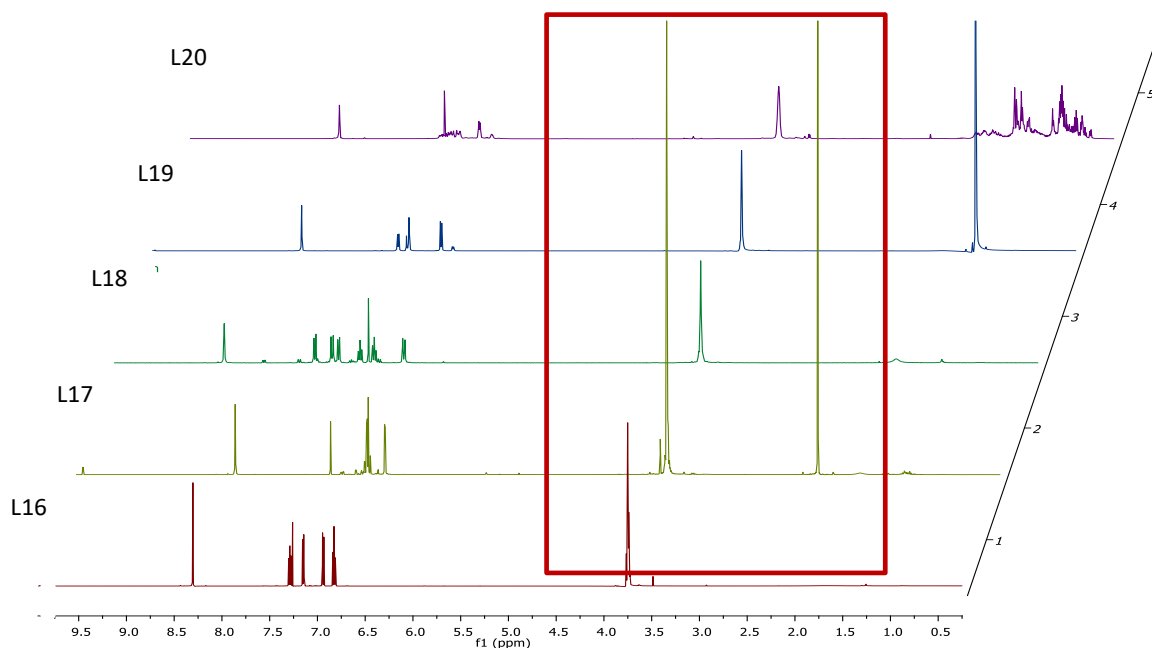


Figure 3. 11 The  $^1\text{H}$  NMR stacked spectra of ligand L16, L17, L18, L19 and L20 in  $\text{CDCl}_3$  (The spectra are stacked at  $15^\circ$  angle to show the differences in the effect of the change of substituents).

From the results shown in Figure 3.11 there was no observable change in the deconvolution of peaks even with the change of substituent which causes different inductive effects to the  $\alpha'$  proton of the imine. These spacer protons could not be resolved and appears as one signal which further indicates that they are chemically equivalent despite the two different donor groups attached to it. It is therefore possible to hypothesize that the O-donor and the imine bond have an equal deshielding effect; consequently, the addition of the different substituent on the phenyl ring would not alter the electronic system of the molecule and therefore no effect on the overlap of these protons.

### 3.6.2.3 $^{13}\text{C}$ $\{^1\text{H}\}$ NMR Analysis

The results from the  $^{13}\text{C}$   $\{^1\text{H}\}$  NMR in this case showed the expected peak of the different carbons as shown in Figure 3.12.

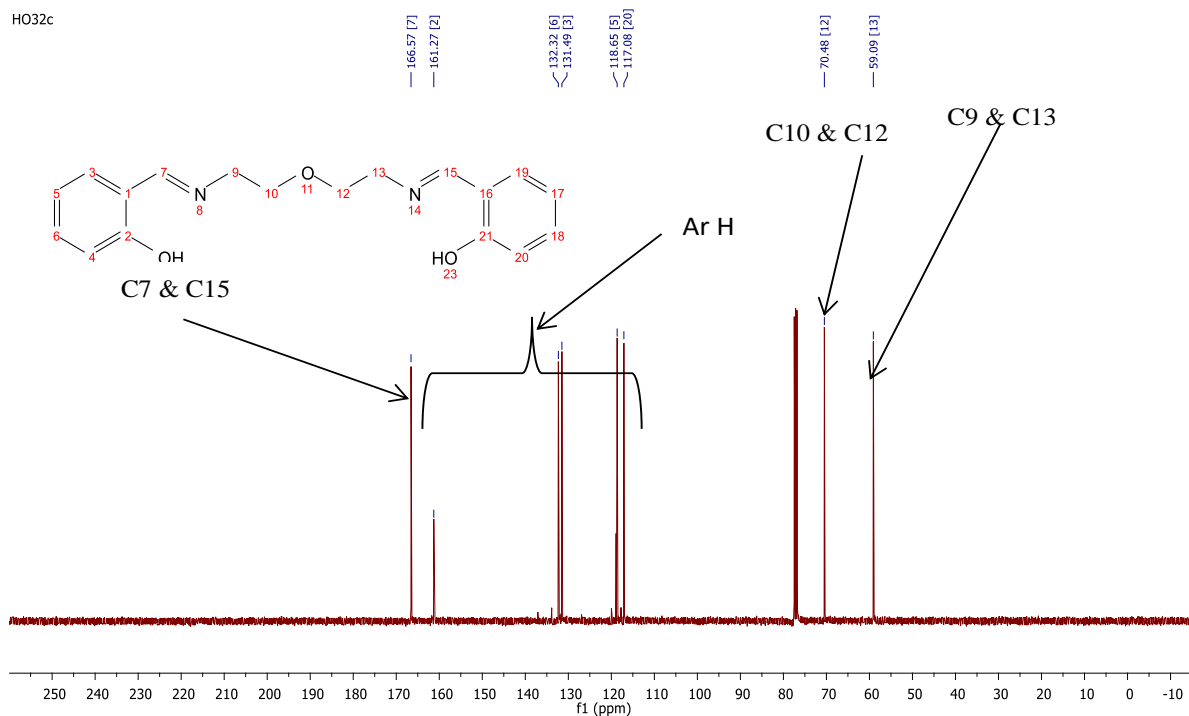


Figure 3. 12 shows the spectrum of  $^{13}\text{C}$   $\{^1\text{H}\}$  NMR, for ligand **L16** for purposes of this discussion in  $\text{CDCl}_3$ .

The spectra for the others are shown in the stacked diagram in Figure 3.13.

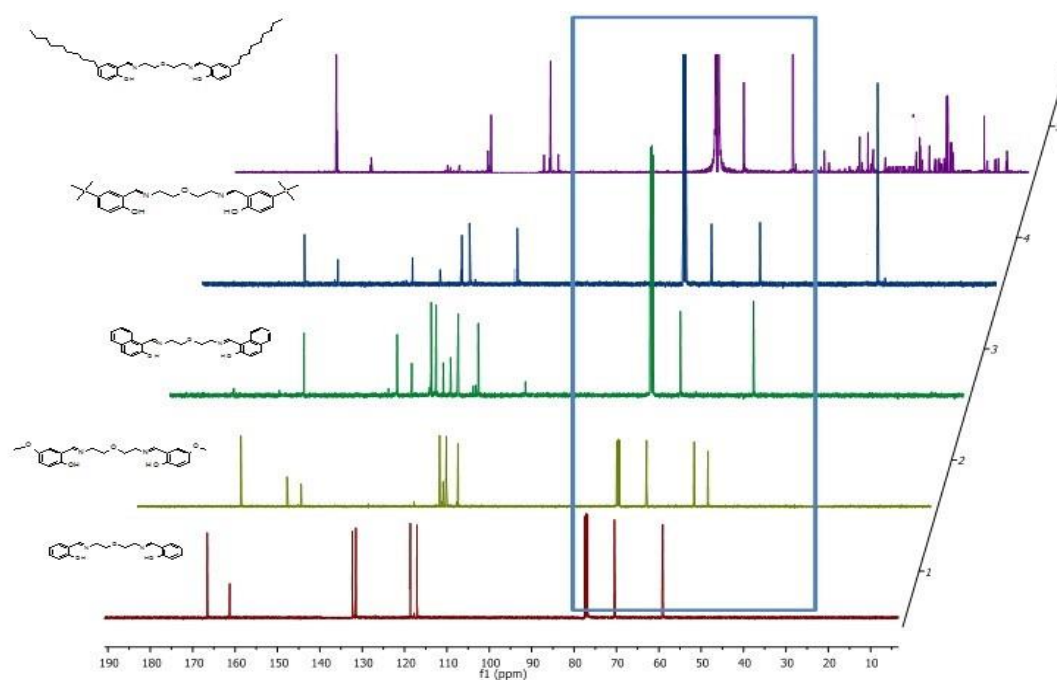


Figure 3. 13 The stacked spectra of  $^{13}\text{C}$   $\{^1\text{H}\}$  NMR of class D ligands in  $\text{CDCl}_3$ .

The imine signal for **L16** was observed at 165 ppm, the aromatic carbons were assigned to the signals from 120-160 ppm with the aromatic phenyl carbon attached to the **OH** being the outlier between 150-160 ppm. One of the carbons attached to the imine system in the aromatic system

is overlapping to another. The two proton decoupled spacer carbons were also observed in this case at 59 ppm and 69 ppm as expected due to the wider chemical shift range of the  $^{13}\text{C}$   $\{^1\text{H}\}$  NMR as compared to the  $^1\text{H}$  NMR. This was also the case for the other ligands in this class; all the carbons are assigned in section 3.14.

### 3.6.3 General discussion of the NMR results

From the above NMR result the desired O-donor ligands with the different substituents were synthesized. It was however shown that the spacer carbons are non-equivalent from the various studies. However, for the  $^{13}\text{C}$   $\{^1\text{H}\}$  NMR results, the two carbon signal peaks were observed. These results can be shown by the correlation studies of the proton and carbon HSQC (Heteronuclear Shift Quantum Correlation) analysis as shown in Figure 3.14.

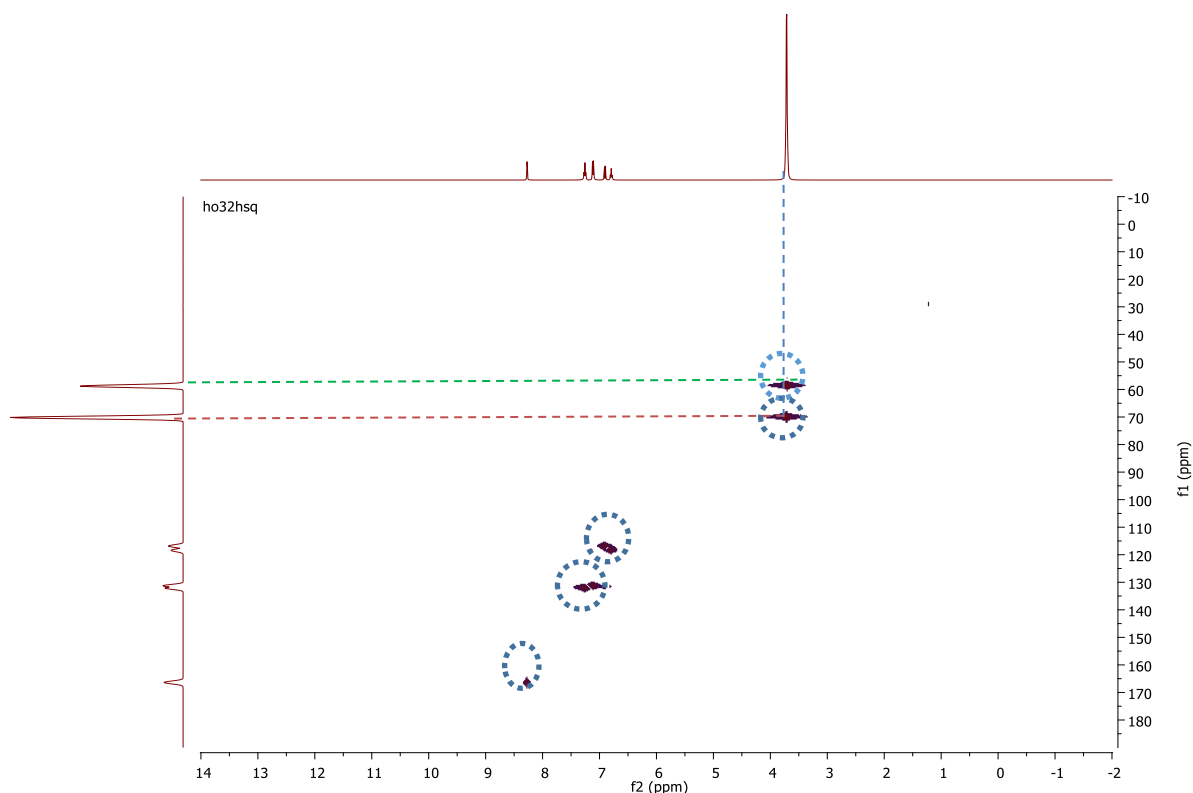


Figure 3. 14 HSQC NMR results for ligand **L16** in  $\text{CDCl}_3$

The reason for the protons not being resolved on the  $^1\text{H}$  NMR was postulated to be due to the symmetry and the flexibility of the ligand which renders the spacer protons to be equivalent.

### 3.7 Synthesis of hexadentate OCH<sub>2</sub>CH<sub>2</sub>O- ligands

This class of ligands were synthesized from 2,2'-[ethane-1,2-diylbis(oxy)]diethanamine spacer. The existence of the extra O-donor group increases the cleft between the two imines. This property will therefore enable these ligands to be structurally analogous to the *oligo-salen* ligands discussed in the introduction. Due to the presence of the imine group in these ligands. This enabled the ligand to be synthesized as per the above method 3.1 and all the results are given in section 3.14.2 of the experimental section. These results are discussed below.

### 3.8 Results and discussion

Equally in this class of ligands the formation of the Schiff base products in this class of ligands was confirmed by the formation of the imine peak as discussed in the analysis below. However, one of the ligands (**L22**) in this class was serendipitously observed to undergo a photochromic effect. This ligand was studied further for the photochromic effect as discussed in section 3.9. The initial results obtained for the stable product was nevertheless studied for the electronic and steric effect together with the other ligands in the same class. All the characterization results are discussed below.

#### 3.8.1 IR analysis

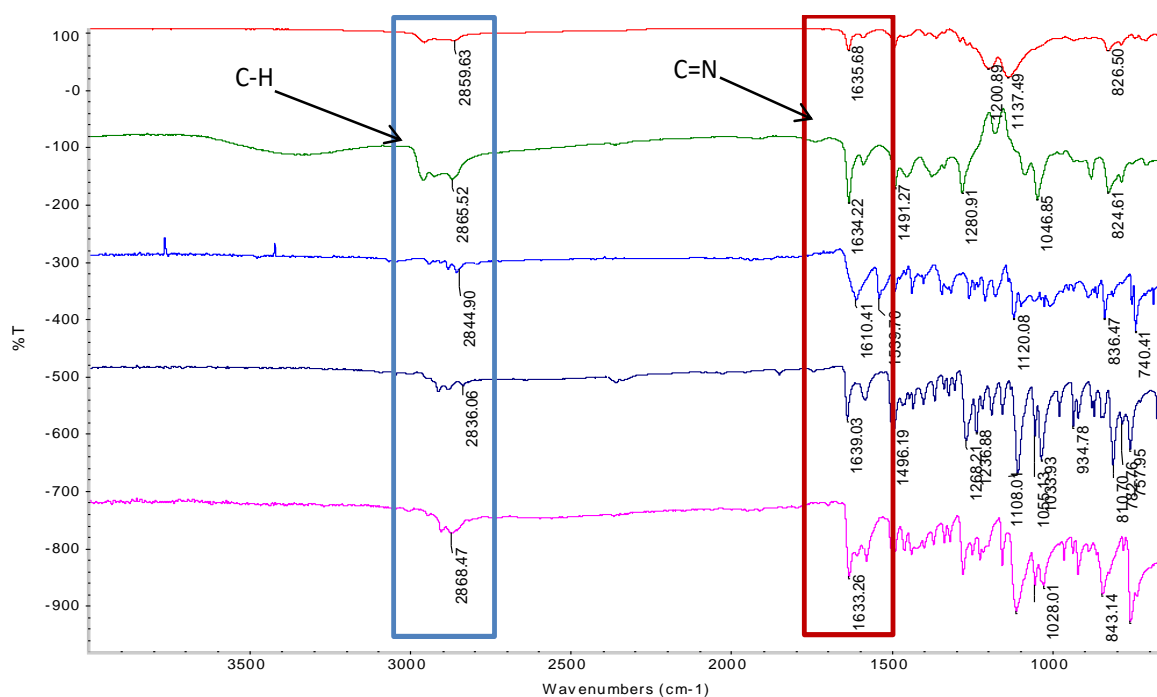


Figure 3. 15 Stacked IR spectra of class E ligands

The obtained results indicate that the imine functional group was observed between  $1633\text{ cm}^{-1}$  to  $1639\text{ cm}^{-1}$  for ligands **L21** to **L25** as shown in Figure 3.15. The spectra indicate that the formation of ligand **L22** with the *methoxy* substituent has a larger red shift compared to the other ligands in the same series with the imine peak observed at  $1639\text{ cm}^{-1}$ . This shift was attributed to the *methoxy* substituent compared to the base ligand the unsubstituted **L21** at  $1633\text{ cm}^{-1}$ .

### 3.8.2 $^1\text{H}$ NMR analysis

The unsubstituted *salicylaldehyde* based ligand **L21** was considered as the representative ligand. The  $^1\text{H}$  NMR analysis was done and the result obtained is shown by the spectrum in Figure 3.16.

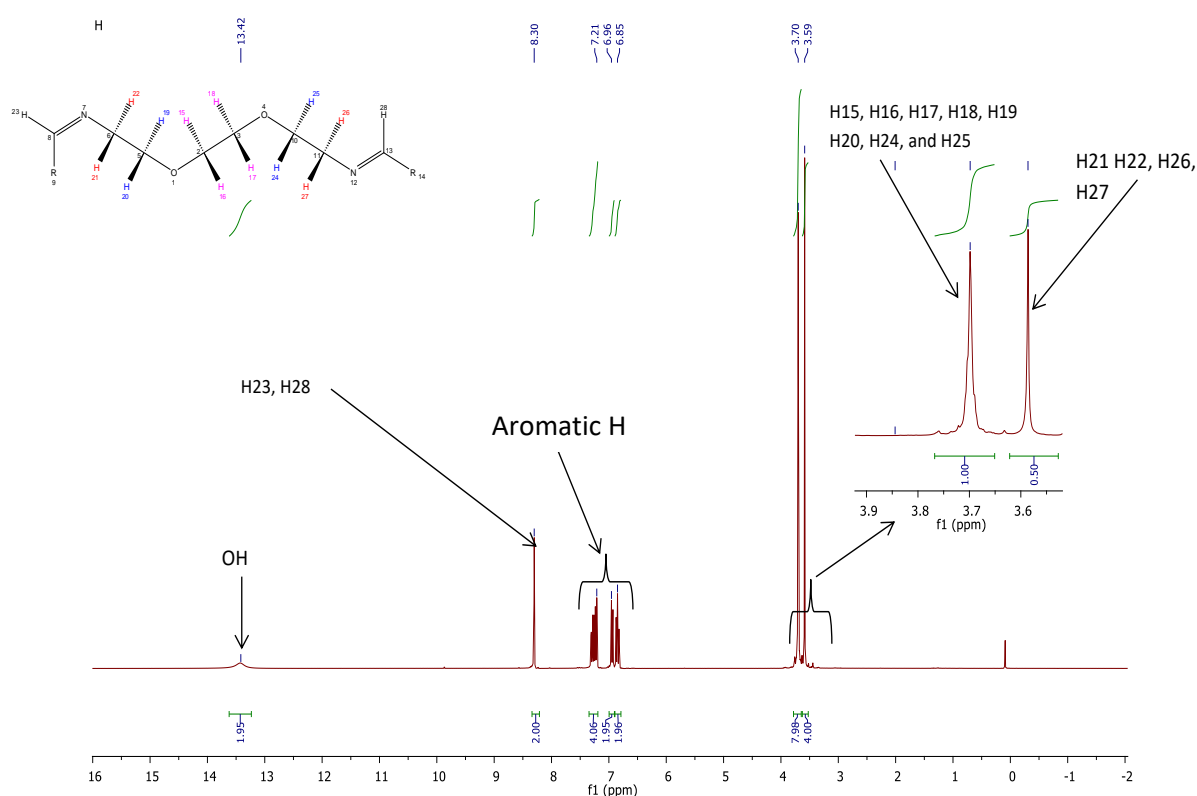


Figure 3. 16  $^1\text{H}$  NMR for Ligand **L21** in  $\text{CDCl}_3$  with explicit hydrogen atoms no observable third signal for the spacer protons.

The results from this *hexadentate* ligand system indicate that the products were obtained with the imine peak observed at 8.30 ppm as shown in Figure 3.16 for ligand **L21**, the aromatic region was observed between 7.21-6.85 ppm. For the spacer protons between 3.70 ppm and 3.59 ppm, these were observed to be comparable to the ones obtained for the *pentadentate* O-system discussed above. From the spectrum shown in Figure 3.16, only two signals were

observed on the  $^1\text{H}$  NMR spectrum with integration ratio of 2:1, with the downfield signal integrating to 8 protons while the upfield signal integrates to 4 protons. The protons for **H21-H22** and **H26-H27** are chemically equivalent indicated by the upfield signal with the 4 protons. The protons **H15-H20** and **H24-H25** are also chemically equivalent shown by the downfield signal with the 8 protons. This was similar in comparison to the O-donor *pentadentate* system where the overlap of the 4 protons of **H19-H20** and **H24-H25** occur in a similar manner to the *pentadentate* system discussed above.

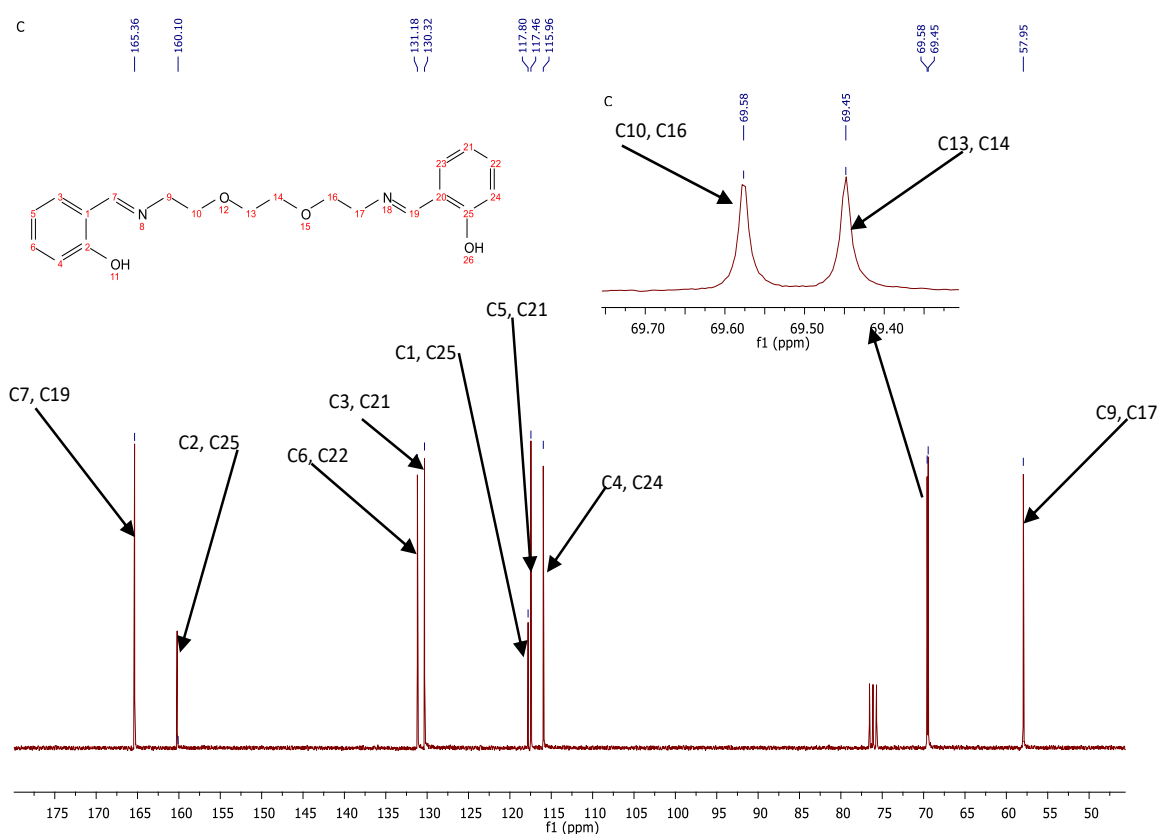


Figure 3. 17 The  $^{13}\text{C}$   $\{^1\text{H}\}$  NMR for ligand **L21** system in  $\text{CDCl}_3$ .

The  $^{13}\text{C}$   $\{^1\text{H}\}$  NMR was also obtained showing the non-equivalence of the spacer protons indicating 3 signals (70.62 ppm, 70.49 ppm and 58.99 ppm,) as shown in Figure 3.17. The sample was also further studied through the HSQC analysis as shown in Figure 3.18. In this case a third signal was observed at 2.12 ppm equivalent to the third C-atom observed in the  $^{13}\text{C}$   $\{^1\text{H}\}$  NMR that was not observable in the proton NMR.

Further analysis of these results shows that the  $^1\text{H}$  NMR spectrum did not show the resolution of the spacer protons as expected, however under the HSQC analysis two signals are observed in relation to the carbon atoms. Because of this resolution under HSQC and the lack of

symmetry, this indicates that these protons are not similar as shown in Figure 3.18. This was observed to be different from the *pentadentate* systems which have symmetry which leads to overlapping of the signals and hence only one signal, whereas the *hexadentate* systems without the symmetry will not have the same overlap of protons.

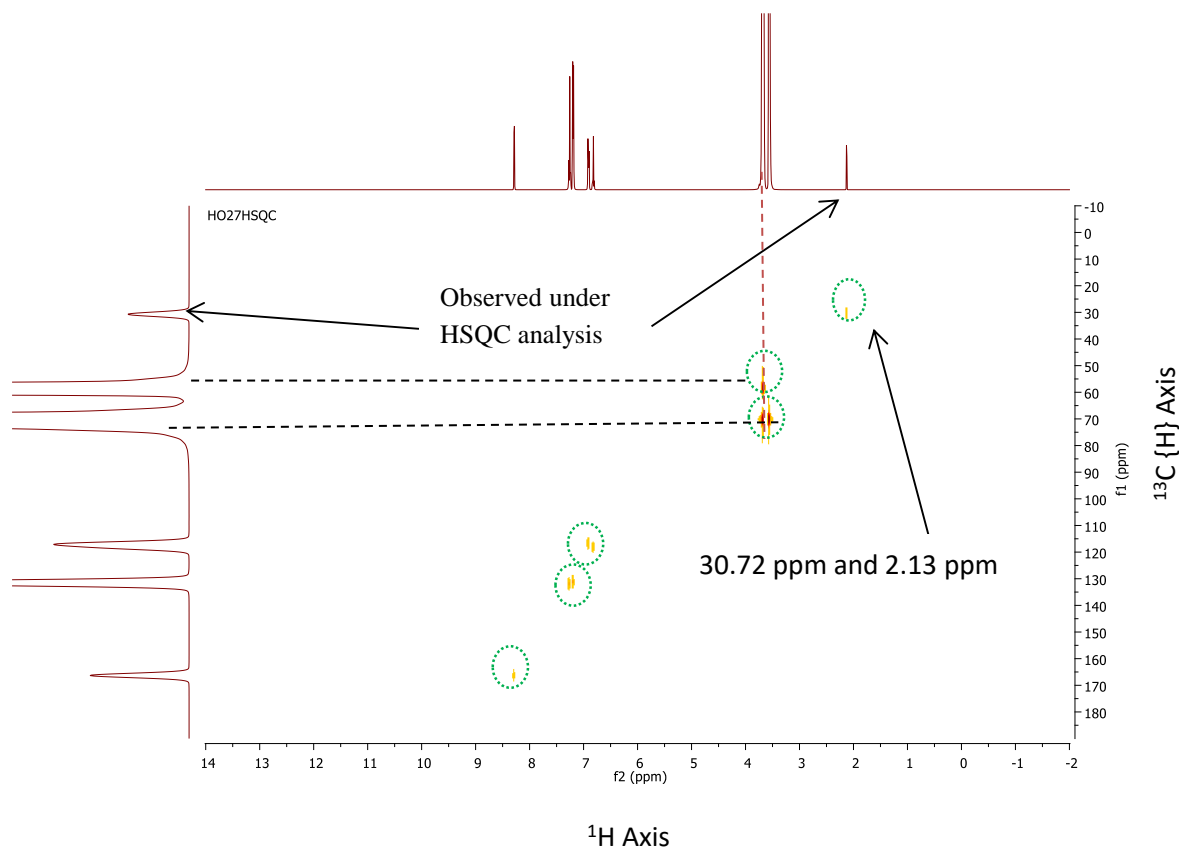


Figure 3. 18 HSQC analysis of ligand **L21** in  $\text{CDCl}_3$

### 3.8.2.1 Effect of added substituents

The introduction of the added substituent on the phenyl ring did not have much better resolution of these protons as shown in the stacked  $^1\text{H}$  NMR spectra in Figure 3.19. In comparison to the base ligand **L21**, the imine peak was shown to shift slightly due to the inductive effect caused by adding the different substituents to the phenyl ring as shown in the imine shift of all the ligands in Table 3.3.

Analysis of the electronic effect due to the added substituent therefore shows that the *methoxy* group with the electron withdrawing group has the greatest chemical shift as shown by the order starting from the highest chemical shift to the lowest as *naphthyl* > *nonyl* > *tert-butyl* > *H* > *methoxy* on both the  $^1\text{H}$  NMR, and the  $^{13}\text{C}$   $\{^1\text{H}\}$  NMR.

The *tertbutyl* group and the *nonyl* group are observed to shift the imine proton towards down field. This was consistent with Pouramin *et al.* [126, 127] and Andrade *et al.* [61] working with various Schiff base ligands. On the other hand, the IR spectra showed the order of the red shift to be from *naphthyl* <H <*tertbutyl*<*nonyl* <*methoxy*. From the IR, the *methoxy* containing substituent was observed to have the largest red shift in all the ligands.

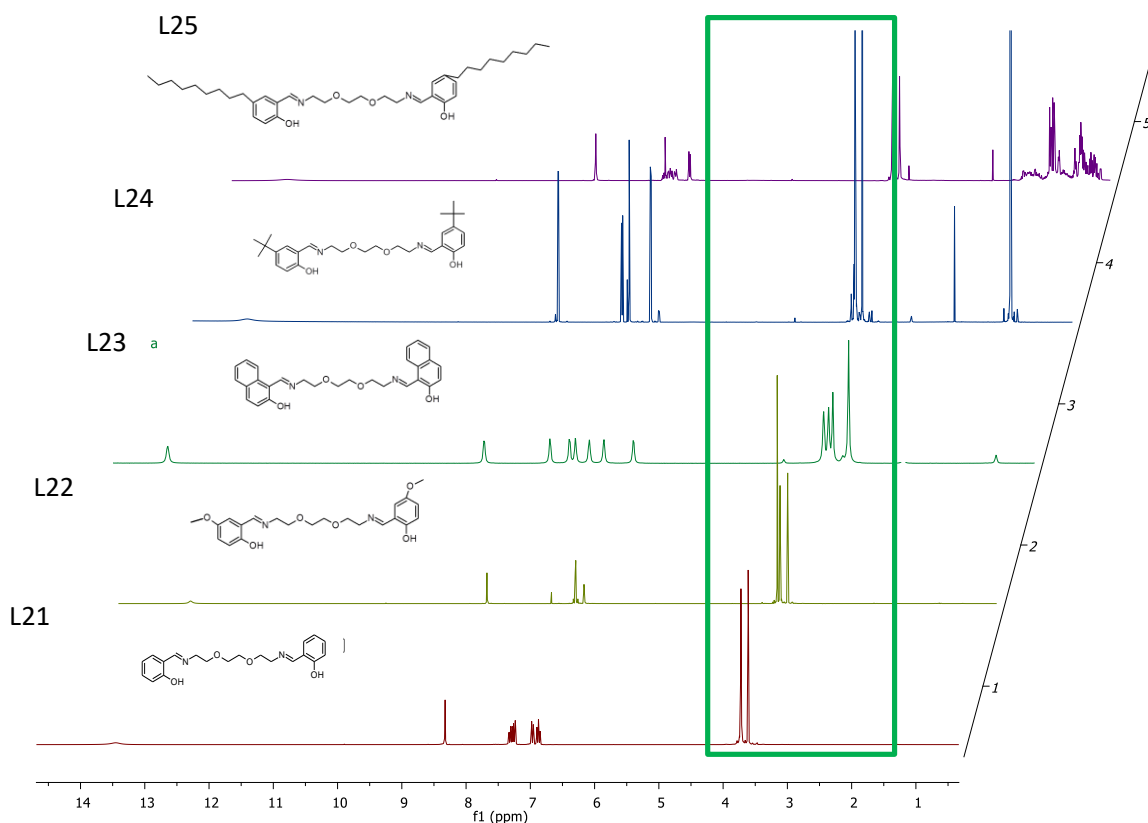


Figure 3. 19 The stacked  $^1\text{H}$  NMR spectra of hexadentate Schiff base ligands O-donor salen type ligand systems in  $\text{CDCl}_3$ .

### 3.8.2.2 Discussion of the effect of the added donor groups

The effect of the change in linker or the increased number of donor groups from 5 to 6 donors is shown by the shift in imine peak in Table 3.2. This indicates that the change of the linker has marginal effect on the imine peak in comparison to the effect due to the substituent of the phenolic ring. The use of analogous ligands bearing different substituents on the phenyl ring shows a much broader shift as compared to the shift due to the added donor groups. While these results are not giving much insight, the overall effect of the systematic increase in the number of the donor groups according to the chelate effect is expected to be much more pronounced when dealing with solvent extraction studies covered in detail in Chapter 7.

Table 3. 1 The spectra showing the shift of the imine in the different substituents of the different O O-donor salen type of ligands

	IR	HNMR	CNMR		IR	HNMR	CNMR
	cm-1	Ppm	ppm		cm-1	ppm	ppm
<b>L16</b>	1633	8.30	166.57	<b>L21</b>	1633	8.21	165.36
<b>L17</b>	1639	8.26	166.23	<b>L22</b>	1639	8.17	165.05
<b>L18</b>	1614	8.77	159.26	<b>L23</b>	1611	8.64	176.89
<b>L19</b>	1633	8.37	166.86	<b>L24</b>	1634	8.33	166.93
<b>L20</b>	1634	8.37	166.91	<b>L25</b>	1635	8.34	167.06

### 3.9 Photochromic effect studies

As had been mentioned in section 3.8 above, ligand **L22** shown in Figure 3.20 below containing the 5-methoxy-substituent was observed to undergo colour change in the presence of direct sunlight.

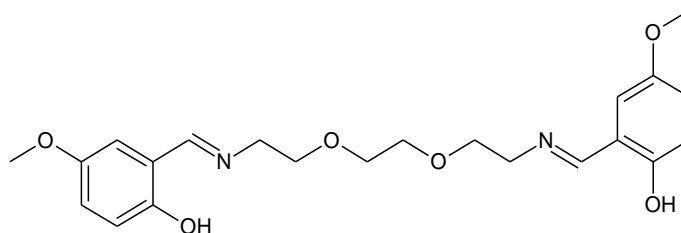
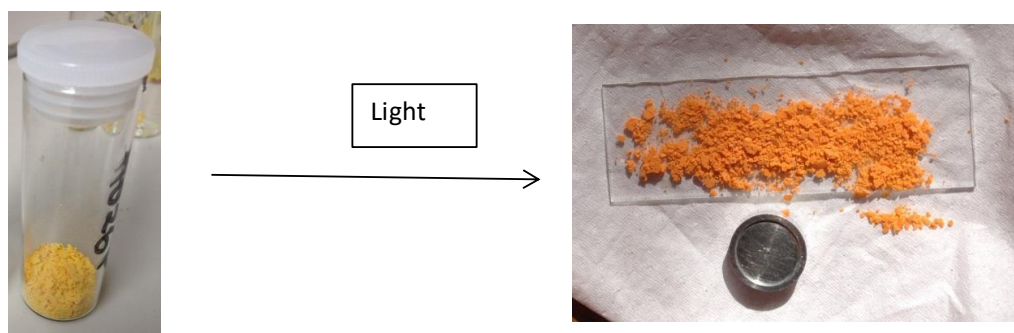


Figure 3. 20 schematic of Ligand **L22**

This ligand was observed to undergo photochromic colour change from a bright yellow product in the lab to a bright orange in the presence of direct sunlight as shown in Figure 3.21. From further analysis of this product this effect was observed to be limited to direct sunlight and not under ordinary fluorescent light in the laboratory. This photochromic colour transition was also limited to this ligand alone and was not observed for the other ligands in this series. It was also observed that when the ligand is dissolved in a solvent such as ethanol or chloroform, the colour transition is no longer observed. For this reason, the study of this ligand using the solvent based analytical technique was ruled out. Therefore, these ligands were analysed using solid state analytical techniques that were available to try and show how this ligand is able to undergo colour transition.



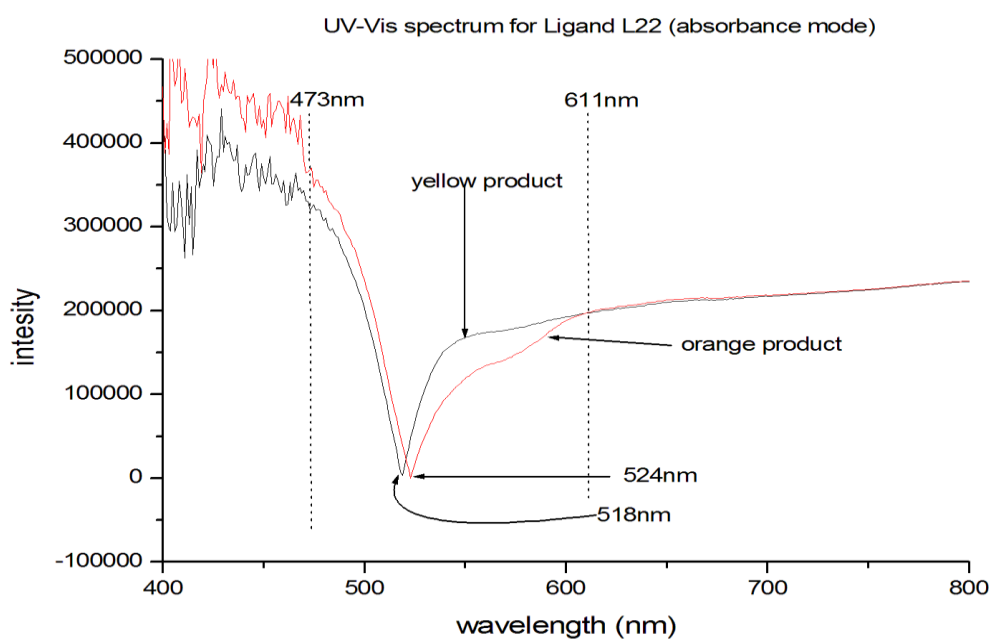
L22 in absence of direct sunlight

L22 in direct sunlight

Figure 3. 21 ligand **L22** and B the ligand **L22** in direct sunlight

### 3.9.1 Solid state UV-Vis Analysis

From the initial naked-eye observation, it was observed that the transition of the colour change is very fast, when the sample was left in open sunlight. Figure 3.21b shows that before transferring the sample to the sample holder of the solid-state UV spectrophotometer, the colour had started to change back to yellow already. The solid-state UV-Vis was therefore carried out in Specord 210 plus analytica solid state UV-Vis spectrophotometer. This was also used to show a slight difference in the transition of the yellow sample and orange sample as shown in Figure 3.21 and discussed as follows.

Figure 3. 22 Solid-state UV of ligand **L22**

The UV analysis in Figure 3.22 shows there is a slight difference in the intensity of the two-coloured products. The yellow product indicates minima intensity at 518 nm while that of the orange product is at 524 nm. The spectra also show that the yellow product has a smooth curve which indicates the uniformity of the transition of the yellow product while that of the orange product indicates a slight shift at 574 nm. Both products show absorbance of radiation at low wavelengths, however at higher wavelength the two products seem to emit radiation from 611 nm to 473 nm.

This is indicated by a deep drop in the absorbance intensity as shown by Figure 3.22. This result shows that transition of the product occurs in this range. It however does not show much more information about the difference of these two products since the colour change was observed to occur very fast. The UV-Vis analysis results however indicate that the transition is much longer and could not be observed by naked-eye. From the above result it can be concluded that there was some form of transition within the molecule in the solid.

Since this ligand was observed to emit or undergo fluorescence at wavelengths above 450 nm, the colour transition was therefore studied for this ligand using the confocal microscope.

### **3.9.2 Confocal microscopy**

Single molecule confocal microscopy is a technique used for study of materials or biological cells using lasers that can be single-plane confocal picture sequences taken at different time intervals at different wavelength [128]. The resultant picture from the study indicates the effect of the radiation on the ligand, with the ligand observed to absorb radiation of wavelengths below 494 nm while it fluoresces at radiation above 503 nm as shown in Figure 3.23.

The result obtained from the confocal study complements the result obtained from the UV study that shows that the ligand has the ability to absorb and emit radiation. From the images in Figure 3.23 the results show that there is no fluorescence below 494 nm, this indicates that the high energy radiations are being absorbed by the molecules and hence no fluorescence observed. However, for the radiations above 503nm, the fluorescence effect was observed in this ligand in solid state. The other effect from this study indicates that the bandwidth of emitted radiation is very wide from about 639 nm to 503 nm.

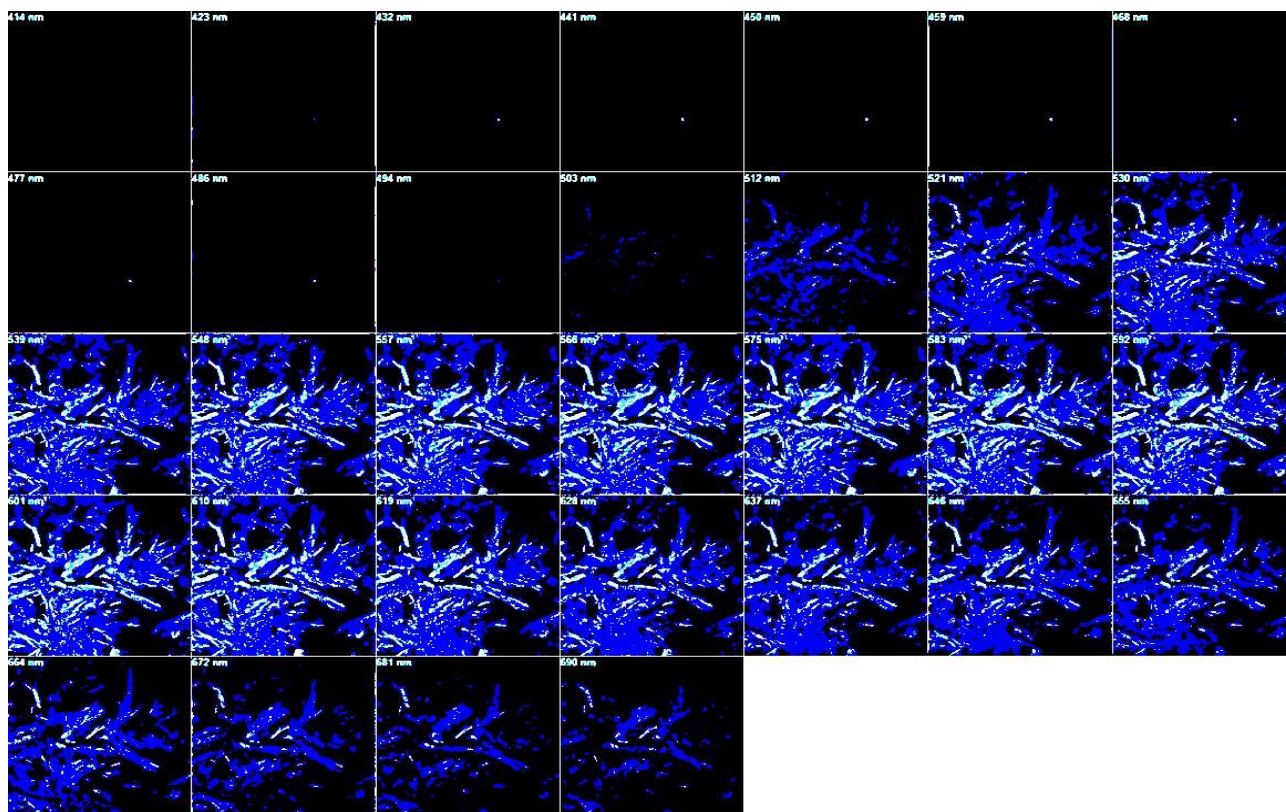


Figure 3. 23 Confocal microscopy image of ligand **L22** picture. (Picture quality obtained from instrument contrast and brightness has been adjusted for better presentation, original pictures available in the provided disc).

The difference between the results from the UV-Vis and confocal analysis is due to the difference in principles through which the two instruments work. The UV-Vis analysis works on the principle of irradiating the samples at different wavelength and recording the absorbance or transmittance of the radiation on the other hand in confocal microscopy tightly focused light spot (laser light) from an illumination pinhole is used to scan a sample through a small detection pinhole at the conjugate image plane. This pinhole allows light originating from the nominal focus to pass while the emitted light from the sampling volume is detected by a photodetector such as a photomultiplier tube or an avalanche photodiode, and a digital image is then constructed by mapping the detected light signal in each scanning spot [128].

By studying this ligand under confocal microscope, it can be observed that the colour transition occurs with release of different wavelength indicated by the rich colour changes shown by Figure

3.24. Since the colours could not be observed by naked eye it is possible to conclude that the colour transition occurs so fast that it cannot be observed by naked eye.

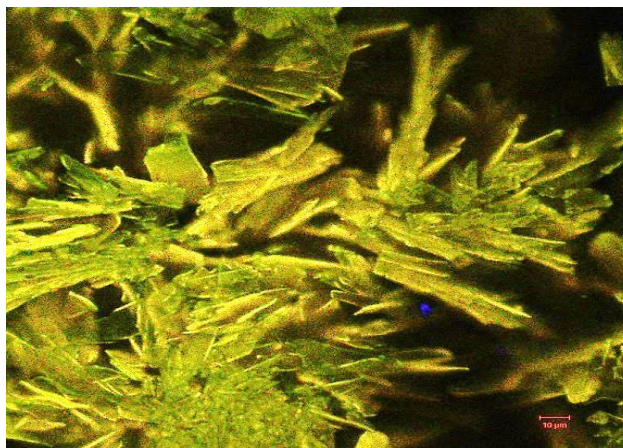


Figure 3. 24 The rich colour interplay due to transition emission of ligand **L22** from 503 nm-639 nm.(Picture quality obtained from instrument contrast and brightness has been adjusted for better presentation original picture provided in the disc).

The sample was also analysed by adding a small drop of ethanol to the samples on the slide and the result indicated that the emission was no longer observed in the confocal microscope. These results therefore indicate that the transitional effect is restricted to the solid state of this molecule. This therefore implies that this effect is related to salient features of crystallinity of the solid samples. It was however not possible to obtain a crystal large enough to be used for single crystal analysis.

### 3.9.3 Discussion of the photochromic study

From literature, the colour change in an organic molecule can be attributed to several factors. These include factors such as structural isomerization for example in ring-opening or closing [129-131] in an organic molecule, free radical formation in the organic molecule [131-133], cis–trans isomerization of an organic molecule [131, 134, 135] or when there is tautomerism in the organic molecule [131, 136, 137]. From the results obtained thus far indicating that some of these ligands undergo tautomerism it is possible to propose that the colour change is attributed to tautomeric behaviour of these ligands. For studies of ligand **L8** in Chapter 2.9.5 the tautomeric behaviour was observed to be due to heat (thermochromic effect). It is however the first time in this case that a reversible colour change is observed for this ligand due to light (photochromism).

### 3.10 Mass spectrometry

The next consideration in the analysis of these ligands was the mass spectrum analysis. The mass analysis was also done on a Waters Synapt G2 High resolution Mass Spectrometer; the conditions are discussed in Chapter 2 with the molecular ion observed as  $m/z$ . The ESI-MS spectrum was obtained for all the ligands bearing the O-donor groups with the analysis carried out in the positive mode. The results were consistent with the results obtained for the N-donor Schiff base ligands in Chapter 2.

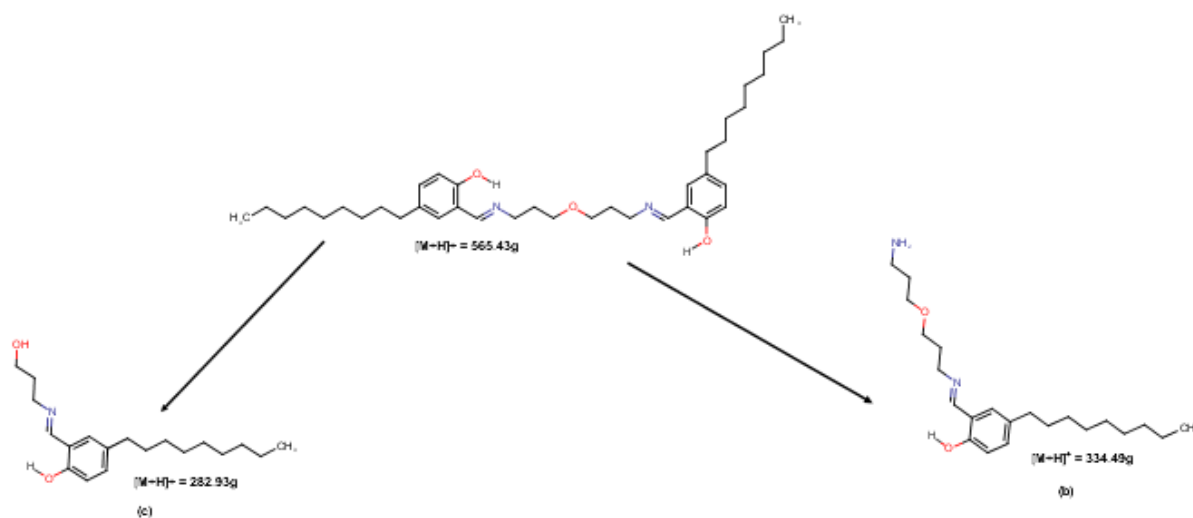


Figure 3. 25 The fragmentation pattern of ligand **L20**, M represents the molecular mass of the ligand **L20**=563.86g/mol

For the *pentadentate* class D ligands, ligand **L20** is used to describe the mass ionisable patterns due to its relatively high mass. The resultant fragmentation patterns for ligand **L20** is shown in Figure 3.25 and Figure 3.26.

The results indicate relative mass abundance of the different fragments. The fragments are obtained from the fragmentation of the molecule and their respective isotopic pattern when bombarded by the different ions from various molecules such as chloride, acetonitrile and sodium [138]. This result shows that the ligand forms fragmented species (a), (b) and (c) as shown by the proposed fragmentation in Figure 3.25, which can be attributed to the molecular ions to  $[M+H]^+$ ,  $[M-C_{16}H_{26}O]$  and  $[M-C_{18}H_{30}N_2O]^+$  respectively. The base peak at 100 % abundance is assigned to species (a), species (b) is observed at 30 % while species (c) is observed at 40 % respectively.

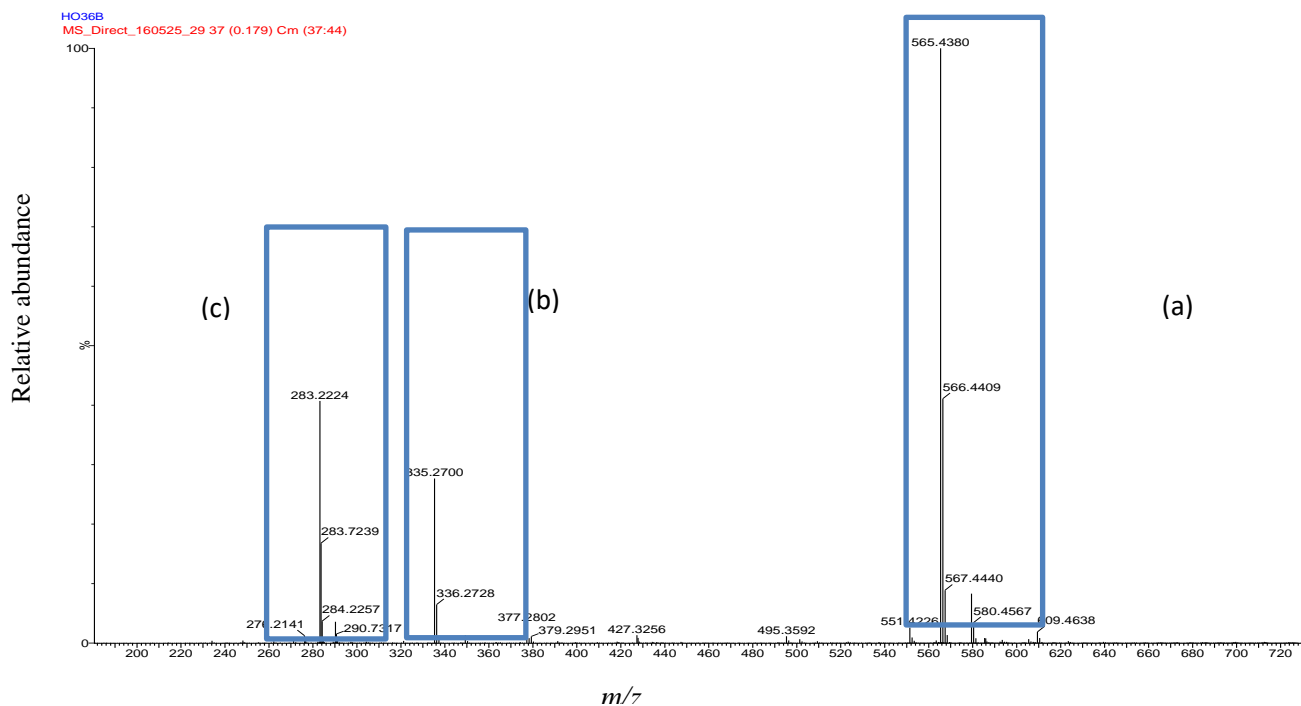


Figure 3. 26 Spectrum of ligand **L20** showing the relative abundance with  $m/z$  value of the ligand.

For the results obtained from other ligands in the same class, **L16-L19**, the ionisable mass species (c) was observed for ligand **L19** and **L20** only, while for ligand **L17** and **L18** species (c) was observed at 100 % relative abundance while species (a) was observed at 60 % relative abundance. These results were similar to the *pentadentate* N-donor class of ligands and are given in section 3.14.2.

### 3.11 Effect of the added donor group

The results from the MS analysis between the class D and E ligands did not differ much in terms of the species formed. The *hexadentate* ligands showed similar distribution of the species. These results are therefore given in the experimental section.

### 3.12 Elemental analysis

The EA/CHN analysis was carried out as described in Chapter 2.11. All the ligands analyzed were confirmed to contain the Schiff base product in high purity. Similarly, these ligands are shown to contain solvent that could not be completely removed. The results are shown in Table 3.3.

Table 3. 2 EA analysis results

LIGAND	FORMULA	%CALCULATED			%OBTAINED		
		C	H	N	C	H	N
L16	C <sub>18</sub> H <sub>20</sub> N <sub>2</sub> O <sub>3</sub>	69.21	6.45	8.97	69.19	6.29	8.83
L17	C <sub>20</sub> H <sub>24</sub> N <sub>2</sub> O <sub>5</sub> (CH <sub>3</sub> OH)	62.36	6.98	7.18	62.33	6.08	7.25
L18	C <sub>26</sub> H <sub>24</sub> N <sub>3</sub> O <sub>3</sub> . (CH <sub>3</sub> O) <sub>2</sub>	70.38	6.54	6.06	70.11	5.70	6.21
L19	C <sub>26</sub> H <sub>36</sub> N <sub>2</sub> O <sub>3</sub> (CH <sub>3</sub> CH <sub>2</sub> O) <sub>0.5</sub>	72.45	8.37	6.26	72.60	8.61	6.09
L20	C <sub>36</sub> H <sub>50</sub> N <sub>2</sub> O <sub>3</sub> (H <sub>2</sub> O)(CH <sub>3</sub> O) <sub>0.5</sub>	73.20	10.10	4.68	73.09	9.68	4.39
L21	C <sub>20</sub> H <sub>24</sub> N <sub>2</sub> O <sub>4</sub>	67.40	6.79	7.86	67.46	6.79	7.86
L22	C <sub>22</sub> H <sub>29</sub> N <sub>2</sub> O <sub>6</sub>	63.45	6.78	6.73	63.63	6.63	6.75
L23	C <sub>28</sub> H <sub>28</sub> N <sub>2</sub> O <sub>4</sub>	73.66	6.18	6.14	73.79	6.14	5.95
L24	C <sub>28</sub> H <sub>40</sub> N <sub>2</sub> O <sub>4</sub>	71.76	8.60	5.98	71.13	8.91	6.16
L25	C <sub>38</sub> H <sub>61</sub> N <sub>3</sub> O <sub>2</sub>	74.96	9.93	4.60	74.84	9.89	4.88

### 3.13 Summary and conclusion

The ten O-bearing Salen type ligands were synthesized through the Schiff base condensation method. The *pentadentate* ligand **L19** with the *tertbutyl* group, *hexadentate* **L21** with *salicylaldehyde* and *hexadentate* **L23** with *naphthylaldehyde* had previously been synthesized. The other seven ligands are to the best of our knowledge, novel. The ligands were obtained in good yield and were fully characterized by IR, <sup>1</sup>H NMR, <sup>13</sup>C NMR, MS and CHN analytical techniques as shown in the experimental section 3.14.

The study of the unsubstituted *salicylaldehyde* ligand of the *pentadentate* system show that the change of substituent on the phenyl ring leads to a red shift on the IR. The *methoxy* containing substituent was shown to exhibit the highest red shift of the *imine*. For the <sup>1</sup>H NMR and <sup>13</sup>C <sup>1</sup>H NMR the change of substituent led to downfield shift in the imine except for the *methoxy* substituent that was observed to exhibit an upfield shift of the *imine*. The *naphthyl* based ligands were shown to exhibit blue shift on the IR and upfield shift of the *imine* on the NMR. The results for the *hexadentate* ligand series also showed the same order of shift. The comparison of the analogous *pentadentate* and *hexadentate* ligands show that the *hexadentate* ligands show an upfield shift on the NMR and a redshift on the IR.

One of the ligands, **L16**, was studied for molecular dynamism which showed the equivalence of these spacer protons. The proton decoupled <sup>13</sup>C NMR on the other hand indicated well resolved signals. This ligand was then analyzed through HSQC analysis, indicating the

equivalence of these protons. These results on unresolved proton signals were therefore hypothesized to occur due to symmetry effect.

One of the *hexadentate* salen O-donor ligands with the *methoxy* substituent on the phenyl ring (ligand **L22**) was observed to undergo reversible colour change in the presence of direct light. This ligand was shown to fluoresce with a broad band gap through confocal microscopy.

### 3.14 Experimental

#### 3.14.1 Characterization of class D ligands

##### 3.14.1.1 Characterization of Salicylaldehyde and 2, 2'-[ethane-1,2-diylbis(oxy)] diethanamine (Ligand L16).

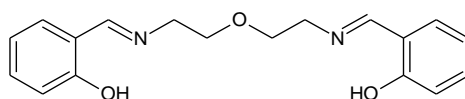


Figure 3. 27 Schematic diagram of **L16**

A 1.22 g (0.0100 moles) of *salicylaldehyde* and 0.006 moles (35 ml of 0.171 M) of 2, 2'-[ethane-1,2-diylbis(oxy)]diethanamine were refluxed. The product obtained as a yellow crystalline precipitate, the yield was 72 % for  $C_{18}H_{20}N_2O_3$  EA calculated (%) C (69.21) H (6.45) N (8.97) EA Found (%); C (69.19), H (6.29), N (8.83)  $^1H$  NMR ppm (600 MHz,  $CDCl_3$ )  $\delta$ H; 13.39 (2 H, s OH), 8.30 (2 H, s NCH), 7.29 (2 H, ddd,  $J$  8.8Hz, 5.9 Hz, 1.7 Hz, ArH), 7.15 (2 H, dd,  $J$  7.6 Hz, 1.7Hz, ArH), 6.95 – 6.92 (2 H, m, ArH), 6.83 (2 H, s, ArH), 3.75 (8 H, s,  $OCH_2CH_2$ ).  $^{13}C$  { $^1H$ } NMR (101 MHz,  $CDCl_3$ )  $\delta$   $c$  166.57 (s, ArCN), 161.27(s,  $C_{Ar}OH$ ), 132.32 (s,  $C_{Ar}H$ ), 131.49 (s,  $C_{Ar}H$ ), 131.49 (s,  $C_{Ar}H$ ), 118.65 (s,  $C_{Ar}CN$ ), 117.08 (s,  $C_{Ar}H$ ), 70.48 (s  $NCH_2CH_2$ ), 59.09 (s  $NCH_2CH_2$ ). IR (ATR, neat,  $cm^{-1}$ ); 3005 (w, OH); 2855 (s, C-H), 1633 (s, C=N), 1575 (s, C=C), 1494 (m, C-H); 1283  $cm^{-1}$  (m,  $C_{Ar}-O$ ). ESI-MS (ES+); Expected  $m/z$  (%) 313.15 Obtained  $m/z$ (%) 313.15 (100)  $[M+H]^+$ .

##### 3.14.1.2 Characterization of 5-methoxy salicylaldehyde and 2,2'-[ethane-1,2-diylbis(oxy)]diethanamine (Ligand L17)

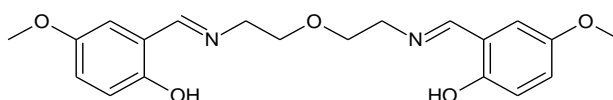


Figure 3. 28 Schematic diagram of ligand **L17**

A 1.56 g (0.0103 moles) of 5-methoxy-Salicylaldehyde and 0.00516 moles of 2, 2'-[ethane-1,2-diylbis(oxy)]diethanamine in ethanol were refluxed in ethanol. Yellow/orange precipitate

was obtained in a yield 84 %. MP 86.5-87.4 °C. For  $C_{20}H_{24}N_2O_5$ . (CH<sub>3</sub>O) EA calculated (%) C (62.36) H (6.98) N (7.18) EA Found (%); C (62.33%), H (6.78), N(7.25); <sup>1</sup>H NMR ppm (400 MHz, CDCl<sub>3</sub>) δ<sub>H</sub> 12.85 (2 H, s OH), 8.26 (2 H, s NCH), 6.94 – 6.83 (4 H, m ArH), 6.69 (2 H, d, *J* 2.8Hz, ArH), , 3.77 – 3.70 (8 H, m, NCH<sub>2</sub>CH<sub>2</sub>), 2.16 (6 H, s, OCH<sub>3</sub>). <sup>13</sup>C {<sup>1</sup>H} NMR (101 MHz, CDCl<sub>3</sub>) 166.23 (s, ArCN), 155.31 (s, C<sub>Ar</sub>OH), 152.03 (s, C<sub>Ar</sub>OCH<sub>3</sub>), 119.35 (s, C<sub>Ar</sub>H), 118.51 (s, C<sub>Ar</sub>H), 117.72 (s, C<sub>Ar</sub>H), 114.98 (s, C<sub>Ar</sub>H), 70.48 (s, OCH<sub>2</sub>CH<sub>2</sub>), 59.24 (s, CH<sub>2</sub>CH<sub>2</sub>O), 31.03 (s, OCH<sub>3</sub>). IR (ATR, neat, cm<sup>-1</sup>); 2886 (w, CH), 1639 (s, C=N), 1587 (w, C=C), 1490 (s, C-H), 1259 cm<sup>-1</sup> (s, C<sub>Ar</sub>-O): ESI-MS (ES+); Expected m/z (%) 372.17, obtained m/z (%) 373.17(100).

### 3.14.1.3 Characterization of naphthylaldehyde and 2,2'-[ethane-1,2-diylbis(oxy)]diethanamine (ligand L18)

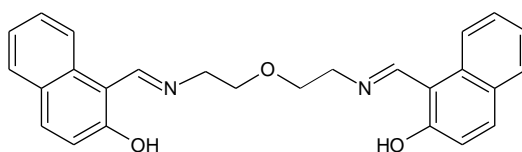


Figure 3. 29 Schematic diagram of ligand L18

A 1.38 g (0.00801 moles) of 2-hydroxy naphthalene and 27 ml (0.00405 moles) of the of 2,2'-[ethane-1,2-diylbis(oxy)]diethanamine (0.15 M solution in the flask) were refluxed. Yellow crystalline flakes were obtained in a yield 87 %. MP 137-139 °C for  $C_{26}H_{24}N_2O_3$ . (CH<sub>3</sub>O)<sub>2</sub>. EA calculated (%) C (70.38), H (6.54), N (6.06). EA Found (%);C (70.11), H (6.70) N (6.21) <sup>1</sup>H NMR ppm (600 MHz, CDC<sub>3</sub>) δ<sub>H</sub>; 8.77 (2 H, s NCH), 7.82 (2 H, d, *J* 8.4 ArOH), 7.64 (2 H, d, *J* 9.3 Hz, ArH), 7.57 (2 H, d, *J* 7.8Hz, ArH), 7.37 – 7.33 (2 H, m ArH), 7.20 (2 H, t, *J* 7.4Hz), 6.89 (2 H, d, *J* 9.3 Hz, ArH), 3.81 – 3.74 (8 H, m, OCH<sub>2</sub>CH<sub>2</sub>). <sup>13</sup>C {<sup>1</sup>H} NMR (400 MHz, CDCl<sub>3</sub>) δ<sub>C</sub>; 159.26 (s, ArCN), 137.28 (s, C<sub>Ar</sub>OH), 133.85 (s, C<sub>Ar</sub>H), 129.26 (s, C<sub>Ar</sub>C), 128.08 (s, C<sub>Ar</sub>C), 126.41 (s, C<sub>Ar</sub>H), 124.67 (s, C<sub>Ar</sub>H), 122.87 (s, C<sub>Ar</sub>H), 118.14 (s, C<sub>Ar</sub>CN), 107.01 (s, C<sub>Ar</sub>CN), 70.45 (s OCH<sub>2</sub>CH<sub>2</sub>), 53.17 (s OCH<sub>2</sub>CH<sub>2</sub>), IR (ATR, neat, cm<sup>-1</sup>); 3050 (w, OH), 2927(m, C-H), 2863 (m, C-H), 1614 (s, C=N), 1588 (s, C=C), 1487 (m, C-H), 1264 cm<sup>-1</sup> (m, C<sub>Ar</sub>-O), ESI-MS (ES+); Expected m/z(%) 412.48 Obtained m/z (%) 207.09 (15) [(M/2)+H]<sup>+</sup>. 413.19 (100) [M+H]<sup>+</sup>.

### 3.14.1.4 Characterization of 5-*t*-butyl salicylaldehyde and 2,2'-[ethane-1,2-diylbis(oxy)]diethanamine (Ligand L19).

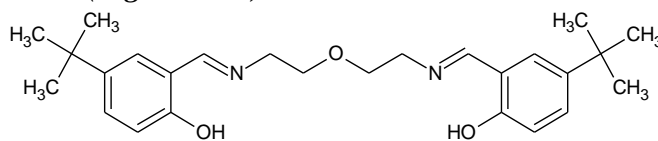


Figure 3. 30 Schematic diagram of Ligand **L19**

A 2.76 g (0.00774 moles) of 2-hydroxy 4-*tert* butyl aldehyde and 26ml (0.00387) moles of 2, 2'-[ethane-1, 2-diylbis (oxy)]diethanamine were refluxed in ethanol. Brownish yellow oil was obtained that slowly solidifies, yield 72 % for  $C_{26}H_{36}N_2O_3 (CH_3CH_2O)_{0.5}$  EA calculated C (72.45) H (8.78) N (6.26). EA Found C (72.60) H (8.61) N (6.09)  $^1H$  NMR (400 MHz,  $CDCl_3$ )  $\delta$   $H$  8.37 (2 H, m, NCH), 7.34 (2 H, dd,  $J$  8.7Hz, 2.5Hz, ArH), 7.23 (2 H, d,  $J$  2.5Hz, ArH), 6.89 (2 H, d,  $J$  8.7Hz, ArH), 3.80 – 3.70 (8H,  $OCH_2CH_2$ ), 1.31 – 1.29 (19 H, m,  $C(CH_3)_3$ ).  $^{13}C$  { $^1H$ } NMR (101 MHz,  $CDCl_3$ )  $\delta$  C; 166.86 (s, ArCN), 158.96 (s,  $C_{Ar}OH$ ), 141.35 (s,  $C_{Ar}CH_3$ ), 129.71 (s,  $C_{Ar}H$ ), 127.91 (s,  $C_{Ar}CN$ ), 116.64 (s,  $C_{Ar}H$ ), 70.82 (s,  $NCH_2 CH_2$ ), 59.33 (s,  $NCH_2 CH_2$ ), 31.41 (s, CCH<sub>3</sub>). IR (ATR, neat,  $cm^{-1}$ ); 2865 (s, C-H); 1633 (s, C=N); 1589 (s, C=C), 1494 (m, C-H), 1265  $cm^{-1}$  (m,  $C_{Ar}-O$ ), ESI-MS (ES+); Expected  $m/z$ (%) 425.28 Obtained  $m/z$  (%) 425.28 (100)[M+H]<sup>+</sup>.

### 3.14.1.5 Characterization of 5-nonyl salicylaldehyde and 2,2'-[ethane-1,2-diylbis(oxy)]diethanamine (ligand L20)

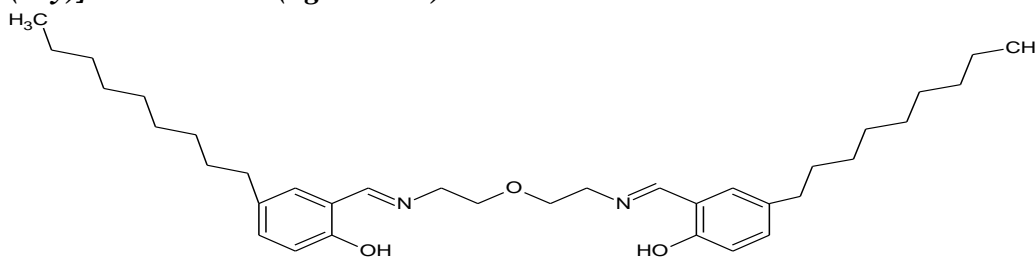


Figure 3. 31 Schematic diagram of Ligand **L20**

A 1.98 g (0.00797 moles) of 2-hydroxy 4-nonylaldehyde and 26.7ml (0.004 moles) of 2, 2'-[ethane-1,2-diylbis(oxy)]diethanamine were refluxed in ethanol. A brownish yellow less viscous oil was obtained. Yield 93%. FM  $C_{36}H_{50}N_2O_3.(H_2O) (CH_3O)_{0.5}$  EA calculated (73.20), H (10.10), N (4.68), Found C (73.09), H (9.68), N (4.39)  $^1H$  NMR ppm (600MHz,  $CDCl_3$ )  $\delta$  8.37 (1 H, m), 7.52 – 6.68 (3 H, m), 4.47 – 2.96 (4H, m), 2.32 – 0.11 (18 H, m).  $^{13}C$  { $^1H$ } NMR (400 MHz,  $CDCl_3$ )  $\delta$  166.91(s, ArCN), 158.83(s,  $C_{Ar}OH$ ), 140.76(s,  $C_{Ar}H$ ), 140.09(s,  $C_{Ar}C$ ), 137.93(s,  $C_{Ar}H$ ), 130.46(s,  $C_{Ar}H$ ), 118.08(s,  $C_{Ar}H$ ), 116.49(s,  $C_{Ar}H$ ), 70.85(s,  $NCH_2 CH_2$ ), 59.24(s,  $NCH_2 CH_2$ ), 51.88-8.75(( $CH_2$ )<sub>8</sub>CH<sub>3</sub>). IR (ATR, neat,  $cm^{-1}$ ); 3005 (w, OH), 2926(m,

C-H), 2868 (m, C-H), 1633 (m, C=N); 1588 (s, C=C); 1491 (m, CH); 1280  $\text{cm}^{-1}$  (m,  $\text{C}_{\text{Ar}}\text{-O}$ ): ESI-MS (ES+); Expected  $m/z$ (%) 564.84, obtained  $m/z$  (%) 283.32 (40)  $[(M/2)+\text{H}]^+$ , 335.27 (30)  $[\text{M}-\text{C}_{16}\text{H}_{26}\text{O}]$ , 566.44 (100)  $[\text{M}+\text{H}]^+$ .

### 3.14.2 Synthesis of class E ligands

#### 3.14.2.1 Characterization of Salicylaldehyde and 2,2'-[ethane-1,2-diylbis(oxy)]diethanamine (Ligand L21)

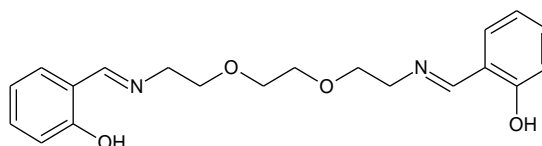


Figure 3. 32 Schematic diagram of **L21**

A 2.44 g (0.01998 moles) of *salicylaldehyde* and 1.48 g (0.0100 moles) of 2,2'-[ethylenedioxy]bis ethylamine was refluxed. Product obtained is yellow crystalline powder (3.1895 g) yield 89.92 %. MP 49.0-50.8 °C FM  $\text{C}_{20}\text{H}_{24}\text{N}_2\text{O}_4$ , EA calculated C (67.40) H (6.79) N (7.86). EA Found C (67.46) H (6.62) N (7.86).  $^1\text{H}$  NMR (300MHz,  $\text{CDCl}_3$ )  $\delta_{\text{H}}$  8.30 (2 H, s, NCH), 7.46 – 7.15 (4 H, m, ArH), 7.05 – 6.90 (2 H, m, ArH), 6.85 (4 H, td,  $J$  7.5Hz, 1.1Hz, ArH), 3.77 – 3.64 (8 H, m, ,  $\text{OCH}_2\text{CH}_2$ ), 3.59 (4 H, s,  $\text{NCH}_2\text{CH}_2$ ).  $^{13}\text{C}$   $\{^1\text{H}\}$  NMR (400 MHz,  $\text{CDCl}_3$ )  $\delta$  ppm (300 MHz,  $\text{CDCl}_3$ ) 166.40 (s, ArCN), 161.26 (s  $\text{C}_{\text{Ar}}\text{OH}$ ), 132.22 (s  $\text{C}_{\text{Ar}}\text{H}$ ), 131.36 (s,  $\text{C}_{\text{Ar}}\text{H}$ ), 118.67 (d,  $J$  25.8,  $\text{C}_{\text{Ar}}\text{H}$ ), 117.01 (s,  $\text{C}_{\text{Ar}}\text{H}$ ), 70.56 (d,  $J$  9.7,  $\text{OCH}_2\text{CH}_2$ ), 58.99 (s,  $\text{NCH}_2\text{CH}_2$ ). IR (ATR, neat,  $\text{cm}^{-1}$ ); 3005 (w, OH); 2905, 2871 (w, CH); 1632 (s, C=N); 1578 (s, C=C); 1490 (m, CH); 1278  $\text{cm}^{-1}$  (m,  $\text{C}_{\text{Ar}}\text{-O}$ ); ESI-MS (ES+); Expected  $m/z$ (%) 356.42, (ES+): $m/z$  obtained  $m/z$ (%)253.15(53)  $[\text{M}-\text{C}_7\text{H}_8\text{O}]^+$ , 357.18(100)  $[\text{M}+\text{H}]^+$ .

#### 3.14.2.2 Characterization of 5-methoxy salicylaldehyde and 2,2'-[ethane-1,2-diylbis(oxy)]diethanamine (Ligand L22)

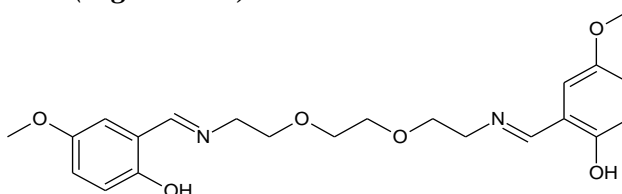


Figure 3. 33 Schematic diagram of **L22**

A 1.52 g (0.000999 moles) of *salicylaldehyde* 0.753 g (0.00509 moles) of 2,2'-[ethylenedioxy]bis ethylamine. A yellow solid was obtained. Yield 78% MP 98.1-100.4°C FM  $\text{C}_{22}\text{H}_{28}\text{N}_2\text{O}_6$ , EA calculated C (63.45) H (6.78) N (6.73). EA Found C (63.63) H (6.63) N (6.75),  $^1\text{H}$  NMR (400MHz,  $\text{CDCl}_3$ )  $\delta$  ppm; 8.64 (s, 2H, NCH), 7.64 (s, 2H), 7.37 – 7.00 (m, 6H), 4.13

(s, 6H, OCH<sub>3</sub>), 4.07 (d, *J*=6.9, 8H, NCH<sub>2</sub>CH<sub>2</sub>), 3.96 (s, 4H, OCH<sub>2</sub>CH<sub>2</sub>O). <sup>13</sup>C {<sup>1</sup>H} NMR (75 MHz, CDCl<sub>3</sub>) 166.15 (s, ArCN), 155.32 (s, C<sub>Ar</sub>OH), 151.99 (d, *J* 1.6, C<sub>Ar</sub>OCH<sub>3</sub>), 119.25 (s, C<sub>Ar</sub>CN), 118.54 (s, C<sub>Ar</sub>H), 117.72 (s, C<sub>Ar</sub>H), 114.95 (s, C<sub>Ar</sub>H), 70.60 (d, *J* 9.1, OCH<sub>2</sub>CH<sub>2</sub>O), 59.23 (s, NCH<sub>2</sub>CH<sub>2</sub>), 55.98 (s, OCH<sub>3</sub>). IR (ATR, neat, cm<sup>-1</sup>); 3043 (w, OH); 2912, 2883 (w, C-H); 1639 (s, C=N); 1588 (s, C=C); 1496 (a, CH); 1268<sup>1</sup> (m, C<sub>Ar</sub>-O); ESI-MS (ES+); Expected m/z(%) 417.2, obtained (ES+) m/z (%) 283.2 (80) [M-C<sub>8</sub>H<sub>11</sub>O<sub>2</sub>]<sup>+</sup>. 417.2 (100) [M+H]<sup>+</sup>.

### 3.14.2.3 Characterization of bis (2-*{(E)-[(2-oxyethyl)imino]methyl}*-naphthalene (Ligand L23)

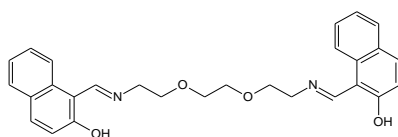


Figure 3. 34 Schematic diagram L23

A 10.33 g (0.05941 moles) of 2-hydroxy naphthylaldehyde and 4.58 g (0.0309 moles) of 2,2'-[ethane-1,2-diylbis(oxy)]diethanamine. Product obtained as a yellow/green crystalline powder. Yield 79.7 %. MP 170-171°C. C<sub>28</sub>H<sub>30</sub>N<sub>2</sub>O<sub>4</sub> EA calculated C (73.66) H (6.18) N (6.14). EA Found C (73.79) H (6.14) N (5.95). <sup>1</sup>H NMR (600MHz, DMSO-*d*<sup>6</sup>) δ ppm 13.10 (2 H, s, OH), 8.17 (2H, d, *J* 7.2, NCH), 7.15 (2 H, s, ArH), 6.96 – 6.66 (4 H, m, ArH), 6.53 (2 H, s, ArH), 6.31 (2 H, s, ArH), 5.79 (2 H, t, *J* 58.1, ArH), 2.92 – 2.73 (12 H, m, NCH<sub>2</sub>CH<sub>2</sub>O). <sup>13</sup>C {<sup>1</sup>H} NMR (75 MHz, CDCl<sub>3</sub>) δ ppm 159.02 (s, ArCN), 137.44 (s, C<sub>Ar</sub>OH), 134.05 (s, C<sub>Ar</sub>C<sub>Ar</sub>), 129.28 (s, C<sub>Ar</sub>C<sub>Ar</sub>), 128.02 (s, C<sub>Ar</sub>H), 126.21 (s, C<sub>Ar</sub>H), 125.27 (s, C<sub>Ar</sub>H), 122.74 (s, C<sub>Ar</sub>H), 117.99 (s, C<sub>Ar</sub>H), 106.67 (s, C<sub>Ar</sub>CN) 70.61 (d, *J* 49.5, OCH<sub>2</sub>CH<sub>2</sub>O), 52.38 (s, NCH<sub>2</sub>CH<sub>2</sub>), 31.04 (s, NCH<sub>2</sub>CH<sub>2</sub>). IR (ATR, neat, cm<sup>-1</sup>); 3048 (w, OH); 2882, 2856 (w, CH); 1611 (s, C=N); 1540 (s, C=C); 1490 (s, CH); 1259 cm<sup>-1</sup> (s, C<sub>Ar</sub>-O); ESI-MS (ES+); Expected m/z(%) 457.53, observed m/z (%) (ES+): m/z(%) 229.11(100) [(M/2)+H]<sup>+</sup>. 457.21(40) [M+H]<sup>+</sup>.

### 3.14.2.4 Characterization of bis (2-*{(E)-[(2-oxyethyl)imino]methyl}*-4-*tert*-butylphenol (Ligand L24)

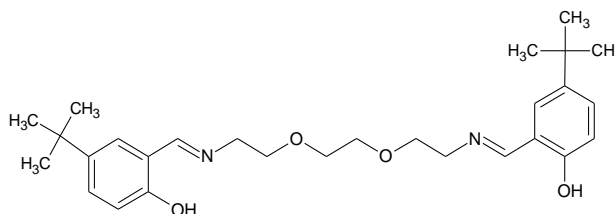


Figure 3. 35 Schematic diagram of L24

6.37 g (0.0136 moles) of 4-*tert* butyl salicylaldehyde and 1.04 g (0.00702 moles) of 2,2'-[ethane-1,2-diylbis(oxy)]diethanamine. Product obtained as yellow viscous oil (3.136 g). Yield

78.4 %. FM  $C_{28}H_{40}N_2O_4$  EA calculated C (71.76) H (8.60) N (5.98) EA Found C (71.13) H (8.91) N (6.16)  $^1H$  NMR (400MHz,  $CDCl_3$ )  $\delta$  ppm 13.17 (2 H, s, OH), 8.33 (2 H, s, NCH), 7.35 (2 H, dd,  $J$  8.7, 2.5, ArH), 7.25 (2 H, dd,  $J$  6.6, 2.3, ArH), 6.90 (2 H, dd,  $J$  8.6, 4.1), 3.73 (8 H, t,  $J$  2.8,  $OCH_2$ ), 3.62 (4 H, s,  $NCH_2CH_2$ ), 1.30 (18 H, s,  $C(CH_3)_3$ ).  $^{13}C$   $\{^1H\}$  NMR (101 MHz,  $CDCl_3$ )  $\delta$  ppm 166.84 (s, ArCN), 158.97 (s,  $C_{Ar}OH$ ), 141.29 (s,  $C_{Ar}C(CH_3)_3$ ), 129.64 (s,  $C_{Ar}H$ ), 127.86 (s,  $C_{Ar}H$ ), 116.62 (s,  $C_{Ar}H$ ), 70.71 (d,  $J$  2.3Hz,  $OCH_2CH_2O$ ), 59.24 (s,  $NCH_2CH_2$ ), 34.08 (s  $C(CH_3)_3$ ), 31.57 (s,  $NCH_2CH_2$ ). IR (ATR, neat,  $cm^{-1}$ ); 3064 (w, OH); 2953, 2864 (m, CH); 1631 (m, C=N); 1588 (s, C=C); 1490 (m, CH); 1264  $cm^{-1}$  (m,  $C_{Ar}-O$ ); ESI-MS (ES+); Expected  $m/z$ (%) 468.31, obtained  $m/z$  (%) 469.30(100)  $[M+H]^+$ .

### 3.14.2.5 Characterization of bis (2-*(E)*-[(2-oxyethyl) imino]methyl]-4-nonyl-butylphenol (ligand L25)

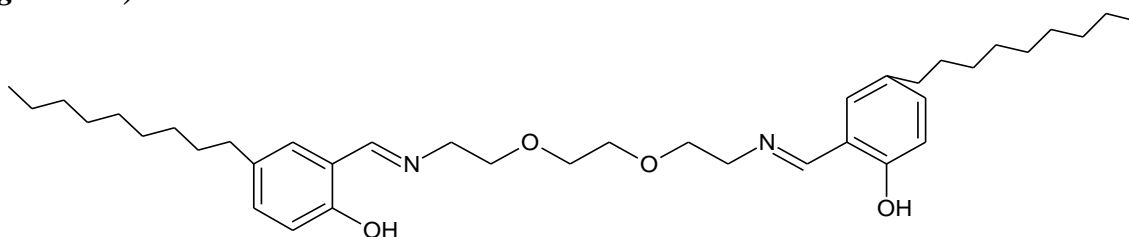


Figure 3. 36 Schematic diagram of L25

A 3.36 g (0.0135 moles) of 4-nonyl salicylaldehyde and 1.001 g (0.006760 moles) of 2,2'-[ethane-1,2-diylbis(oxy)]diethanamine. Product obtained as a yellow oil (3.1866g). Yield 77 %. FM  $C_{38}H_{60}N_2O_4$ , EA calculated C(74.96) H (9.93) N (4.60) EA Found C (74.84) H (9.89) N (4.88)  $^1H$  NMR (400MHz,  $CDCl_3$ )  $\delta$  ppm 13.15 (2 H, s, OH), 8.34 (2 H, s, NCH), 7.32 – 7.07 (3 H, m, ArH), 6.87 (3 H, s, ArH), 3.75 – 3.70 (8 H, m,  $OCH_2$ ), 3.62 (4 H, s,  $NCH_2CH_2$ ), 1.74 – 1.37 (4H, m,  $C_{Ar}CH_2$ ), 1.31 – 1.12 (14 H, m,  $CH_2$ ), 0.91 – 0.86 (4 H, m,  $CH_2$ ), 0.85 – 0.72 (12 H, m,  $CH_2$ ), 0.68 – 0.47 (6 H, m,  $C(CH_3)_3$ ).  $^{13}C$   $\{^1H\}$  NMR (400 MHz,  $CDCl_3$ )  $\delta$  ppm 166.96 (s, ArCN), 158.82 (s,  $C_{Ar}OH$ ), 140.71 (s,  $C_{Ar}C(CH_2)$ ), 140.04 (s,  $C_{Ar}H$ ), 137.94 (d,  $J$  12.6,  $C_{Ar}H$ ), 131.09 (s,  $C_{Ar}H$ ), 130.41 (d,  $J$  9.3,  $C_{Ar}H$ ), 116.45 (s,  $C_{Ar}H$ ), 70.70 (d,  $OCH_2CH_2O$ ), 59.24 (s,  $NCH_2CH_2$ ), 37.41 – 8.49 (m,  $(C_9H_{19})_2$ ). ATR (ATR, neat,  $cm^{-1}$ ) 2958(m, C-H), 2858 (m, C-H); 1634 (s, C=N); 1588 (w, C=C); 1491 (m, C-H); 1280  $cm^{-1}$  (s,  $C_{Ar}-O$ ); ESI-MS (ES+); Expected  $m/z$ (%) 608.45 (ES+) :obtained  $m/z$  (%) 305.23 (100)  $[(M/2) +H]^+$ , 609.46 (40)  $[M+H]^+$ .

# **CHAPTER 4**

---

## **CRYSTAL STRUCTURE DETERMINATION AND FLOURESCENCE STUDIES**

---

## 4.0 Introduction

In an extraction system, the ability of the ligand to extract the metal ions depend on the ability of the ligand and the metal ion to interact in one phase and then be transferred as a metal complex to a secondary phase. This process has to be selective, disregarding certain metals in favour of others. The design and principle of hydrometallurgy is therefore heavily dependent on this principle and by changing various attributes of the ligand such as donor groups, bite size and the substituents, this can be achieved. Since salen type ligands make excellent candidates due to its various advantages, the study of the complexing of these ligands to the metal ions, before subjecting them to solvent extraction, is therefore important. This chapter will therefore deal with the synthesis of selected salen type ligand complexes and the determination of their mode of coordination through single crystal analysis. Some solution studies through fluorescence studies are also discussed to show the effect of the different donor groups and substituents.

### 4.1 Ligand-metal interaction

The coordination of ligands to metal ions in solution is a fundamental part of any study of solvent extraction technique. The coordination of an extractant to the metal ions can therefore borrow greatly from various fields of chemistry. For example because coordination of an extractant to a metallic ion usually occurs in a bi-phasic immiscible liquid system, the nature of such interactions can therefore borrow from reactions involving heterogeneous and homogenous systems [139]. The study of coordination has therefore been shown to borrow from organometallics, from surface chemistry and from stability and potentiometric studies. This interaction will be explained further in subsequent discussions.

In hydrometallurgy, for metal ions to be extracted the coordination of the extractant to the metal ion in solution can be thought of as the reaction of a ligand to a metal ion in a reactor, where the reactor is the solvent extraction vessel (system). In a standard solvent extraction system for example, the coordination of the ligand to the metal ion usually takes place under standard temperature and pressure. The ligands in the organic phase react with a metal ion in the aqueous phase to completion without the need for the ligand to dissolve in the aqueous phase. This reaction has been shown to occur through the interfacial contacts brought about by intimate shaking [140]. For a good solvent extraction system all the ligands (extractants) have to be able to interact with the selected metal ions leading to complete coordination to effect 100 %

extraction. This reaction must be facile, fast and stable in both phases without any need for a catalyst at standard temperature and pressure.

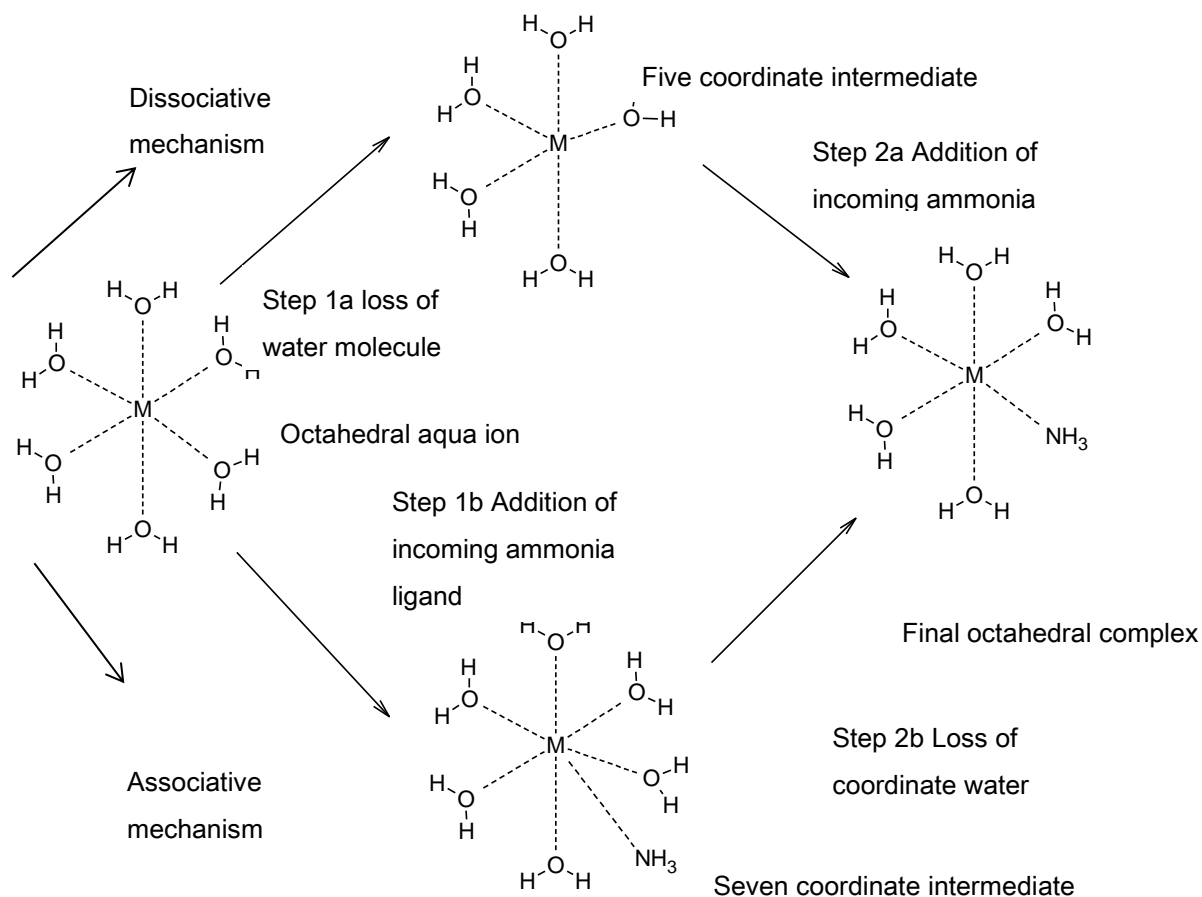
The study of such system therefore involves deeper understanding of the mode of action of the ligands, the physiochemical role of the solvent and the coordination nature of the metal ion (coordination ability and the kinetics of such coordination). This reaction has to also be able to factor the effect of the various extraneous influences such as pH, temperature and the effect of competition of various metal ions to the coordination site of the ligand. In previous discussions in Chapter 1, most of the factors are discussed in detail. This chapter therefore aims to study the coordination behaviour of these ligands and the geometry formed by these ligands and metal ions. The greater aim is therefore to correlate the mode of coordination of these ligands to the nature of the extractant that will be covered in the subsequent chapters (Chapter 5 to Chapter 7). The following discussion therefore shows coordination of the ligand to the metal ion.

#### **4.1.1 Coordination in solution**

From Chapter 1, the products of leaching or the pregnant leach solution is defined as product of corrosion using acid or base. These leaching products can therefore be samples obtained from mining (ore) or from the various other secondary sources. In all these cases the pregnant leach solution will be introduced as an aqueous solution or as concentrated hydrated salt. Therefore, in order for the ligand to coordinate to the metal ion there has to be the replacement of the water molecules or the other counter ions by the chelate ligand. The rate of ligand substitution of the inner sphere water molecules is typical of the rate of coordination of the complex [29]. Scheme 4.1 gives us the possible ways in which the water molecules can be replaced.

From the diagram in Scheme 4.1, it can be observed that the incoming ligand must first form an outer sphere complex to position itself correctly to move into the inner sphere. In this way there are therefore two possible mechanisms that the process can follow. The first process is nucleophile substitution reaction ( $S_N1$  mechanism) in which the metal ion loses a water molecule or one of its anions from its inner sphere leading to the metal lowering its coordination number to five to create the gap. This gap can then be filled by the incoming ligand as shown through step 1a and step 2a in Scheme 4.1. The second method occurs through  $S_N2$  mechanism where the incoming ligand moves into the coordination sphere first raising the coordination

number to seven and then a departing ligand or water molecule is lost as shown through step 1b and 2b. For this to occur, the chelated ligand and the departing ligands will exhibit different coordinate attraction by the metal ions [29].



Scheme 4. 1 Dissociation and association mechanism of hydrated complex Dissociation and association mechanism of hydrated complex redrawn courtesy of Martell *et al.* [29].

#### 4.1.2 Factors affecting coordination of extractant to metal ions

There are several factors that affect the ability of the ligand to coordinate to the metal ions. Some of these factors include pH, the donor group which has been considered in Chapter 1. In this chapter however, the consideration will be on the factors that affect the geometrical coordination of the ligand to the metal ions such as Jahn-Teller distortion, hydrogen bonding and ligand pre-organization.

##### 4.1.2.1 Jahn-Teller distortion

The explanation of Jahn-Teller distortion will be restricted to the divalent metal cations only. This is since the focus of this thesis is on divalent cations. The second reason is that the base metals considered in this work are more prevalent in this oxidative state in nature.

Jahn-Teller distortion can therefore be defined as the ability of a divalent atom to achieve stability by forming distorted geometry due to the unequal occupancy of degenerate orbitals [141]. From ligand field theory the metal orbitals are under repulsion from those of the ligand. For divalent transitional metals such as  $\text{Cu}^{2+}$  ( $d^9$  configuration) [139] with partially occupied  $e_g$  (electronic ground state) orbital (three electrons in the  $e_g$  level) of the d shell. These electrons are distributed such that two  $e^-$  are in the  $d_{z^2}$  orbital and one is in the  $d_{x^2-y^2}$  orbital leading to uneven repulsion experienced by the coordinating ligands. The  $d_{z^2}$  orbitals are usually in the axial position while the  $d_{x^2-y^2}$  are in plane. Therefore, the four donor atoms of the ligand coordinated to the metal in plane usually feels the effect of repulsion due to the one electron in the  $d_{x^2-y^2}$  orbital. The bonds formed in plane will therefore be much shorter and stronger than the ones on the axial position experiencing the repulsion effect of the two electrons.

Normally in the process of complex formation by *bidentate* ligands, the ligands usually make use of these shorter and stronger bonds first. This means  $\text{Cu}^{2+}$  with this ability to form the shorter bonds will form more stable complexes with these kinds of ligands than the next available metal such as  $\text{Ni}^{2+}$  and  $\text{Zn}^{2+}$  ions without these bonds. This effect is only applicable to metals coordinating to 5 donor atoms and not six covalent bonds where the two axial orbitals are both used. For the metals with 6 donor atoms, the  $\text{Ni}^{2+}$  will form much stronger bonds than  $\text{Cu}^{2+}$  according to the ligand field stabilization energy theory [141-143].

#### **4.1.2.2 Effect of hydrogen bonding in solution**

Although hydrogen bonding are weaker bonds than the common electrostatic interactions, they can also play a crucial role in the ligand-metal recognition and stability process [115]. The formation of hydrogen bonds in solution or even in solid state depends on proper orientation of the hydrogen donor group and the functional groups of the receiving phase. This can either lead to intramolecular H-bonding or intermolecular H-bonding.

#### **4.1.3 Pre-organization and bite size**

So far, the discussions have exclusively been on the synthesis of the multidentate Schiff base ligands which can form 5-coordinate, 6-coordinate or 7-coordinate systems. However, for the metal ions to coordinate to the ligands, the donor groups have to be arranged in a special manner or be flexible enough to switch to a conformation that favours the coordination. The special

arrangement of ligands to coordinate is referred to as ligand pre-organization [29]. Ligand pre-organization is very important for the crown ether and crown ether type ligands.

From studies of these types of ligand systems it can be observed that the ability of the metal ion to coordinate to form a complex is dependent on the position of the donor group in the ring. The formation of a metal-ligand complex therefore determines the stability of the ligand and hence its ability to be extracted.

From studies of *bidentate* ligands, the metal ions prefer to coordinate to the two donor groups when the ring size has either 5 or 6 atoms in the ring as shown by Figure 4.1.

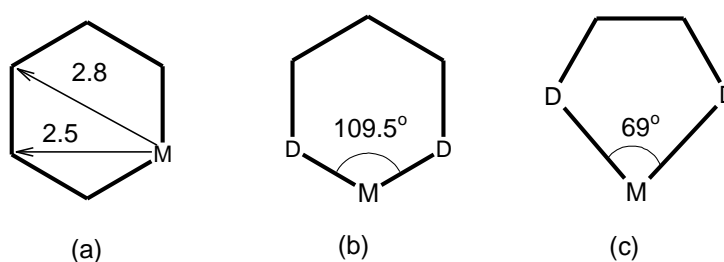


Figure 4. 1 The bite size of idealized cyclohexane (b) the ideal geometry for six membered ring and (c) idealized five membered ring redrawn courtesy of Martell et al [29].

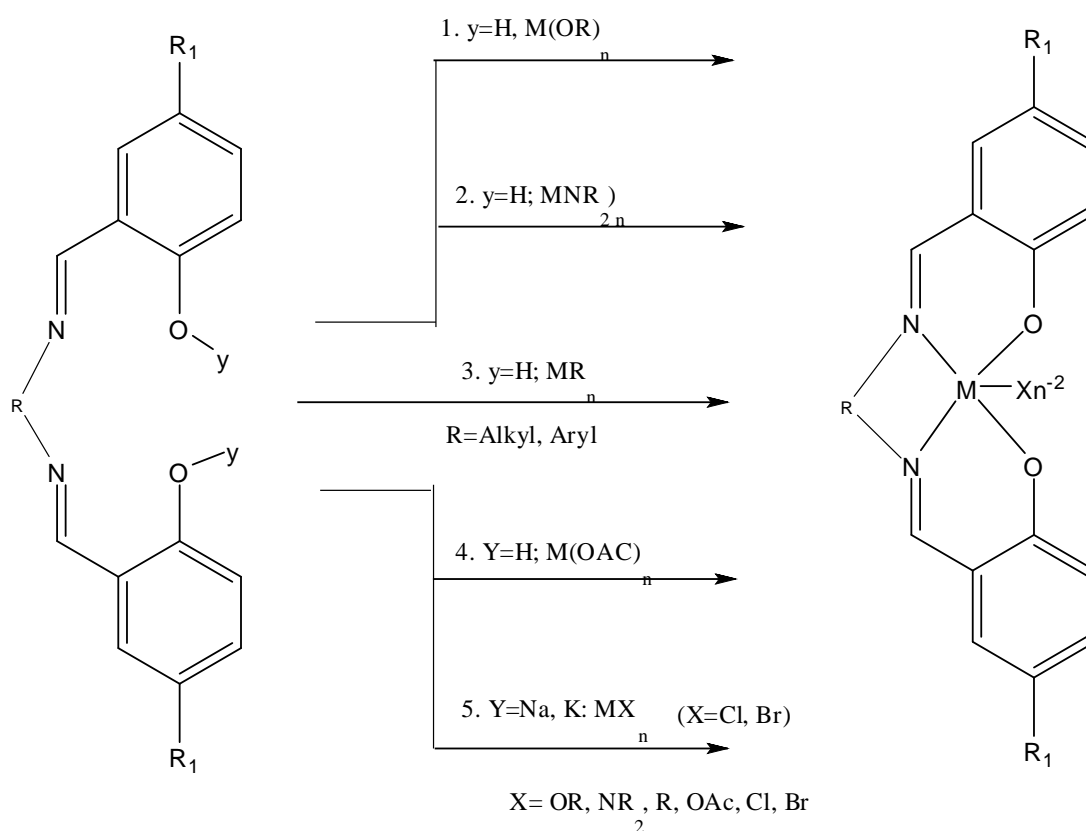
The ability of the ligand to form this 5 or 6 sided ring is therefore called the ligand bite size and this determines whether the ligand will coordinate to a large metal ion or a smaller metal ion [29]. From Figure 4.1, if bite size is composed of 6 atoms (hexagonal system) the D-M-D (D donor group, M metal ion) bond angle will be  $109.5^\circ$  and the torsion angles will be  $60^\circ$  [144]. This allows for sufficient strain for smaller metal ions to coordinate, on the other hand if the bite size is reduced to 5 atoms the bond angle is reduced to  $69^\circ$  but the bond length is increased to  $2.8 \text{ \AA}$  which is ideal for the larger metal ions. Therefore, if larger metal ions coordinate to a hexagonal system (composed of 6 atoms) this will be characterized with distorted geometry and strained rings. The same will be observed for the smaller metal ions with the pentagonal system.

#### 4.1.4 Coordination of salen type ligands

From Chapter 2 it is now known that the imine in Schiff base ligands easily reacts with various transitional metal ions such as  $\text{Cd}^{2+}$ ,  $\text{Co}^{2+}$ ,  $\text{Cu}^{2+}$ ,  $\text{Ni}^{2+}$ ,  $\text{Pb}^{2+}$  and  $\text{Zn}^{2+}$  to form Schiff base complexes under suitable experimental conditions [60]. The coordination of the imine centre can therefore be enhanced by the addition of other functional or donor groups in the vicinity of

the imine centre. The effect of increased donor groups therefore acts as an added centre for coordination of the metal ion. This makes the Schiff base ligand act as chelating agents that stabilize the metal ions in various oxidation states. Schiff base ligands have excellent chelation ability which has greatly enhanced their uses in metal complex formation and studies [60].

There are various methods used for the syntheses of Schiff base-metal complexes. The commonly used synthetic routes for the preparation of metal complexes can be summarized by this diagrammatic representation from literature by Cozzi *et al.* [66] showing different routes of synthesis as shown in Scheme 4.2.



Scheme 4. 2 Common routes for the synthesis of salen type Schiff base metal complexes redrawn courtesy of Itrat *et al.* [60].

The summary of Scheme 4.2 indicates that Schiff base ligands can be synthesized using various salts such as metal alkoxide given by route 1, using metal amides in route 2. Route 3 involves deprotonating of the hydroxyl proton to form alkyl metal complexes, route 4 involves refluxing with metal acetate, chlorates or nitrates and finally route 5 involves the use of the halides in the presence of sodium hydride NaH, or potassium hydride KH. For our work our preference was using route 4.

## 4.2 Problem statement

The studies of the complex geometry in extraction systems has always been a difficult issue, this is due to the lack of understanding of all the interactions that take place in a mixed solvent system. This is further exacerbated by the scarcity of instruments for the studies of the ligand complexes in solutions. Techniques such as X-ray diffraction, neutron diffraction, and isotope dilution are some of the more exotic methods for the determination of structural geometry of coordinate complexes in solution. However, there are various studies on metal complexes and ligands in various solutions that can be used to establish the behaviours of the ligand with the metal cation. This includes spectroscopic methods such as UV-Vis spectroscopy, fluorescence, IR and NMR spectrometry. In this chapter the study will be on the pre-organization of the ligand through single crystal determination of various ligands synthesized in both Chapter 2 and 3. A detailed study on the coordination mode of these ligand systems will be done and the development of some novel crystal structures for both the ligands and their related complexes.

## 4.3 Chapter objective

The objective for this chapter is to determine the nature of coordination of selected Schiff base complexes. Therefore, different complexes will be synthesized and analyzed through spectroscopic techniques such as IR, UV-Vis studies and fluorescence and also determine their crystal structure through single crystal X-ray diffraction technique.

## 4.4 Instrumentation

Most of the instruments used for analysis such as IR and MS have already been discussed in Chapter 2 and 3. The other instruments used are therefore discussed as follows.

### 4.4.1 Single crystal x-ray diffraction

X-ray diffraction usually involves two types of analysis, powder diffraction for the analysis of bulk powder samples or single crystal analysis. Our work focuses on the single crystal analysis which involves the study of microcrystalline solid compounds for the purpose of understanding their mode of coordination [145]. The use of this technique therefore involves the study of molecular and intermolecular interactions which are derived from crystal packing forces. This study therefore involves the identification of conserved features of the ligand [146] and how they influence the final geometry [115]. These features may involve the responses of the ligand to the influence of geometrical requirements of the metal or due to forces of crystallinity. The

second feature involves the study of geometry around the metal ion are observed if the metal cation sits at the centre of the complex with non-ideal metal-donor distances or if the metal cation deviates from the centre, making shorter or longer contacts with some of the donor atoms, or when the metal cation exhibits dynamic or static crystal disorder. These disorders are usually characterized by either large anisotropic displacement parameters or resolvable, discrete cationic positions for static ligand framework [115].

#### **4.4.2 UV-Vis study**

One of the spectroscopic methods for analysis of complexes is by use of UV-Vis spectroscopy. This is usually done by observing the absorbance of the ligand at a certain wavelength in the solution which upon addition of the metal ion leads to a new absorption peak at another wavelength; this new peak is attributed to the formation of complex.

### **4.5 Results and discussion**

#### **4.5.1 Single crystal X-ray diffraction (SXRD) analysis of the ligands**

After the characterization of all the ligands synthesized in Chapters 2 and 3, the crystals of some of the new ligands were developed. In this series of ligands, 3 novel crystal structures were obtained as discussed below.

##### **4.5.1 Formation of ligand crystals**

All the above crystals were obtained from slow evaporation in ethanol solution.

##### **4.5.1.1 Data collection**

All the data collection and refinement were carried out by myself at the supramolecular XRD lab at Stellenbosch University. Suitable crystals were selected and mounted on the Bruker SMART-APEX II DUO diffractometer instrument under liquid nitrogen stream at 100 K. For ligand **L18** this was collected at room temperature at 293 K. The results from the crystal analysis data are therefore shown in Table 4.1 for all the ligands obtained while Table 4.4 indicates the refinement data for the complexes obtained. All the crystals discussed in this section are to the best of my knowledge, novel. All the cif check reports, the HKL, INS and the CIF file for each of these ligands are attached and placed on the CD attached to this thesis. The results are therefore discussed as follows.

Table 4. 1 Crystal structure data for ligand **L16**, **L17** and **L18**

Ligand	<b>L16</b>	<b>L17</b>	<b>L18</b>
Empirical formula	C <sub>18</sub> H <sub>20</sub> N <sub>2</sub> O <sub>3</sub>	C <sub>41</sub> H <sub>45</sub> N <sub>5</sub> O <sub>8</sub>	C <sub>27</sub> H <sub>24</sub> NO <sub>3</sub>
Formula weight	312.36	735.82	410.47
Temperature/K	99.98	100.77	293
Crystal system	orthorhombic	orthorhombic	monoclinic
Space group	<i>Pbcn</i>	<i>Pca2</i> <sub>1</sub>	<i>Pc</i>
a/Å	5.6768(14)	35.766(4)	20.097(11)
b/Å	8.978(2)	4.5011(5)	6.877(4)
c/Å	31.322(8)	22.753(3)	7.900(4)
α/°	90	90	90
β/°	90	90	101.34
γ/°	90	90	90
Volume(Å <sup>3</sup> )Dcalc	1596.3(7)/ 1.3	3663.0(7)/ 1.334	1070.6(10)/ 1.273
Z	4	4	2
F(000)	664	1560	434
Θ range for data collection	2.6 to 56.92°	1.78 to 57.1°	4.14 to 57.18°
Index ranges	-7 ≤ h ≤ 7, -12 ≤ k ≤ 12, -40 ≤ l ≤ 41	-42 ≤ h ≤ 42, -6 ≤ k ≤ 5, -27 ≤ l ≤ 27	-25 ≤ h ≤ 26, -9 ≤ k ≤ 9, -10 ≤ l ≤ 10
Reflections collected/unique	16680/1954[R(int) = 0.0294]	52635/6669[R(int) = 0.0990]	10275/4346[R(int) = 0.0803]
Data/restraints/parameters	1954/0/108	6669/37/459	4346/68/280
Goodness-of-fit on F <sup>2</sup>	1.147	1.055	0.892
Final R indexes [I ≥ 2σ (I)]	R <sub>1</sub> = 0.0370, wR <sub>2</sub> = 0.1052	R <sub>1</sub> = 0.0824, wR <sub>2</sub> = 0.2107	R <sub>1</sub> = 0.0882, wR <sub>2</sub> = 0.2006
Final R indexes [all data]	R <sub>1</sub> = 0.0453, wR <sub>2</sub> = 0.1234	R <sub>1</sub> = 0.1181, wR <sub>2</sub> = 0.2529	R <sub>1</sub> = 0.1452, wR <sub>2</sub> = 0.2309
Largest diff. peak/hole / e Å <sup>-3</sup>	0.32/-0.23	0.92/-0.46	0.83/-0.20

#### 4.5.1.1 Measurement parameters

Single crystal diffraction intensity data were therefore collected using a SMART CCD area-detector diffractometer. Using a graphite-monochromated Mo-K radiation source ( $\lambda=0.71073$  Å). Data reduction and cell refinements were carried out by SMART and SAINT programs. The structures were solved by direct methods (Bruker SHELXTS [147]) and refined by full-matrix least squares techniques (Bruker SHELXL [147]) using all unique data. The non-H atoms in the structure were refined anisotropically. All hydrogen atoms were placed in calculated idealised positions. The refinement was carried out using SHELXL98[147] using the WinGX [148] and OLEX 2 [149] crystal interfaces. The programme mercury, OLEX2 and Ortep were used for the graphic representation of the crystal structure.

#### 4.5.1.1.2 Discussion of crystal structure of ligand L16

The ligand crystallized in an orthorhombic crystal system. The ligand was obtained in a primitive space group (*Pbcn*) with symmetry elements perpendicular to the b-plane. The molecule undergoes symmetrical transition and is also next to a glide plane perpendicular to the b-axis. The symmetrical unit shows half of the molecule with the other half generated by symmetry.

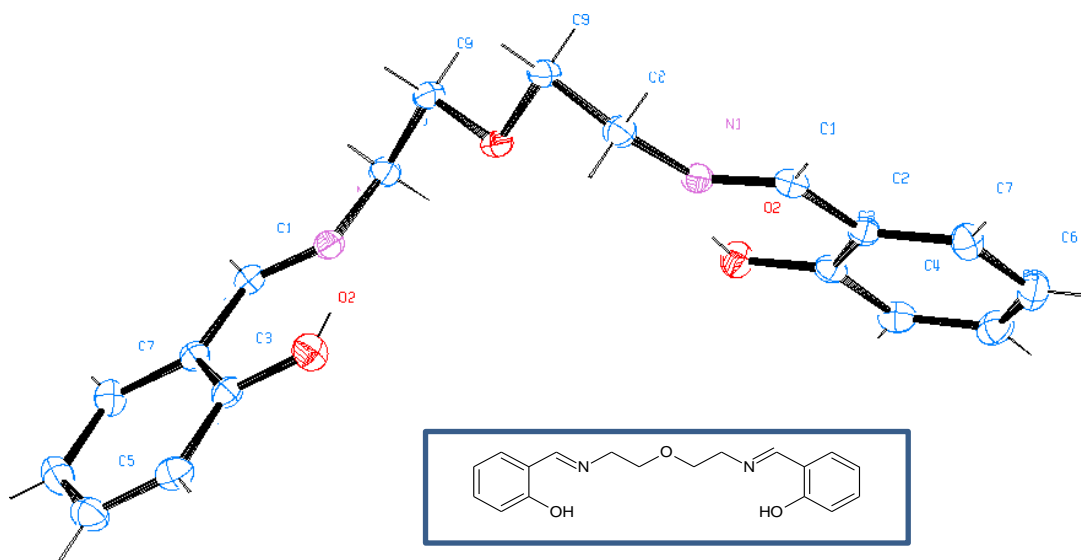


Figure 4. 2 Ortep diagram of **L16** asymmetric molecule of the ligand with the insert showing the Schematic diagram

Further analysis of this crystal shows that the molecule has intermolecular hydrogen bonding between the imine nitrogen and the hydroxyl proton. The unit cell contains four molecules of the above asymmetric molecule lying parallel to each other as shown in Figure 4.3.

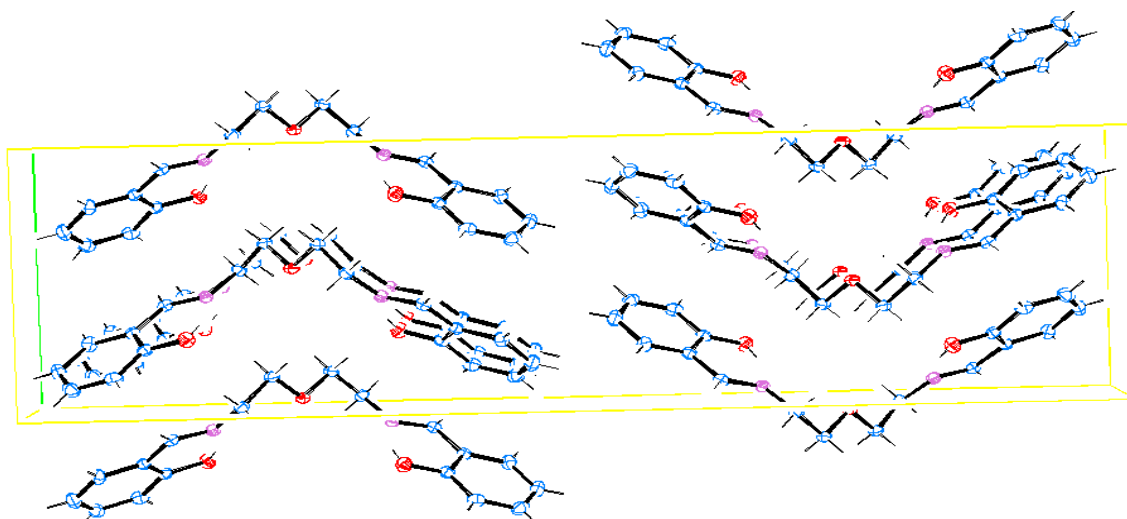


Figure 4. 3 The asymmetric unit cell of **L16** ligand showing the packing of the unit molecules

Since all these ligands were synthesized with the 2,2-dioxy ethylamine spacer, these ligands therefore show an angle of bent if viewed from the spacer atoms as shown by Figure 4.4 for **L16**. This bend is also observed for all the other ligands in this class. This bent structure can be as a result of forces of crystallinity or the ligands resistance to forming the linear molecules shown by the schematic diagrams in Figure 4.2. It is also possible to hypothesize that the bent shape once dissolved in a solution like  $\text{CDCl}_3$  might be able to show dynamism that leads to the proton overlap as discussed in Chapter 3.7.

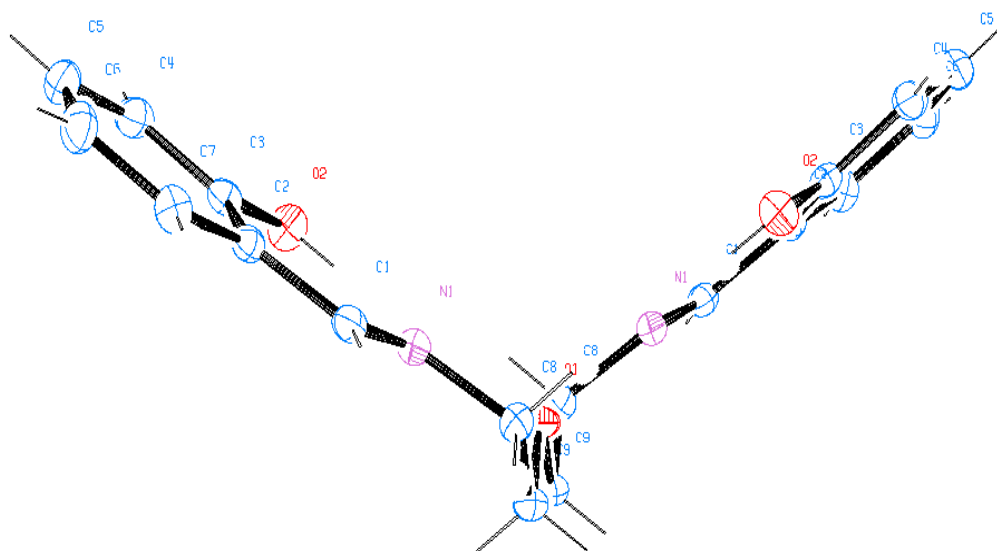


Figure 4. 4 Ortep diagram of L16 ligand viewed from the spacer proton indicating the V-shaped bend of the ligand

Table 4. 2 Selected bond lengths and angles for ligand **L16**

Bond lengths			Bond Angles		Torsion Angles	
Atoms	Length (Å)		bond	Angle (°)	bond	Angle °
O1 C9	1.4235(13)		C1 C9 C8	108.23(9)	O2 C3 C4 C5	179.33(11)
O2 C3	1.3486(14)		C1 N1 C8	120.70(10)	N1 C8 C9 O1	62.17(11)
N1 C1	1.2778(15)					

#### 4.5.1.1.3 Discussion of crystal structure of Ligand L17

The obtained crystal was obtained in crystallised orthorhombic crystal system in a  $Pca2_1$  space group. The crystal system indicates a body centred ligand with two-fold screw axis and a glide plane perpendicular to the  $c$  plane. This is shown by the asymmetric unit with two molecules lying next to each other. The ligands show that one of the molecules has undergone a two-fold rotation lying almost opposite to the other. This is shown with oxygen labelled O6 as shown in Figure 4.5. Selected bond lengths and angles are given in Table 4.3.

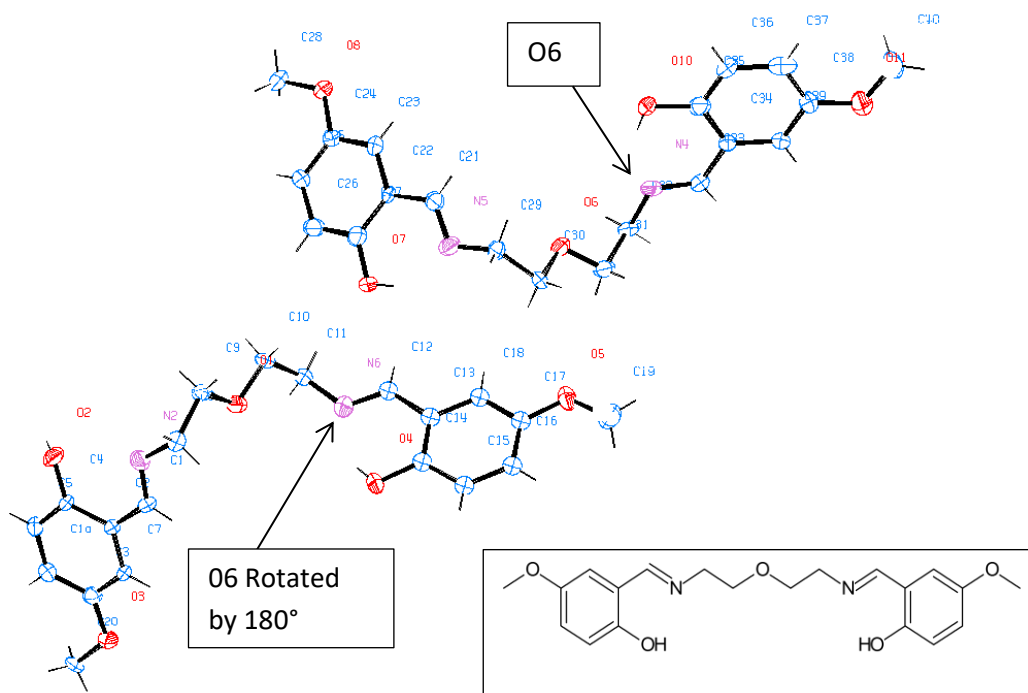
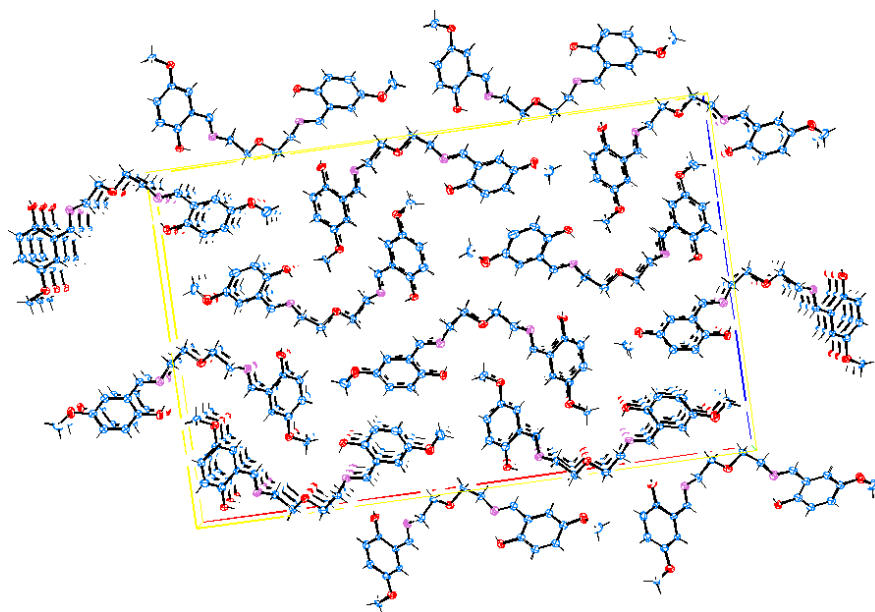


Figure 4. 5 The two-unit molecules in the asymmetric unit of the crystal (insert shows the schematic diagram of L17).

Table 4. 3 Selected bond lengths and bond angles for ligand **L17**

Bond lengths			Bond Angles			Torsion Angles		
Atoms	Length (Å)		bond	Angle (°)		bond	Angle (°)	
O1 C9 <sup>l</sup>	1.419(6)		C9 O1 C10	112.2(4)		O1 C11 N6 C12	-120.4(5)	
O2 C4	1.359(6)		C1 N O8	119.8(4)		O1 C9 C8 N2	62.17(11)	
N1 C1	1.436(7)		C10 C11 N6	110.1(4)				
			N C8 C9	113.2(5)				

The ligand also shows that there is intramolecular hydrogen bonding in the system; however, one of the ligands that have undergone a symmetrical operation indicates that the hydrogen bond is lying opposite to the imine. The selected bond lengths and angles are shown in Table 4.3 and in Figure 4.6 shows the packing diagram indicating the format of arrangement of the ligands in the unit cell. The ligand does not show any inter molecular interaction such as hydrogen bonding.

Figure 4. 6 Packing diagram of ligand **L17**.

#### 4.5.1.1.4 Discussion of crystal structure of Ligand **L18**

The crystal of this ligand was obtained in a monoclinic crystal system with a primitive C-centred space group. The obtained structure shows the ligand with the hydroxyl protons coordinating to the N-atom of the imine as had been postulated in Chapter 2 and 3. The ligands reflections were collected at room temperature with slight disorder. The obtained structure was obtained as an inversion twin leading to relatively high R<sub>f</sub>-factor as shown in Table 4.1. The

obtained crystal structure diagram is therefore shown in Figure 4.7 (a), while Figure 4.7 (b) shows the packing diagram of the ligand.

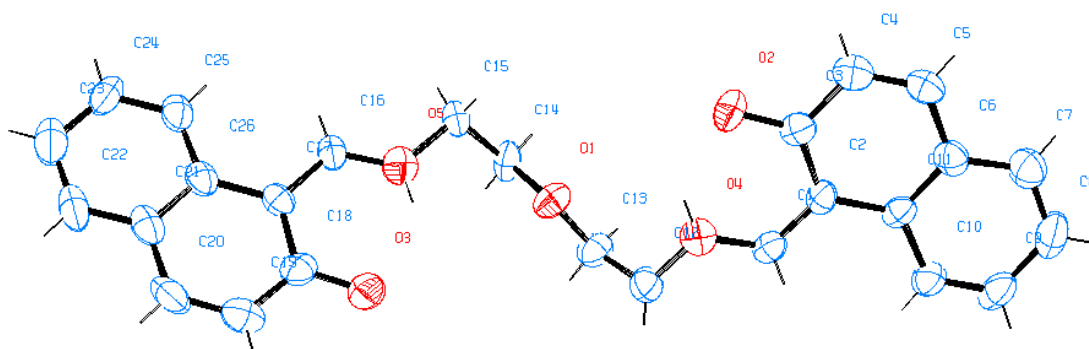


Figure 4. 7 (a) The structure of ligand **L18** with the hydrogen atom bonded to the imine rather than the phenolic oxygen.

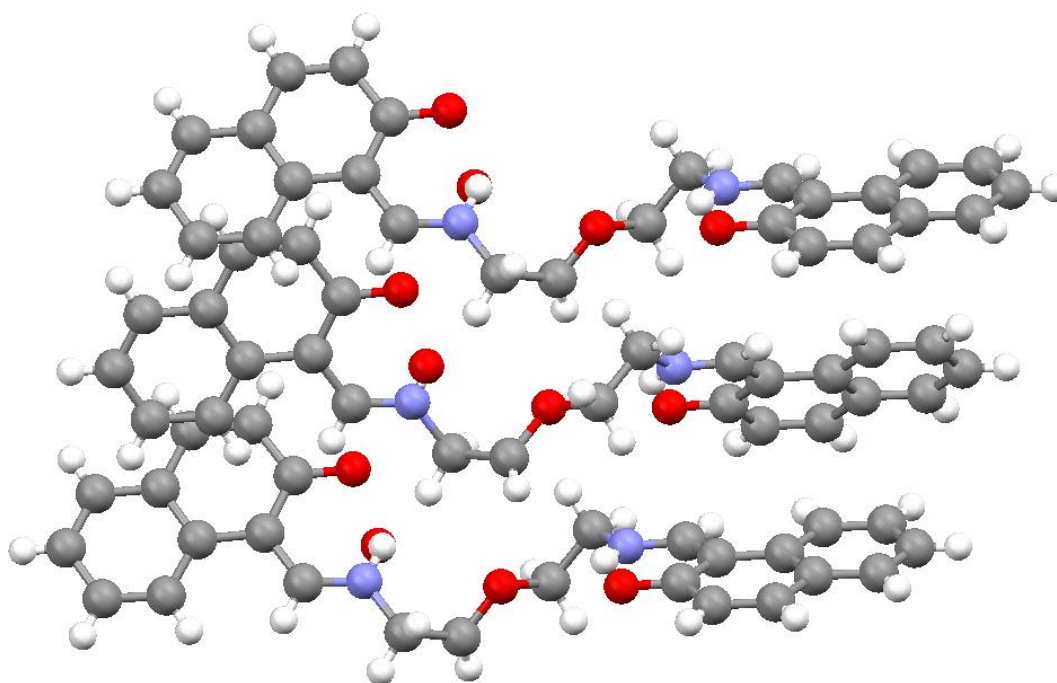


Figure 4. 7 (b) The packing diagram of **L18** ligand (packing diagrams do not usually contain the labels).

in this ligand there was no intermolecular interaction in the unit cell of the ligand as shown in Figure 4.7b. However, the ligand was obtained showing that the H-atom is coordinated to the N-atom in a quinoidal form as had been explained in section 2.9.5 which showed that the naphthyl group undergoes tautomerism. The obtained structure showed the O2-C2 or O3-C18 bond length much shorter than the normal C-O bond. The N-H bond is also showed to be much shorter than the normal N-H bond at 0.8 Å as shown by table 4.3b.

Table 4. 3 (b) Selected bond lengths for ligand **L18**

Atom	Atom	Length/Å	Atom	Atom	Length/Å
O2	C3	1.292(8)	N1	C1	1.322(7)
O3	C18	1.290(8)	N1	C12	1.395(8)
O1	C13	1.419(8)	N2	C16	1.279(8)
O1	C14	1.421(7)	N2	C15	1.465(8)

#### 4.5.2 Summary of the study of crystal structure of the ligands alone

From the results of crystal structure determination of class D ligands, it was observed that these ligands form crystal structures with a slight bent structure as shown in Figure 4.4. This slight bent can therefore be postulated to be part of the reason for non-equivalent protons on the  $^1\text{H}$  NMR in Chapter 3.6.4 (Figure 3.12). This was however not confirmed since the  $^1\text{H}$  NMR was obtained in D-chloroform solvate and therefore can be due to a solvent effect while the crystal structure is in solid state.

#### 4.6 Determination of crystal structure of the complexes

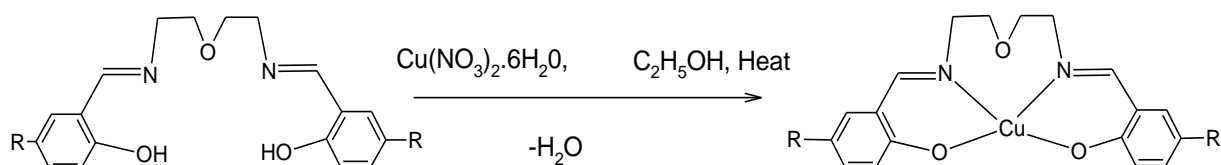
Various attempts were made to synthesize the different complexes using the synthesized ligands. For crystals obtained from the novel ligands these were fully characterized through IR, UV-Vis and MS. While those that form non-novel crystals (obtained through analysis of unit cell) or the samples that did not crystallize, were analyzed through IR and UV-Vis only. This was done to reduce chances of repeat analysis of the formed complexes on the SXRD. The synthesis procedure for these complexes is therefore discussed below.

##### 4.6.1 Experimental

The following reagents were used for the synthesis of the salen type complexes: copper acetate ( $\text{Cu}(\text{Ac})_2 \cdot 6\text{H}_2\text{O}$ ), copper nitrate ( $\text{Cu}(\text{NO}_3)_2 \cdot 3\text{H}_2\text{O}$ ), cobalt acetate ( $\text{Co}(\text{Ac})_2 \cdot 6\text{H}_2\text{O}$ ) and lead perchlorate ( $\text{Pb}(\text{ClO}_4)_2 \cdot 2\text{H}_2\text{O}$ ) all purchased from Sigma Aldrich. The solvents used for the reaction and crystallization include DCM, diethyl ether, dry ethanol purchased from B & M Scientific. The other reagents and instruments used for analysis have previously been discussed.

#### 4.6.2 Synthesis of L17-Cu and L18-Cu and L19-Cu

The method used for synthesis was a literature method by Saban *et al.*[71]. 0.0513 g ( $1.26 \times 10^{-4}$  moles) of ligand **L17** was weighed and dissolved in ethanol under reflux. A stoichiometric equivalent amount of 0.0306 g ( $1.26 \times 10^{-4}$  moles) of  $\text{Cu}(\text{NO}_3)_2 \cdot 6\text{H}_2\text{O}$  was weighed and immediately dissolved in 5 ml ethanol. The ethanol salt solution was then added drop wise to the ethanol-ligand solution slowly and the solution allowed to reflux for 4 hours. The reflux products were removed by rotary evaporation and the product washed with cold methanol. The product was then dried under vacuum and the products were obtained as greenish-black powder which was analyzed as follows. Scheme 4.3 shows the reaction equation for the synthesis of the complexes. The crystals were then obtained through vapour diffusion with DCM-diethyl ether after 3 weeks at ambient temperature and pressure.



Scheme 4. 3 Reaction scheme for the synthesis of the neutral Schiff base copper complex for ligand **L17** R=  $\text{OCH}_3$  where the phenyl group is replaced by a naphthyl group

The other complexes were also synthesized using this method and the results obtained are discussed as follows.

##### 4.6.2.1 Results

The obtained product was therefore analysed by IR as described in Chapter 2.7.1 to prove coordination of the ligand to the metal ion as shown by the spectra of **L17** alone and that of its Cu-complex as shown in Figure 4.8.

The IR analysis results shows that upon coordination there is a shift of the imine peak on the IR from  $1639 \text{ cm}^{-1}$  to  $1630 \text{ cm}^{-1}$  for ligand **L17**. This is also accompanied with the shift of the aromatic C-O peak and the disappearance of the OH peak at  $3000\text{-}3500 \text{ cm}^{-1}$ . Table 4.4 shows the shift of the imine for the various complexes analysed on the IR. These results therefore confirm the formation of the complex.

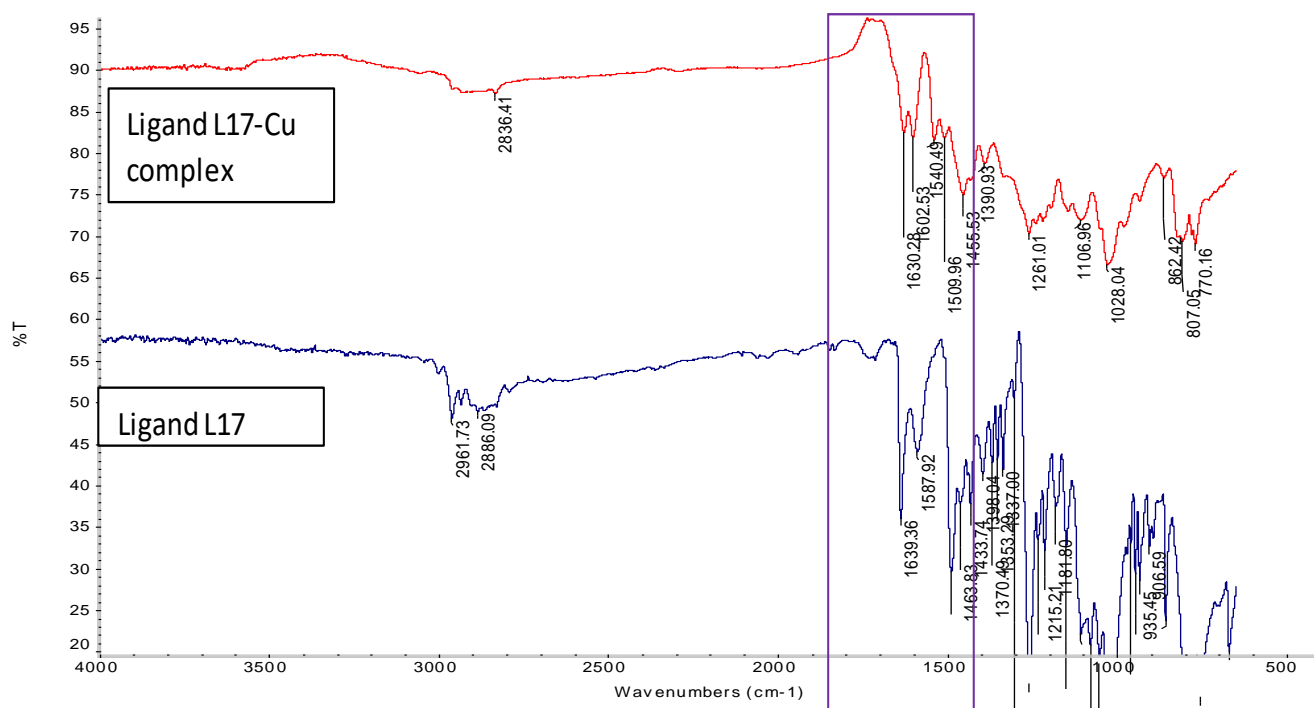
Figure 4. 8 IR of ligand **L17** alone and the **L17-Cu** complex

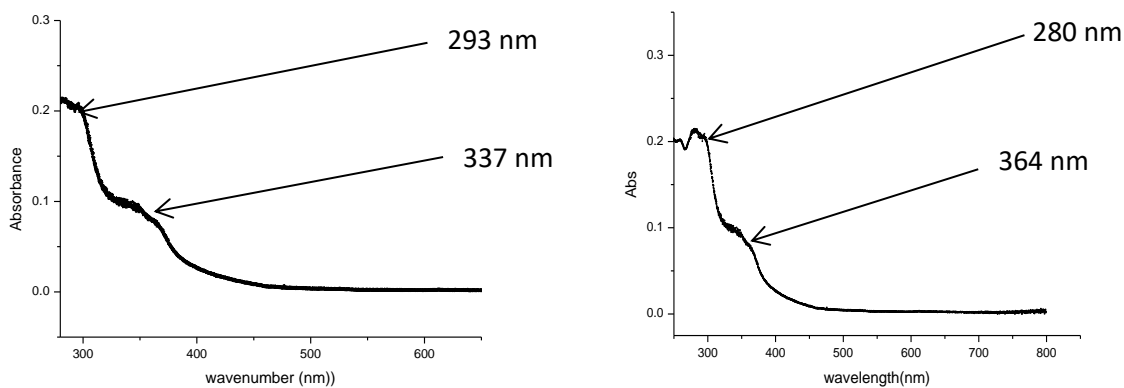
Table 4. 4 FT-IR spectra for the imine stretching frequencies

Name	IR		Name	IR	
	Imine ( $\nu_{C=N}$ , $\text{cm}^{-1}$ )			Imine ( $\nu_{C=N}$ , $\text{cm}^{-1}$ )	
	L	C		L	C
<b>L1-Cu</b>	1627	1636	L17-Cu	1639	1630
<b>L1-Co</b>	1627	1635	L18-Cu	1614	1618
<b>L4-Cu</b>	1633	1621	L19-Cu-pb	1633	1621

Note: L= the uncoordinated ligand. C= complex formed between ligand and metal ion.

#### 4.6.2.2 UV-Vis spectroscopy

The UV-Vis spectra for the Cu-complex for **L17** were obtained as shown in Figure 4.9 (a) and Figure 4.9 (b) shows the spectrum for ligand **L18-Cu** both of which were carried out at  $10^{-7}$  molar solution in chloroform. The results from the UV-Vis spectroscopy shows that both complexes shows the two absorbance maxima with **L17-Cu** two maxima at 293 nm and 338 nm while for **L18-Cu** being at 280 nm and 364 nm which can be attributed to the  $\pi-\pi^*$  and  $n-\pi^*$  transition respectively [150]. The bands above 500 nm usually attributed to the d-d transition could not be observed due to low sensitivity.

(a) **L17-Cu** UV-Vis spectrum in CHCl<sub>3</sub>(b) **L18-Cu** UV-Vis spectrum in CHCl<sub>3</sub>Figure 4. 9 **L17-Cu** UV-Vis spectrum in CHCl<sub>3</sub> and **L18-Cu** UV-Vis spectrum in CHCl<sub>3</sub>

### 4.6. 3 Determination of crystal structure

Selected crystals from each of these complexes were found and mounted on the Bruker Apex II duo instrument. The reflection data were collected as indicated in section 4.6.1.

**Please note** the CIF check report, the HKL, INS and the CIF file for each of these ligands are attached in the CD which is attached to this thesis.

#### 4.6.3.1 Discussion of crystal structures

##### 4.6.3.1.1 L17-Cu and L18-Cu complexes

The class D ligands with the O-donor *pentadentate* system complexes bearing the O-donor group were analyzed first. For this class of ligands, the crystal structure results show that both ligands **L17** and **L18** have a propensity to form a *metallocycle* with the Cu<sup>2+</sup> ion. The *metallocycle* is composed of two ligands coordinating to two copper ions in a 1:1 ratio and are related by an inversion centre as shown by the schematic diagrams in Figure 4.10 (a), Figure 4.11 and Figure 4.12 for ligands **L17-Cu** and **L18-Cu**. The coordinate geometry shows two copper ions coordinating to a highly bent ligand molecule.

Table 4. 5 For class D ligands complex

Identification code	L17-Cu	L18-Cu	L19-CuPb
Empirical formula	C <sub>20</sub> H <sub>24</sub> CuN <sub>2</sub> O <sub>5</sub> Cl <sub>0.5</sub>	C <sub>26</sub> H <sub>24</sub> N <sub>2</sub> O <sub>3</sub> Cu	C <sub>54</sub> H <sub>69</sub> Cu <sub>2</sub> N <sub>4</sub> O <sub>7</sub> Pb <sub>0.5</sub> S
Formula weight	506.88	683.2	2297.73
Temperature/K	293.15	100	296(2)
Crystal system	triclinic	monoclinic	monoclinic
Space group	P-1	P2 <sub>1</sub>	P2 <sub>1</sub> /c
a/Å	8.62(4)	10.8837(6)	19.3936(8)
b/Å	15.86(8)	20.3520(12)	16.0536(7)
c/Å	17.02(8)	10.5257(6)	20.0167(13)
α/°	90.12(6)	90	90
β/°	89.96(6)	116.0950(10)	90.685(5)
γ/°	100.44(8)	90	90
Volume/Å <sup>3</sup>	2288(20)	2093.8(2)	6231.5(5)
Z	2	4	2
ρ <sub>calc</sub> /mm <sup>3</sup>	0.736	2.167	1.225
m/mm <sup>-1</sup>	0.712	9.08	2.106
F(000)	517	1316	2368
Index ranges	-10 ≤ h ≤ 10, -18 ≤ k ≤ 18, -19 ≤ l ≤ 19	-14 ≤ h ≤ 14, -27 ≤ k ≤ 27, -14 ≤ l ≤ 14	-23 ≤ h ≤ 23, -19 ≤ k ≤ 19, -23 ≤ l ≤ 24
Reflections collected	44050	42181	64849
Independent reflections	6163[R(int) = 0.0930]	10380[R(int) = 0.0520]	11145[R(int) = 0.1096]
Goodness-of-fit on F <sup>2</sup>	0.72	0.91	1.098
Final R indexes [I ≥ 2σ (I)]	R <sub>1</sub> = 0.0570, wR <sub>2</sub> = 0.1721	R <sub>1</sub> = 0.0380, wR <sub>2</sub> = 0.1154	R <sub>1</sub> = 0.1095, wR <sub>2</sub> = 0.2091
Final R indexes [all data]	R <sub>1</sub> = 0.0766, wR <sub>2</sub> = 0.1891	R <sub>1</sub> = 0.0561, wR <sub>2</sub> = 0.1333	R <sub>1</sub> = 0.1418, wR <sub>2</sub> = 0.2254
Largest diff. peak/hole / e Å <sup>-3</sup>	0.65/-0.77	0.58/-0.54	2.88/-1.36

Table 4. 6 For class A ligands complex

Identification code	L1-Co	L1-Cu	L4-Cu
Empirical formula	C <sub>18</sub> H <sub>21</sub> N <sub>3</sub> O <sub>2</sub> Cl <sub>0.5</sub>	C <sub>11</sub> H <sub>19</sub> N <sub>4</sub> O <sub>5</sub> Cu	C <sub>24</sub> N <sub>4</sub> O <sub>6</sub> Cu <sub>1</sub> ClH
Formula weight	388.03	350.84	533.09
Temperature/K	293.15	293.15	102.15
Crystal system	triclinic	monoclinic	monoclinic
Space group	P-1	P2 <sub>1</sub> /c	C2/c
a/Å	11.790(11)	9.271(17)	49.035(12)
b/Å	12.936(13)	14.82(3)	7.3271(18)
c/Å	14.479(14)	11.04(2)	27.846(7)
α/°	86.111(13)	90	90
β/°	86.289(15)	102.40(6)	122.015(4)
γ/°	64.50(2)	90	90
Volume/Å <sup>3</sup>	1987(3)	1482(5)	8483(4)
Z	2	4	12
ρ <sub>calc</sub> mg/mm <sup>3</sup>	0.649	1.572	1.252
m/mm <sup>-1</sup>	0.472	1.5	1.056
F(000)	403	728	3153
Index ranges	-14 ≤ h ≤ 14, -15 ≤ k ≤ 15, -17 ≤ l ≤ 17	-13 ≤ h ≤ 13, -21 ≤ k ≤ 21, -15 ≤ l ≤ 15	-58 ≤ h ≤ 45, -8 ≤ k ≤ 8, -32 ≤ l ≤ 33
Reflections collected	31956	44639	22231
Data/restraints/parameters	7194/0/534	4564/3/200	7811/20/491
Goodness-of-fit on F <sup>2</sup>	0.895	1.096	1.052
Final R indexes [I ≥ 2σ (I)]	R <sub>1</sub> = 0.0510, wR <sub>2</sub> = 0.1283	R <sub>1</sub> = 0.0425, wR <sub>2</sub> = 0.1183	R <sub>1</sub> = 0.0755, wR <sub>2</sub> = 0.2131
Final R indexes [all data]	R <sub>1</sub> = 0.0960, wR <sub>2</sub> = 0.1616	R <sub>1</sub> = 0.0597, wR <sub>2</sub> = 0.1245	R <sub>1</sub> = 0.1251, wR <sub>2</sub> = 0.2531

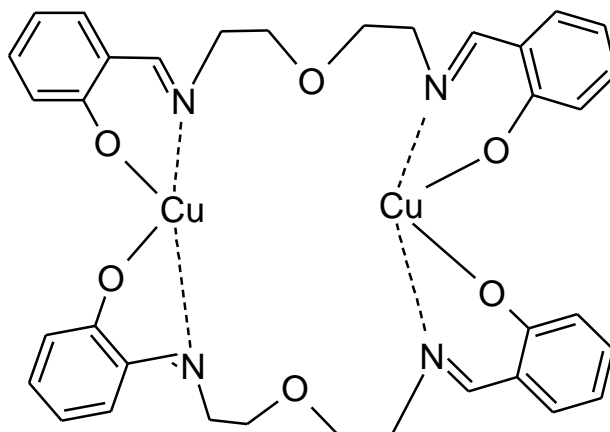


Figure 4. 10 (a) Schematic diagram of the tetrahedral **L17-Cu** complex drawn to represent the inversion mode of coordination of the  $\text{Cu}^{2+}$  to the **L17** ligand. (Note the bond lengths are not drawn to scale).

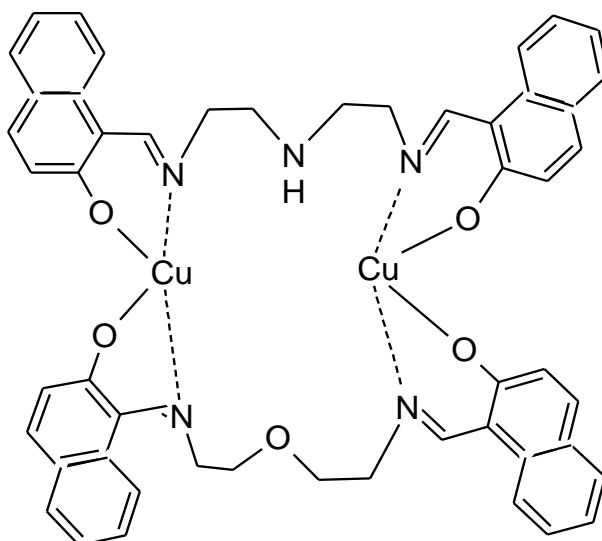


Figure 4. 11 Schematic diagram of the tetrahedral **L18-Cu** complex drawn to represent the inversion mode of coordination of the  $\text{Cu}^{2+}$  to the **L18** ligand (Note the bond lengths are not drawn to scale).

The asymmetric unit cell contains two units which are lying perpendicular to each other and contains the solvent DCM used in the crystallization. The formed complex **L17** contains a mono solvate of DCM and consists of two-unit molecules in the asymmetric units while the *naphthyl* derivative is non-solvated in Figure 4.12. For both complexes the geometry around the Cu-centre is four coordinated with two O-atoms and two N-atoms.

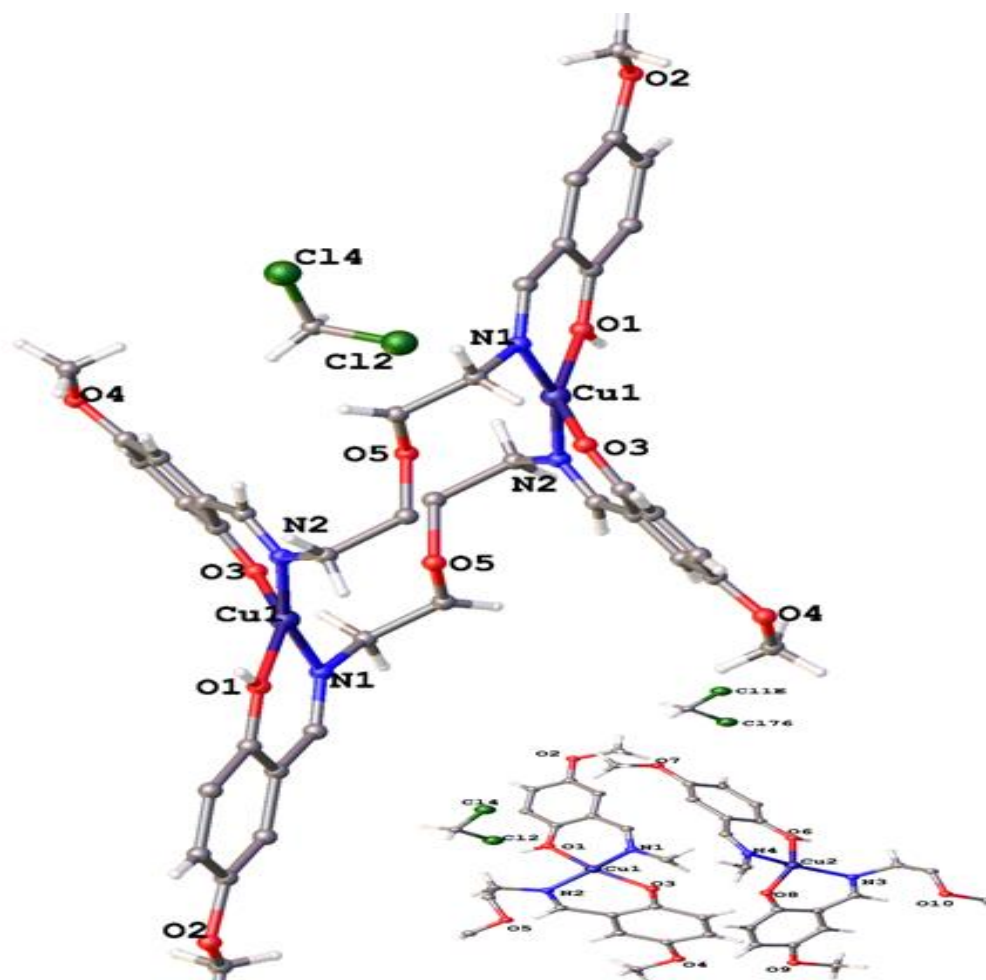


Figure 4. 12 Ortep diagram of ligand **L17-Cu** complex, ellipsoids drawn at 50% probability, some atoms have been deleted for picture clarity. Insert shows a different perspective to show the coordination of the Cu atom

For both the **L17-Cu** and **L18-Cu** in Figure 4.12 and 4.13 shows a distorted square planar geometry and the structure is analogous to our previous work by Saban *et al.*[71] and the N-donor group derivative by Quintero-Tellez *et al.* [151]. The work by Saban *et al.* using ligand **L19** which was also synthesized, and the crystal structure obtained. The obtained complex was subsequently used to make the bi-metallic system in **L19-CuPb** complex discussed in section 4.3.7.1.2. On the other hand, the work by Quintero-Tellez *et al.* consists of the unsubstituted *pentadentate* salen type N-donor ligand.

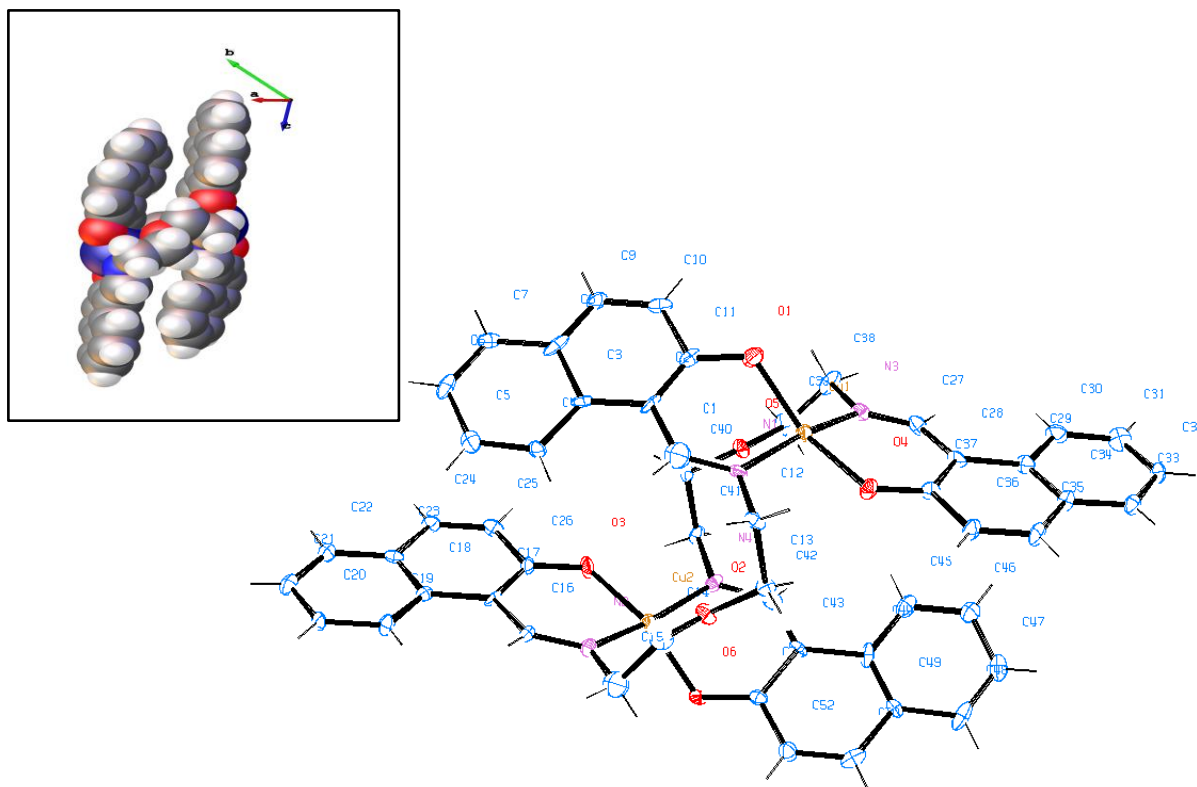


Figure 4. 13 Ortep diagram of ligand **L18-Cu** complex, ellipsoids drawn at 50% probability. Insert shows the space filled model indicating existence of channels caused by resistance between the electron clouds of the naphthyl groups.

For these complexes, all bond lengths and bond angles were all consistent with the literature [151, 152] and are given in Tables 4.7a and 4.7b.

Table 4. 7 Selected bond lengths for ligand **L17-Cu** and **L18-Cu**

(a) For <b>L17-Cu</b>			(b) For <b>L18-Cu</b>		
Bond		Length (Å)	Bond		Length (Å)
Cu1	N1	1.773(7)	Cu2	O3	1.897(5)
Cu1	N2	1.890(8)	Cu2	O6	1.914(5)
Cu1	O1	2.275(9)	Cu2	N4	1.980(6)
Cl4	C50	1.600(9)	Cu2	N2	1.945(7)
Cu2	O8	2.078(8)	Cu1	O1	1.925(5)
Cu2	N4	1.775(7)	Cu1	O4	1.906(5)
Cu2	O6	2.283(9)	Cu1	N1	1.974(6)
Cu2	N3	1.880(8)	Cu1	N3	1.970(6)



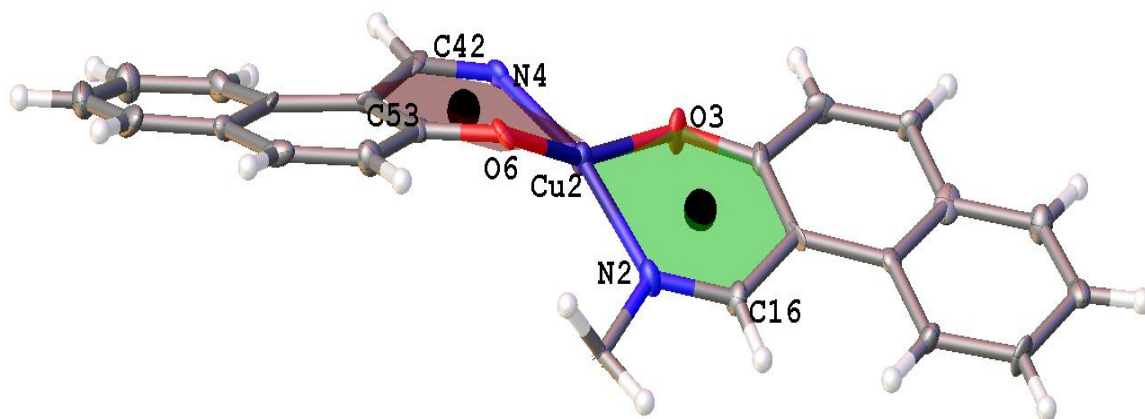


Figure 4.15 Plane showing the slight twist of the bonds around the Cu-centre which are out of plane for **L18**  
 For the solvate in the complex in **L17-Cu** the existence of the substituent is observed to allow the complex solvent molecule to exist in the channels as shown by the packing diagram in Figure 4.16.

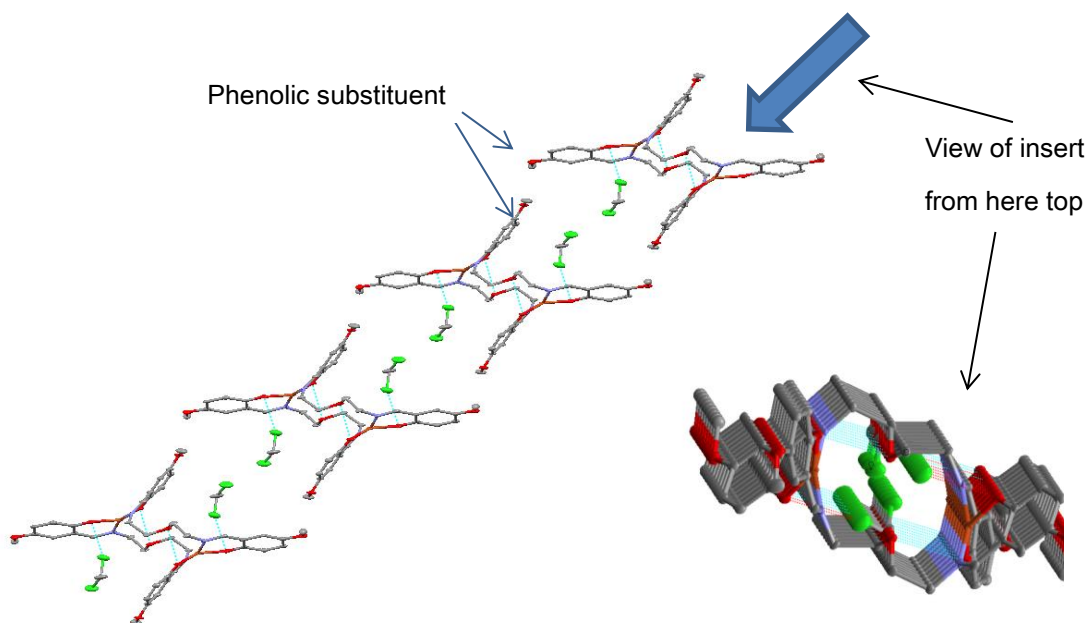


Figure 4.16 Packing diagram indicating the solvent interaction in the **L17-Cu**

On the other hand, for the unsubstituted **L18-Cu** the coordination mode is in such a manner that they are almost perpendicular to each other with each successive complex a line below each other as shown by the packing diagram of **L18** Figure 4.17.

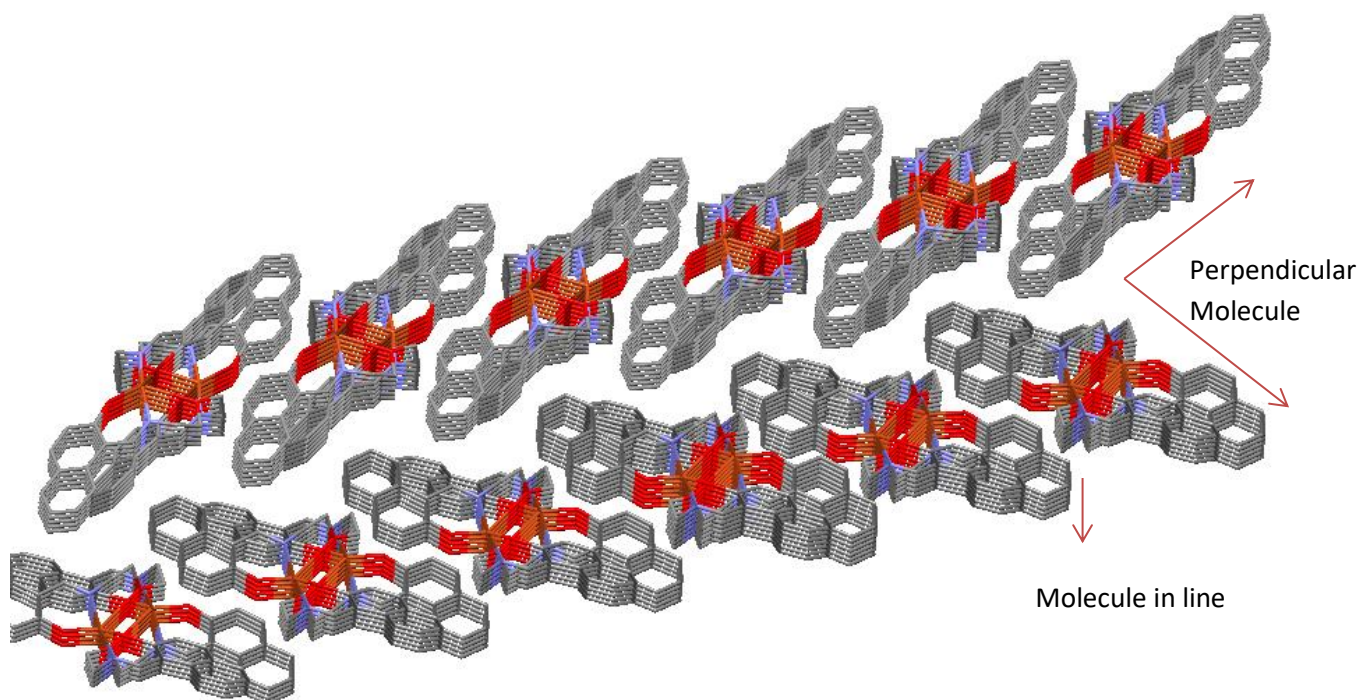


Figure 4. 17 Packing diagram of **L18-Cu** Insert shows the two molecules perpendicular to each other and viewed from the top.

#### 4.6.3.1.1.2 Discussion of the crystal structure of bi-metallic complex **L19-Cu-Pb**

The initial complex **L19-Cu** complex was synthesized as shown by procedure 4.7.2. The obtained product from procedure 4.7.2 was dissolved in ethanol and further reacted with lead perchlorate in a 4:1 ratio. The resultant product was further dried and recrystallized in DMSO/ethanol solution. The crystal was obtained through vapour diffusion with DCM and diethyl ether with the crystal data shown in Table 4.9.

The bi-metallic Cu-Pb metal complex was obtained consisting of four copper ions with four **L19** ligands, the geometry around this copper is analogous to the above square planar complexes for **L17-Cu** and **L18-Cu** as shown in the schematic diagram Figure 4.18. For this complex the coordinated Pb-metal was observed to coordinate in an octahedral geometry (Figure 4.19) with bonds with the hydroxyl O-donor group forming a bi-metallic *metallocycle*. These types of bimetallic complexes with Schiff bases have been reported by Betul *et al.* [153] who used a **Cu-Hg** complex and also by Shi-ping *et al.* [154] who used a two centre Cu system.

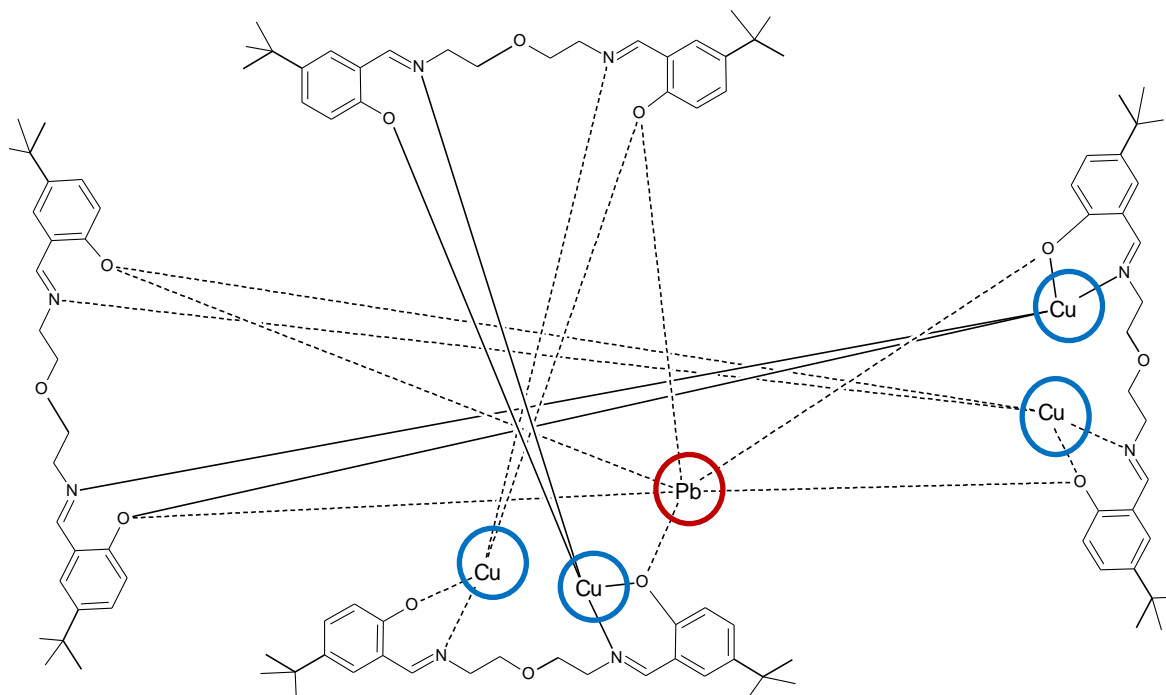


Figure 4. 18 Schematic diagram of **L19-CuPb** bimetallic complex drawn to represent the inversion mode of coordination of the  $\text{Pb}^{2+}$  and the  $\text{Cu}^{2+}$  to the four **L19** ligands (note the bond lengths are not drawn to scale).

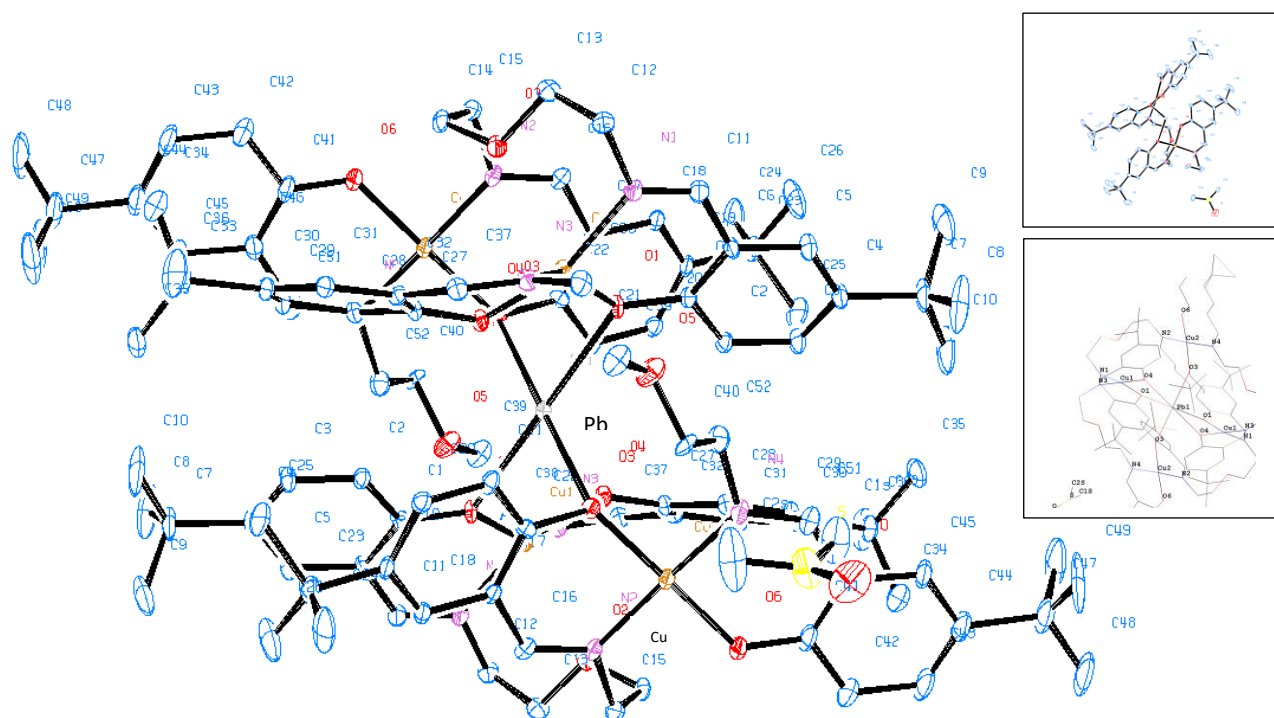


Figure 4. 19 Ortep diagram of disordered **L19-CuPb** complex with four copper **L24** ligands and one  $\text{Pb}^{2+}$  metal the ellipsoids are drawn at 10% displacement probability. Some atoms have been deleted for picture clarity (insert shows wireframe diagram showing the octahedral  $\text{Pb}^{2+}$  and square planar  $\text{Cu}$  geometries and the asymmetric unit with half of the molecule).

Table 4. 9 selected bond lengths for **L19-Cu-Pb**

Atom	Atom	Length (Å)	Atom	Atom	Length (Å)
Cu1	N1	1.946(10)	Pb1	O3 <sup>1</sup>	2.603(8)
Cu1	O1	1.936(14)	Pb1	O3	2.603(8)
Cu1	O1A	1.95(3)	Pb1	O1	2.619(13)
Cu1	O4	1.992(19)	Pb1	O1A	2.39(3)
Cu1	N3	2.07(2)	Pb1	O1A <sup>1</sup>	2.39(3)
Cu1	O4A	1.861(16)	Pb1	O4	2.583(19)
Cu1	N3A	1.892(18)	Pb1	O4A	2.698(17)
Cu2	N2	2.034(10)			
Cu2	O3	1.920(7)			
Cu2	N4 <sup>1</sup>	1.93(2)			
Cu2	O6 <sup>1</sup>	1.956(17)			
Cu2	N4A <sup>1</sup>	2.039(18)			
Cu2	O6A <sup>1</sup>	1.846(15)			

Table 4. 10 Selected bond angles for **L19-Cu-Pb**

Atom	Atom	Atom	Angle(°)	Atom	Atom	Atom	Angle(°)
N1	Cu1	O1A	97.8(8)	O3 <sup>1</sup>	Pb1	O3	180.0(3)
N1	Cu1	O4	163.1(8)	O3 <sup>1</sup>	Pb1	O1	99.2(4)
N1	Cu1	N3	100.9(6)	O3	Pb1	O1	80.8(4)
O1	Cu1	N1	90.4(5)	O3 <sup>1</sup>	Pb1	O1 <sup>1</sup>	80.8(4)
O4	Cu1	N3	87.6(7)	O3	Pb1	O1 <sup>1</sup>	99.2(4)
O4A	Cu1	N1	154.1(9)	O3	Pb1	O4A <sup>1</sup>	103.0(5)
O4A	Cu1	N3A	97.0(7)	O3 <sup>1</sup>	Pb1	O4A	103.0(5)
N3A	Cu1	N1	93.8(7)	O3	Pb1	O4A	77.0(5)
N2	Cu2	N4A <sup>1</sup>	176.2(5)	O3 <sup>1</sup>	Pb1	O4A <sup>1</sup>	77.0(5)
O3	Cu2	N2	89.7(4)	O1	Pb1	O1 <sup>1</sup>	180
O3	Cu2	N4 <sup>1</sup>	94.3(7)	O1A <sup>1</sup>	Pb1	O3 <sup>1</sup>	87.8(11)
O3	Cu2	O6 <sup>1</sup>	169.3(8)	O1A	Pb1	O3 <sup>1</sup>	92.2(11)
O3	Cu2	N4A <sup>1</sup>	87.2(5)	O1A	Pb1	O3	87.8(11)
N4 <sup>1</sup>	Cu2	N2	169.5(11)	O1A <sup>1</sup>	Pb1	O3	92.2(11)
N4 <sup>1</sup>	Cu2	O6 <sup>1</sup>	93.0(7)	O1A <sup>1</sup>	Pb1	O1A	180
O6 <sup>1</sup>	Cu2	N2	84.4(5)	O4	Pb1	O3 <sup>1</sup>	97.4(6)

The obtained structure was obtained as a highly disordered system and the sample was therefore refined into two positions as shown in Figure 4.19. The bond angle around the  $\text{Pb}^{2+}$  ions is therefore refined to two positions this is despite various attempts to synthesise this complex and rerun the crystal on the SXRD.

#### 4.6.3.1.2 For the N-donor group ligands

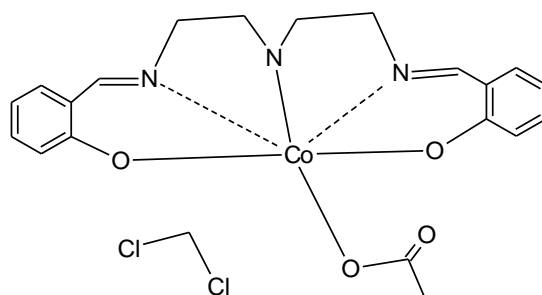
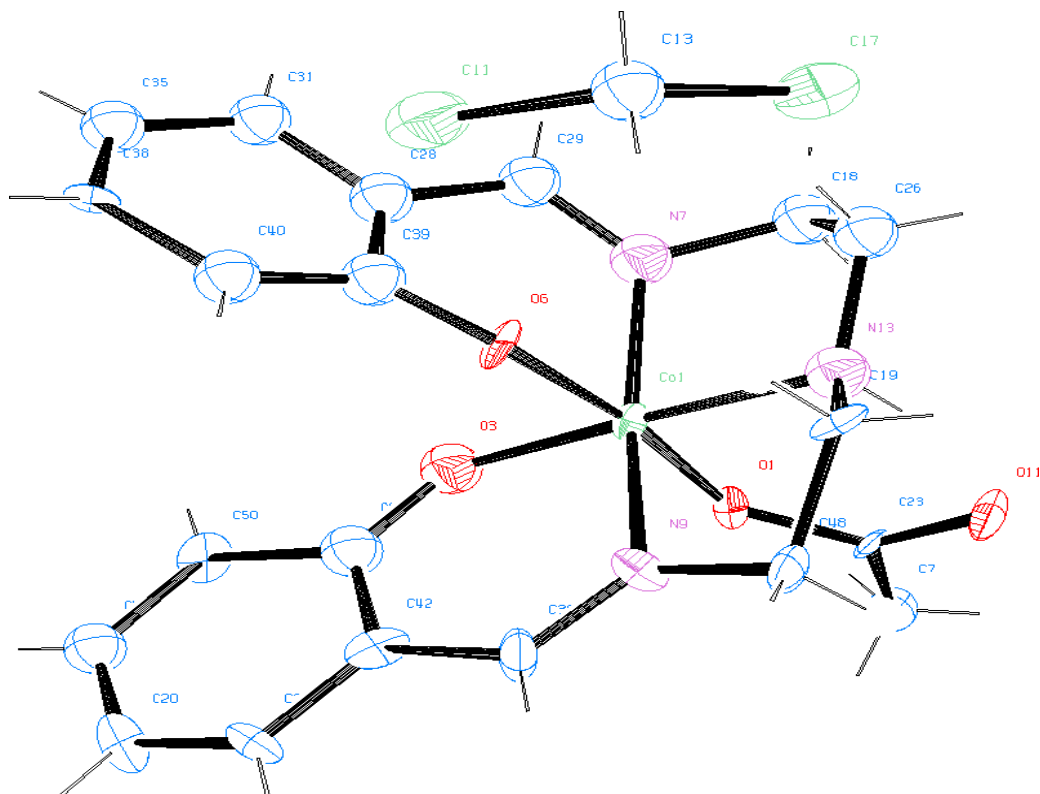
These complexes were also synthesized as described in the procedure 4.6.2 and analyzed with the various analytical techniques. For **L1** ligand; two crystal structures were obtained **L1-Co** and **L1-Cu**. For the ligand **L4** the **L4-Cu** complex was also obtained. These structures are all discussed with the crystal data shown in Table 4.6. all the crystal bond length and angles are shown by table 4.9 and 4.10.

##### 4.6.3.1.2.1 Discussion of the crystal structure of complex **L1-Co**

This was the only complex that was obtained with a cobalt metal as **L1-Co**. The schematic diagram of the complex and the Ortep diagrams are shown in Figure 4.20 and Figure 4.21 respectively. (The IR, UV-Vis and mass spectra are attached to Appendix 3 and 4 confirming formation of these complexes).

This complex was obtained with the *pentadentate salen* ligand coordinated to the metal centre. The Cu atom is therefore coordinated to three N-atoms and two O-atoms of the ligand. The Co is also coordinated to the acetate counter ion forming an octahedral geometry. The asymmetric unit contains two of these octahedral units with one DCM solvate. The bond angles and bond length were consistent with octahedral geometry. From literature, Yilmaz *et al.*[155] studied the analogous Cu complex of this ligand showing a square planar geometry around the Cu metal, while Francis *et al.* [156] studied an analogous Co complex and obtained the same coordination geometry around the Co metal centre.

It is also known that the octahedral geometry for Co complexes are very common since Co prefers this coordination geometry[156]. There are various types of this ligand coordinated to Co that have been synthesized and have found widespread use in oxygen adsorption, however this is the first time its DCM solvate is being reported in this work.

Figure 4. 20 Schematic diagram of **L1-Co** with DCM solvateFigure 4. 21 Ortep diagram **L1-Co** with the DCM solvate and some atoms have been removed for picture clarity

#### 4.6.3.1.2.1 Discussion of crystal structure for complex **L1-Cu** and **L4-Cu** complex

The crystal structure obtained for ligand **L1-Cu** and **L4-Cu** was unexpected since the ligands alone did not show any sign of hydrolysis as discussed in chapter 2.9. The crystal structure for **L1-Cu** was therefore obtained as a mono solvated coordinate square planar complex while the **L4-Cu** obtained as a highly disordered crystal with one coordinate water molecules and 4 hydrated waters of crystallization. Ligand **L1** is used in the above synthesis of the cobalt complex discussed above. The two complexes are therefore discussed and shown in Figure 4.22 and 4.23.

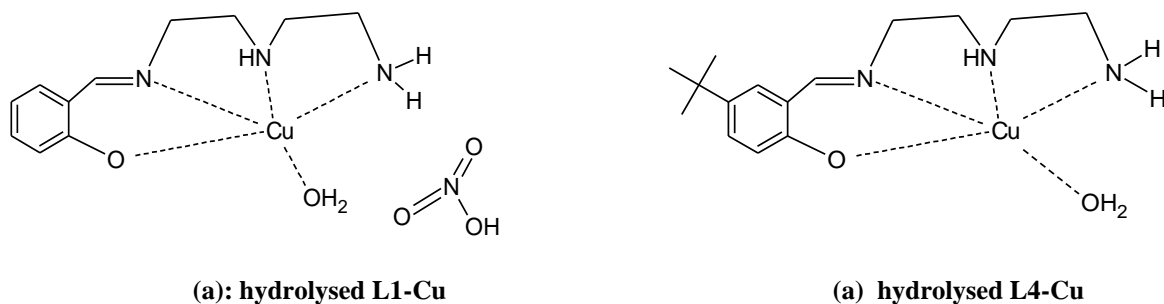


Figure 4. 22 Schematic diagram for hydrolysed L1-Cu with nitrate counter ion

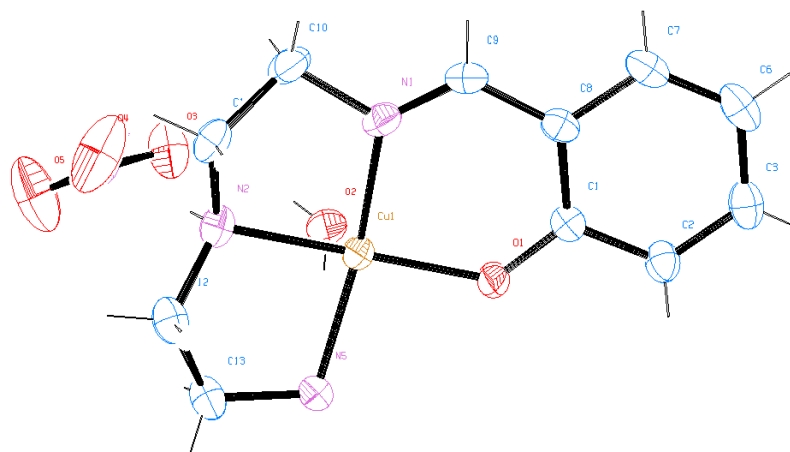


Figure 4. 23 The Ortep diagram of hydrolysed L1-Cu structure. The ellipsoids are drawn at 30% displacement probability level

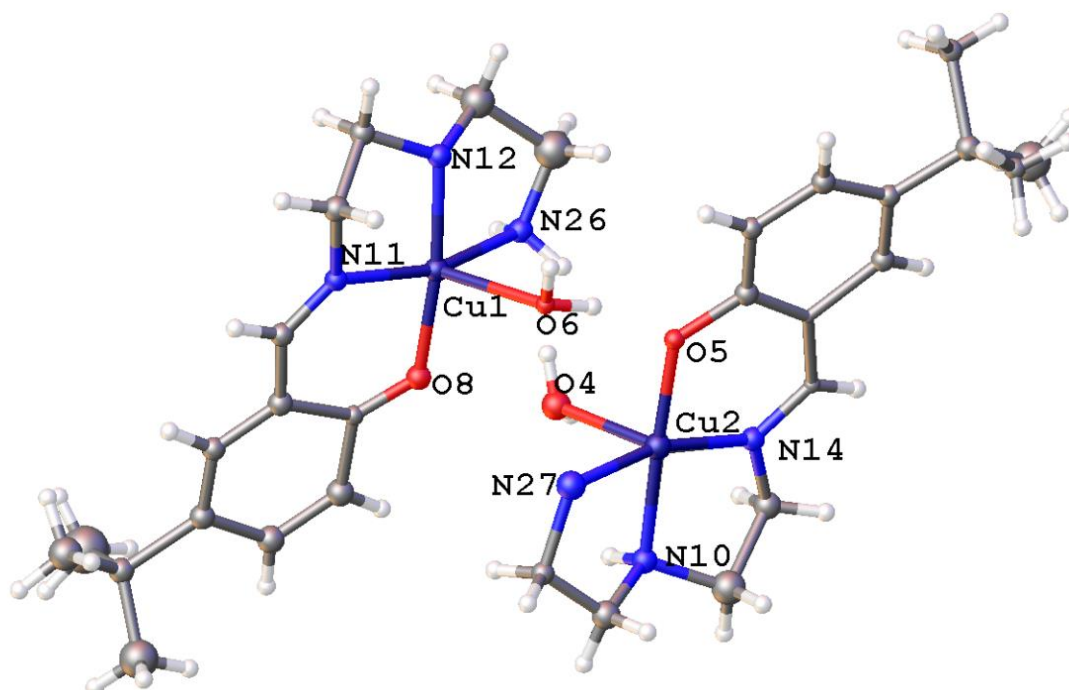


Figure 4. 24 The Ortep diagram of the disordered crystal structure of hydrolysed L4-Cu some atoms have been deleted for picture clarity. Ellipsoids are drawn at 30% displacement probability.

These two complexes were obtained as products of partial hydrolysis of the imine bond as shown by the schematic diagram and crystal structure in Figures 4.22 (a) and 4.22 (b). Because of this; these hydrolyzed complexes were subsequently fully characterized by IR, UV-Vis and MS as shown by the results in Appendix 2 and 3 respectively.

The hydrolysis of the imine bond in salen type ligands is not usually common this is because the ligands are known to be robust and stable in strongly acidic condition [157, 158]. However, there are some literature for example the work of Bhattacharyya *et al.* [159] and Zhou *et al.* [158] on analogous *tripodal* ligand systems and the one of hexadentate O-donor ligand system indicate the ability of these ligands to be partially hydrolysed in ambient conditions in the presence of  $\text{Cu}^{2+}$ ,  $\text{Zn}^{2+}$  or  $\text{Cd}^{2+}$  as shown in Figure 4.25. In the case of the *tripodal* ligands the replacement of  $\text{Cu}^{2+}$  with  $\text{Sn}^{2+}$  leads to full hydrolysis of the imine bond and oxidation of the  $\text{Sn}^{2+}$  to  $\text{Sn}^{4+}$ .

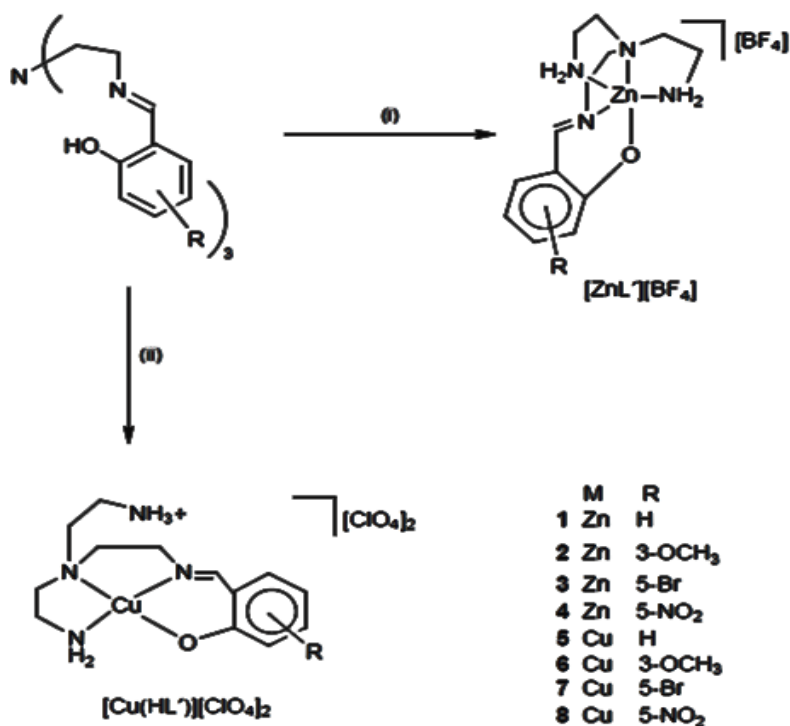


Figure 4. 25 Hydrolytic degradation of Schiff base ligand *courtesy of Brattacharyl et al. [159]*

The hydrolysis of the imine bonds is therefore proposed to occur due to the co-ordination of one arm of the *tripodal* ligand to the metal ( $\text{M}^{2+}$ ) which generates small quantities of  $\text{H}_3\text{O}^+ \text{X}^-$  ( $\text{X} = \text{ClO}_4$  or  $\text{BF}_4$  or  $\text{NO}_3$ ) in situ. This then catalyzes the hydrolysis of the remaining unbound

*salicylidene* arms back to amine groups more rapidly than the rate of complexations of the remaining *salicylidene* units. The amine group generated will then bind to the metal centre in preference to any condensation reaction with free *salicylaldehydes* present in solution [26] as shown by Zhou *et al.* [25] Figure 4.26.

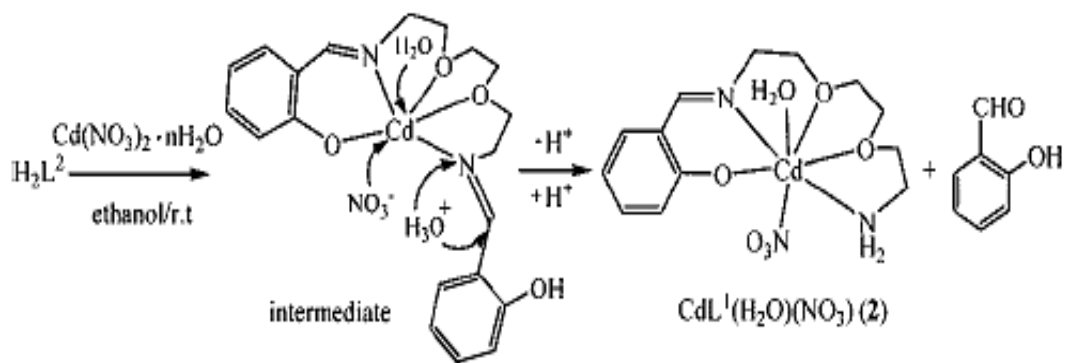


Figure 4. 26 Coordination induced hydrolysis of salen type hexadentate ligand redrawn courtesy of Zhou *et al.* [25]

Since the aim of this work is to study the ability of these ligands to coordinate to the metal, the formed complexes are further discussed as potential product of solvent extraction due to the ease of formation of these products. These complexes are therefore discussed below.

#### 4.6.3.1.2.1.1 Discussion of the crystal structure of hydrolysed L1-Cu complex (Figure 4.23)

A dark purple/blue coloured crystal was selected, and diffraction images of the crystal obtained; the refined images show that the asymmetric unit contains 4-unit molecules in a monoclinic unit cell in a  $\text{P}2_1/\text{C}$  space group. The asymmetric unit shows the analogous **L1** ligand with one of the *salicylaldehyde* groups partially hydrolysed while the other end shows the coordination of Cu metal with three N-donor groups and one O-group. A fifth O-donor atom from the water of crystallization is coordinated in an axial position with a bond length of 2.37Å in distorted trigonal bipyramidal geometry. The trigonal bipyramidal geometry has a small twist mechanism [160, 161] leading to its distortion. Selected bond angles and bond lengths are given in Table 4.11 and are all consisted with the trigonal pyramidal geometry for Cu metal

Table 4. 11 Selected bond lengths and bond angle table of **L1-Cu**

Selected bond lengths (Å)			Selected bond angles		
Bond	lengths		Bond	Angles (°)	
Cu1 O1	1.939(4)		O1 Cu1 O2	95.95(9)	
Cu1 O2	2.370(5)		O1 Cu1 N1	93.32(10)	
Cu1 N1	1.961(4)		O1 Cu1 N2	173.03(9)	
Cu1 N2	2.024(4)		O1 Cu1 N5	94.99(10)	
Cu1 N5	2.046(4)		N1 Cu1 O2	101.80(8)	
			N1 Cu1 N2	84.84(11)	
			N1 Cu1 N5	164.23(10)	
			N2 Cu1 O2	91.01(9)	

#### 4.6.4.3 Discussion of the hydrolysed complex For **L4-Cu** (Figure 4.24)

Equally like the above crystal, light green crystals were obtained and analysed on the SXRD and the asymmetric unit shows two-unit molecules. The Cu metal centre shows a distorted trigonal pyramidal structure just like the above case of the hydrolyzed **L1-Cu**. The bond angles and bond lengths are given in Table 4.12 and 4.13. The obtained hydrolyzed products are analogous to Garvis *et al.*[162] and the bond lengths and angle are consistent with this literature.

Table 4. 12 Selected bond lengths for ligand **L4-Cu**.

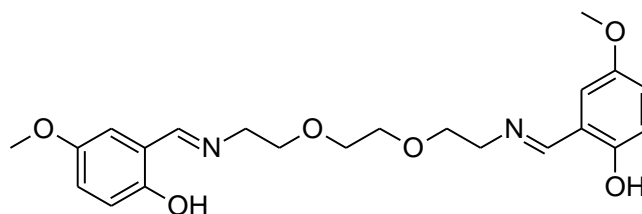
Bond	Length(Å)		Bond	Length (Å)	
Cu2 O11	1.932(4)		Cu1 N1	1.955(5)	
Cu2 N24	2.008(6)		Cu1 N2	2.016(5)	
Cu2 N3	1.950(6)		Cu1 O5	2.279(4)	
Cu2 N4	2.007(6)		O1 C7	1.323(7)	
Cu2 O6	2.327(4)		N36 C15	1.490(8)	

Table 4. 13 Selected bond angles around the Cu metal

Bonds				Angles (°)	bond				Angles (°)
O11	Cu2	N24		95.8(2)	O1	Cu1	N2	174.9(2)	
O11	Cu2	N3		93.0(2)	O1	Cu1	O5	93.57(17)	
O11	Cu2	N4		172.8(2)	N36	Cu1	N2	85.1(2)	
O11	Cu2	O6		94.62(17)	N36	Cu1	O5	91.97(19)	
N24	Cu2	N4		85.1(3)	N1	Cu1	N36	160.5(2)	
N24	Cu2	O6		97.51(19)	N1	Cu1	N2	83.9(2)	
N3	Cu2	N24		163.5(2)	N1	Cu1	O5	104.4(2)	
N3	Cu2	N4		84.5(3)	N2	Cu1	O5	91.4(2)	
N3	Cu2	O6		95.7(2)					
N4	Cu2	O6		92.4(2)					

#### 4.7 Fluorescence studies

This study was developed as a result of the photochromic effect in section 3.92 for ligand **L22**. Shown in Figure 4.27. This ligand had been observed to undergo reversible colour change. This colour change was attributed to fluorescence of the ligand as observed through confocal microscope study.

Figure 4. 27 Schematic diagram of ligand **L22**

Fluorescence which is the ability of an organic ligand to absorb and emit radiation at different wavelengths is a very important property for the design of organic light emitting diodes (OLED). In sensors this property has successfully been exploited in design of cationic chemosensors discussed as follows.

For organic molecules containing a *fluorophoric* unit with site(s) for guest binding, these have found application in detection of metal ions. This is because metal ions effectively act as guests for these molecules through coordination. The resulting effect of the formed complex can be enhancement, shift or quench of the luminescent emissions of these organic ligands. Quenching of fluorescence by metal ion during complexation, is a common phenomenon whereas

enhancement is rare [163, 164]. The fluorescence enhancement is often of much interest as it opens up the opportunity for photochemical applications of these complexes.

The changes brought about by metal ion coordination to *fluorophoric* unit occurs primarily through four methods. These include methods such as; photoinduced electron transfer (PET), photoinduced charge transfer (PCT), formation of monomer/excimer, energy transfer and proton transfer. Transition metal ions with partially filled d-orbitals are known to induce fluorescence quenching by oxidative or reductive PET and energy transfer processes. One known example from literature is  $\text{Cu}^{2+}$  [164] which forms complexes that lead to quenching. The fluorescence behaviour of selected ligands in the presence of the selected divalent metal ions was therefore investigated as follows.

#### 4.7.1 Instrumentation

The 2010 Perkin-Elmer fluorescence spectrophotometer was used for the analysis with a scan range of 200-800nm.

#### 4.7.2 Experimental

All the solutions used were diluted to  $10^{-7}$  moles and the procedure carried out as follows. Class E ligands were used for this study since **L22** ligand belongs to this class.

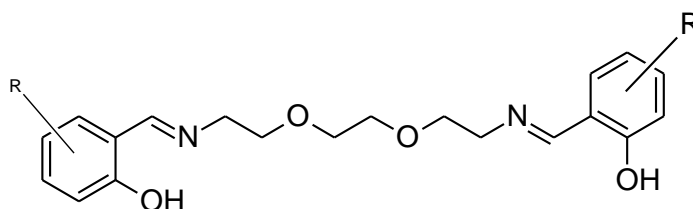


Figure 4. 28 Schematic diagram of hexadentate O-donor salen type ligand

The results from Figure 4.29 shows that all the *hexadentate* O-donor ligands are all fluorescence active with the unsubstituted salicylaldehyde based ligand **L21** showing the highest fluorescence, while **L22** with the electron withdrawing substituent shows the lowest fluorescence. This result was equally quite unexpected considering that the ligand **L22** had shown the transitional light effect under confocal microscopy study. It was observed that ligand **L23** undergoes excimer formation. The formation of the excimer which is a dimeric unit in the excited state in solution can therefore help explain why its high fluorescence in solution is not observed in the solid state similar to the methoxy containing **L22** ligand as a solid state.

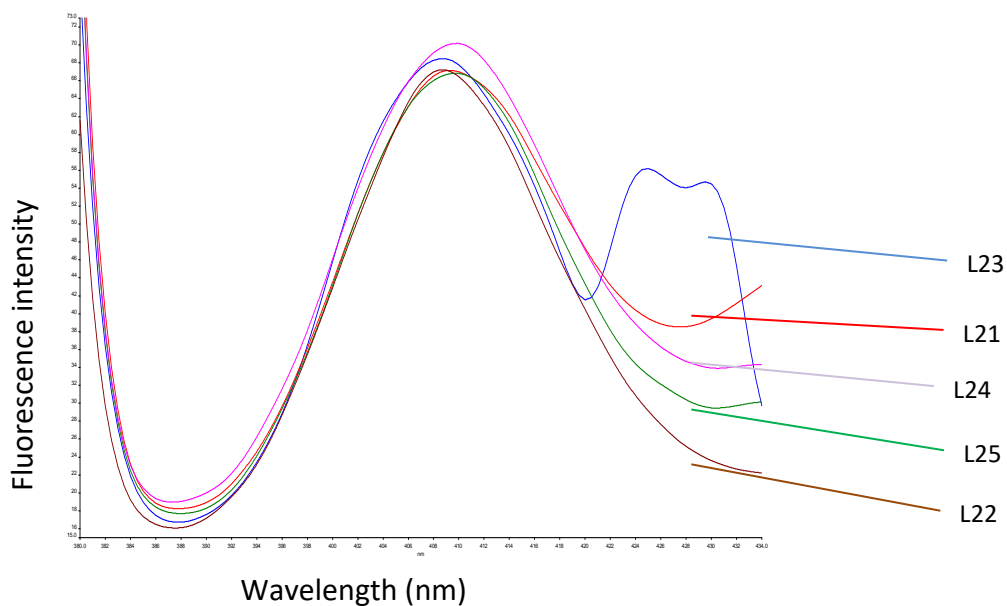


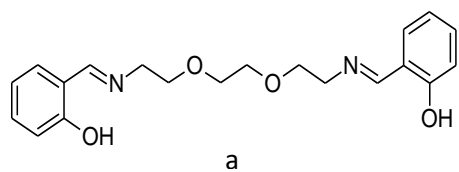
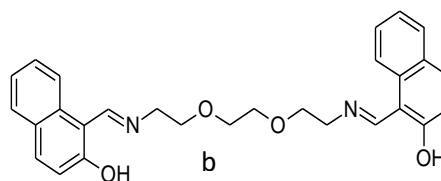
Figure 4. 29 The stacked spectra of the hexadentate O-donor salen type ligands

#### 4.7.2.1 Proposed mechanism of fluorescence of the ligands

The fluorescence of these ligands is mainly attributed to the transition of the ligand from the hydroxyl tautomer (enol form). The enol form is then excited to a ( $\pi-\pi^*$ ) state from where the hydroxyl proton is quickly transferred to the nitrogen of the imino atom as had been discussed in both Chapter 2 and Chapter 3 to form the keto form. The ketone-tautomer (also a  $\pi-\pi^*$  state) may then undergo relaxation toward a ground state releasing the energy through fluorescence [163]. The results as shown above therefore indicate that since the ligand **L22** which had been shown to undergoes this transition in the presence of direct sunlight will have very minimal transition to ground state. The other highly stable ligands **L21** with unsubstituted *salicylaldehyde* group will therefore form the higher shift due to the absorbance of light energy to transit it to the ketone form and subsequent release of this energy as the high fluorescence.

#### 4.7.3. Study of solvent effect in fluorescence

Two ligands were selected for this study. This included the high molecular weight ligands **L21** and **L23**. These two ligands were selected due to their lack of substituents and because they showed comparably higher fluorescence by themselves. These two ligands are shown by their schematic diagrams in Figure 4.30 (a) and 4.30 (b).

Figure 4.16 Schematic diagram of ligand **L21**Figure 4.17 Schematic diagram of ligand **L23**Figure 4.30 Schematic diagrams of (a) **L21** and (b) **L23**

From the results in Figure 4.31, it is observed that the ligands themselves showed varied response in the different solvents. Ligand **L21** showed higher fluorescence than the ligand **L23** with the naphthyl substituent.

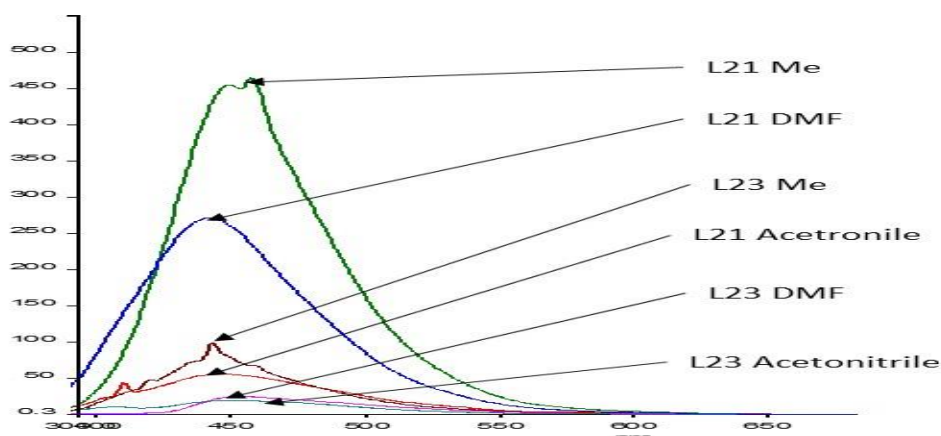


Figure 4.31 Fluorescence spectra of **L21** and **L23** using Me (methanol), DMF (dimethylformamide) and acetonitrile solvents (full spectrum attached as appendix 3) at excitation at 360 nm

By comparing the ligands fluorescence responses in different solutions, it is observed that in methanol, the fluorescence is higher than both DMF (dimethyl formamide) and acetonitrile. In subsequent studies DMF is used over the highly fluorescent active methanol solvent since the formed complexes have lower solubility in methanol.

#### 4.7.4 Metal ligand studies

##### 4.7.4.1 Procedure

The two ligands of *hexadentate* O-donor ligands **L23** and **L25** were chosen and were weighed and made to a concentration of  $10^{-7}$  moles in a 1:1 DMF water solution. Each of the 6 metal nitrate salts were subsequently weighed and made to a solution of  $10^{-7}$  moles in the 1:1 DMF water solution. 2 ml of each of this solution was subsequently mixed and analysed on the fluorimeter.

#### 4.7.4.2 Results

From the results it is observed that despite the two ligands having the same spacer group, they respond differently towards the selected divalent transitional metal ions. The highly aromatic *naphthyl* containing ligand **L23** is observed to be highly responsive towards  $Zn^{2+}$  ion compared to any of the other metal ions. This is followed by  $Cd^{2+}$  which is much less responsive than the  $Zn^{2+}$  but higher than the other base metals. On the other hand for ligand **L25** with the nonyl group it is observed that  $Zn^{2+}$  ions are relatively highly fluorescent active than the other divalent transitional metal ions. It is also observed that  $Pb^{2+}$  ion has a relatively high response than the  $Cd^{2+}$  ions.

These results indicate that the different substituents affect the fluorescence of these ligands towards various divalent base metal ions. Hence the study of the effect of the change of donor groups (changed from the O donor to the N donor group) was undertaken by using ligand **L8** and **L10**. The results are discussed below.

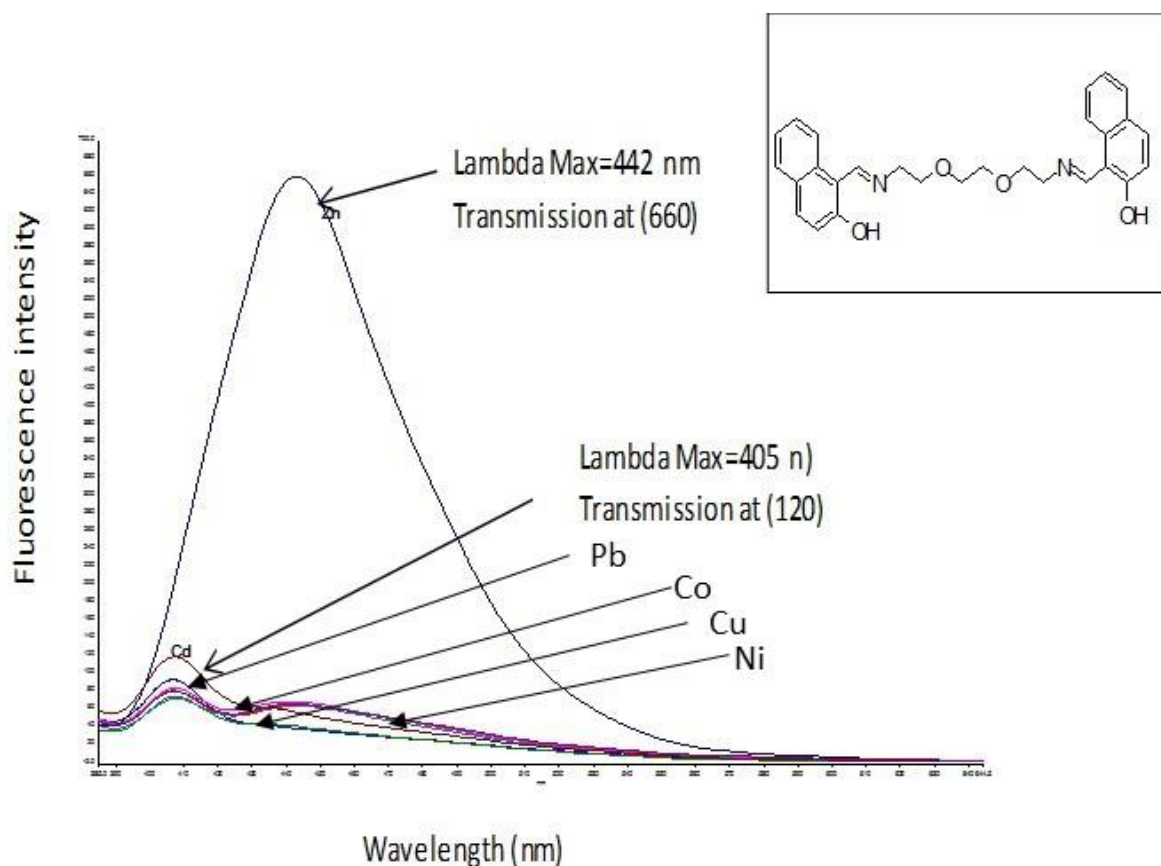


Figure 4. 32 Fluorescence spectra of different metal ions with **L23** at ratio of 1:1 in DMF and H<sub>2</sub>O 1:1 solution at excitation at 360 nm at 25°C.

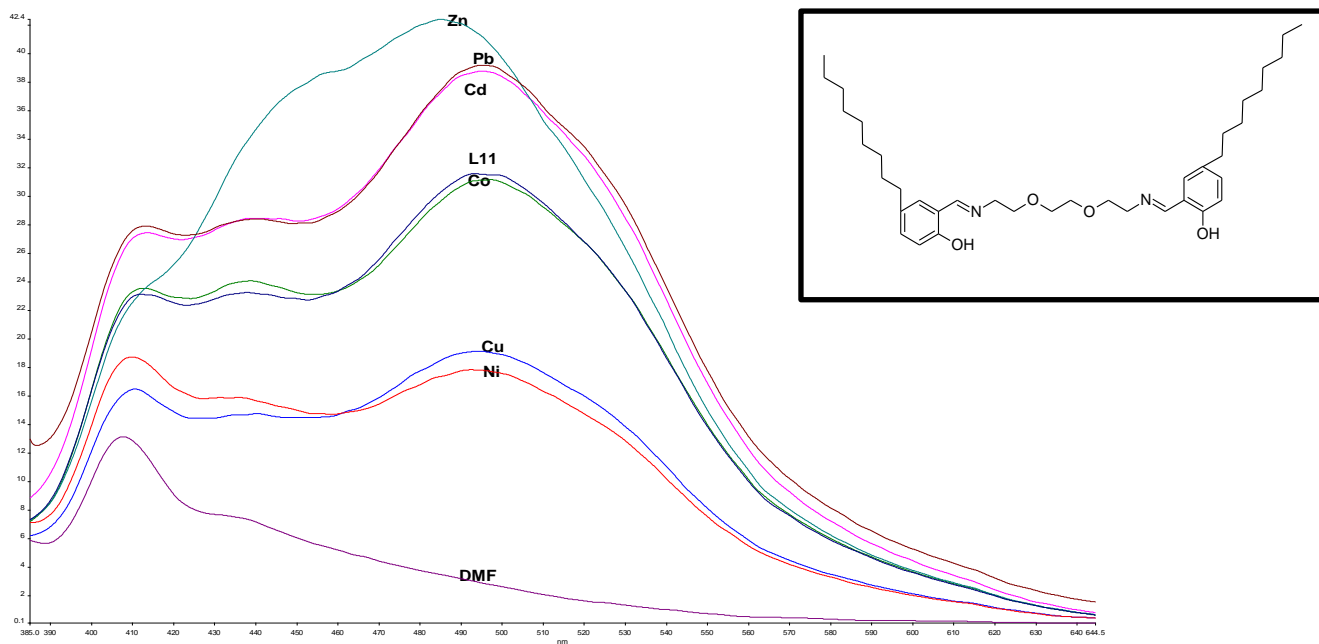


Figure 4. 33 Fluorescence spectra of base metal ions with **L25** at ratio of 1:1 in DMF and H<sub>2</sub>O 1:1 solution at excitation at 360 nm at 25°C.

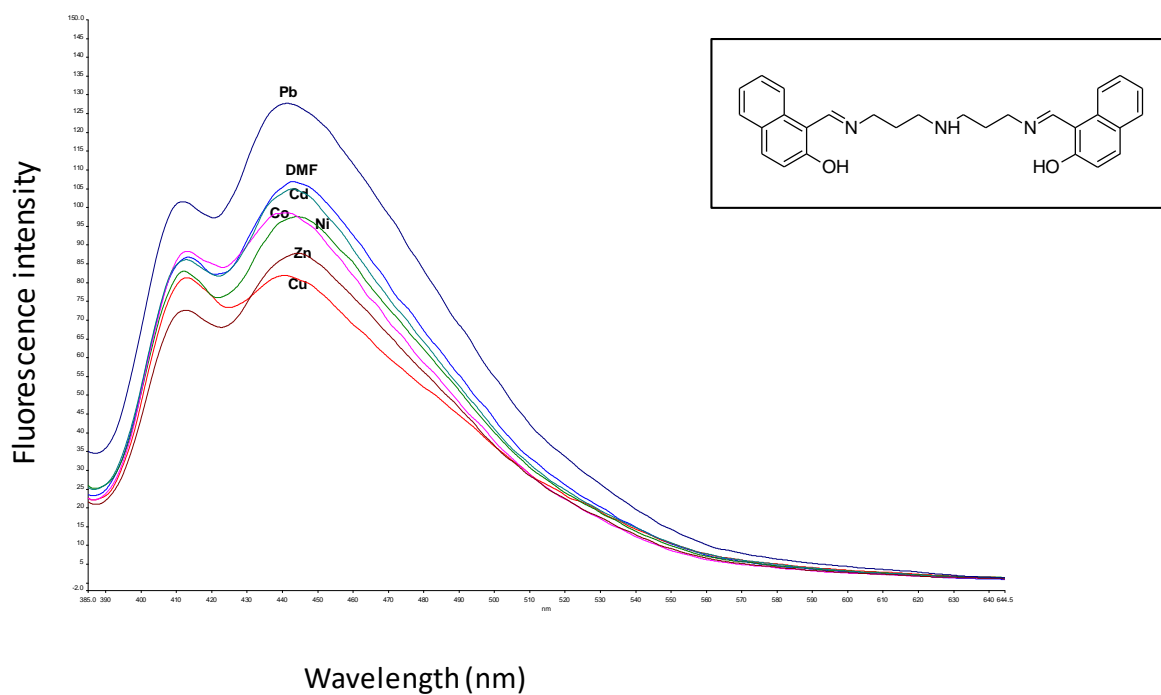


Figure 4. 34 Fluorescence spectra of base metals with ligand **L8** at ratio of 1:1 in DMF and H<sub>2</sub>O 1:1 solution at excitation at 360 nm at 25°C

The observed results completely differ from the above results for the O-donor groups with these ligands showing higher fluorescence of Pb<sup>2+</sup> ions than Zn<sup>2+</sup>.

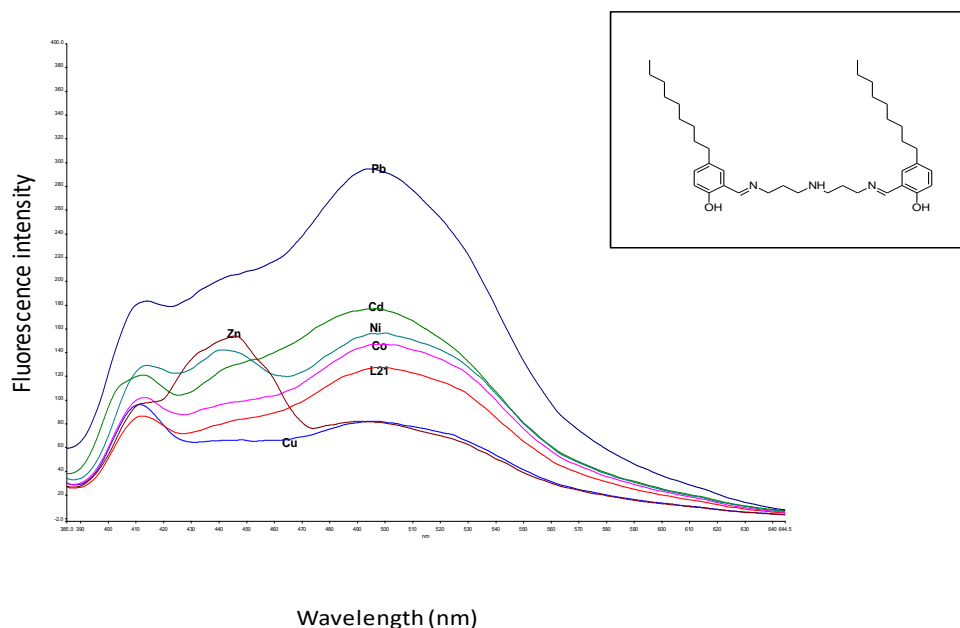


Figure 4. 35 Fluorescence spectra of base metals with ligand **L10** at ratio of 1:1 in DMF and H<sub>2</sub>O 1:1 solution at excitation at 360 nm at 25°C

#### 4.7.5. Mechanism of metal induced fluorescence

The fluorescence of these ligands due to the presence of the metal ions is usually attributed to the photo induced charge transfer that occurs when the metal is coordinated to the ligand. In most cases ligands usually undergo intramolecular charge transfer due to the lone pairs on the N or O-donor group [165]. However due to coordination these donor groups are usually involved in coordination therefore restricting the fluorescence upon coordination. For metal ions that have high charge transfer capability these usually lead to higher fluorescence as observed for the metal ion such as Zn<sup>2+</sup>, Pb<sup>2+</sup> or Cd<sup>2+</sup>. On the other hand, for metal ions without charge transfer capability for example Cu<sup>2+</sup> usually leads to quenching as observed by the results.

#### 4.8 Summary and conclusion

Since the aim of this dissertation is to study the salen type ligands bearing different donor groups and substituents in solvent extraction process, this work was limited to selected ligands and complexes. From these selected ligands three crystals of sufficient size were obtained and analyzed through single crystal X-ray diffraction technique. The results show that these *pentadentate* Schiff base ligands with the O-donor in their spacer were obtained showing a bent out of plane due to a stability effect and conformation change due to crystallinity forces or ligand preorganization.

Six complexes were then synthesized and fully characterized by IR, UV-Vis and MS where appropriate, before analysis on the SXRD instrument. The pentadentate class D ligands had a predisposition to coordinating with  $\text{Cu}^{2+}$  ions forming a metallocycle with the metal centre coordinated in square planar geometry. On the other hand, the pentadentate class A ligand **L1** was observed to coordinate with  $\text{Co}^{2+}$  ion in an octahedral geometry. Both this ligand **L1** and the **L4** derivatives were observed to coordinate with  $\text{Cu}^{2+}$  in unexpected metal induced degradation of the ligand through partial hydrolysis to form trigonal bi-pyramidal geometry.

For the pentadentate O-donor class D ligands, the copper complexes **L17-Cu** and **L18-Cu** were obtained as metallocycles with the Cu-metal centre coordinated in square planar geometry. The Cu-Pb complex of ligand **L19** with a  $\text{Pb}^{2+}$  centre coordinated to four Schiff base complexes of  $\text{Cu}^{2+}$  was also obtained. The results were a confirmation of the ability of these ligands to form a bi-metallic system where the  $\text{Cu}^{2+}$  are coordinated in a similar manner to **L17-Cu** and **L18-Cu** complexes then coordinated to the  $\text{Pb}^{2+}$ .

Finally, selected ligands were studied for fluorescence which showed the ligand **L23** with the hexadentate O-donor showing higher fluorescence and exciplex formation. Upon introduction of the metals it was observed that the *hexadentate* salen type O-donor ligands have a strong response to  $\text{Zn}^{2+}$  ions, while the *pentadentate* N-donor were observed to have a higher response towards  $\text{Pb}^{2+}$ .

# **CHAPTER 5**

---

## **SOLVENT EXTRACTION OF THE N-DONOR SCHIFF BASE LIGANDS**

---

## 5.0 Introduction

Schiff base ligands have various properties which include ease of synthesis and ease of modification. These properties can be exploited in solvent extraction operations to design ligands that are selective and efficient in extraction of different metal ions. In most cases the selectivity can be obtained by simply varying the substituents and the alkyl group between the donor group(s). The N-atom as a donor group is classified as a softer donor in the hard and soft acid base classification (HSAB). This softer nature allows this donor group to coordinate to various metal ions, by adding different alkyl groups on this atom it can therefore be tuned to coordinate to a wide range of metal ions. This chapter will focus on the study of solvent extraction, transport and stability of the N-donor ligands. The work will further consider how the different substituents and the alkyl groups affect the extraction property of these ligands.

### 5.1 The donor group

In ligand design for solvent extraction, the addition of donor groups in a ligand system provides various advantages. The most significant advantage is that it is an added centre of coordination for the ligand as had previously been discussed in Chapter 1. Apart from this, the added donor group alters the physical or the chemical characteristics of the ligand. The electronic effect of this donor can often be measured by the electronegativity of the donor group. Therefore, the highly electronegative donor groups tend to encourage the extraction of hard metal ions in the **HSAB** classification. The level of changes due to the electronic effect of the added donor group can be attributed to the position of the added donor group in relation to other functional groups or atoms in the ligand system. For N-donor ligands or even the O-donor ligands the ability of this donor groups to coordinate lies in the various groups attached to the donor group as discussed below.

#### 5.1.1 N-Donor group

The reactivity of the imine (*azomethine*) centre has been comprehensively discussed in Chapters 1, 2 and 4. This chapter will focus on the ability of the added N-donor group to coordinate in the salen type ligand's backbone and how this coordination can affect the ability of these ligands to be used in solvent extraction systems.

The reactivity of the N-donor in the salen type ligand backbone is based on the standard model of coordination of ammonia as an example of a saturated nitrogen atom [166]. The addition of

an alkyl group(s) to this saturated amine shows that the enthalpy of protonation in a gaseous system increases along the Series 5.1.



Series 5. 1 The order of protonation of N-atom in a gaseous system courtesy of Martell *et al.* [166].

On the other hand in aqueous systems the protonation constants (pKaH) in aqueous systems for the different amines are known by the Series 5.2.



Series 5. 2 Protonation constant of saturated amines in aqueous systems courtesy of Martell *et al* [166].

These contrasting results indicate that the addition of the alkyl groups to the N-donor prompts an inductive effect in gaseous systems [166]. The addition of the alkyl group in the aqueous system is however restricted by the presence of the H-atom. Any reaction of the amine will therefore focus on the replacement of the H-atoms by the different alkyl groups. This is observed in the transitioning from primary amine (i.e. RNH<sub>2</sub> showing 2H), to secondary amine (RNH) to tertiary amine (R<sub>3</sub>N).

### 5.1.1.1 Effect of added alkyl groups between the donor groups

The addition of an alkyl group to N-donor atoms can be shown by studies of protonation equilibrium of gaseous ammonia as shown in Series 5.1. For the Schiff base ligands, the added alkyl groups R as shown in Figure 5.1 offers greater advantages in terms of modification of these ligand systems to allow for coordination of either larger or smaller metal ions as discussed in ligand bite size in Chapter 4.

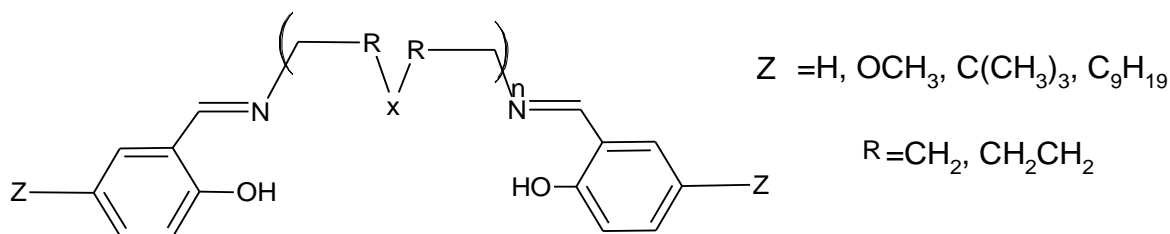


Figure 5. 1 Salen type ligands where R can be different alkyl groups and X being different donor groups.

The increased number of alkyl groups between the two donor groups therefore has three important effects on the Schiff base ligand system. The first consideration is that it has an inductive effect. Studies of this inductive effect show that this effect is often very minimal

due to the dominant nature of the donor group X shown in Figure 5.1. The effective inductive effect will therefore greatly depend on the nature (electronegativity) of this donor group [29]. In most cases the inductive effect and steric hindrance to the donor group will often outweigh this inductive effect as had been shown in Chapter 2.9.2.2 by the observed shift of the imine upon addition of the alkyl group. The general trend of this inductive effect can be shown by

Series 5.3.



Series 5.3 The inductive effect due to the alkyl group courtesy of [29].

The second factor to be considered has to do with the chelating ability. The chelate effect in polydentate ligand systems as theorized by Bjerrum [167] and Schwarzenbach [29] shows that the increased alkyl group in polydentate ligand systems has the effect of changing the coordination mode of the metal. The mode of metal coordination is controlled by the permissible geometry around the metal ions [166]. This geometry can be tetrahedral, square planar, square pyramidal, trigonal bi-pyramidal or octahedral geometry. The chelation of the metal by the ligand will therefore be controlled by the size and the flexibility of the chelate ring. The degree and freedom allowed by these ligands sometimes leads to the distortion of these geometries such as distorted square planar, distorted square pyramidal or distorted octahedral geometry [166] depending on the charge and size on the metal ion.

The third effect due to the added alkyl group R (Figure 5.1) on the N-containing donor group is towards its solvation ability. This is discussed by considering the effect of saturation of the N-donor group in tetradentate N ligand systems discussed below.

## 5.2 Tetradentate N-containing ligands

The tetradentate ligands are derivatives of the protonation of the ammonia molecules as described above with three alkyl groups around the N-donor. These were first synthesized by Trofimenko *et al.* in the 1960s [168, 169] and are considered to be an important class of ligands in coordination chemistry. For these types of ligands, the tertiary functionalized N-atom will have a greater steric effect as shown by both Series 5.1 and 5.2 above.

From the above discussion, the different alkyl groups influence the basicity (alkaline) character of the ligand. The addition of an electron donating group to ammonia will increase its electron density. This will have the effect of raising the energy of the lone pair, making it more available for protonation. The successive increase of the alkyl group will therefore lead to increased

basicity of the amine as shown in Table 5.1. The addition of an electron withdrawing substituent will have the opposite effect by withdrawing electron density from the N-donor which makes it less basic [170]. The addition of an aromatic group on the other hand will lead to stability of the lone pair [170]

Table 5. 1 The pKaH values of different alkyl groups to different amines courtesy of Clayden *et al.*[170]

<b>R</b>	<b>RNH<sub>2</sub></b> (pKaH)	<b>R<sub>2</sub>NH</b> (pKaH)	<b>R<sub>3</sub>N</b> (pKaH)
Me	10.6	10.8	9.8
Et	10.7	11.0	10.8
n-Pr	10.7	11.0	10.3
n-Bu	10.7	11.3	9.9

From the Table 5.1 it can be observed that the basicity of the amine increases from primary amine to secondary amine. The addition of the third alkyl group to form the tertiary amine however shows reduction in the pKaH which is referenced by Series 5.2 above. The change in pKaH can therefore be explained in terms of the stability of the system brought about by the presence of the H-atom. This H-atom is stabilized by the solvent such as water through hydrogen bonding [29, 170]. By considering the primary and secondary amine both containing unsaturated H-atom, by reducing the H atom from secondary amine to tertiary amine there is no H-bonding therefore the systems will have reduced stability hence a reduced pKaH [170] as shown by Series 5.1 above. The removal of solvent (water) leads to increased basicity of the system as the series indicates.

From the above discussions it can be observed that the different substituents and the solvents have a very important role to play in the stability of the N-atom and its associated mode of coordination to any metal. This will subsequently affect the nature of extraction of the ligands.

### 5.3 Chapter objective

The objective for this chapter is to subject the 15 salen type ligands with the N-donor group previously synthesized in Chapter 2 to solvent extraction and bulk liquid membrane transport studies. The effect of the different substituents and the added alkyl groups will also be studied. The 15 ligands used are therefore shown in Figure 5.2, 5.3 and 5.4.

## Class A ligands.

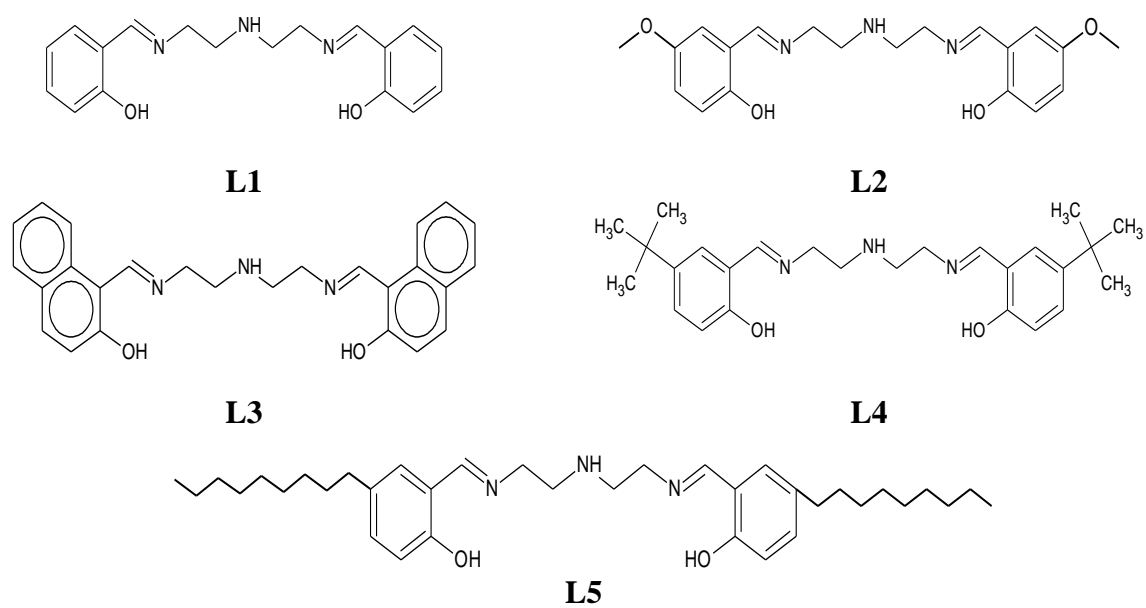


Figure 5. 2 Class A ligands

## Class B ligands

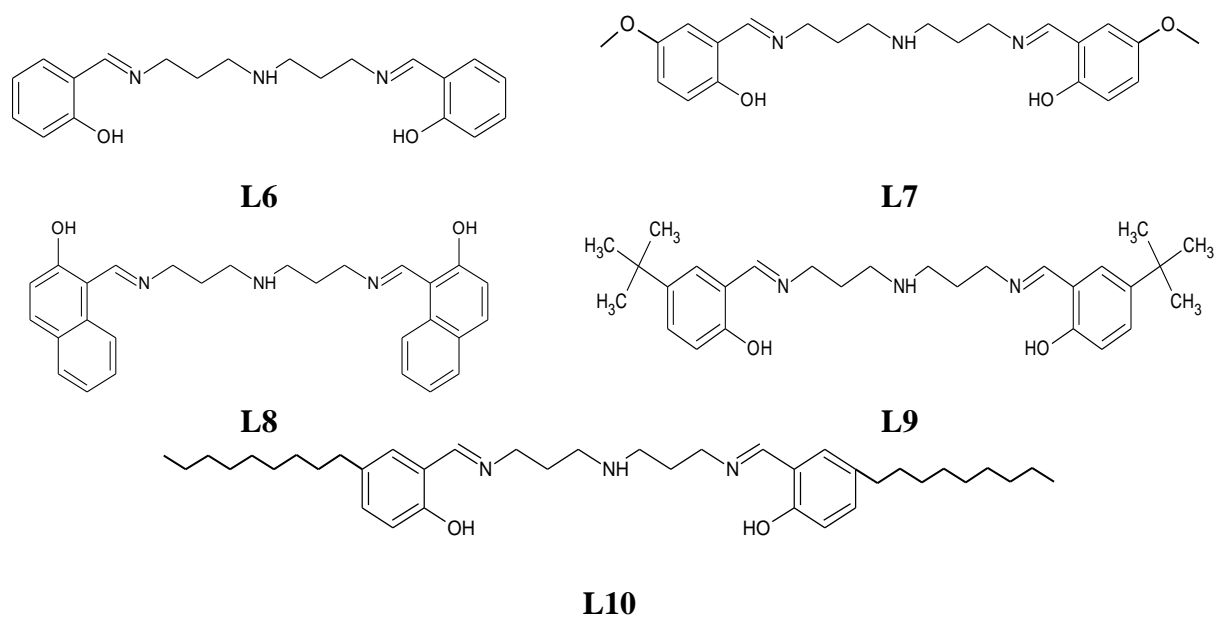


Figure 5. 3 Class B ligands

## Class C ligands

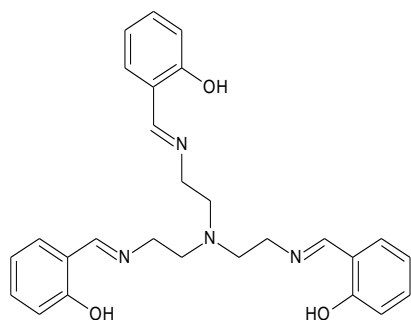
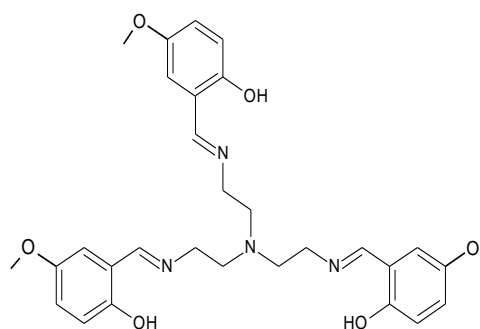
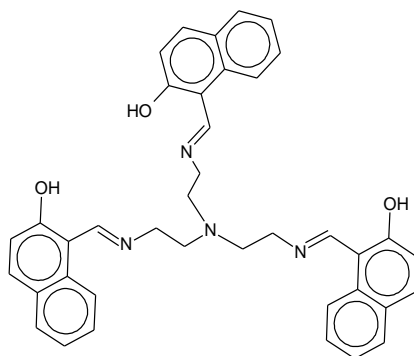
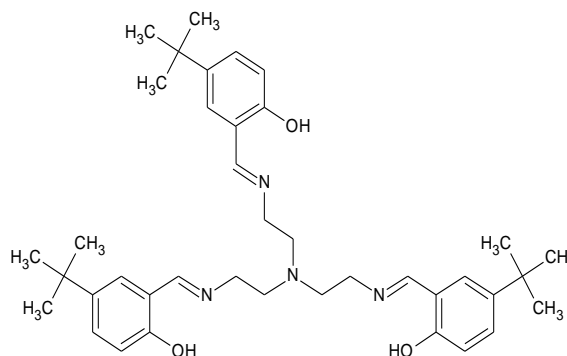
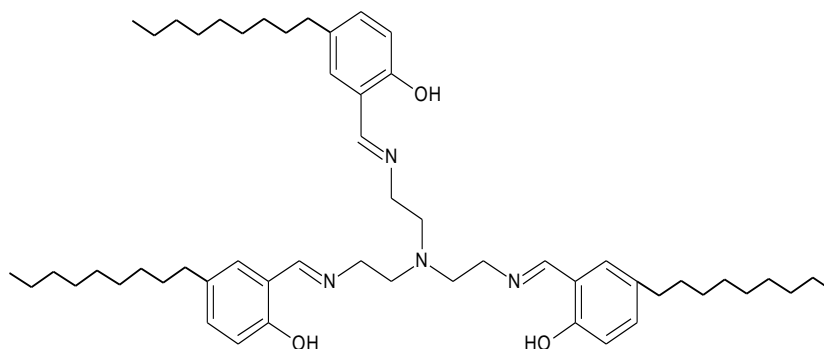
**L11****L12****L13****L14****L15**

Figure 5. 4 Class C ligands

**5.4 Solvent extraction studies**

Solvent extraction was undertaken for the different ligands using the following reagents and instruments.

### 5.4.1 Reagents

Metal mix at pH 4.98 containing 0.01 M of the 6 different metal ions ( $\text{Cd}^{2+}$ ,  $\text{Co}^{2+}$ ,  $\text{Cu}^{2+}$ ,  $\text{Ni}^{2+}$ ,  $\text{Pb}^{2+}$  and  $\text{Zn}^{2+}$ ). The metal mix solution was prepared using hydrated nitrate salts of the different transitional and post transitional metals purchased from Saarchem, a subsidiary of Merck chemicals PTY Ltd. It was buffered at pH 4.98 using sodium acetate and acetic acid purchased from Sigma Aldrich. 0.01 M solution of each of the ligands synthesized in chapter 2 were also prepared in 100 ml volumetric flasks in aqueous chloroform. The saturated aqueous chloroform was obtained by shaking 750 ml of chloroform and 250 ml of deionized water in a 1 litre separating funnel. Finally, the 0.1 M nitric acid was prepared from dilution of the 1 litre standard 1 M (1 molar) Nitric acid solution bought from Merck chemicals PTY Ltd.

### 5.4.2 Instrumentation

All instruments used were available at Stellenbosch University CAF or at the hydrometallurgy research lab. The following instruments were therefore used.

#### 5.4.2.1 pH Meter

The pH was measured using a Thermo Orion 420A+ pH meter, using the standards (pH 4, 7 and 10) to calibrate it before each set of measurements. Figure 5.5 shows the pH instrument used.



Figure 5. 5 The thermo Orion 420A+ pH meter with the two standard pH buffers besides it

#### 5.4.2.2 Lab shaker

The extraction was carried out using a SPL-MP15 Labcon linear platform shaker. For intimate mixing of the different phases the instrument was set at 220 revolutions per minute for 24 hours as shown in Figure 5.6.



Figure 5. 6 The SPL-MP15 Alcon linear platform shaker with the instrumental parameters shown

### 5.4.2.3 Inductively coupled plasma (ICP-OES)

The analysis of the aqueous product from extraction was performed at the central analytical facility (CAF) at Stellenbosch University in the ppm range using the Thermo ICap 6300 ICP-OES. The Ultra-trace analysis was performed on an Agilent 7900 ICP-OES or Agilent 8800 QQQ ICP-OES.

### 5.5 Competitive solvent extraction

The competitive extraction study was carried out using a literature method by Saban *et al.*[71]. 10 ml of 0.01 M solution of the ligand in aqueous chloroform was measured into a vial. 10 ml of the 0.01 M metal mix solution at pH 4.98 containing the 6 different base metal ions ( $\text{Cd}^{2+}$ ,  $\text{Co}^{2+}$ ,  $\text{Cu}^{2+}$ ,  $\text{Ni}^{2+}$ ,  $\text{Pb}^{2+}$  and  $\text{Zn}^{2+}$ ) was then transferred into the same vial to form two immiscible layers as shown in Figure 5.7. The samples were closed sealed and fastened on the lab shaker set at the described conditions of 220 rpm. The samples were allowed to shake for 24 hrs. After the agitation process, 1 ml of the aqueous phase containing the metal mix was then transferred into the ICP tube and topped up to 10ml with 0.1 M nitric acid.



Before extraction



After extraction

Figure 5. 7 Samples before extraction and after 24 hr extraction on the lab shaker

The samples were then analysed for metal ions extracted with the percentage metal extracted calculated based on the percentage metal originally extracted as

$$\% \text{ Extracted (E)} = \frac{\text{Control(C)} - \text{sample(S)}}{\text{control(C)}} \times 100$$

Equation 5. 1 Calculation of % extraction

Where:

**Control (c)** = value obtained from the control sample prepared by placing the 10 ml of the metal mix at pH 4.98 and the 10 ml of the aqueous chloroform solution, however in this case the aqueous chloroform layer contains no ligand when shaken on the lab shaker for 24 hrs.

**Sample (s)** = the value obtained from the extraction with the different ligands.

### 5.5.1 Results

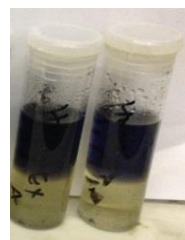
The ICP extraction results were obtained and calculated by equation 5.1 above. During the process of extraction there were several observations that were made and are discussed as follows.

#### 5.5.1.1 Bleeding of the ligand

For class A ligands, ligand **L1**, it was observed that immediately upon the addition of the aqueous layer containing the metal mix to the chloroform layer with the ligand, there was immediate formation of two colours. The upper aqueous layer formed a deep blue colour indicative of  $\text{Cu}^{2+}$  ions complexing to the ligand. However, after the 24 hours of extraction the lower chloroform layer formed a pale green colour and after a while the upper layer darkened (black colour) as shown in Figure 5.7 below.



**L1** Before extraction



**L1** after extraction

Figure 5. 7 The ligand **L1** before and after the extraction process (The colouring of the upper aqueous layer indicates that the ligand is leaching to the aqueous layer).

**L2** Before extraction**L2** after extractionFigure 5. 8 The ligand **L2** before and after extraction

The colour change was also observed for the other ligands in this class (i.e. ligand **L2**, **L3** and **L4**) which all showed the final pale green colour of the chloroform layer and the very dark blue colour of the aqueous layer. For these ligands however, the initial colour upon contact was green and not deep blue as shown by Figure 5.7. These observations can be attributed to a bleeding of the ligand to the aqueous phase effect. The result from Thermo ICap 6300 ICP-OES confirms these observations and the results are discussed as follows.

**Note:** All the values below 5 % are considered to fall within the experimental error ranges. These arise during handling samples and calculation errors and therefore are not considered in the extraction discussion. They are however shown in the results to show the general trend of extraction.

#### 5.5.1.1 Discussion of competitive extraction results from class A ligands

The results obtained from the ICP analysis in Figure 5.8 shows the extraction of ligands **L1** to **L5** bearing the different substituents on the phenyl ring. The results for ligand **L1** to **L4** indicate that these ligands did not make good candidates for extraction. The results are dominated by the leaching effect which is shown by the low extraction values and high standard deviation obtained from the 4 repeat readings. This high standard deviation is shown by the large error bars in the results. The ICP results showed limited extraction for the *salicyl* derived ligand **L1**, *methoxy* substituted *salicyl* ligand **L2**, the *naphthyl* group ligand **L3** and the *5-tert butyl* substituted *salicyl* group ligands. The *tert butyl* substituted *salicyl* ligands **L4** showed the highest extraction among the ligands suspected of leaching to the organic phase. The metal extraction results are also relatively equal. Even with the leaching the ligands still show slightly higher extraction of  $\text{Cu}^{2+}$  with **L4** showing the highest extraction at 20 %. This selectivity of  $\text{Cu}^{2+}$  over the other metal ions is further shown by the extraction of ligand **L5** which did not show any sign of leaching as discussed below.

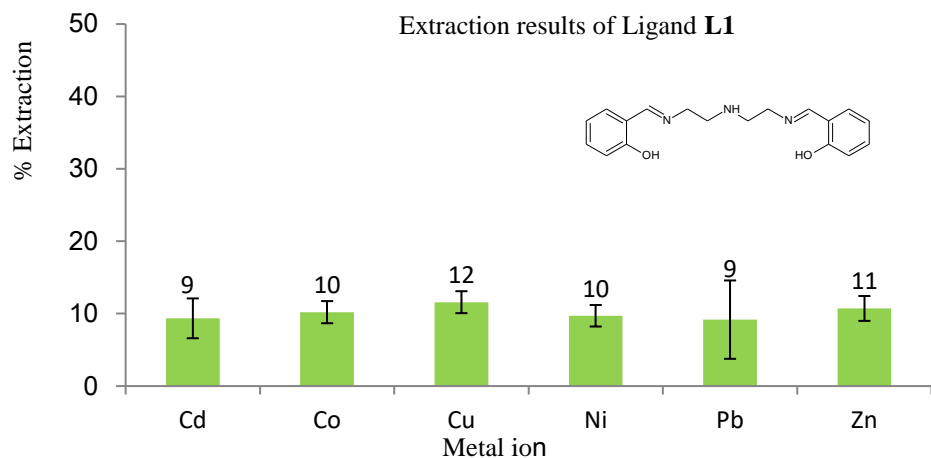


Figure 5.8 (a): Graphical representation of extraction results for ligand **L1** characterized by high standard deviation shown by the large error bars.

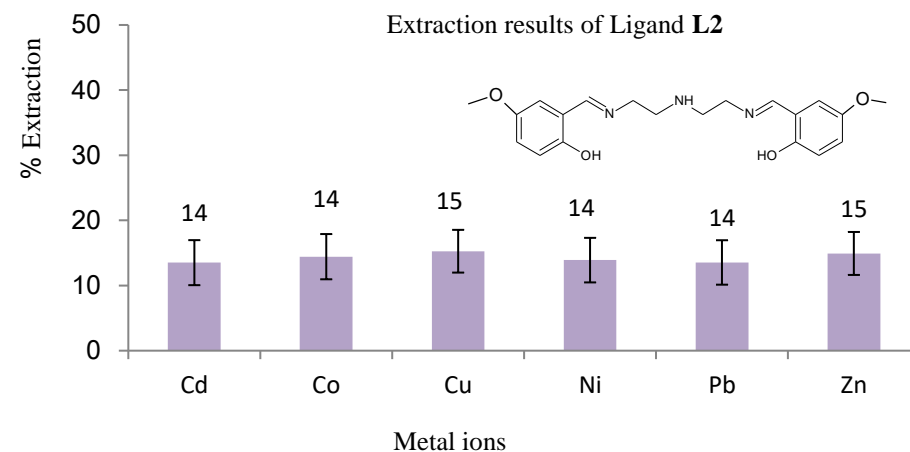


Figure 5.8 (b): Graphical representations of extraction results for ligand **L2**. No selectivity is observed with the leaching.

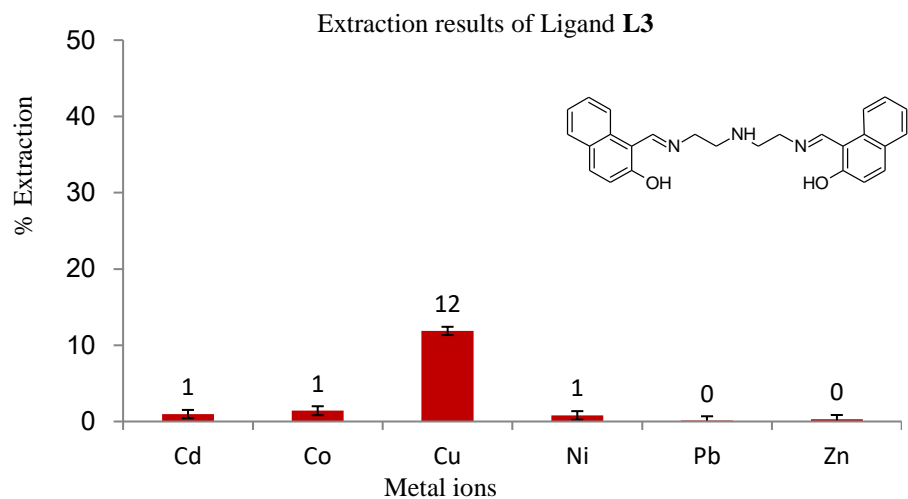


Figure 5.8 (c) Graphical representation of extraction results for ligand **L3** showing high leaching but with selectivity of  $\text{Cu}^{2+}$ .

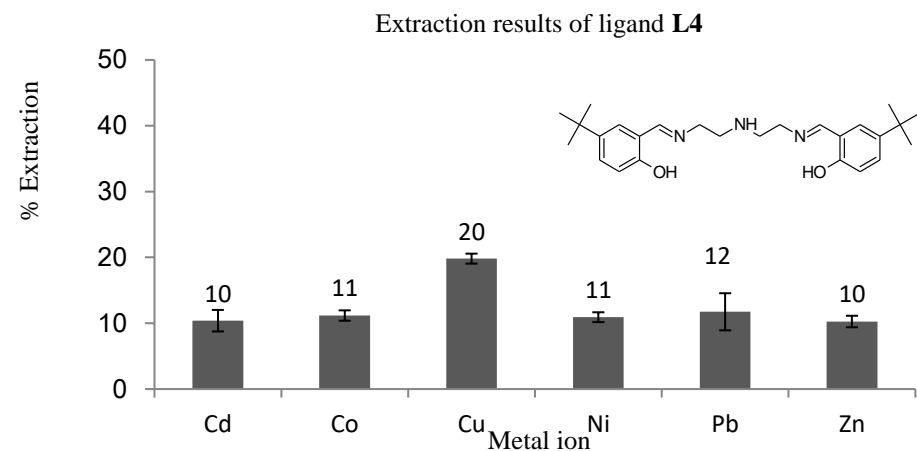


Figure 5.8 (d): Graphical representation of extraction results for ligand **L4** showing the highest extraction for the leaching product.

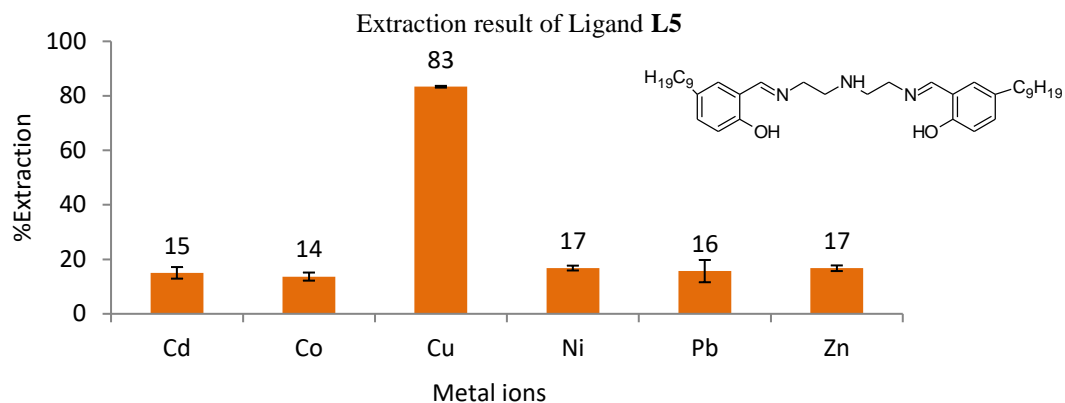


Figure 5. 9 (d) Graphical representation of extraction results for ligand **L5** showing very high extraction of  $\text{Cu}^{2+}$

The Ligand **L5** with *nonyl* substituent was the only ligand in this series that did not leach into the aqueous phase. This was attributed to the presence of the highly organic *nonyl* substituent. This ligand shows a high extraction and selectivity of  $\text{Cu}^{2+}$  with the other metal ions being extracted at less than 20 %. The higher extraction of  $\text{Cu}^{2+}$  by this ligand is consistent with the Irving-Williams series [73] which shows that  $\text{Cu}^{2+}$  will be selectively extracted over other divalent metal ions. The selectivity of  $\text{Cu}^{2+}$  for class A ligands is therefore summarized in Table 5.2.

Table 5. 2 Summary of the % extraction of  $\text{Cu}^{2+}$  with the different class A (N-donor ethyl) ligand systems (results in brackets indicate standard deviation errors).

Ligand	<b>L1</b>	<b>L2</b>	<b>L3</b>	<b>L4</b>	<b>L5</b>
% $\text{Cu}^{2+}$	12(2.2)	15(3.3)	12(3.17)	20(2.4)	83(2.0)

**Note:** Values in brackets indicate the % standard deviation between the consecutive values.

### 5.6 Competitive Solvent extraction of Class B ligands

The solvent extraction results for class B ligands with the increased alkyl groups between the donor groups showed improved extraction. There was better extraction across all the 5 ligands of this class of ligands over that of class A ligands. This improved extraction value can be attributed to the effect of the added alkyl group between the two-donor nitrogen's. The results from ICP-OES are therefore shown in Figure 5.9.

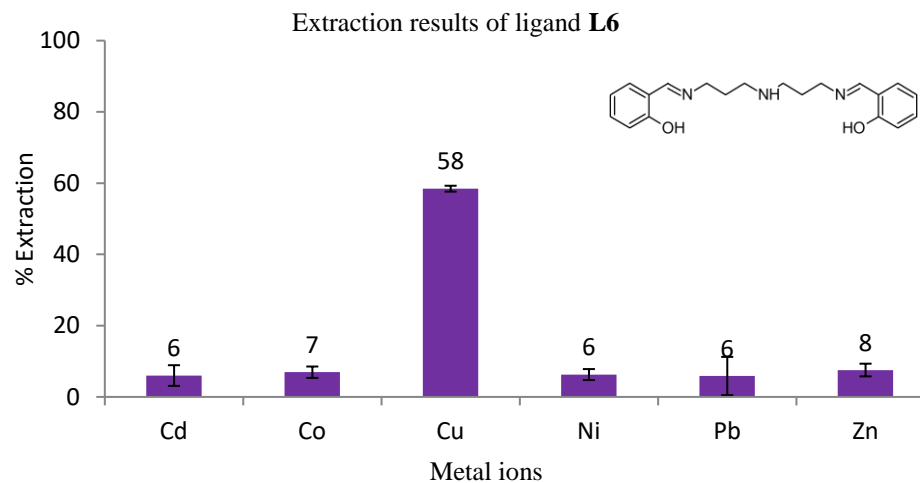


Figure 5.9 (a): Graphical representation of extraction results for ligand **L6**

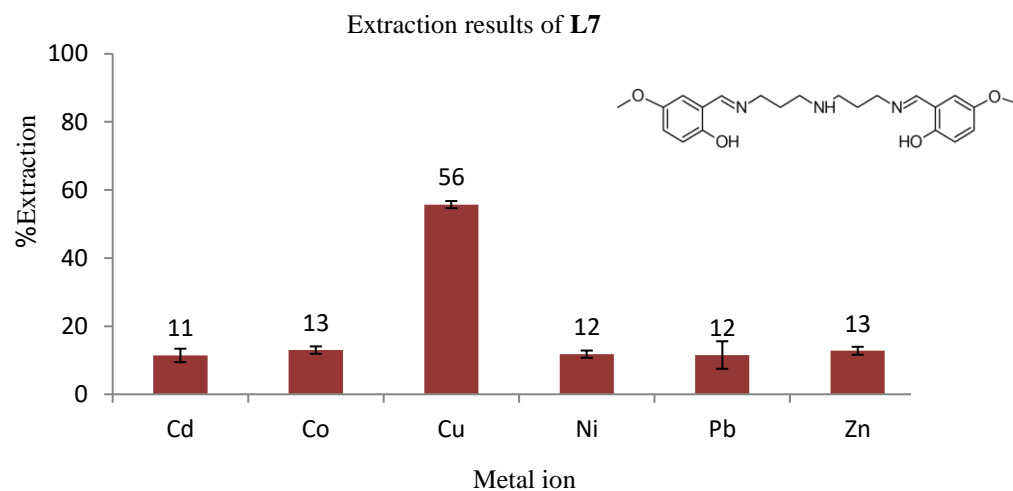


Figure 5.9 (b): Graphical representation of extraction results for ligand **L7**

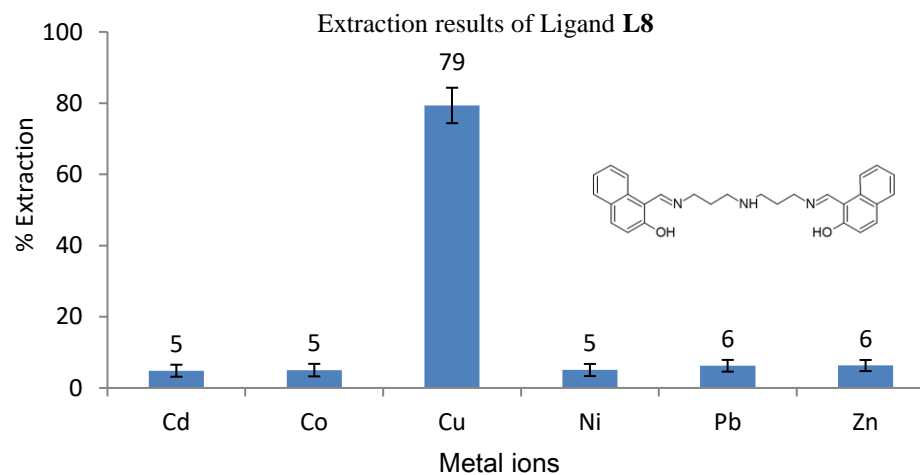


Figure 5.9 (c): Graphical representation of extraction results for ligand **L8**

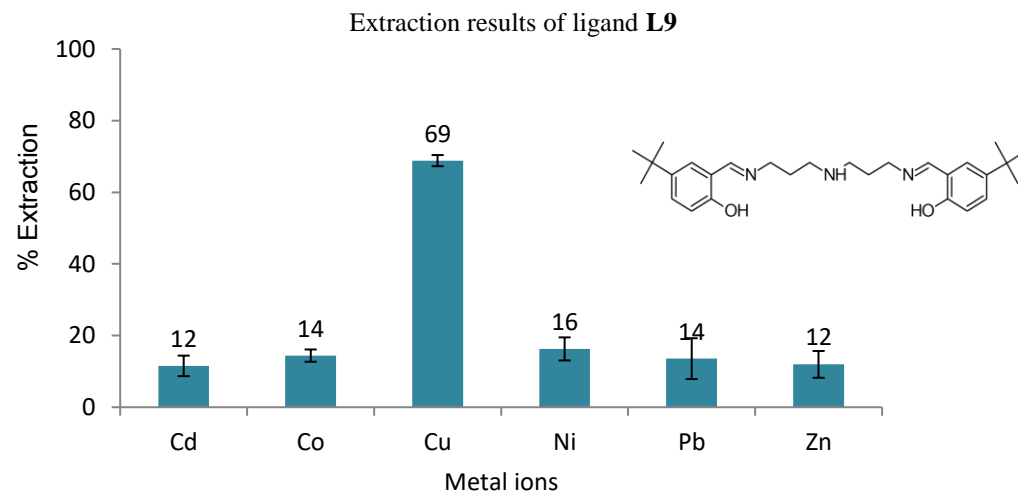


Figure 5.9 (d): Graphical representation of extraction results for ligand **L9**

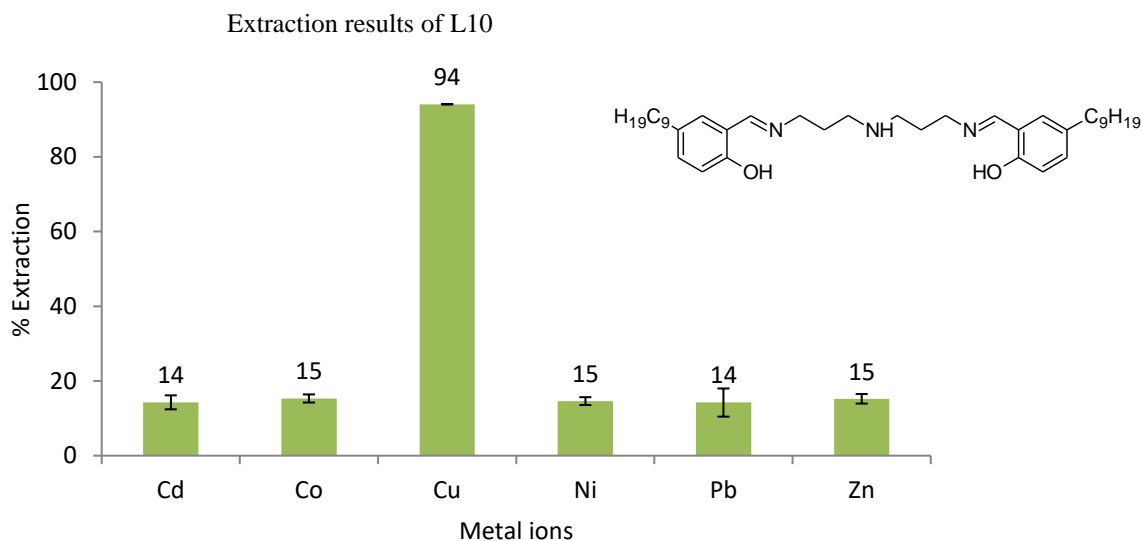


Figure 5.9 (d) Graphical representations of extraction results for ligand **L10**

### 5.6.1 Discussion of extraction results from class B ligands

All the ligands in this class showed extraction for  $\text{Cu}^{2+}$  of over 50 %. Ligand **L10** showed the highest extraction at 94 %. Ligands **L6**, **L7**, **L8** and **L9** also showed better selectivity towards the  $\text{Cu}^{2+}$  as opposed to their analogous class A ligands. The ligand **L8** with the *naphthyl* substituent showed the highest selectivity towards  $\text{Cu}^{2+}$ , this was comparatively higher than anticipated. The results for the extraction of  $\text{Cu}^{2+}$  are summarised in Table 5.3.

Table 5.3 The summary of the % extraction of the different base metal ions using the class B (N-N-N propyl) ligand systems ( $\text{Cu}^{2+}$  results are highlighted).

Ligands	L6	L7	L8	L9	L10
<b>Cu</b>	58(0.2)	56(1.5)	79(5.0)	63(1.3)	94(0.1)

The comparison of the results obtained between **L8** (*naphthyl* containing substituent) and **L9** (*tert-butyl* containing substituent) for class B ligands showed an unexpected result. The bulkier *tert-butyl* group showed much lower extraction of  $\text{Cu}^{2+}$  as compared to the *naphthyl* group. These two ligands have relatively the same mass with both the ligands having the same number of carbon atoms. The *tert-butyl* is however much more saturated with more hydrogen atoms than the *naphthyl* group. The high extraction of the *naphthyl* group over the *tert-butyl* group can therefore be attributed to the inductive and steric effect differences.

From Chapter 2, on the discussion of the electronic effect of the added substituents to the imine group as was shown, each of these phenyl substituents showed an inductive effect. This was indicated by shift of the imine proton or the imine carbon in the  $^1\text{H}$  NMR,  $^{13}\text{C}$   $\{^1\text{H}\}$  NMR and IR studies in Chapter 2. The high steric effect due to the bulky *tert-butyl* group together with higher saturation should make this ligand much more soluble in the organic phase, therefore in principle lead to greater extraction. But from the results, it is observed that the *naphthyl* substituent showed better extraction and selectivity. This can be attributed to the stability offered by the aromatic *naphthyl* group over the *tert-butyl* group described as follows.

As had been described in Chapter 1 and Chapter 2, the chelation of salen type ligands to the metal ions is attributed to the coordination of the ligands to the metal ions. For this to occur the hydroxyl group in the salen type ligands has to be deprotonated. The results above can be postulated that the higher extraction of the *naphthyl* group is due to the ligand having the ability to offer better stability of the deprotonated hydroxyl group through the aromatic system. This means that the hydroxyl proton of the *naphthyl* substituent can easily be deprotonated in the system leading to better coordinating of the ligand. This is shown by the higher shift of the imine proton in both of the *naphthyl* groups in each of the class A and class B ligands over the *tert-butyl* group. Also, ligand **L8** was shown to undergo *tautomerism* where the OH proton of the *naphthyl* group is transferred to the imine, indicating the ease of deprotonation of this proton Figure 5.10. The net effect is better coordination of this ligand to the metal ions and therefore increased extraction as indicated by the results between **L7** and **L8**.

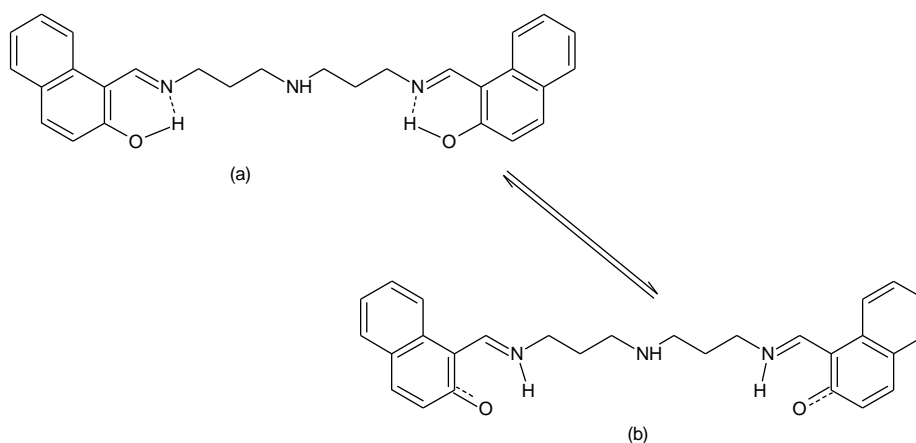


Figure 5. 10 Showing the tautomerism of the Schiff base product (referenced from scheme 2.20 in chapter 2).

## 5.7 Competitive solvent extraction of class C ligands (tripodal ligands)

Due to the leaching effect of the class A ligands, the class C ligands (*tripodal* ligand) system were developed as discussed in Chapter 2. The aim of using these ligands was that with increased molecular weight and increased bulkiness, this would lead to improved organic character for the systems while still providing the effect of the ethyl spacer group between the N-donor atoms. The second assumption made was that by increasing the number of donor groups this would in principle allow for increasing the chelating ability of the ligands therefore there would be an effect on selectivity. These ligands would therefore be comparable to class A ligands. The results obtained were however not as expected as shown by the graphical representation in Figure 5.11.

### 5.7.1 Discussion of results from the competitive solvent extraction of the tripodal ligands

The extraction results for the *tripodal* ligand systems were very disappointing; they were also characterized by a high degree of leaching. The high degree of leaching was attributed to the increased number of imine moieties in the system. From the result, the *naphthyl* substituent ligand **L13** and the *nonyl* containing substituted ligand, **L15** are the only ligands that showed appreciable levels of extraction. These results are consistent with the results obtained for the class A ligands containing the ethyl spacer.

The selectivity and the % extraction of these ligands were also similar to those of the class A ligands. These ligands were also shown to be selective towards  $\text{Cu}^{2+}$  ions. Ligand **L15** showed an extraction of 86 % with good selectivity for  $\text{Cu}^{2+}$  over the other metal ions. The selectivity of ligand **L15** was very encouraging showing that the ligand can make an excellent extractant for the  $\text{Cu}^{2+}$  ions. The selection of  $\text{Cu}^{2+}$  is also in agreement with the Irving-Williams series[75]. The results for  $\text{Cu}^{2+}$  extraction are therefore summarised in Table 5.4.

Table 5. 4 The summary of the % Extraction of  $\text{Cu}^{2+}$  with the different class C, N- tripodal ligand systems (results in brackets indicate standard deviation errors).

ligand	<b>L11</b>	<b>L12</b>	<b>L13</b>	<b>L14</b>	<b>L15</b>
% $\text{Cu}^{2+}$	-	-	20 (0.9)	11 (3.3)	86 (1.5)

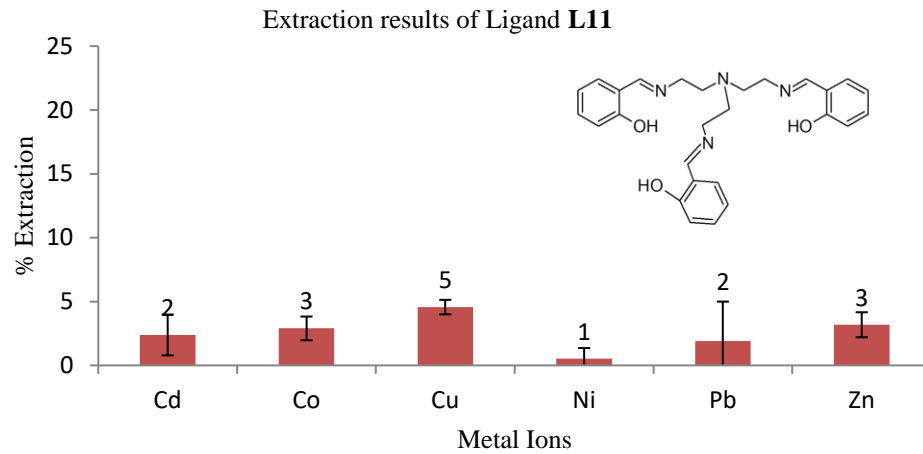


Figure 5.11 (a): Graphical representations of extraction results for ligand **L11**

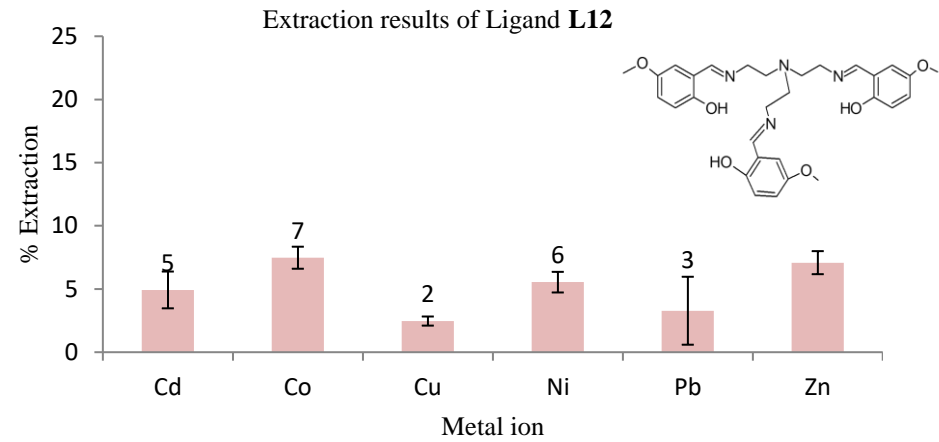


Figure 5.11 (b): Graphical representations of extraction results for ligand **L12**

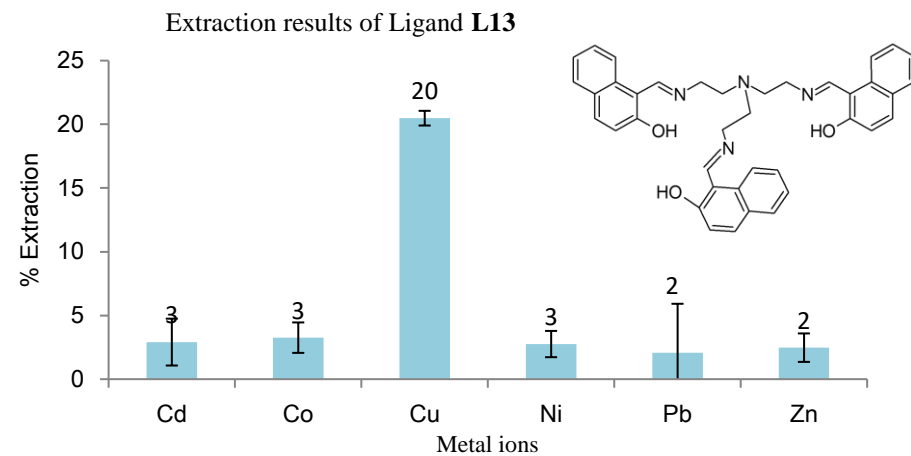


Figure 5.11 (c): Graphical representations of extraction results for ligand **L13**

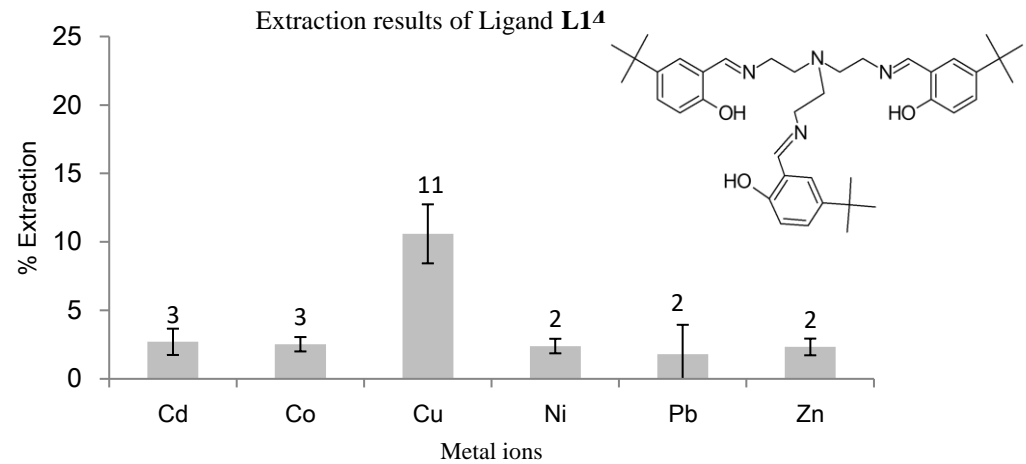


Figure 5.11 (d): Graphical representations of extraction results for ligand **L14**

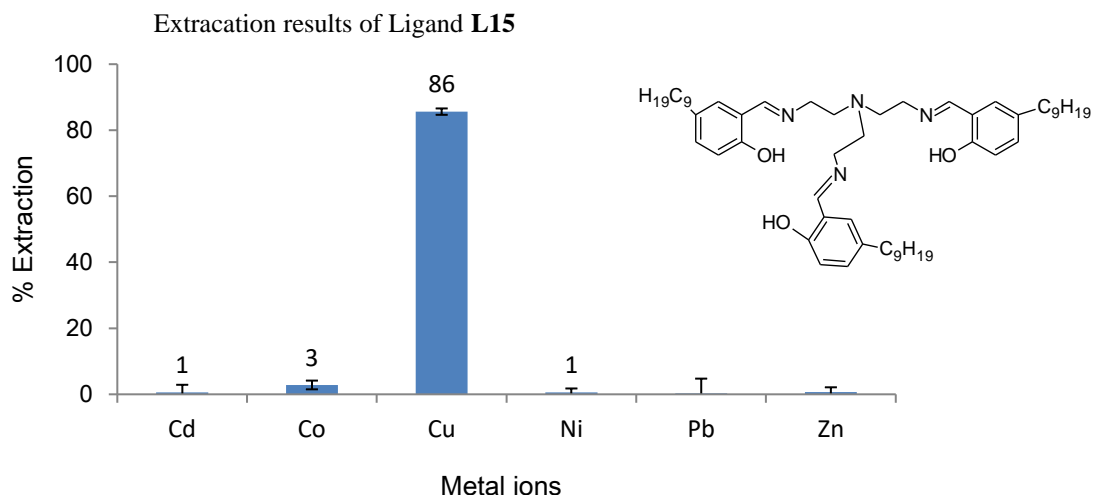


Figure 5. 11 (e) Extraction results of ligand **L15** showing very high selectivity for  $\text{Cu}^{2+}$

### 5.8 Discussion of leaching based on ICP results

The class A ligands **L1 – L4**, and class C ligands **L11-L14** showed very low extraction, this low extraction was attributed to the leaching effect. There are no clear mechanisms for this observation since most extraction processes do not give much consideration to this effect. However, discussion of this effect can lead to better understanding of ligand solvent effect. This effect can also bring in better understanding of the mode of coordination to allow for the design of better low molecular weight extractants. There are therefore two reasons that are postulated to show how this leaching effect takes place.

The first reason has to do with the property of the ligand where the extra N-donor group induces polarity and increases the solvation of these coordinate products. This reason can be derived from the various *bis imine* ligand systems that have been used in solvent extraction process but did not show leaching effect due to the lack of the N-donor. Examples of these ligands are shown in Figure 5.12. All these three ligands have been used in our laboratory for solvent extraction studies and did not show any leaching effect by Hensberg [171].

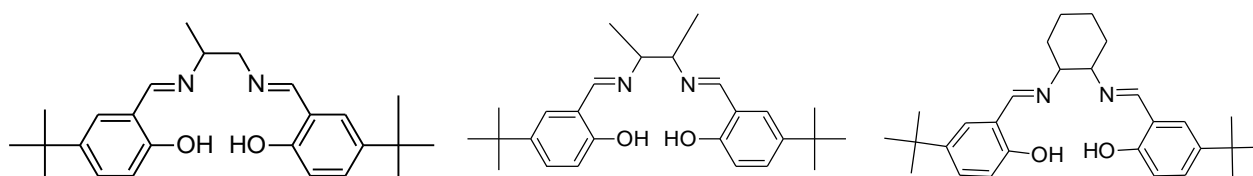


Figure 5. 12 Examples of monotopic salen type ligands used for solvent extraction ( redrawn courtesy of Hensberg [171]).

The addition of the donor group therefore leads to the increased solubility of the ligand in aqueous solution which is seen by comparing these ligands in Figure 5.12 to the **L4** ligand.

The second postulated reason deals with the nature of coordination leading to leaching. In this theory it can be hypothesized that the chelated Cu-complex in solution is coordinated in a manner to allow for the water molecules being weakly coordinated as indicated by Equation 5.2.



Equation 5. 2 Coordination of the water molecules

The existence of this coordinate water molecule means that the chelated complex formed is much more hydrated that would render the complex more soluble in aqueous phase as opposed to the organic phase. This type of coordination is seen by the crystal structure obtained in Chapter 4 of the N-donor ligands as shown in Figure 5.13 (a) and 5.13(b) for ligand **L1** and **L4** the class A. The other theory based on coordination can also be attributed to the hydrolysis of the ligands shown in Figure 5.13 (a) and 5.13 (b) indicating that the complex formed is missing one of the aldehydes. This will then lead to the formed complex being less organic in nature and therefore will be pushed towards the aqueous phase.

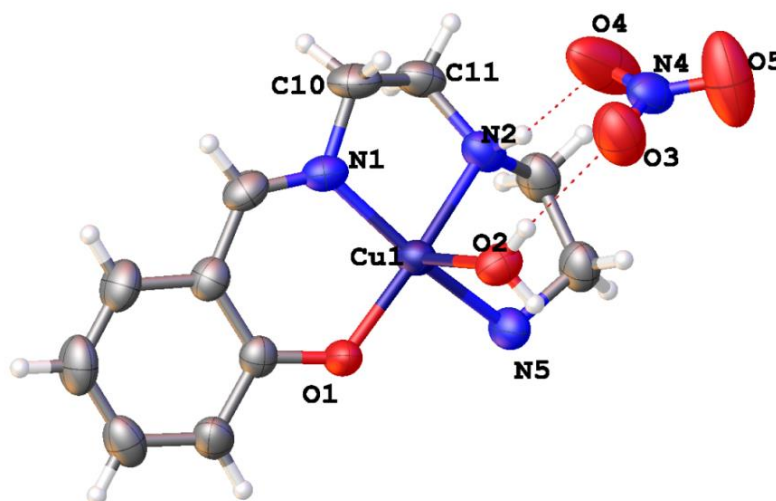


Figure 5. 13 The crystal structure for ligand **L1-Cu** indicating water molecule coordinated to copper centre

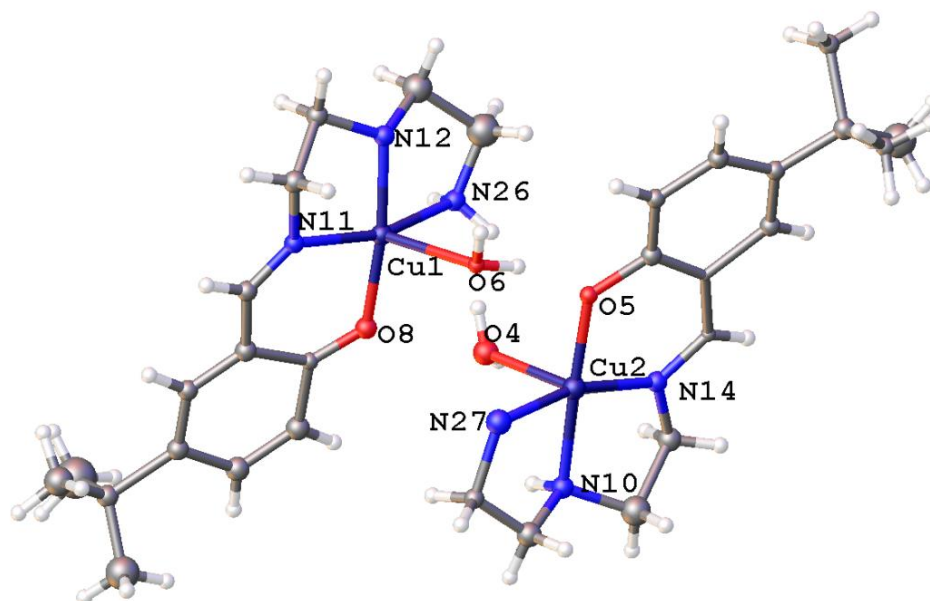


Figure 5. 14 The disordered crystal structure of **L4-Cu** with the water molecules found at the centre of the molecule (some atoms have been deleted for picture clarity).

## 5.9 Summary of extraction results

Even though these results were not as expected, due to the high leaching effect, the ligands were studied further by counteracting this effect by using different synergists to get a better understanding of these systems. These results are therefore discussed in Chapter 6. The ligands that did not show a leaching effect were used for competitive bulk liquid membrane transport as follows.

## 5.10 Competitive bulk liquid membrane transport studies

The ligands that had shown minimal or no leaching were then subjected to competitive bulk liquid membrane transport. The principle behind this study is that an organic phase containing the extractant is placed between an aqueous source phase consisting of the mixed metal ions and another aqueous receiving phase at a much lower pH. At the interface metal ions coordinate to the ligand and form neutral complexes that diffuse to the bulk of the organic phase. The other end of this organic phase is in contact with the receiving phase at a lower pH. Here the complex diffuses across the interface to the receiving phase where the metal ion is released. The ligand is reprotonated due to the pH difference and diffuses back to the organic phase to repeat the process. There are two processes occurring in this system. Extraction occurs between the source phase and the membrane phase and the stripping of the metal ion occurs between the membrane phase and the receiving phase. The pH difference creates the driving force that

allows for the processes to take place and is further expedited by gently stirring the bulk of these phases using a stirrer. New ligands are exposed to extract more metal ions at one phase while at the opposite end some metal ions are being released to the receiving phase without the need for the vigorous intimate mixing as used in competitive extraction study. This process was carried out using the following apparatus.

### 5.10.1 Transport apparatus

The bulk liquid membrane transport studies were carried out using the bulk liquid transport apparatus built by the inorganic chemistry hydrometallurgy research group. This apparatus comprises of a cylindrical glass cell (4.0 cm, internal diameter (i.d)) holding an internal glass tube (2.0 cm, i.d), for separating the two aqueous phases as shown by the schematic diagram in Figure 5.15. The experiment was carried out by using a thermostated water bath at 25 °C to keep the temperature under control. A motor creating 10 revolutions per minute was used to provide agitation without breaking the surface of the bulk liquid membrane created. The procedure used is therefore described as follows.

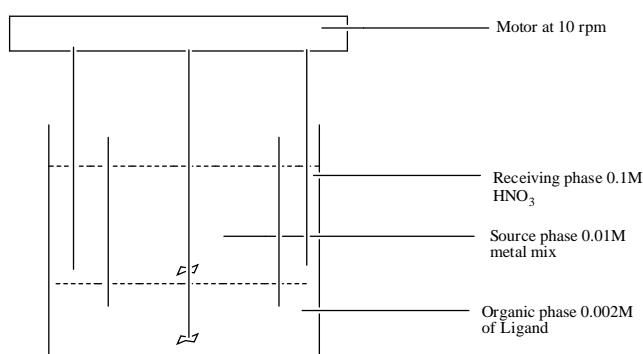


Figure 5. 15 Schematic diagram of the concentric transport cell for bulk liquid membrane transport of metal ions (Redrawn courtesy of Davarkhah et al. [78]).

### 5.10.2 Procedure

All the transport experiments were carried out by the above mentioned concentric transport cells. 50 cm<sup>3</sup> of 0.002 M extractant was measured first into the concentric cell. The aqueous source phase contained 10 cm<sup>3</sup> of the 0.01 M concentration of the mixed base metal ions at pH 4.98 which was added in the middle column and the receiving phase contained 30 cm<sup>3</sup> of 0.1 M nitric acid at pH 1 was then added in the receiving column. These two layers were separated by an organic chloroform phase containing the extractant. The set up was then left to stir slowly at 10 rpm for 24 hrs at ambient pressure. The pH gradient between the receiving and the source

phase was used to facilitate the transport of the metal cations across the membrane by counter transport of protons [172]. The ligands **L5**, **L10** and **L15** were chosen as the only ligands with the same substituents that did not leach.

The following terms are used in the discussion of the results and are defined as follows.

**C** = Control, determined from the analysis of the amount of base metal ions present before transport of the metal mix at pH 4.98.

**SP** = Source phase, determined from the analysis of base metal ions present in the source phase after transport.

**%MP** = The % membrane value (%MP) is the difference between the control and the source phase. It gives the amount of metal ions into the membrane phase as shown by equation 5.3.

$$\% \text{ MP} = \frac{(\text{Control}-\text{SP})}{\text{control}(\text{C})} \times 100$$

Equation 5. 3 Calculation of % metal in the membrane phase

**% RP** = receiving phase, determined from the analysis of base metal ions in the receiving phase (% RP) calculated from the amount of metal ions present in the receiving phase after transport. This was obtained through factoring in the dilution due to the volume difference between the source phase and the receiving phase as shown in equation 5.4.

$$\% \text{ RP} = \frac{(\text{sample} \cdot \text{DF})}{\text{control}(\text{C})} \times (100/1)$$

Equation 5. 4 Calculation of % receiving phase

The dilution factor (DF) for the transport set-up was therefore determined to be 3 since the source phase volume is 10 ml and the receiving phase volume is 30 ml.

### 5.10.3 Results

The following results were obtained from the ICP-OES for the transport study of the different class of ligands containing the *nonyl* substituents as shown in Figure 5.16.

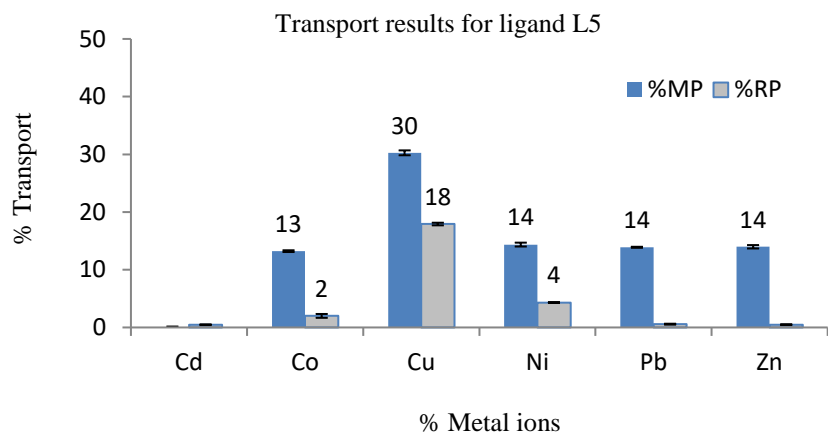


Figure 5.16 (a): Graphical representation of bulk liquid membrane transport results for ligand **L5**

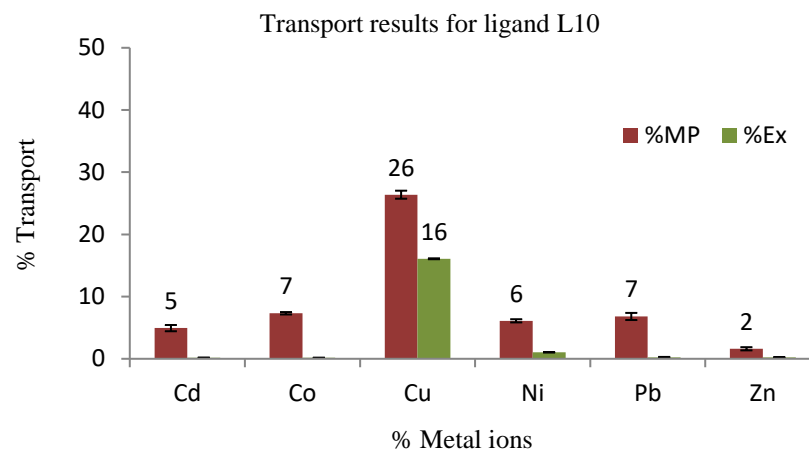


Figure 5.16 (d): Graphical representation of Bulk liquid membrane transport results for ligand **L10**

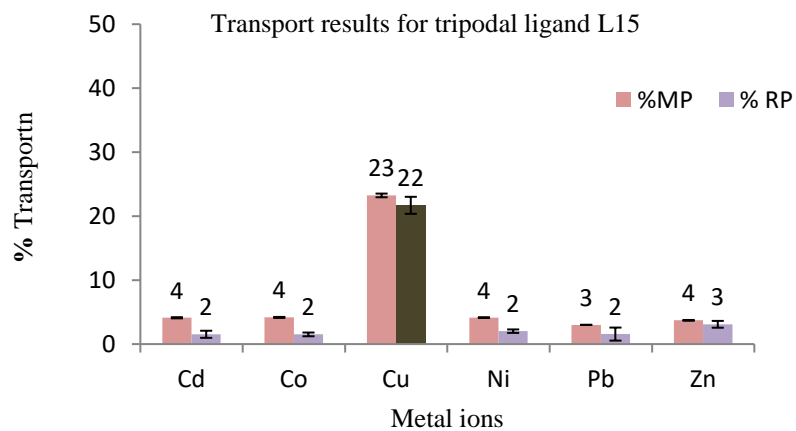


Figure 5.16 (d): Graphical representation of Bulk liquid membrane transport results for ligand **L15**

**% MP** = The total amount of metal ions extracted to the membrane phase (MP=control-source phase after transport).

**% RP** = The total amount of ions transported through the bulk liquid membrane.

#### 5.10.4 Discussion of transport results

From the 3 samples that were studied for bulk liquid membrane transport, ligands **L5**, **L10** and **L15** all transported  $\text{Cu}^{2+}$  ions. Ligand **L15** showed the highest transport at about 22 % ( $21.7 \pm 0.01$ ). The two ligands **L5** and **L10** showed varied results with ligand **L5** transporting  $\text{Cu}^{2+}$  at 18% ( $17.9 \pm 0.22$ ) and ligand **L10** extracting 1% less at 17 % ( $16.9 \pm 0.1$ ). The second observation from the results showed that the  $\text{Ni}^{2+}$  was the second highest transported metal ion for both of these ligands had a maximum at 4% ( $4.3 \pm 0.1$ ) for ligand **L5**.

The third observation was on the difference of % MP and % RP in the graph. The closeness of these two indicates a very efficient transport system where all the metals in the membrane phase are stripped to the receiving phase. From this it was observed that the stripping efficiency of ligand **L15** is at 93 %. This value is obtained by calculating the % of metal ions that passed through source phase to the membrane phase and how much of this was received in the 0.1M  $\text{HNO}_3$  solution after 24 hours. For ligand **L5** and **L10** these showed an efficiency of 61 % and 59 % respectively for the transport of  $\text{Cu}^{2+}$ . This efficiency indicates the degree of ease to which these ligands are able to release the  $\text{Cu}^{2+}$  metal ions due to pH difference.

From these results, despite extracting the least amount, the *tripodal* ligand also has the highest releasing efficiency, followed by the **L5** which releases 61 % through the stripping process and finally the ligand **L10** which releases 60 %. Lastly for ligand **L5**, between 13 % to 14 % of four other metal ions ( $\text{Co}^{2+} = 13$  %,  $\text{Ni}^{2+}$ ,  $\text{Pb}^{2+}$  and  $\text{Zn}^{2+}$  all at 14 %) are shown to have been transported to the membrane phase, however less than 3 % of this has been transported to the receiving phase. This indicates the low degree of release of the other metal ions as opposed to the  $\text{Cu}^{2+}$  that is easily released due to the pH difference.

#### 5.11 pH studies

The aim of this study was to understand the competitive nature of this ligand as a function of pH. The principle of this study lays in the fact that certain metals coordinate better at lower pH condition than others. This is used a lot in commercial solvent extraction to develop pH profiles called pH isotherms. The implication of this is that by changing the pH, the selectivity of one metal ion over the other can be attained. This would indicate the best effective extraction pH of the metal ions. The second consideration is to show the stability of these ligands and its formed complexes under lower pH (acidic conditions).

The experiment was carried out as shown in section 5.5 and the results are shown below.

### 5.11.1 Results

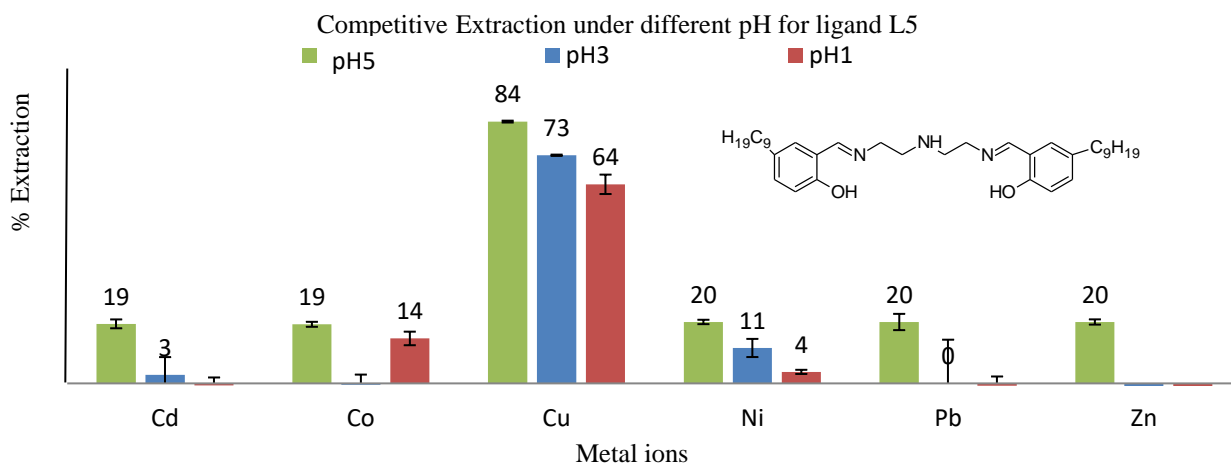


Figure 5. 17 Graphical representation of the stripping study results for **L5** at pH 5, pH 3 and pH 1

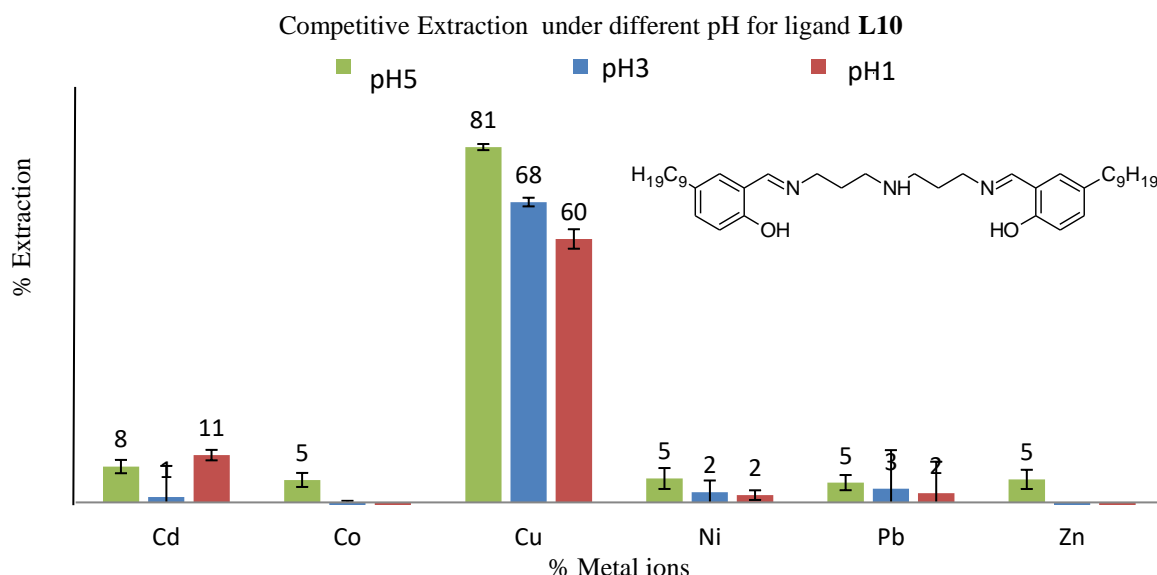


Figure 5. 18 Graphical representation of the stripping study results for **L10** at pH 5, pH 3 and pH 1.

### 5.11.2 Discussion of pH study effect

From the results it is observed that there is a drop in the amount of metal ions extracted into the organic phase by using the lower pH. For the ligands **L5** and **L10**, the % drop of  $\text{Cu}^{2+}$  ions extracted is between 10 -15 % by using the 2-different pH. The ligand **L5** shows the highest extraction % in lower pH at  $64.0 \pm 3.1$ . The system also showed other unexpected results, both of the ligands showed that the second highest extracted metal ion was that of  $\text{Ni}^{2+}$ . These ligands have a higher resistance to hydrolysis showed by extraction of over 50 % in pH 1. This ability to extract at lower pH is an indication of the improved property of these ligands over

the ketoxime based ligands that do not show extraction at pH lower than 1.6 [52]. The reduced extraction of these ligands can however be attributed to the increased resistance to deprotonation of the ligand at lower pH. The net effect is that there will be resistance to the extraction due to lowering of pH.

### 5.12 Summary and conclusion

The results from solvent extraction for class A and class C ligands were observed to give extensive leaching to the aqueous phase. Only the ligands **L5** and **L10** with nonyl substituents were observed to show substantial extraction of  $\text{Cu}^{2+}$  at 83 % and 86%. The ligands from class B ligands **L6-L10** were also shown to extract  $\text{Cu}^{2+}$  over other metal ions.

All the ligands synthesized from *nonyl* substituents from each class did not leach and were shown to selectively extract  $\text{Cu}^{2+}$ . These ligands were subsequently used in bulk liquid transport and were shown to effectively transport  $\text{Cu}^{2+}$  over other metal ions. Two of the ligands from the *nonyl* substituent groups were studied for pH effect indicating the ability of these ligands to be used in different pH's to effect extraction. All the ligands which showed leaching will be used in the proceeding Chapter 6 in the study of the synergistic effect.

# **CHAPTER 6**

---

## **SYNERGISTIC EXTRACTION OF THE N- DONOR LIGANDS**

---

## 6.0 Introduction

This chapter attempts to shed light on the concept of synergism in solvent extraction. A comprehensive discussion on synergistic effects in solvent extraction is undertaken with postulated theories on how the synergistic effect can occur. A study of the synergistic effect of three synergists and the 12 different ligands is investigated as shown below.

### 6.1 Synergistic effect in solvent extraction

In Chapter 1, solvent extraction is defined as the use of a biphasic liquid system in extracting of metal ions. The two phases are the aqueous phase with the target solute and the immiscible organic phase containing the extractant. These two phases are in contact with each other. The targeted solute, which are the metal ions, are bound selectively by the extractant into the organic phase causing the separation of the targeted ions from the aqueous phase [173]. In most hydrometallurgical processes, particularly in commercial operations, the reagents used will often comprise of mixtures of two or more extractants as formulas. These formulations contain the extractants blended together with other organic reagents that enhance solubility, phase disengagement properties, and metal transfer ability [7]. The organic compounds which enhance metal extraction property are called synergists; the converse to this is called depressants.

The enhancement of extraction was first observed in 1954 by Cuninghume *et al* [174] in the extraction of Pr(III) (praseodymium) and Nd(III) (neodymium) and the term synergism was first used four years later in 1958 by Blake *et al.* [175]. The process of using a synergist has since found great application in most hydrometallurgical operations with various synergists having been developed. One of the quintessential qualities of a synergist is that the synergists are by themselves extractants and when used together with other ligated-extractants they produce enhanced extraction. This improved extraction is the core measure of synergism and the reverse to synergism is referred to as antagonism [25, 173, 176, 177]. The synergistic effect can therefore be shown by Equation 6.1.

$$SF = D_{AB} / (D_A + D_B)$$

Equation 6. 1 Synergistic factor calculation.

From Equation 6.1, the enhanced extraction will be obtained from the summation of the performance of the two reagents separately and can therefore be calculated by the term

synergistic factor (SF)[178] as shown by the above Equation 6.1. The synergistic factor is derived from the distribution ratios  $D$  defined in Chapter 1.2.2.

## **6.2 Mode of action of synergist**

The use of different ratios of synergist, ligand and metal ions usually lead to drastic enhancement of separation efficiency. There have been various proposed modes of action of these synergists, however the true origin and the fundamental driving force leading to synergistic action is still not fully understood. Some of the proposed modes of action rely on the fact that most synergists are surface active amphiphilic molecules [179]. Because of this it is therefore assumed that the synergist would bind (either coordination or general interaction like H-bonding, Van-Der Waal attraction, electrostatic interaction etc.) and push the extracting material to the required phase. In this regard, for these amphiphilic molecules to work as synergists, they have to exhibit both molecular chelating properties as well as the ability to form supramolecular aggregates [179] brought about by the discrete assemblies of metal complexes [180].

The study of synergism therefore requires intimate knowledge of metal ligand coordination, as well as supramolecular coordination through aggregate formation [173]. This kind of study therefore involves principles grounded on understanding the roles of interfacial activity (including phase transfer, catalysis and micelle formation) and mixed complex formation (including adduct formation and ion pair formation) in metal extraction processes [181]. In this regard the process of synergism and its mode of action can be looked at from these two approaches.

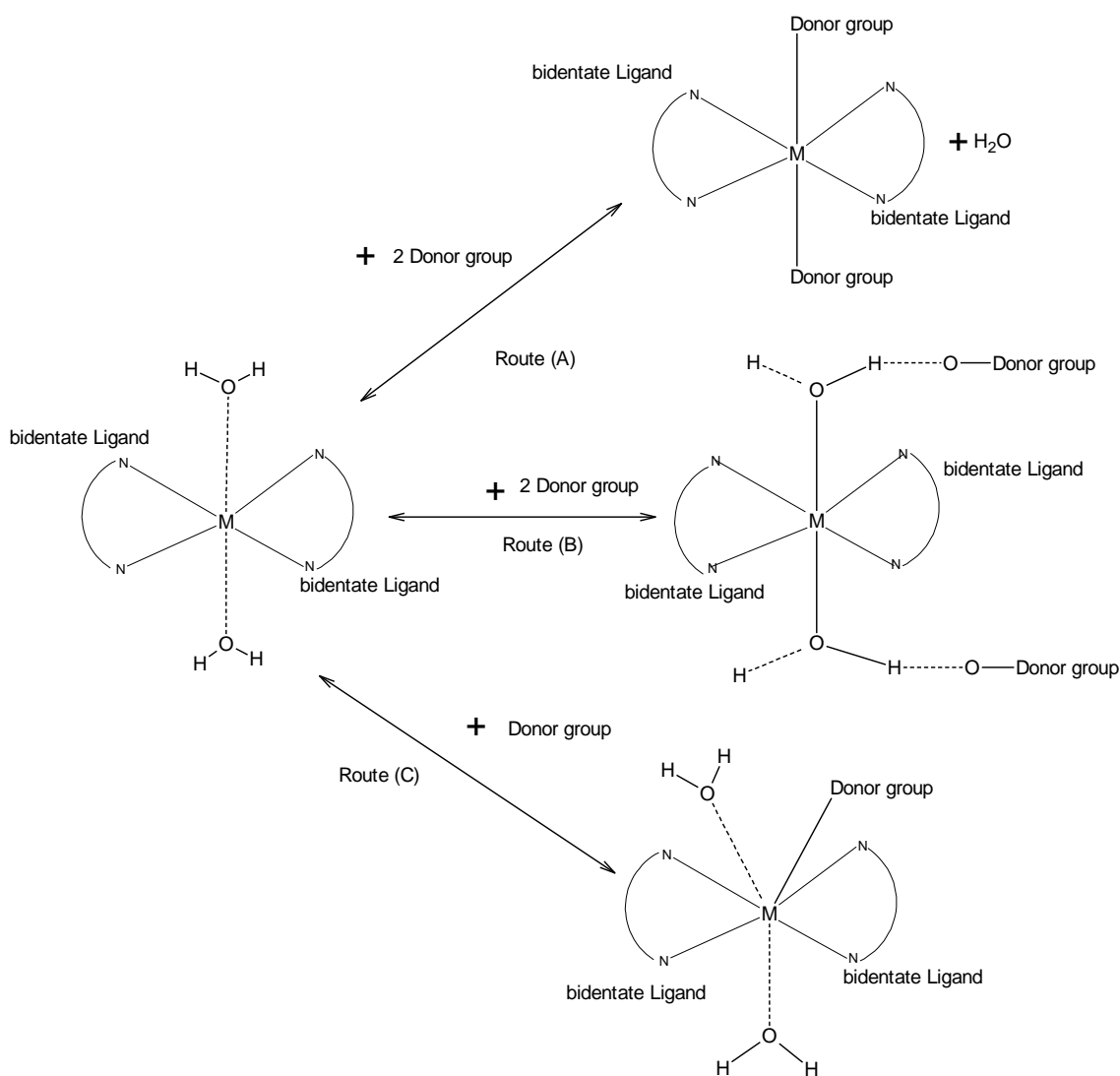
### **6.2.1 Classical metal ligand coordination**

The classical ligand coordination approach to synergistic action in solvent extraction is an infrequently applied explanation. However recently with the availability and accessibility of single crystal analysis there are various commercial extractants whose structure have been published showing the complexes of known extractants coordinated to different synergists [180, 182, 183]. This approach to synergism therefore explains synergistic action in terms of the enhancement of the hydrophobic character of the extracted complex. This approach proposes that the metal ion is not co-ordinately saturated by the ligand anion and therefore it will retain some residual water in its coordination sphere [184] as shown by the Equation 6.2.



Equation 6. 2 Coordination hydrated complex.

In the Equation 6.2, the neutral organo-metallic complex formed remains hydrated, consequently, it is slightly extractable [185, 186]. The water of hydration is subsequently replaced by polar solvents such as carboxylic acids, alcohols, ketones or esters that acts as simple donor group [186-188]. This residual water can therefore be replaced through various ways as shown by our proposed mechanism in Scheme 6.1.



Scheme 6. 1 Possible mechanism of synergistic classical coordination

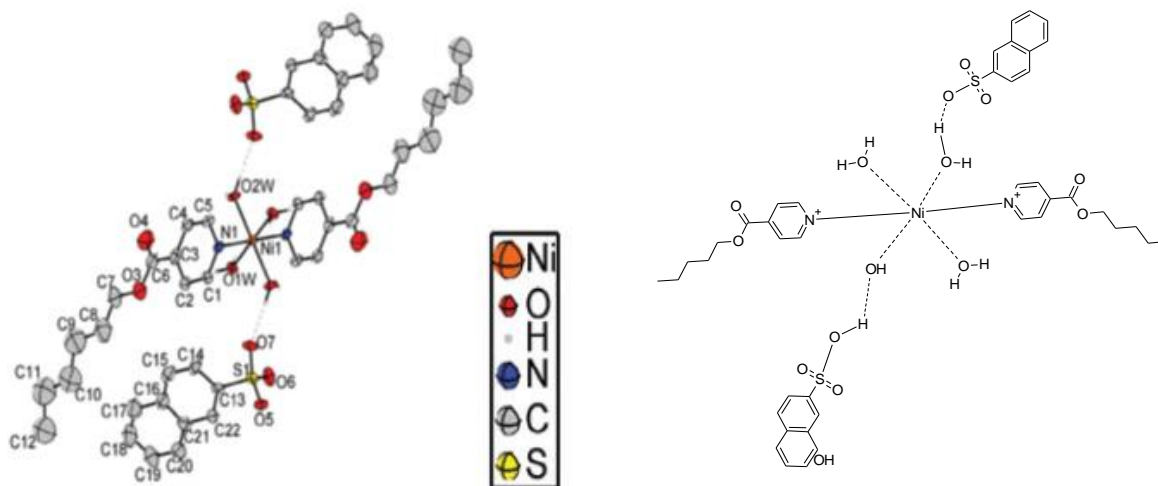


Figure 6. 1 Ortep diagram of Ni-complex drawn at 30% probability ellipsoids (b) Schematic diagram of the Ni-complex courtesy of Jiyuan et al. [189]

In Scheme 6.1 there are different ways in which this mechanism is proposed to occur. The first proposed mode of coordination is through Route A and involves the non-saturated metal complex (made of the ligand and the metal salt) that is co-ordinately saturated by the water molecules, therefore the metal complex is retained in the aqueous phase [184] and therefore no extraction or partial extraction takes place. By adding the synergist in Route A, the water molecules are replaced by the synergistic donor group and therefore kept in the organic phase. This has been shown by the study of  $\alpha$ -hydroxyoxime systems which have shown partial coordination by the synergist as shown by Bearnard *et al* [182].

In the Route B, the water molecules are not removed but are hydrogen bonded to the donor group of the synergist which leads to the formation of aggregates. This is shown by Jiyuan *et al* [189] showing the crystal structure of  $\text{Ni}^{2+}$  hydrogen bonded to a *naphthyl* sulfate based synergist as shown by Figure 6.1 above.

In Route C, there is an expansion of the coordination sphere of the metal ion that is proposed to take place. This will allow bonding of the adduct donor molecule of the synergist. From literature Reza *et al.* [190], Kazuhife *et al.*[191] and Shan Zhu *et. al.* [192] show the synergist coordinated to various ligands. The end result of such coordination will lead to partial replacement of the water molecules by the donor group, in such a system there will be much more dispersed saturated system which leads to the formation of third phase in the extraction

systems. In such a system the secondary effect might be synergistic effect accompanied by suppression of other metals in the solvent extraction system.

## 6.2.2 Supramolecular aggregates

As discussed earlier most types of synergists such as tri-n-butyl phosphate (TBP) and di-n-butyl phosphoric acid (HDBP) used in the PUREX (plutonium uranium recovery solvent extraction) process are amphiphilic molecules. It is known that amphiphilic molecules have a tendency to aggregate [193]. Consequently, the proposed supramolecular aggregates are based on literature evidence of self-assemblies in studies of amphiphilic molecules in both polar and non-polar solvents [180]. It has also been recognised that the presence of supramolecular association between ligands can be employed to influence the selectivity and efficiency of separation processes [180].

Since the synergists are by themselves extractants, the use of discrete ligand-complex assemblies in solution in equilibrium has the potential to result in the enhanced complex stability-behaviour. This stability was previously referred to as the ‘assembly effect’ [180]. This effect was proposed to reflect the presence of assembled ligand components and their influence on formation of other metal complexes [180].

The aggregate formation by amphiphilic molecules is usually characterized by the formation of macromolecular structures called micelles. The formation of these micelles will therefore have a profound influence on the physical properties of the system [173, 194]. Now depending on the system used, aqueous or organic. These amphiphilic molecules have the ability to assemble to form, micelles or reverse micelles (RMs) or water-in-oil (W/O) microemulsions [173, 195-198] as shown in Figure 6.3 below.

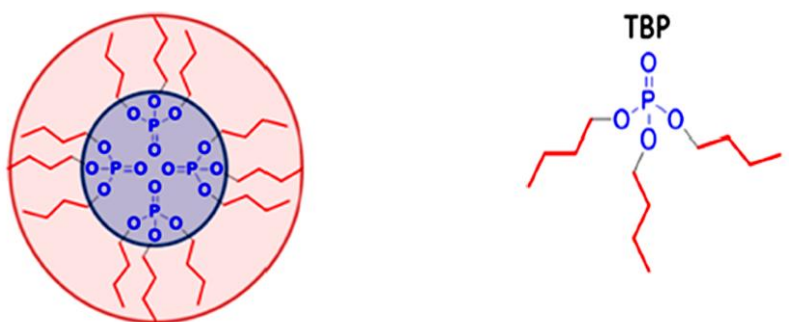


Figure 6. 2 Example of reverse micelle made up from four TBP molecules TBP molecule shown on the side  
Redrawn courtesy of Ross *et. al* [173].

The architecture of the aggregated/micelles or reverse micelles (RM) formed is usually characterized by polar cores made up of the amphiphile head-groups or other hydrophilic moieties. These hydrophilic moieties therefore include metal ions, acidic anions and water molecules, all of which are surrounded by the organic amphiphilic tail-groups in the organic solvent [173, 195-198]. The size and shape of RMs is usually highly sensitive to the conditions within the system [173]. From experimental studies, the only available method for the analysis of the formation of these aggregates is through X-ray scattering experiments or small angle X-ray (SAXS) or neutron scattering techniques (SANS) to provide structural information about large-scale assemblies in solution [173].

### **6.2.3 Factors affecting aggregation**

Based on the aggregate formation mechanism, common surfactants have low critical aggregation concentrations (CACs) compared to other extractants and are therefore strongly affected by factors such as quantity of water and acids [179, 199], the nature and amount of cations in the system, as well as nature of the organic diluent [193, 200, 201].

### **6.3 Type of synergist**

Since most synergists are known extractants by themselves, they therefore work as a combination of mixed extractants. There are several synergistic combinations that have been developed with various known mixtures of extractants and synergist. The choice and design of each combination is usually based on the chemical and physical properties of the targeted metal ion [25]. These combinations can include: neutral synergists such as alcohols, organophosphorus or nitrogen containing ligands with acidic extractants [25] or water soluble extractants which typically contain; carbon–oxygen compounds (amides, ethers, ketones); phosphorus–oxygen compounds and are usually characterized by H-bonding. The last class is the chelating extractant for example two chelated amine-based ligands which usually form mixed amine complexes in solution. Extraction is therefore achieved by the mixed amine complex [25, 202].

### **6.4 Problem statement and justification**

There are various types of extractants that have been developed. However, only a small percentage have been extensively tested and commercialised [7, 203]. This is not only because of the various regulations and safety requirements which have to be met before commercialization. There are also cost implications of introducing new extractants to a solvent

extraction operation. Introducing new extractants will often involve various changes to the extraction process. These changes can be simple processing changes to fundamental changes that involve overhaul of the entire process of extraction. The development of a synergist to enhance the process of extraction or to alter the type of analytes being extracted is therefore a more appropriate cost saving method. It would therefore suffice to look at the development of new synergists as the future of solvent extraction [25].

#### 6.4.1 Choice of synergist

Three acidic amphiphilic molecules have been selected as the synergist for the study as shown below in Figure 6.3.

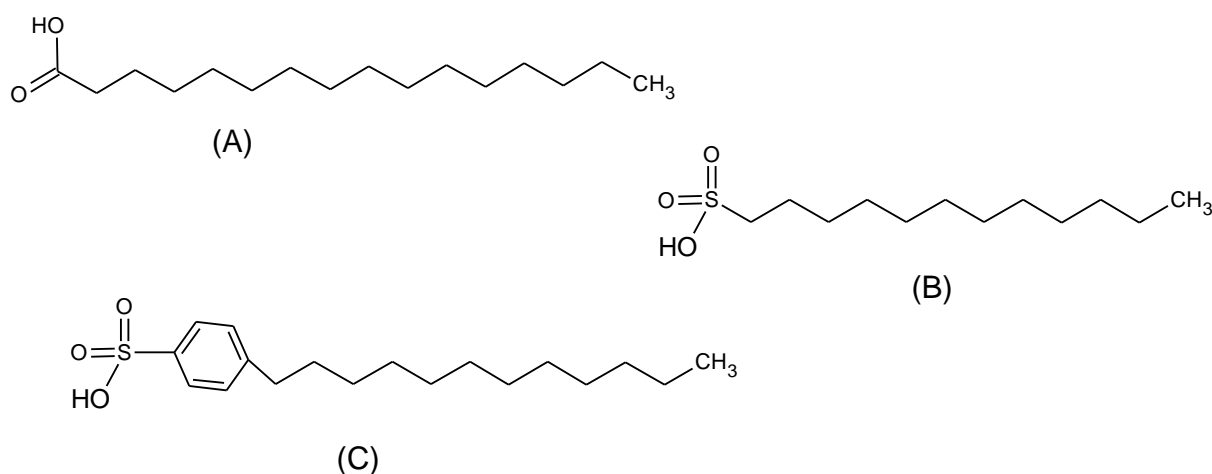


Figure 6. 3 Acidic co-extractants used in the synergistic studies (a) palmitic acid (hexadecanoic acid), (b) indicates dodecasulfonic acid (dodecane-1-sulfonic acid) and (c) indicates benzyl dodecasulfonic(4-dodecane-benzylsulfonic acid)

##### 6.4.1.1 Alkyl Sulfonates

Alkyl benzene sulfonate and alkyl sulfonates are anionic surfactants, they form major constituents of most synthetic detergents, they are widely used in various industrial processes, such as in paper industries, electroplating, cosmetics, food processing, laundry and vehicle washing [204]. Apart from this, these types of surface active reagents have found use in hydrometallurgical processes such as in the flotation cell where they are used as collectors. These reagents have a high specificity for certain mineral surfaces and are therefore usually utilized in relatively low dosages [204]. The two alkyl sulfonate synergists have low use in literature and from our knowledge have not been used for synergistic studies with any of our Schiff base ligands.

### 6.4.1.2 Carboxylic acid

Carboxylic acids are some of the most used synergists. Their mode of action is usually similar to those of phosphorus (V) acids used in uranium recovery. Examples include TBP and HDBP used in PUREX process mentioned earlier. *Palmitic* acid has found use in various literature works with known synergistic ratio of 1:4. [71, 180, 205] This molecule gives us a comparative standard to use in comparing our results to the published work.

## 6.5 Chapter objective

The main objective for this chapter is to use the ligands that were shown to leach in Chapter 5 to study the effect of synergism. Three synergists will be used to show the effect of the various substituents and their influence in synergistic action.

## 6.6 Experimental

A 0.01 M concentration of the mixed metal ions were prepared as described in section 3.5 at pH 4.98; 10 ml of this metal mix was measured into a vial containing 10 ml of 0.04 M, concentration of the amphiphilic molecule alone in aqueous chloroform. The samples were then placed on the Labcon shaker as per procedure in section 5.5 after which 1 ml of the aqueous layer was obtained and diluted to 10 ml with 0.1 M nitric acid before analysis on the ICP-OES. The results obtained are as shown in Figure 6.4 for the different synergists.

Please note the 1:4 ratio of metal ion to synergists and later 1:1:4 of metal ion to ligand to amphiphilic molecules (synergistic) was arrived at from literature work [180] and from two of our previous work on use of *palmitic* acid Saban *et al.* [71] and the use of benzyl dodecasulfonic synergist by Pearce *et al.* [205].

## 6.7 Results

From the results it was observed that the different synergist extracts different metal ions with maximum extraction achieved for the different synergists as shown in Figure 6.4

### 6.7.1 Discussion of results from synergist extraction alone

The result obtained below showed variable results, for synergist C containing the benzyl dodecasulfonic group which showed the highest extraction of  $Pb^{2+}$  at 59 % followed by synergist B at 47 % and then A at 30 %. The different synergists show varied selectivity with



Because *palmitic* acid has C16 which is more than C12 in dodecyl group in synergist B and C, it was therefore expected that the *palmitic* acid would extract higher amount of metal ions. However, the observed results showed that by using the carboxylic functional group there is good selectivity of  $\text{Pb}^{2+}$  over any of the base metals ions as shown by Figure 6.4 (a). The use of sulfonate functionality on the other hand leads to selectivity of  $\text{Pb}^{2+}$  and  $\text{Cu}^{2+}$  as shown by Figure 6.4 (b). The introduction of the benzyl group on synergist C at first confirms the tendency of the sulfonate functionality to select  $\text{Pb}^{2+}$  and  $\text{Cu}^{2+}$ . However, there is increased synergism for all the metal ions with reduced selectivity since there extraction across all the metal ions as shown by Figure 6.4 (c).

## 6.8 Synergistic effects

Synergistic study was therefore undertaken based on the 1:1:4 ratio of metal ion, ligand and synergist. The ligands used in this study were mainly from the ligands that showed very high degree of leaching. The synergistic effect of class B ligands that did not show a high degree of leaching was also investigated which will be covered later in section 6.8.3. The ligands used are therefore as follows.

### 6.8.1 Class A ligands

Except for ligand **L5**, containing the *nonyl* substituent this class of ligand **L1-L4** had very high degree of leaching as shown in Chapter 5.5.1.1. The results obtained from studies of their extraction indicated very low extraction with ligands **L4** showing the highest observed extraction of  $\text{Cu}^{2+}$  at close to 20 %. These ligands shown in Figure 6.5 were therefore chosen as good candidates for the study of synergistic effect. This was done by using them together with the different synergist in a 1:4 ratio to extract the selected divalent metals ions. This was carried out as explained in the experimental below.

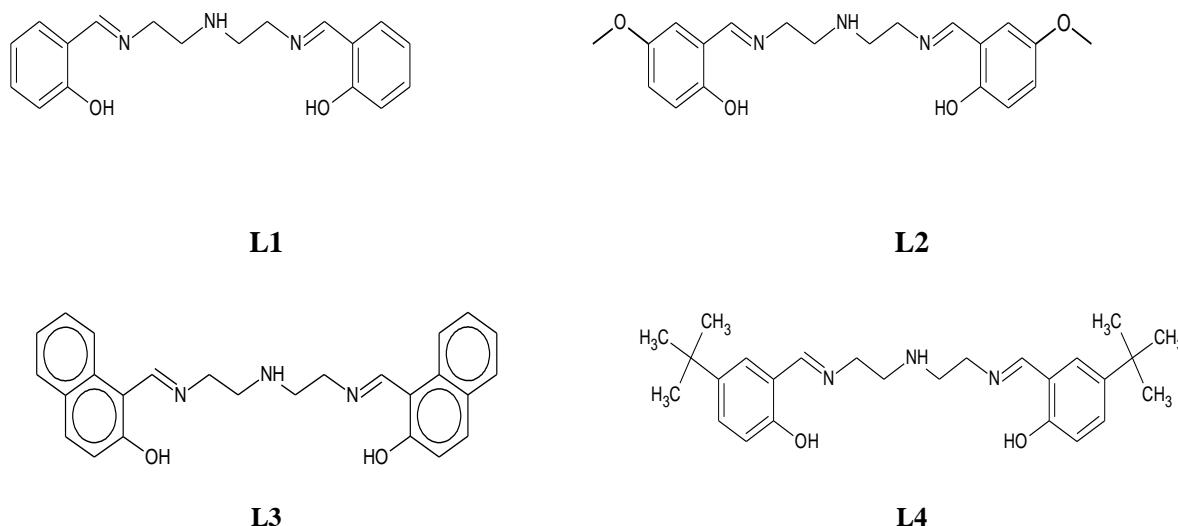


Figure 6. 5 Showing the schematic diagram of class A ligands

### 6.8.1.1 Experimental

The experimental set up was similar to the previous procedure in Chapter 5.5 and 6.6 above for the synergist alone. 10 ml of the standard 0.01M solution of metal mix at pH 4.98 was measured and added to aqueous chloroform containing 10 ml of 0.01M ligand and 0.04M of *palmitic* acid. This was then allowed to shake at 220 RPM for 24 hours. After this the products were processed and analyzed on the ICP-OES. The same procedure was used for the other two synergists with the same ligand. The results are therefore shown below in Figure 6.6.

Note: From the results below.

%E= the % of metal ions extracted with the ligand alone in absence of any synergist

SAL= synergist A and the corresponding ligand L

SBL= synergist B and the corresponding ligand L

SCL= synergist C and the corresponding ligand L

Graphical representation of the synergist extraction for **L1-L4** is therefore shown below.

### 6.8.1.2 Discussion of competitive synergistic extraction results for class A ligands

The obtained results as shown in Figure 6.6 indicated that there was synergistic extraction that occurred in using these ligand systems with the different amphiphilic molecules. Previously in Chapter 5, the amount of metal ion extracted by the ligands alone (indicated as (% ExL) in each

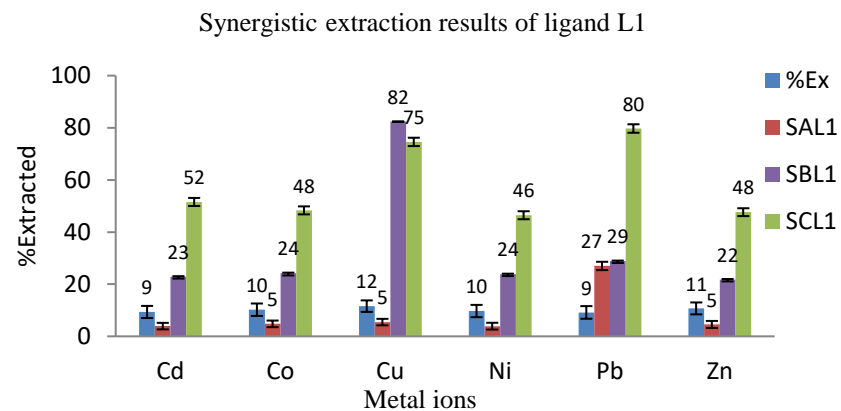


Figure 6.6 (a): Graphical representation of synergistic extraction of ligand **L1**.

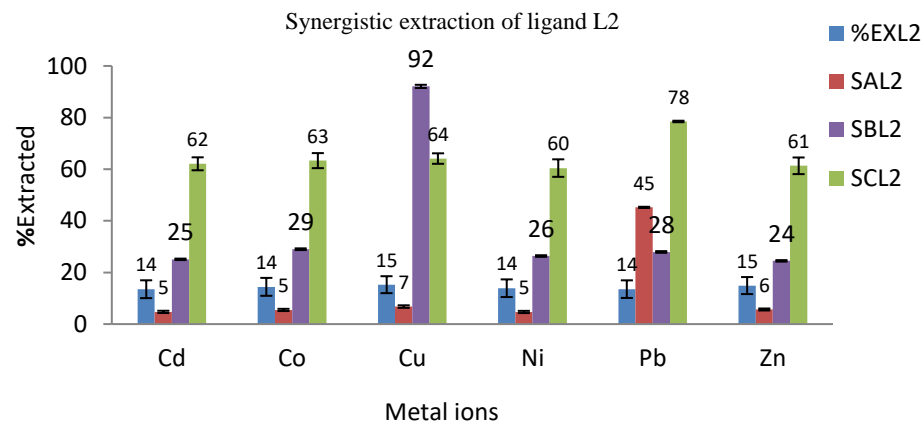


Figure 6.6 (b): Graphical representation of synergistic extraction results of ligand **L2**.

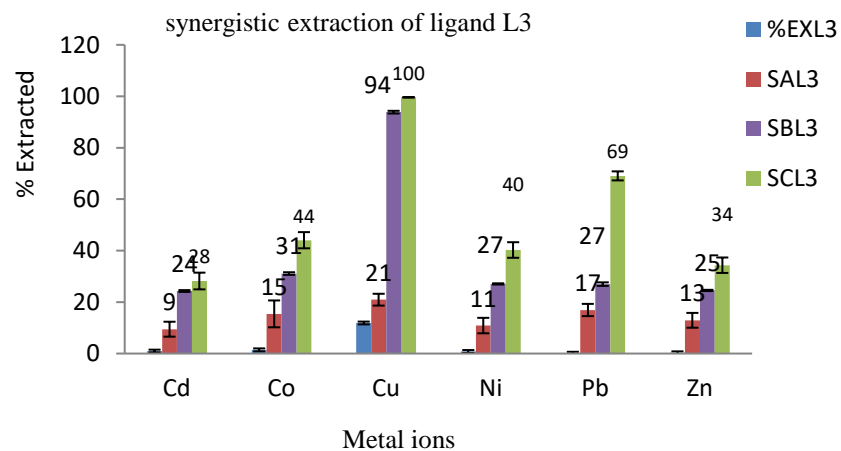


Figure 6.6 (c): Graphical representation of synergistic extraction results of ligand **L3**.

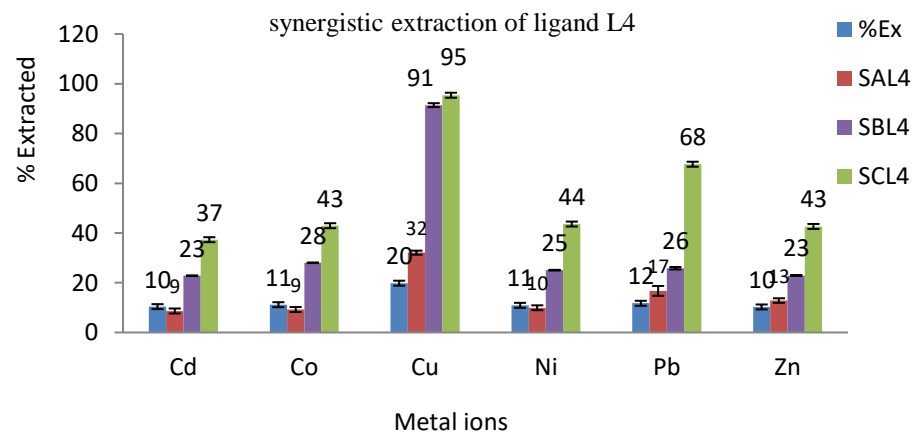


Figure 6. 6 (d) Graphical representation of synergistic extraction results of Ligand **L4**.

-of these graphs Figure 6.6 (a) to Figure 6.6 (d) had shown very minimal extraction due to the high leaching effect. With the addition of the synergist, both synergistic effects and antagonistic effects are observed. Co-extraction of some of the metal ions is also observed.

By observing the results from Figure 6.6 (a), the ligand **L1** shows various effects. For example, the ligand alone extracts slightly less than 12 % for the highest extraction of  $\text{Cu}^{2+}$ . However, when the synergist is added, only a slight increase in the extraction of the  $\text{Pb}^{2+}$  ions at 27 % is observed. In all the cases antagonistic effect with reduction of extraction of all the metal ions is observed.

For synergist B, using the same ligand **L1** (Figure 6.6a), a synergistic effect for all the metal ions is observed. With the highest synergistic effect obtained for  $\text{Cu}^{2+}$  at 82 % considering that the ligand alone had 12 % and the synergist alone had 40 % extraction of  $\text{Cu}^{2+}$  (increase of 30% ( $82\% - (40\% + 12\%)$ )). The synergistic factor was obtained as 1.58 as calculated by Equation 6.1.

Lastly for synergist C, for the same ligand in this case there is greater synergistic effect observed with  $\text{Pb}^{2+}$  ions showing the highest synergistic extraction at 80 % followed closely by  $\text{Cu}^{2+}$  at 75 %. This synergist effect however shows the lowest selectivity among the three synergists with the lowest synergistically extracted metal being  $\text{Ni}^{2+}$  at 46 %. The trend discussed above is observed for all the ligand series and through this, the effect of synergist on the selectivity is discussed below.

#### 6.8.1.2.1 Effect of synergist on selectivity

From these results, the effect of the synergist and that of the ligand is observed. The introduction of synergist A to the ligand **L1** system induces the selectivity of the  $\text{Pb}^{2+}$ . This shows that the selectivity is greatly influenced by the synergist over the selectivity of the ligand. This observation is based on the results indicating that the synergist alone extracted only  $\text{Pb}^{2+}$  ions as shown in Figure 6.7 (a). The same is true for ligand **L2**. However, for ligands **L3** and **L4**,  $\text{Cu}^{2+}$  is selectively extracted over the synergistic preference which is  $\text{Pb}^{2+}$  as shown by the summarised results for  $\text{Cu}^{2+}$  and  $\text{Pb}^{2+}$  below.

For synergist B (dodecyl sulfonate),  $\text{Cu}^{2+}$  is selectively extracted over  $\text{Pb}^{2+}$  in the series. From Figure 6.7 (b), the synergistic preference is for both of these metal ions. However the introduction of the ligands pushes selectivity of  $\text{Cu}^{2+}$  over  $\text{Pb}^{2+}$  as shown by Figure 6.7 (b). The

general trend observed indicates that the % of  $\text{Cu}^{2+}$  extracted increases as the alkyl content increases, except for the sterically bulky **L4** which shows a slight reduction. The reverse is observed for  $\text{Pb}^{2+}$  where the amount of  $\text{Pb}^{2+}$  is being reduced across the series.

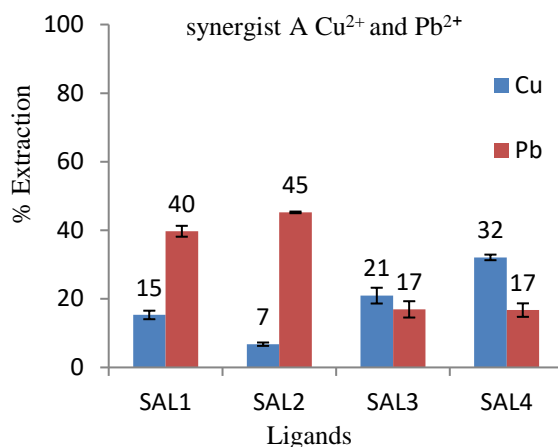


Figure 6.7 (a): Graphical representation of the trends of synergist extraction for  $\text{Cu}^{2+}$  and  $\text{Pb}^{2+}$  with synergist A.

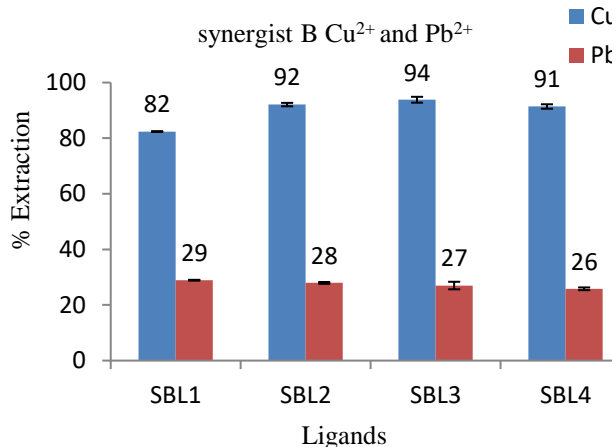


Figure 6.7 (b): Graphical representation of the trends of synergist extraction for  $\text{Cu}^{2+}$  and  $\text{Pb}^{2+}$  with synergist B.

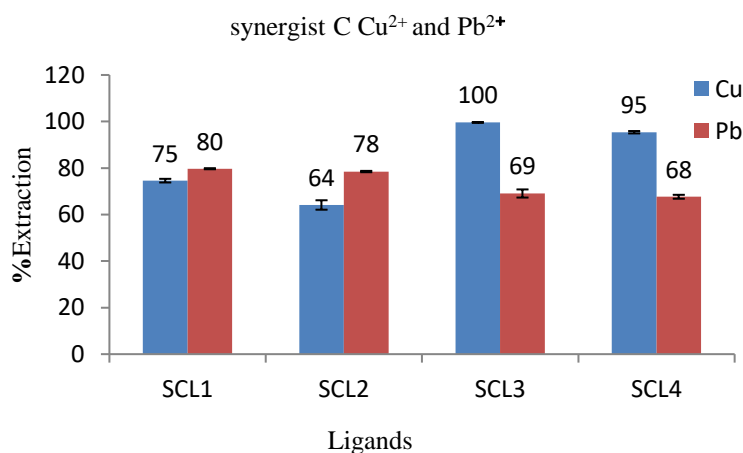


Figure 6.7 (c): Graphical representation of the trends of synergist extraction for  $\text{Cu}^{2+}$  and  $\text{Pb}^{2+}$  with synergist C.

For synergist C (dodecyl benzyl sulfonate), an almost equal measure of extraction of  $\text{Cu}^{2+}$  and  $\text{Pb}^{2+}$  is observed as shown by Figure 6.7 (c). The introduction of the high electron density benzyl group reduces selectivity of the sulfonate functionality towards  $\text{Cu}^{2+}$  while enhancing the preference of  $\text{Pb}^{2+}$  as shown by Figure 6.7 (c). However because of the presence of the ligand which seems to synergistically favour  $\text{Cu}^{2+}$  the net effect is that both  $\text{Pb}^{2+}$  and  $\text{Cu}^{2+}$  are extracted in equally high measure.

### 6.8.2 Class C ligands

Finally, the class C ligands (*tripodal* ligands shown in Figure 6.8 below) that had shown excessive leaching except for ligand **L15** with the *nonyl* substituent were studied. The ligands **L11-L14** were therefore subjected to synergistic solvent extraction. The procedure used was similar to the experimental in section 6.8.1 above and the results obtained are shown in Figure 6.8.

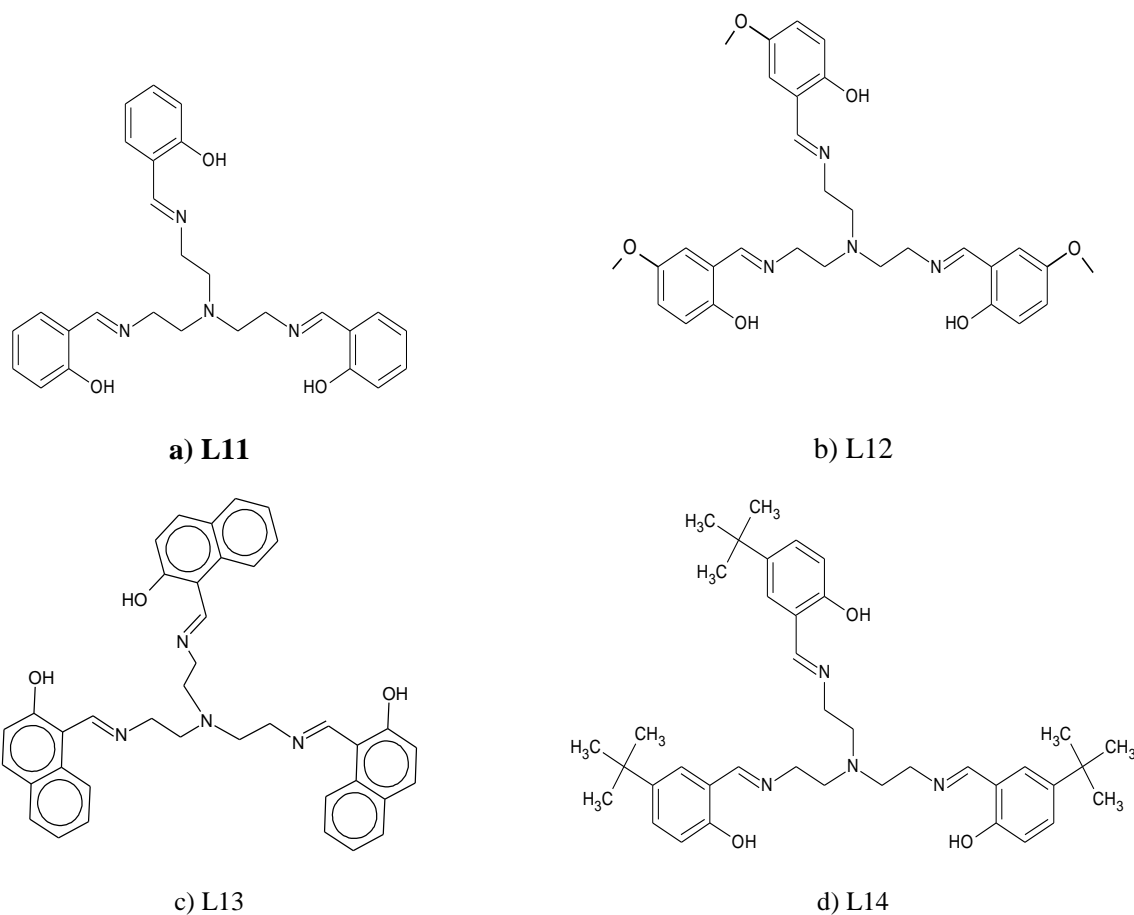


Figure 6. 8 Schematic diagrams of class C ligands used for synergistic solvent extraction

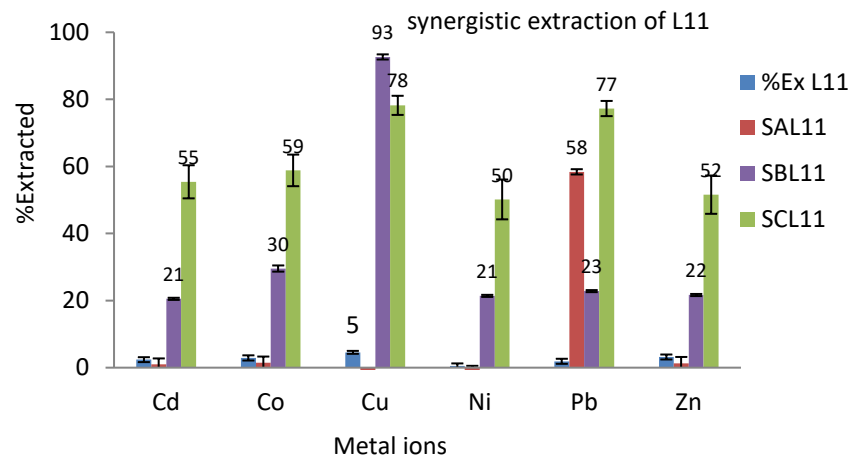


Figure 6.9 (a): Graphical representation of synergistic extraction of ligand **L11**.

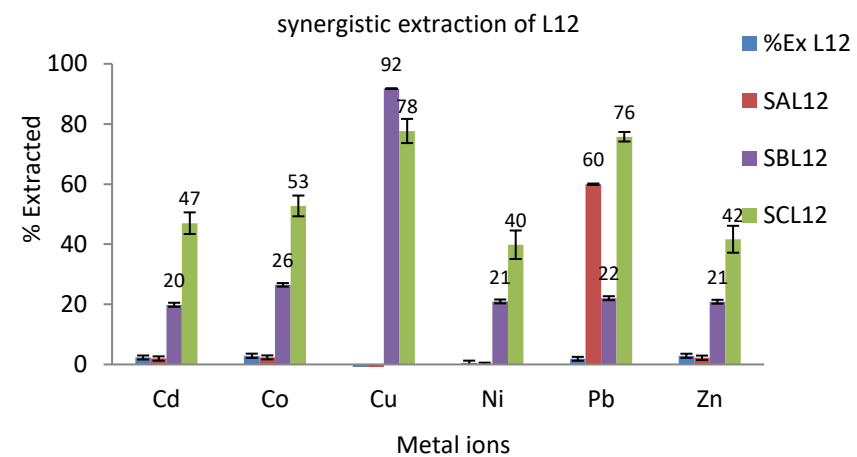


Figure 6.9 (b): Graphical representation of synergistic extraction of ligand **L12**.

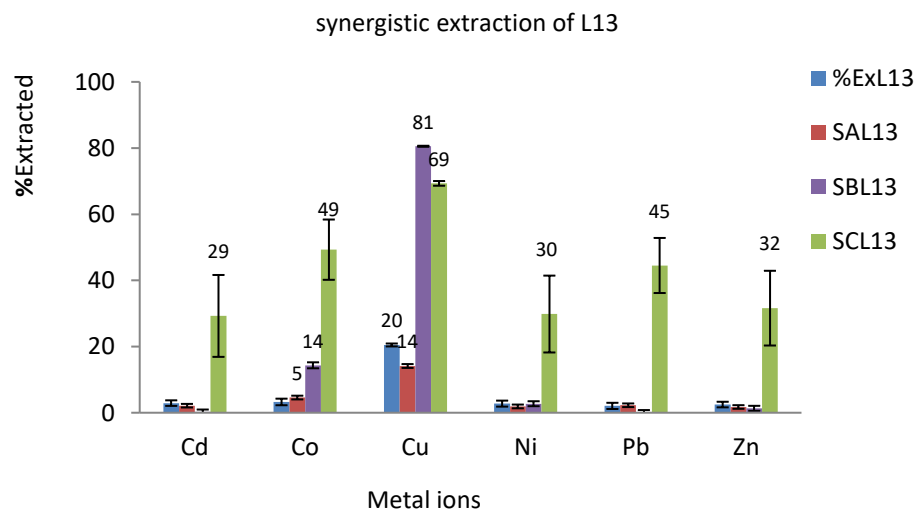


Figure 6.9 (c): Graphical representation of synergistic extraction of ligand **L13**.

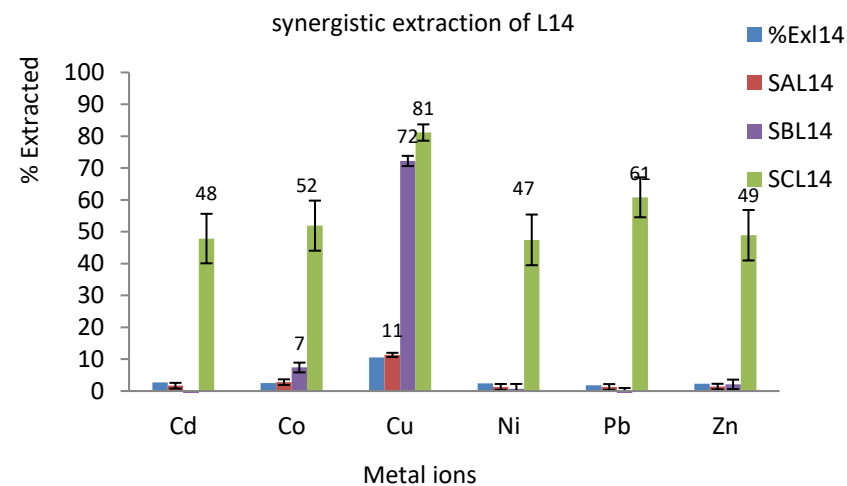


Figure 6.9 (d): Graphical representation of synergistic extraction of ligand **L14**.

### 6.8.2.1 Discussion of competitive synergistic extraction results for class C ligands

The results from the synergistic study of the *tripodal* ligands **L11-L14** indicate the high degree of synergistic effect. Previously as discussed in Chapter 5, these ligands had shown excessive bleeding with the highest extracted metal ion  $\text{Cu}^{2+}$  being 20 % for ligand **L13** with the *naphthyl* group. Upon addition of the different synergists, it is observed that synergist A containing the carboxylic functionality with longer hexadecane alkyl group had minimal to no synergistic effect when working in conjunction with ligands with the highly organic alkyl groups like *naphthyl* group ligand **L13** and *tert*-butyl groups ligand **L14** while showing synergistic effects for  $\text{Pb}^{2+}$  with the un-substituted *salicyl* group. This is however not the case for both synergist B and C which all show selectivity towards  $\text{Cu}^{2+}$  over  $\text{Pb}^{2+}$  as shown by the summarised results for  $\text{Cu}^{2+}$  and  $\text{Pb}^{2+}$  in Figure 6.10b and 6.10c.

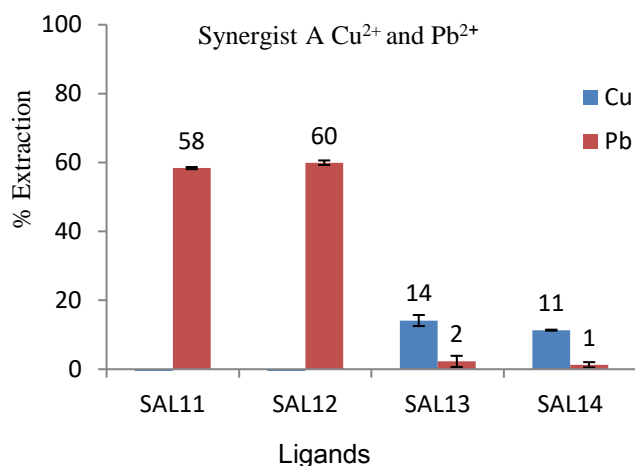


Figure 6.10 (a): Graphical representation of the trends of synergist extraction for  $\text{Cu}^{2+}$  and  $\text{Pb}^{2+}$  with synergist A.

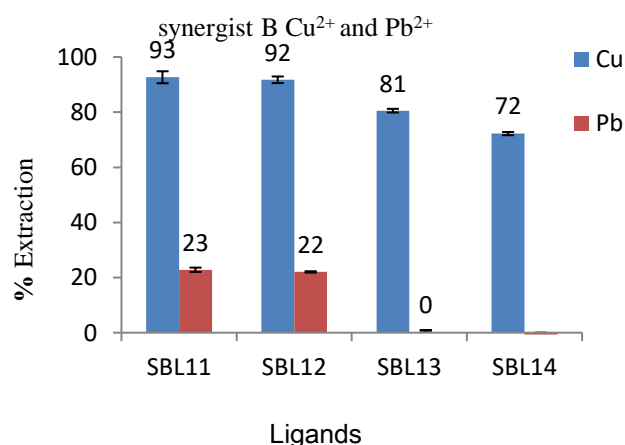


Figure 6.10 (b): Graphical representation of the trends of synergist extraction for  $\text{Cu}^{2+}$  and  $\text{Pb}^{2+}$  with synergist B.

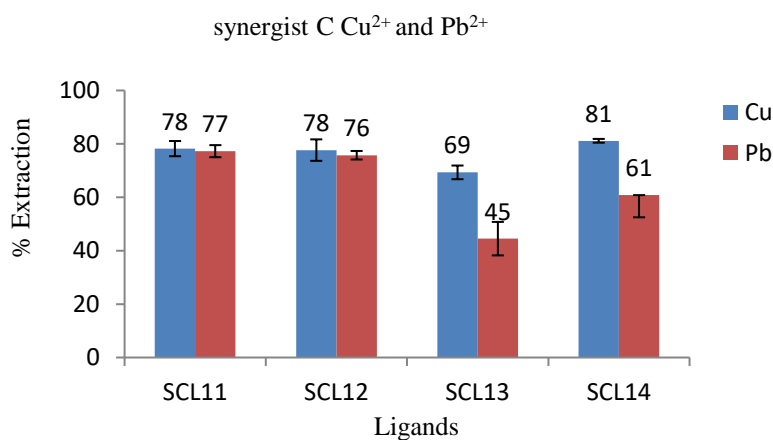


Figure 6.10 (c) Graphical representation of the trends of synergist extraction for  $\text{Cu}^{2+}$  and  $\text{Pb}^{2+}$  with synergist C

This result in addition to that from the competitive synergistic extraction of class A ligands, indicate a major difference in the two synergistic modes of action. Synergist A was observed to undergo both synergistic effects and antagonistic effects in this series. Its preference for  $Pb^{2+}$  is observed when in a lower molecular weight ligand while for the highly organic higher molecular weight ligands its preference for  $Pb^{2+}$  is greatly reduced. This can be attributed to its mechanism of action discussed as follows.

From literature, carboxylic acid and phosphoric acid based functional groups mode of action tends to be towards interaction (H-bonding or van der Waals) as opposed to the aggregate formation [206] which is synonymous with the sulfonate based functional group. This can be shown by the  $^1H$  NMR titration study below. The results obtained indicate that the addition of the *palmitic* acid to a solution of **L1** ligand in chloroform shows a shift of the spacer protons as shown by Figure 6.11 and Figure 6.11. This shift was however not observed for the sulfonate based synergists B and C as shown in Figure 6.11. This shows a form of interaction of the ligand to the synergist as discussed below.

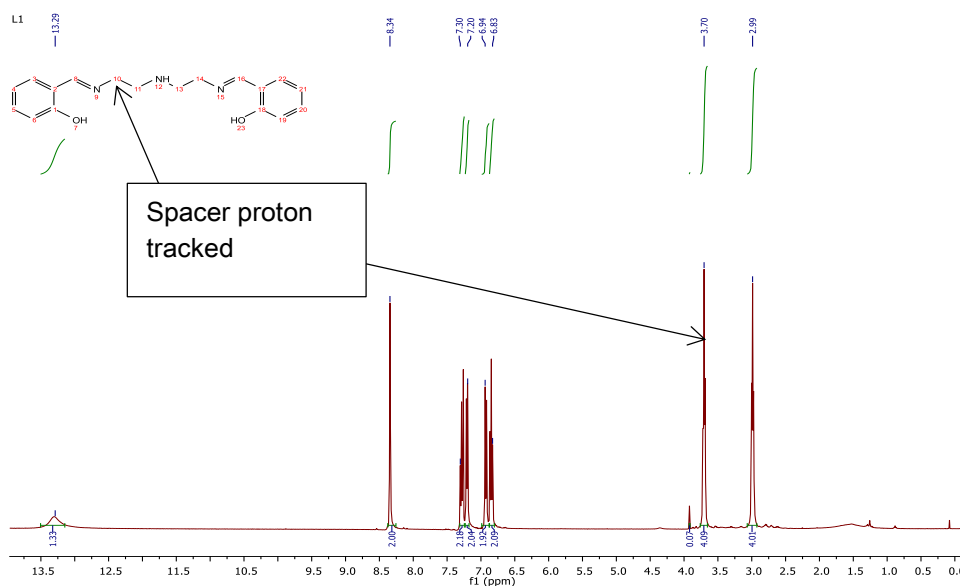


Figure 6. 11  $^1H$  NMR spectra of the ligand **L1** indicating the spacer proton being tracked (please note this ligand has been fully characterized in chapter 2 (Figure 2.6) and this diagram only shows the proton being tracked below).

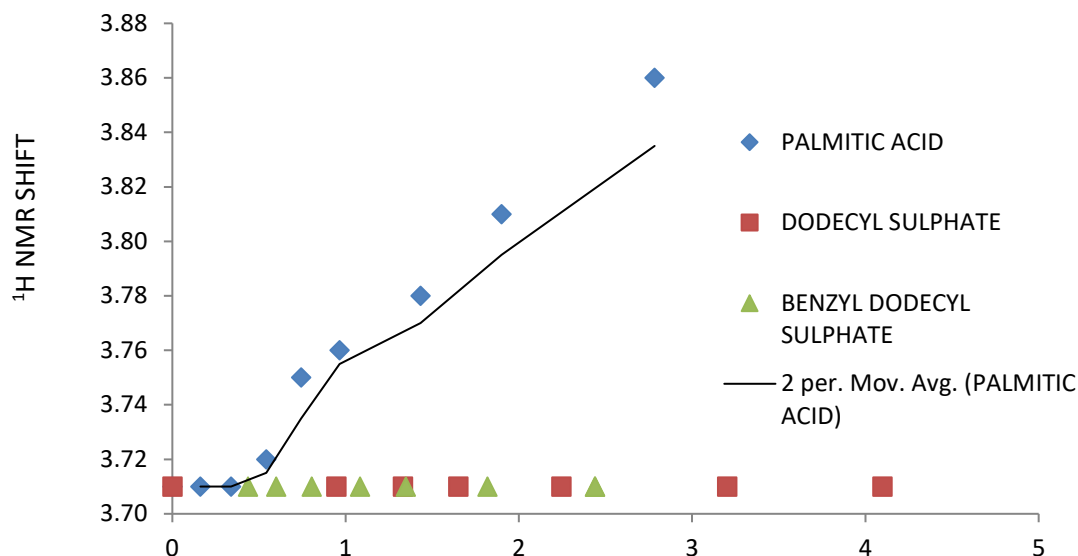


Figure 6. 12 The induced shift of the spacer methylene signal in the  $^1\text{H}$  NMR Spectrum of **L1** on titration with different synergists in  $\text{CDCl}_3$ .

The graph in Figure 6.13 shows that there is an interaction with increased *palmitic* acid whereas the sulfonate-based synergists B and C do not show any form of interaction. The 1:5 ligand palmitic acid maxima were achieved due to supersaturation. There were also attempts at the development of some crystal structures based on the ligand **L4** and any simple acid such as hexanoic acid which led to some crystals which were however intrinsically twinned and therefore could not be separated out for refinement. The mechanisms are discussed in Section 6.2 and the proposed modes of coordination are given by Scheme 6.1.

From the results in Figure 6.12, showing that *palmitic* acid tends to interact, it can therefore be observed that larger metal ions such as  $\text{Pb}^{2+}$  (series 6.1) will have greater ability to coordinate to the synergist. This leads to  $\text{Pb}^{2+}$  being selectively highly extracted over the other metals ions.

$$\text{Pb}^{2+} = 1.23 \text{ \AA}, \text{Zn}^{2+} = 0.74 \text{ \AA}, \text{Ni}^{2+} = 0.69 \text{ \AA}, \text{Cu}^{2+} = 0.73 \text{ \AA} \text{ and } \text{Co}^{2+} = 0.75 \text{ \AA}.$$

Series 6. 1 Ionic size of selected metal ions (courtesy of Shannon R. D online database [207]).

Since  $\text{Co}^{2+}$ ,  $\text{Cu}^{2+}$  and  $\text{Zn}^{2+}$  have an almost equal ionic size almost similar extraction values are observed by the synergist alone as shown in Figure 6.5a. However because of the influence of the different ligands there is preference for the  $\text{Cu}^{2+}$  over the  $\text{Co}^{2+}$  and  $\text{Zn}^{2+}$  in these systems. The other factor that must be considered in the synergistic preference of  $\text{Cu}^{2+}$  is the stability of the formed complex as shown by the Irving-Williams series.

For the other synergist containing the alkyl sulfonates functionality as discussed, their mode of action is through aggregate formation through reverse micelle formation. Therefore, by introducing a highly organic benzyl group next to the highly polar sulfonate group will have the effect of reducing the electronegativity (polarity) of the sulfonate group. This will subsequently reduce the ability of the synergist to agglomerate around a particular metal ion or around its complex. The net effect is a selective interaction with the metal ions present in the solution as shown by the high extraction of the other metal ions.

The synergistic effect of the ligands of the partially leached class B ligands was therefore also investigated as follows.

### 6.8.3 Class B ligands: bis(3-aminopropyl)amine based ligands

This class of ligands did not show extensive bleeding as shown in Figure 6.13 where ligand **L6**, **L7** and **L9** were used in this study. These ligands had been shown to extract  $\text{Cu}^{2+}$  over the other ions as a result of complex stability as shown by the Irving-Williams series as discussed in Chapter 5. These three ligands were used because they showed relatively lower extraction in this series. The extraction set up was again similar to the experimental in section 6.6.1 above. The results obtained are shown in Figure 6.14 below.

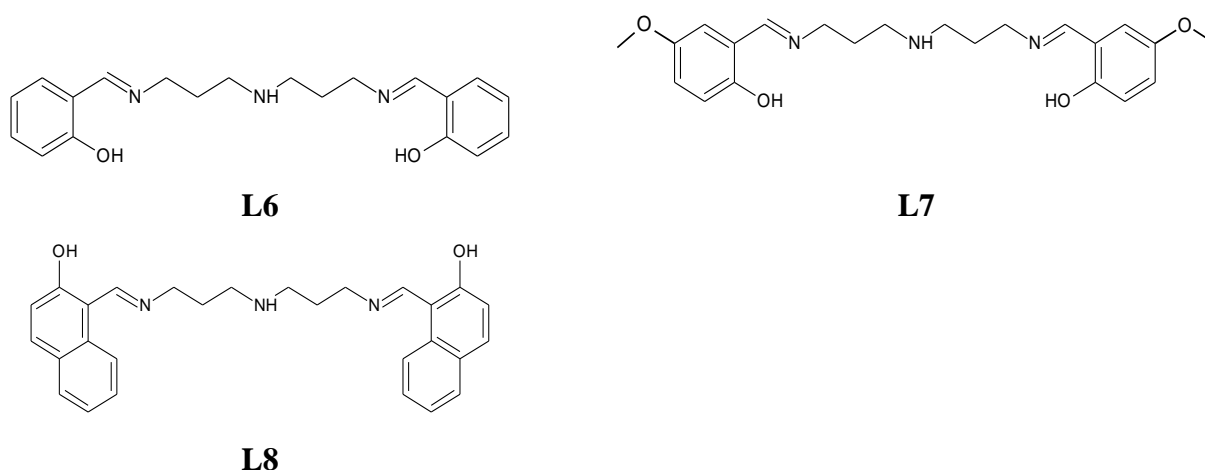


Figure 6. 13 Schematic diagram of the class B ligands used for synergistic solvent extraction studies.

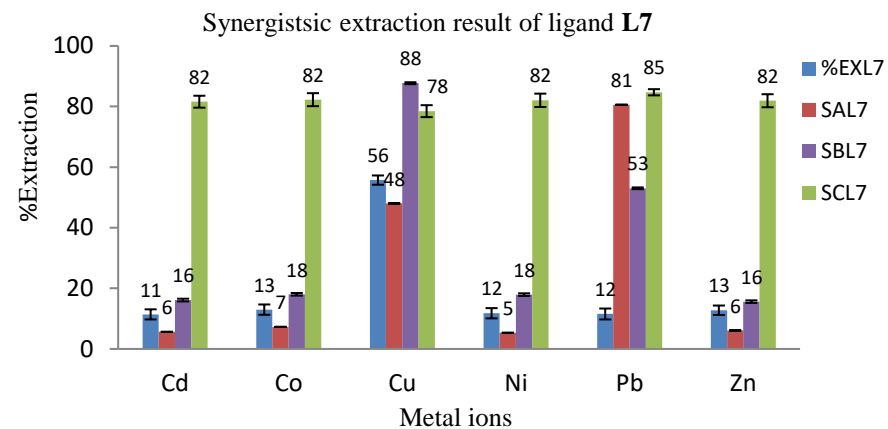
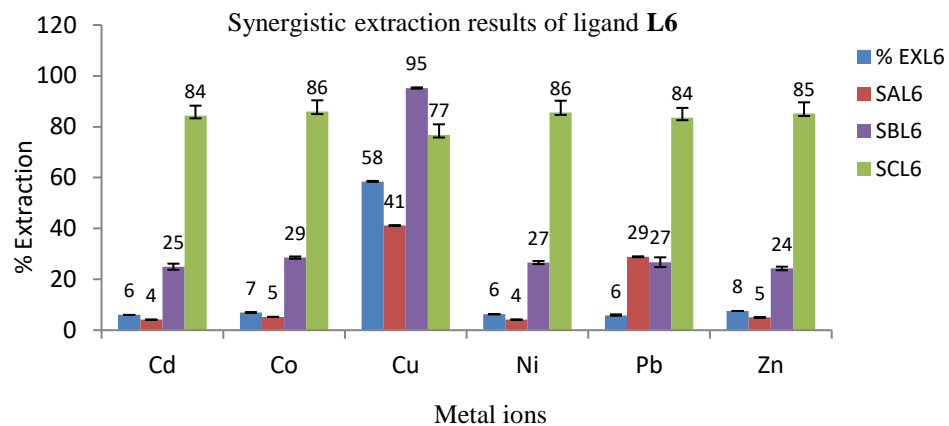
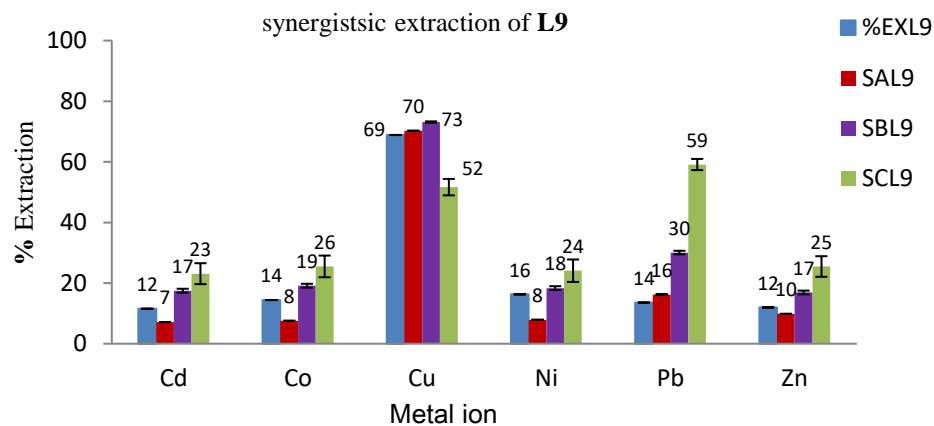


Figure 6.14 (a): Graphical representation of synergistic extraction results of ligand L6.

Figure 6.14 (b): Graphical representation of synergistic extraction results of ligand L7.



EXL      Extraction of Ligand  
 SA      Synergistic A  
 SB      synergist B  
 SC      Synergistic C  
 Key

Figure 6. 14 (c) Graphical representation of synergistic extraction results of ligand L9

### 6.8.3.1 Discussion of competitive synergistic extraction results for class B ligands

In this ligand series there was a synergistic effect in the extraction of  $\text{Cu}^{2+}$ . Only ligand **L7** showed a slight reduction of  $\text{Cu}^{2+}$  extracted. The ligand alone extracted about 60 % of  $\text{Cu}^{2+}$  in competitive solvent extraction %**EXL7** in Figure 6.15 (b). Upon Extraction with the synergist % **SAL7** there is a slight reduction in the extraction of the  $\text{Cu}^{2+}$  ions to 48 %. While it could be observed that there is an antagonistic effect, the two values 54 % and 48 % are within the experimental error range and are therefore not considered substantial to deduce an antagonistic effect. For the same system synergist A and ligand **L7** a synergistic effect is however observed for the  $\text{Pb}^{2+}$  ion. The use of the other two ligands is accompanied by antagonistic effects of  $\text{Pb}^{2+}$  while synergistic effect in the extraction of  $\text{Cu}^{2+}$ . In lower molecular weight ligands without substituent the synergist preference is towards the bigger  $\text{Pb}^{2+}$  ions. However due to the increased inductive effect of the alkyl group and the increased alkyl content the  $\text{Cu}^{2+}$  ions are selectively being extracted over the other synergistic preference.

### 6.9 Summary of the synergistic action

From these results it can be observed that the different ligands and the different synergists induce different synergistic results. Based on these results it is therefore possible to conclude that the different functional groups in the synergist have important contribution in the selectivity of the different metal ions.

In all these ligand classes synergist A and B both have straight chain aliphatic groups and can be said to be structural analogues with different functional head groups. The results also bears this effect showing that synergist A favours selectivity of  $\text{Pb}^{2+}$  on the other hand synergist B containing the sulfonate group prefers the  $\text{Cu}^{2+}$  over the other metal ions.

For synergist C having the benzyl sulfonate group with the dodecyl straight chain alkyl group. The results consistently showed that selectivity is reduced even though the  $\text{Cu}^{2+}$  and  $\text{Pb}^{2+}$  ions are extracted to a slightly higher extent.

These ligands were further subjected to competitive bulk liquid transport to study the selectivity of these synergistic systems as follows.

### 6.10 Study of selectivity in synergistic transport

To study the ability of these ligands to transport the metal ions ligand **L11** (Figure 6.15) was subjected to competitive bulk liquid transport using the different synergists. This ligand was

selected due to the higher degree of synergism observed in the class C ligands over the class A and B ligands. This ligand was also the only ligand that showed substantial synergistic effect using synergist A in this class of ligands as discussed in section 6.8.2.1. It is important to note that due to the cost and time restraint, not all the ligands could be studied for competitive transport studies. The choice of this ligand had to meet the above criteria to be able to show how the synergists transport the metal ions from the source phase to the receiving phase across the bulk liquid membrane as a result of pH difference.

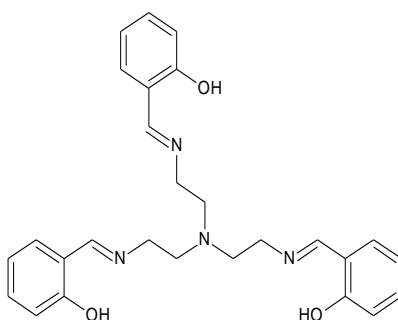


Figure 6. 15 Ligands **L11** used in synergistic transport study

### 6.10.1 Experimental

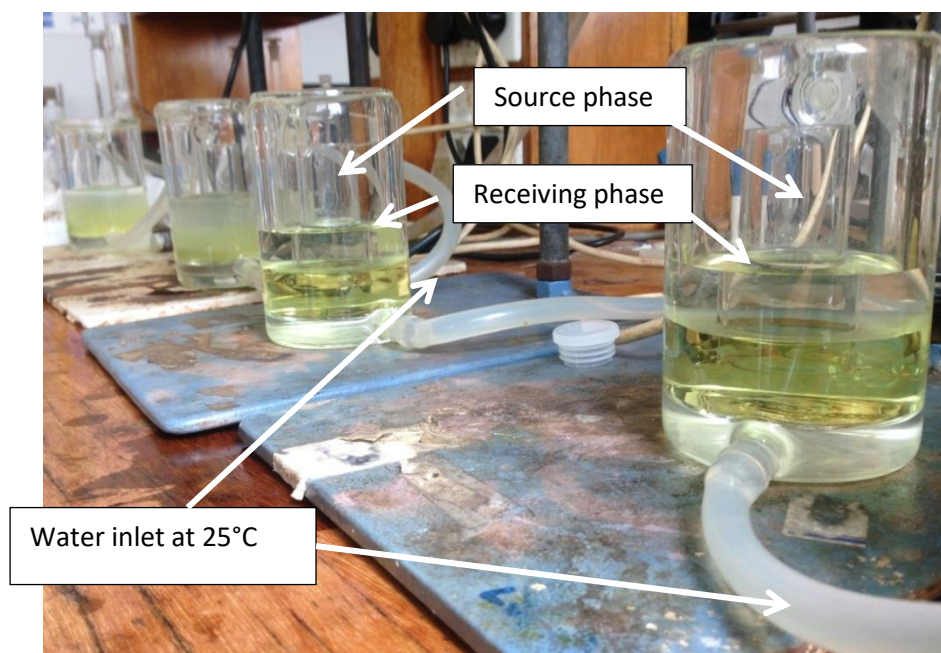


Figure 6. 16 Transport cell containing the synergist and the ligand in the membrane phase and the metal mix in the source phase

The set up for the transport was similar to the procedure used in Chapter 5.9.1 where 50 ml of the aqueous chloroform containing the 0.002 M ligand and 0.008 M of the synergist were

transferred to the transport cell. On the receiving end of the transport cell (shown in Figure 6.16), 30 ml of the 0.1 M nitric acid was added and 10 ml of the metal mix was then added to the source phase similar to the procedure in chapter 5.9.1.

The samples were left to stir at 10 revolutions per minute for 24 hr after which the source phase and the receiving phase are processed by obtaining 1 ml of both the receiving phase and the source phase adding 9 ml of 0.1 M nitric acid. The two samples from each set up were then analyzed by ICP-OES. Each of the samples were set up in duplicate as shown in Figure 6.16.

The ICP results are therefore discussed as follows.

### 6.10.2 Results from competitive transport study of ligand L11

The study of bulk liquid transport for the synergist system is shown in Figure 6.17.

#### Note

**% MP** = Represents the amount of metal ions extracted from the source phase to the membrane phase and is obtained by control minus source phase after transport. (Control is the amount of metal ions in the source phase before transport).

**%RP** = Represents the amount of metal ions in the receiving phase after transport.

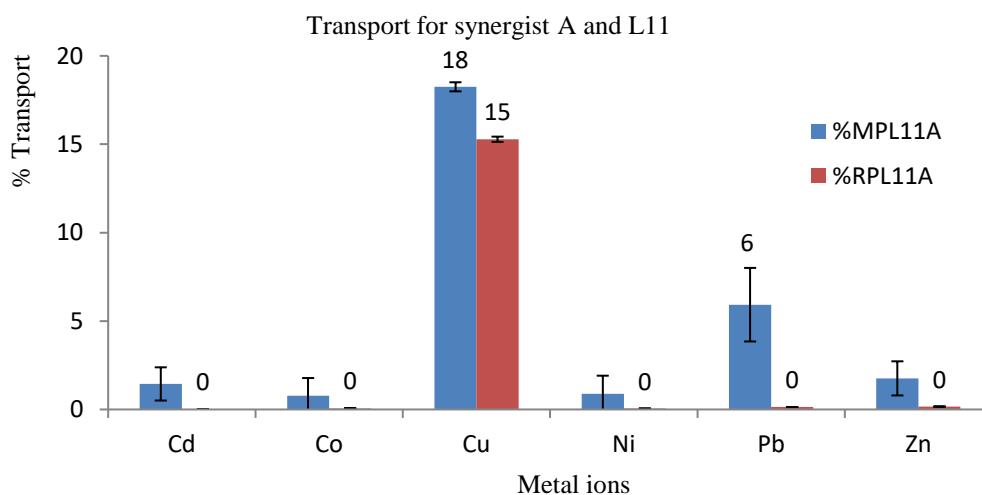


Figure 6. 17 (a) Synergist transport for synergist A-L11

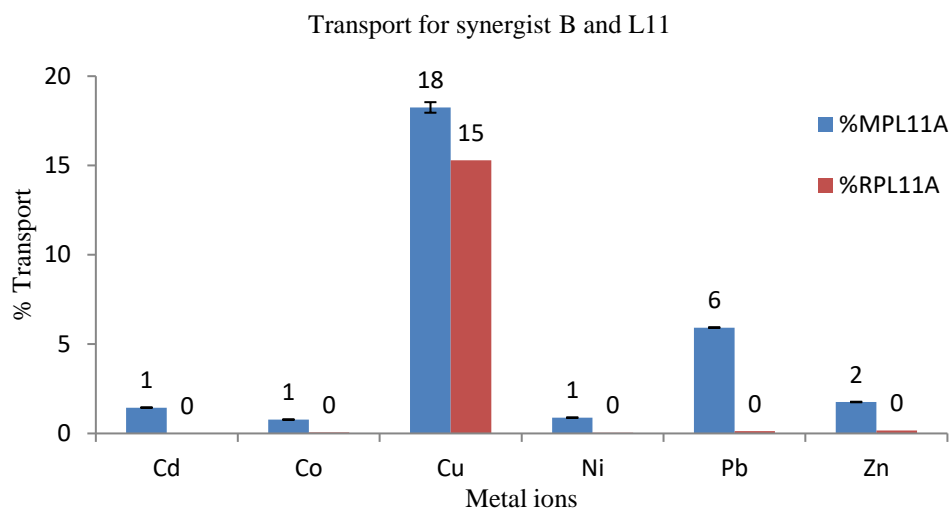


Figure 6. 17 ( b) Synergist transports for synergist B-L11

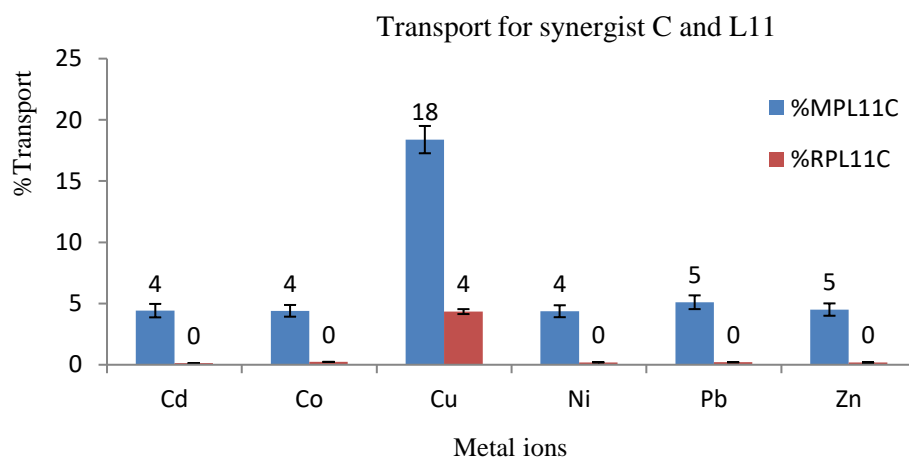


Figure 6. 18 ( c) Synergist transport for synergist C-L11

### 6.10.3 Discussion of the synergistic effect on transport studies

From these transport results, it is observed that only  $\text{Cu}^{2+}$  ions are being transported to the receiving phase. For synergist A, more  $\text{Cu}^{2+}$  is transported than when the other synergists are used. The second highest extracted metal ion is  $\text{Pb}^{2+}$ . For this system, the assumption could be made that the  $\text{Pb}^{2+}$  would be preferentially transported over the  $\text{Cu}^{2+}$  ions. This is because the synergistic competitive solvent extraction results had shown higher extraction of  $\text{Pb}^{2+}$ . In this transport study it is however observed that the nature of interaction between the synergist A, the ligand and  $\text{Pb}^{2+}$  ions is much stronger and therefore the pH difference does not easily allow its release into the receiving phase. These results are consistent with previous work by Saban *et al* who showed that synergistic transport preference is towards  $\text{Cu}^{2+}$  over  $\text{Pb}^{2+}$  [71].

## 6.11 Summary and conclusion

The N-donor *salen* type ligands synthesized previously as discussed in Chapter 2 were used to study the synergistic effect. Twelve out of the fifteen ligands in this group of ligands were used for competitive synergistic studies with three different amphiphilic molecules.

The results indicate that the different functionality in the amphiphilic molecules leads to different proposed mechanisms for the synergistic extraction of the selected metal ions. The carboxylate functionality was shown to undergo coordination while the sulfonate based functional group showing aggregation through reverse micelles.

The introduction of the benzyl group to the sulfonate functional group in the amphiphilic molecule leads to higher extraction but poor selectivity. The sulfonate based ligands have high selectivity for  $\text{Cu}^{2+}$  and  $\text{Pb}^{2+}$  while the carboxylate functional group has high selectivity for the  $\text{Pb}^{2+}$  alone.

The results show that there is a clear trend that developed in the competitive synergistic extraction using these ligands. The different substituents on the ligands will therefore lead to synergistic effects.

For class A ligands with synergist A the order of extraction of  $\text{Pb}^{2+}$  is given as  $\mathbf{L2 > L1 > L3 = L4}$  for  $\text{Cu}^{2+}$  the order is reversed with  $\mathbf{L2 < L1 < L3 < L4}$ . This is also the same order obtained for synergist B and C. The small difference only occurs for  $\mathbf{L1 > L2}$  for  $\text{Pb}^{2+}$  while for  $\text{Cu}^{2+}$  it is  $\mathbf{L3 > L4}$ .

The class B ligands had a reverse order for the extraction of  $\text{Pb}^{2+}$  for these ligands with synergist A and B showing  $\mathbf{L2 < L1 < L3 < L4}$  for synergist C. The extraction of  $\text{Pb}^{2+}$  order is completely reversed with  $\mathbf{L1 > L2 > L3 > L4}$ . On the other hand the synergistic extraction for  $\text{Cu}^{2+}$  is shown by the order  $\mathbf{L1 > L2 > L3 > L4}$  for all the ligands Note for this class  $\mathbf{L3}$  is the only ligand that falls out of the prescribed order.

For the class C ligands, the order of synergistic extraction is similar to the class A ligands however only two results were obtained for  $\text{Cu}^{2+}$ . For synergist B two results for  $\text{Pb}^{2+}$  was obtained. The general trend for this class of ligands follows the same order for class B ligands shown above.

# **CHAPTER 7**

---

## **SOLVENT EXTRACTION OF THE SCHIFF BASE LIGANDS BEARING THE O-DONOR GROUPS**

---

## 7.0 Introduction

This chapter focuses on the Schiff base ligands bearing the O-donor atoms. The coordination ability of the O-donor in the Schiff base ligand series will be discussed. The O-bearing ligands synthesized in Chapter 3 are subjected to competitive solvent extraction studies, bulk liquid membrane transport study and the pH effect study to determine selectivity and extraction efficiency.

### 7.1 Oxygen containing ligand systems

Based on the hard-soft acid base classification of the different donor group, the O donor atom is classified as a hard donor atom with preference to coordinate to the hard metal ions. This is indeed the problem for the ligands bearing the O-donor atoms used in solvent extraction since they are unable to reject hard metal ions such as  $\text{Ca}^{2+}$ ,  $\text{Mg}^{2+}$  and  $\text{Mn}^{2+}$  [208, 209]. Apart from this the ligands bearing the O-donor atoms usually suffer greatly due to ease of poisoning by  $\text{Fe}^{+3}$  ions [208]. Therefore in most solvent extraction processes preliminary steps are usually employed to remove  $\text{Fe}^{+3}$  ions prior to solvent extraction [209]. This extra process usually leads to extra cost using O-donor based ligands. Because of such disadvantages, the uses of O-bearing ligands in solvent extraction is usually restricted to a few metal ions.

There are however certain oxygen-donor (O-donor) based ligands that have found successful use in the commercial base metals extraction processes. Example of these ligands include the oxime ligands such as hydroxyoximes, carboxylic acids [178] in the form of versatic acids [210], and the phosphoric acids [211] and their respective derivatives in the form of di-2-ethylhexylphosphoric acids (D2EHPA) [209] as shown in Figure 7.1. These ligands have therefore found use in solvent extraction processes and have wide ranging extraction ability brought about by the various modifications these ligands can have as shown in Figure 7.1. While these ligands offer various advantages they still have numerous disadvantages brought about by the characteristics of the above-mentioned O donor atom such as the inability to reject  $\text{Ca}^{2+}$  for phosphate based extractant and being poisoned by  $\text{Fe}^{3+}$ . However, studies of the Schiff based hydroxyoxime extractants which have been successfully used in copper extraction show that these types of ligands can be used for base metal extraction.

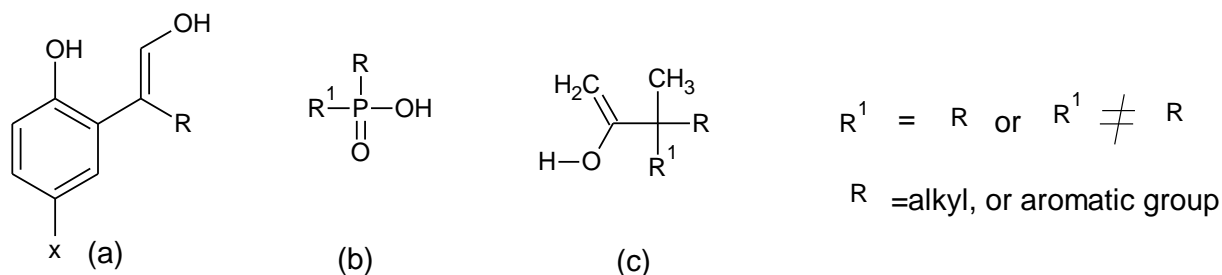


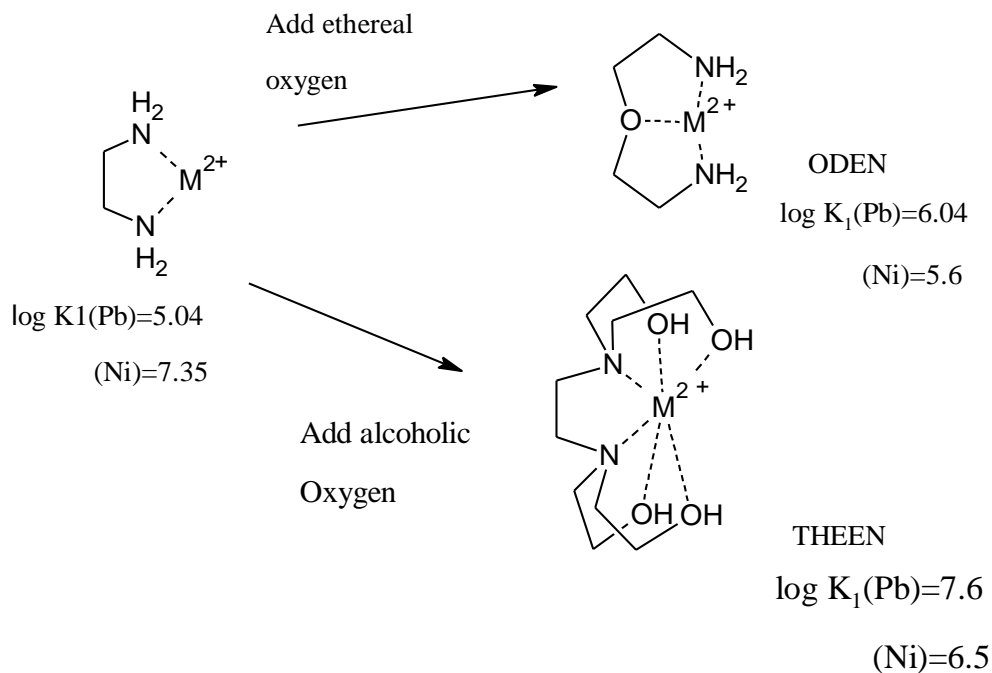
Figure 7. 1 The chemical structures of the O-donor extractants with (a) as hydroxyoximes (LIX reagents), (b) the phosphoric acid derivatives (CYNEX reagents)[209] and (c) the carboxylic acids (Versatic acids)

From studies aimed at improving on the properties and the ability of the O-donor ligands such as in the *oligo salen* type of ligands which was discussed in detail in Chapter 3. The discussion centred on the various modifications that can be made to the O-donor ligands to enable this hard donor group to be successfully incorporated in the design of extractants. The ability of the O-donor atom will therefore be discussed as follows.

### 7.1.2 Coordination of the oxygen donor group

The study of coordination of the O-donor group in Schiff base ligands has its precedence from studies of the analogous unidentate O-ion, which is the OH-(hydroxide) ion. The hydroxyl ion is classified as hard, based on the HSAB classification therefore has preference to coordinate to the hard metals such as alkaline and alkaline earth metals [29]. However due to the presence of electron donating or withdrawing groups such as organic alkyl groups, or electronegative donor groups the hardness character can inductively be adjusted in a systematic way to allow this hard donor group to coordinate to softer metals such as in the hydroxime ligands [29].

There are various studies that have been done to examine the chelating ability of the O-donor group. The simplest known neutral unidentate O-bearing ligand is H<sub>2</sub>O [29]. The preliminary studies of this system have shown that there is increased basicity on the neutral oxygen atom due to the addition of the alkyl groups such as H<sub>2</sub>O < MeOH < Me<sub>2</sub>O. The methyl group (Me) has very limited inductive effect. It is also sterically hindered and does not disperse charge easily. It therefore cannot be used as a basis to investigate coordination to different metal ions. However, the O-ligand systems with larger alkyl groups or aromatic groups containing additional functional groups or more O-donor groups (Figure 7.2) have been known to coordinate to larger metal ions as shown by Scheme 7.1.



Scheme 7. 1 Effect of adding O-donor atom in the system for ODEN and THEEN molecules. The log K<sub>1</sub> value indicates the complex stability. Redrawn courtesy of Arthur E. Martell et al.[29]

The addition of the neutral O-donor atoms to such organic systems shows increased stability for complexes formed by large metal ions. This therefore implies that increasing the O-donor atom will lead to selectivity of larger metal ions over smaller metal ions. This selectivity can be attributed to two important reasons, the first is due to the chelate effect; larger atoms having higher coordination numbers than the smaller atoms [29].

The second reason can be attributed to the inductive effect caused by the addition of the alkyl groups which is known to be very minimal. In principle this inductive effect is not much higher than that of water [29]. For this reason, the main contributing factor is the added donor. For this reason the aim of this study is to therefore study the solvent extraction of the O- bearing salen type ligands and the effect of adding O-donor groups to the solvent extraction of these selected metal ions.

## 7.2 Chapter objective

The objective for this chapter is to use the ligands synthesized in Chapter 3 for solvent extraction studies. The focus will be on the effect of the various substituents and donor groups towards selectivity and extraction. All ten (10) ligands used in this chapter have been fully characterized as discussed in Chapter 3 and are shown below.

## Class D ligands

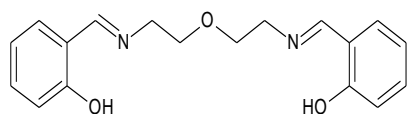
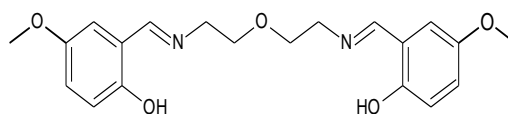
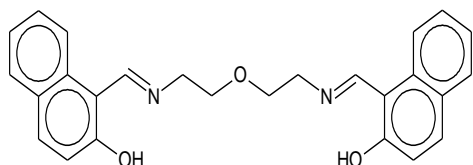
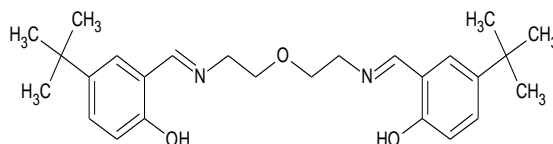
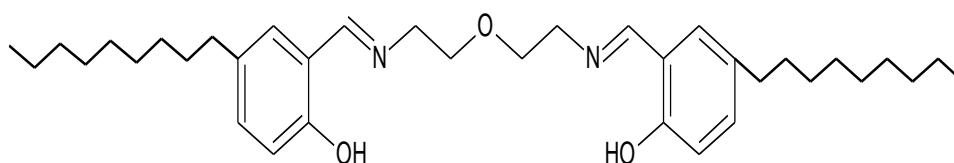
**L16****L17****L18****L19****L20**

Figure 7. 1 The pentadentate salen type ligands bearing the O-donor group class as D ligands

## Class E ligands.

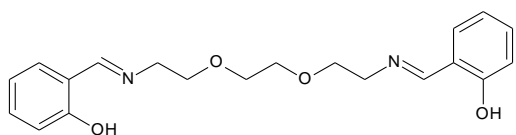
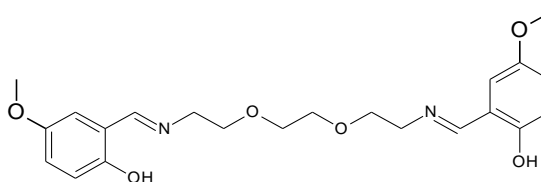
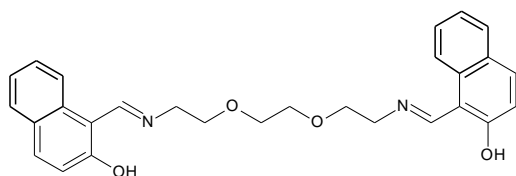
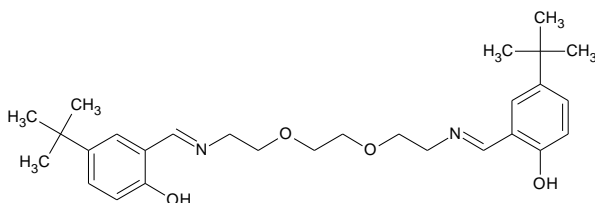
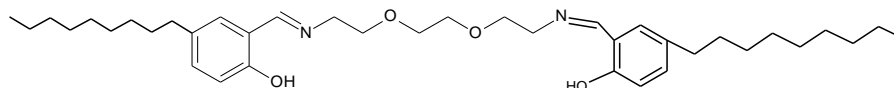
**L21****L22****L23****L24****L25**

Figure 7. 2 The hexadentate salen type ligands bearing O-donor ligands as class E ligands.

## 7.3 Competitive solvent extraction studies

The competitive solvent extraction study was carried out using the method described in Chapter 5.4.2. 10 ml of 0.01 M solution of the ligand in aqueous chloroform was measured into a

sample vial. 10 ml of the 0.01 M metal mix solution at pH 4.98 containing the 6 different divalent metals ions ( $\text{Cd}^{2+}$ ,  $\text{Co}^{2+}$ ,  $\text{Cu}^{2+}$ ,  $\text{Ni}^{2+}$ ,  $\text{Pb}^{2+}$  and  $\text{Zn}^{2+}$ ) was then transferred into the same vial to form two immiscible layers. The ligands used are shown in Figure 7.2 and 7.3

#### 7.4 Extraction results for pentadentate system L16-L20

The extraction results were obtained from the ICP-OES and calculated as previously discussed in chapter 5 equation 5.1. These values were then represented in Figure 7.4 below.

##### 7.4.1 Discussion of results from class D ligands

The results from the ICP show that these ligands show exceptional extraction of  $\text{Cu}^{2+}$  ion. They have high extraction with higher selectivity for the  $\text{Cu}^{2+}$  ions. This high extraction and selectivity can be attributed to stability of the  $\text{Cu}^{2+}$  complex as shown by the Irving-Williams [75] series. This indicates that  $\text{Cu}^{2+}$  will form much more stable complexes than the other divalent base metal ions. This indicates that  $\text{Cu}^{2+}$  will be extracted over the other metal ions.

The results also indicate that the ligand **L16** with unsubstituted phenyl ring bearing the salicylaldehyde group had the highest extraction. The general trend for the extraction of these ligands is given as *salicylaldehyde* > *naphthylaldehyde* > *5-methoxy aldehyde* > *5-nonylsalicylaldehyde* > *5 tert-butyl-salicyaldehyde*. The results obtained are consistent with previous work on the study of the 5-tert butyl ligand by Saban *et al* [71] who showed very low extraction of the *tert-butyl* ligand. The work by Turkington *et al* [27] who used different substituents and hydroxime ligands showed that by using a coherent series of salicylaldoxime ligands, that extractant strength varies in the order  $\text{X} = \text{Br} > \text{NO}_2 > \text{Cl} > \text{OMe} > \text{H} > \text{tBu}$ , with  $\text{pH}_{1/2}$  values indicating that the distribution coefficients for copper extraction for the tBu and Br substituted reagents differ by more than two orders of magnitude.

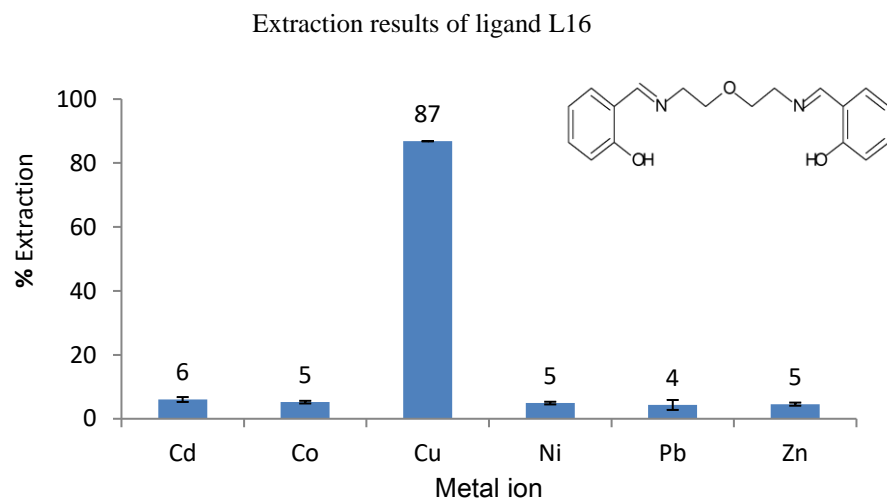


Figure 7.4 (a): Graphical representation of extraction results for ligand **L16**.

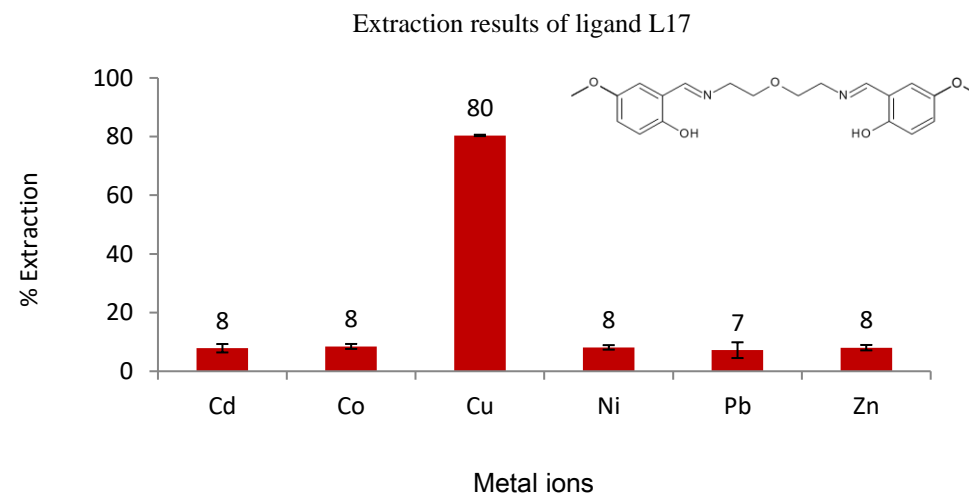


Figure 7.4 (b): Graphical representation of extraction results for ligand **L17**.

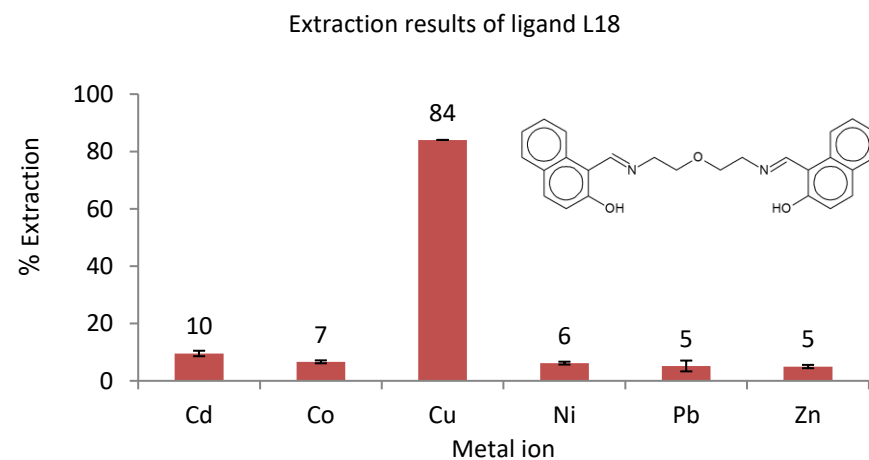


Figure 7.4 (c): Graphical representation of extraction results for ligand **L18**.

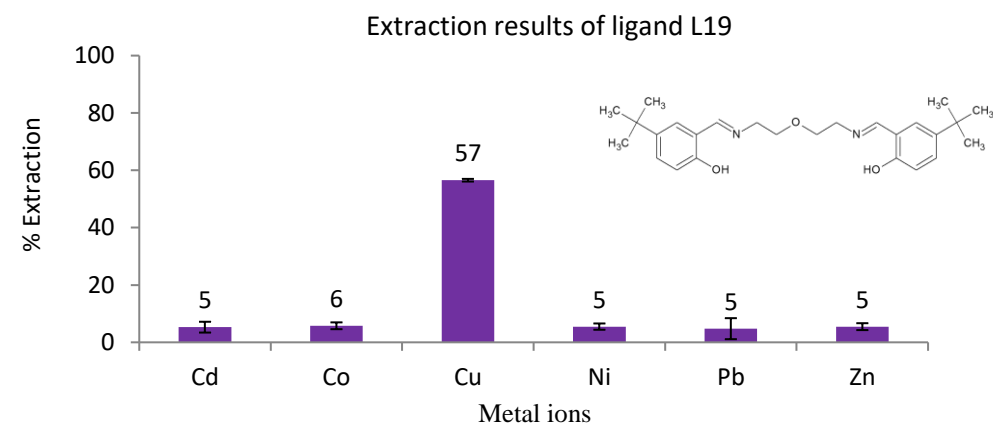


Figure 7.4 (d): Graphical representation of extraction results for ligand **L19**.

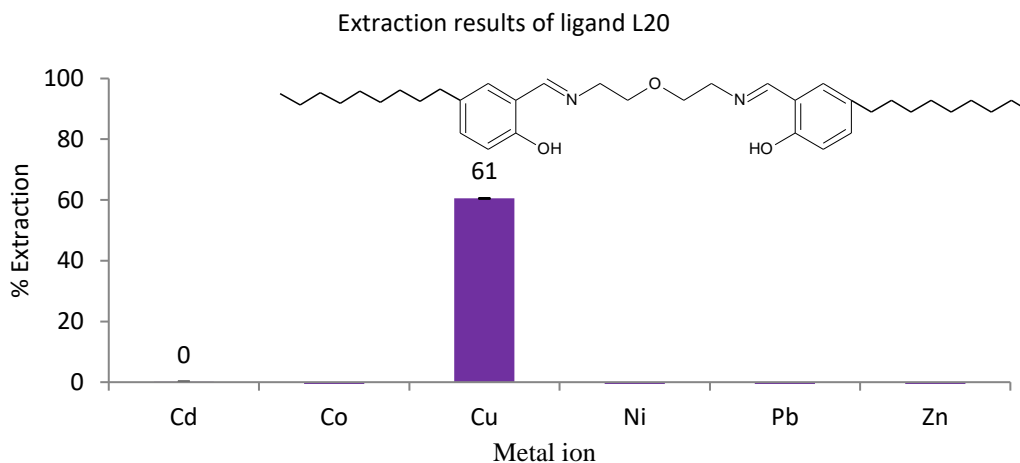


Figure 7. 4 (e) Graphical representation of extraction results for Ligand **L20**

The results obtained also show that lower molecular weight substituents co-extracts other metal ions as shown by ligand **L18** showing 10 % extraction of  $\text{Cd}^{2+}$  ions (Figure 7.4c), on the other hand higher molecular weight ligand **L20** does not show any co-extraction (Figure 7.4e). These results were quite unexpected due to the previous results obtained from the study of the N-bearing salen ligands. The results had indicated that the higher molecular weight substituent containing the *nonyl* group had shown higher extraction of the  $\text{Cu}^{2+}$  ions over the other ligands in the same series. The highly saturated *nonyl* substituent had the effect of resisting leaching and therefore kept the ligand in the organic phase. But since these O-donor group ligands did not show any leaching effect the effective presence of the *-nonyl* group to keep the ligand in the organic phase is therefore reduced and therefore it's effective inductive effect to coordination of the  $\text{Cu}^{2+}$  in solution comes into consideration. From further study of the above results, the bulkier *tert-butyl* group was observed to have lower % extraction than the *nonyl* group, since both the *nonyl* and the *tert-butyl* group are electron donating groups to the phenyl ring. It is therefore possible to postulate that the difference in the order of extraction is due to the mode of coordination of these ligands with the sterically hindered *tert-butyl* group offering higher steric resistance to the coordination of the  $\text{Cu}^{2+}$  ions than the longer *nonyl* group in the ligands system, which can be shown by the following discussion on the coordination of the O-donor ligands which is discussed below.

#### 7.4.2 Coordination structure in relation to extraction

Based on our coordination geometry studies in Chapter 4 where three crystal structures of **L17-Cu**, **L18-Cu** and **L19-Cu-Pb** were obtained as shown below in Figure 7.5, 7.6 and 7.7 respectively.

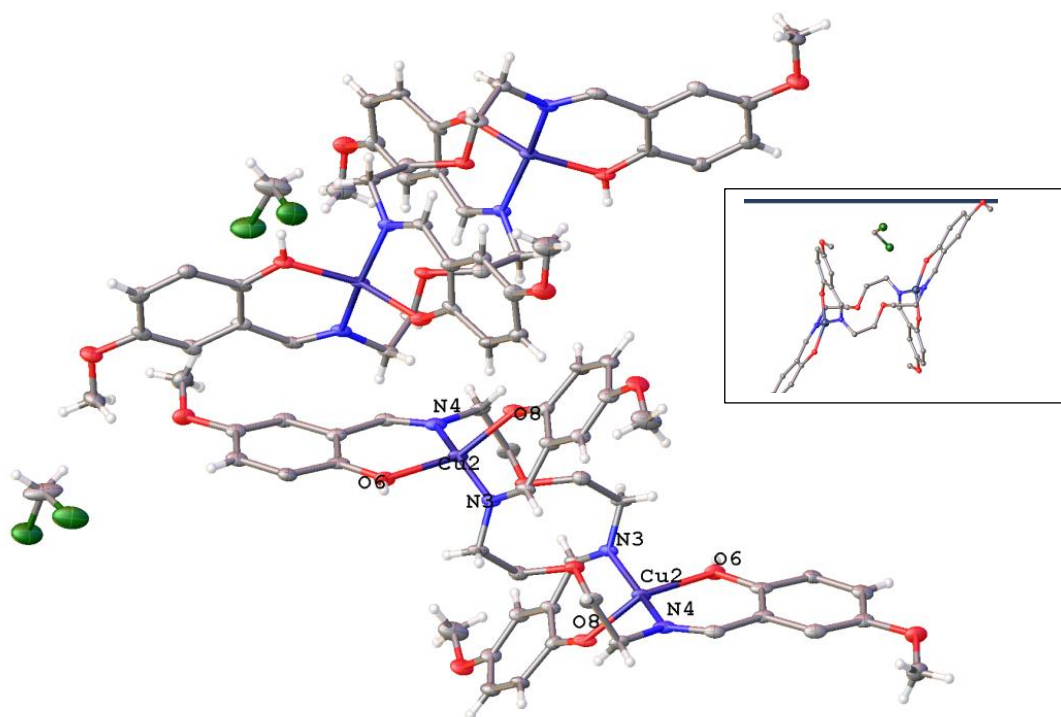


Figure 7. 3 Ortep diagram of ligand **L17-Cu** complex with DCM solvate, ellipsoids drawn at 50% probability, (insert shows one of the asymmetric units)

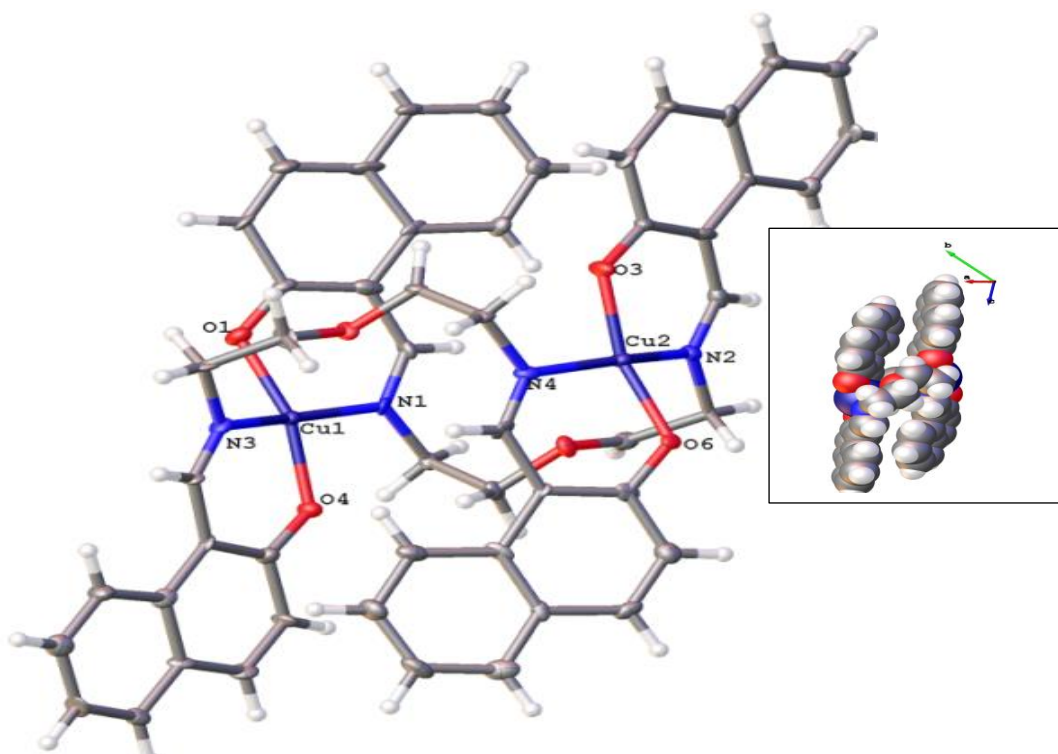


Figure 7. 4 Ortep diagram of ligand **L18-Cu** complex, ellipsoids drawn at 50% probability, insert shows the space filled model indicating existence of channels caused by resistance between the electron clouds of the naphthyl groups

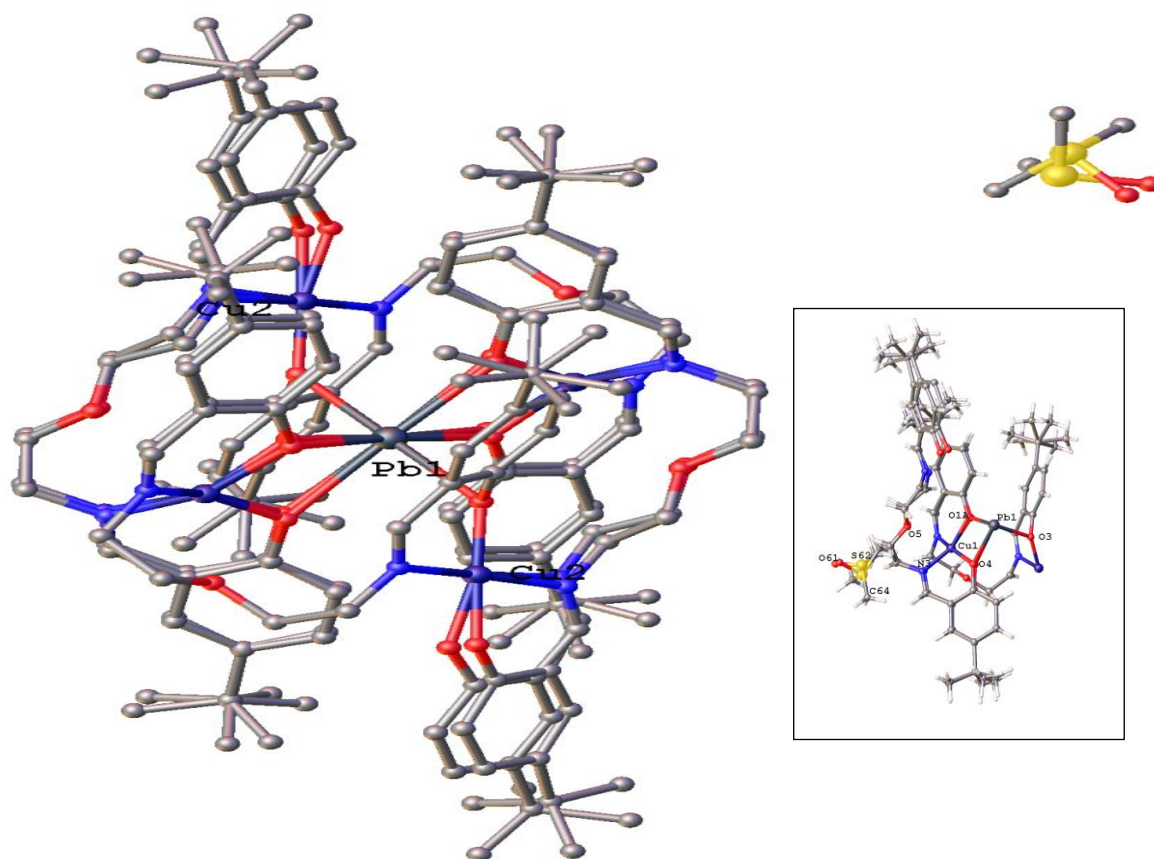


Figure 7. 5 Ortep diagram of **L19-CuPb** complex showing the octahedral coordinated  $\text{Pb}^{2+}$  centre surrounded by 4 planar copper complexes and monosolvate DMSO. H-atoms have been removed for picture clarity. (Insert shows the asymmetric unit with half of the molecule).

From these crystal structures obtained as discussed in Chapter 4, it can be observed that these ligands have a predisposition to coordinate to  $\text{Cu}^{2+}$  forming metallocycles. It is also observed that the introduction of the substituents on the phenyl ring allows for the solvate molecule to interact with the complex as shown in Figure 7.5 and Figure 7.7 with DCM and DMSO solvates respectively. This interaction with solvent molecules will therefore lead to reduction of extraction efficiency. This is what's observed for the different ligands in this class where the non-substituted ligands have better separation than the ligands with *para*-substituents.

### 7.5 Competitive solvent extraction of class E ligands

The hexadentate ligands bearing the two O-donor groups were also subjected to competitive solvent extraction studies. The set up for the extraction was similar to the procedure used in Chapter 2.4.2 and Chapter 7.3 above. The results were then obtained from the ICP and are shown in the representative graphs shown below.

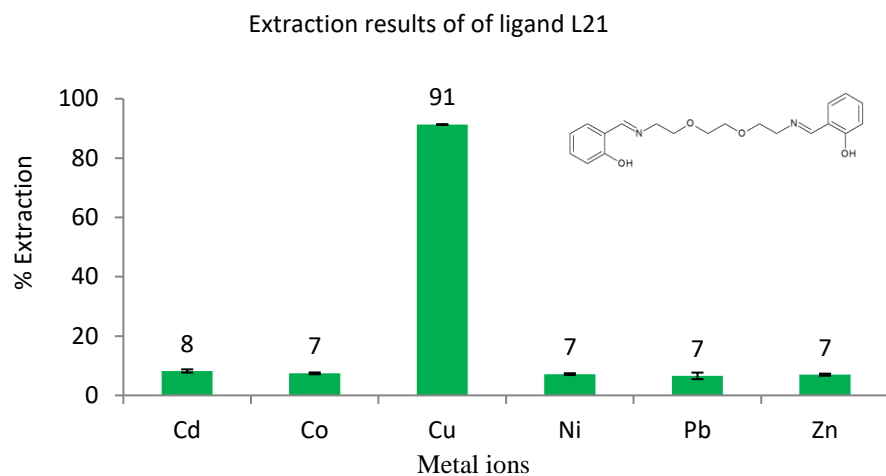


Figure 7.7 (a): Graphical representation of extraction results for Ligand **L21**.

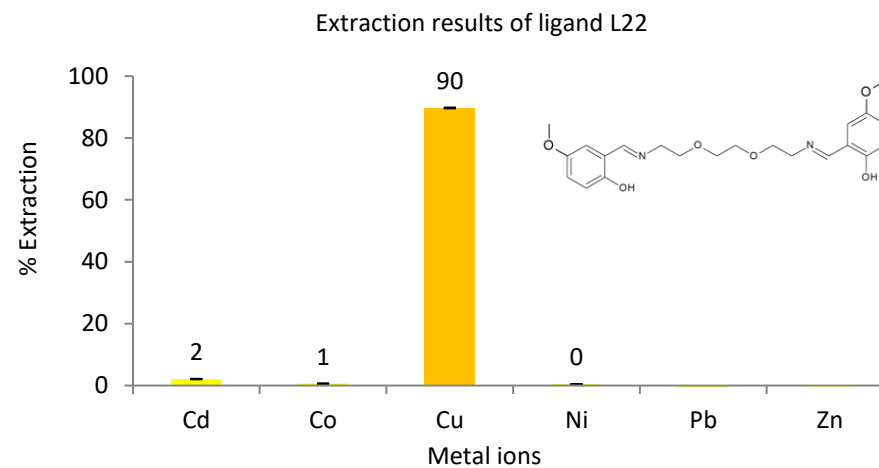


Figure 7.7 (b): Graphical representation of extraction results for Ligand **L22**.

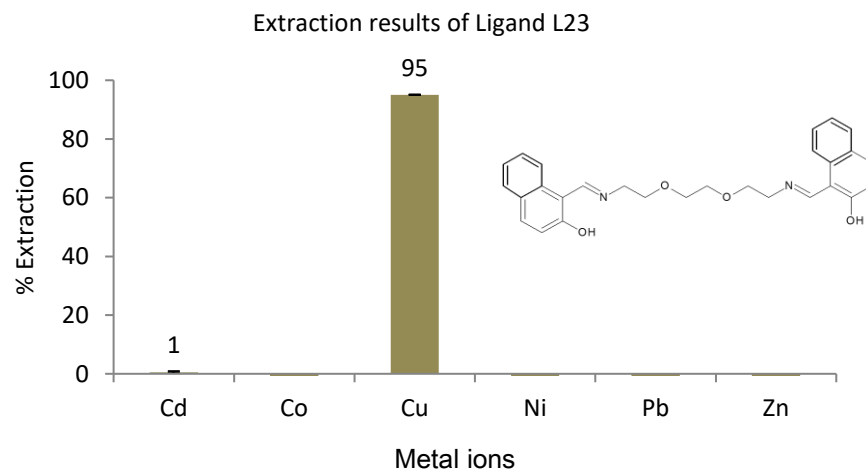


Figure 7.7 (c): Graphical representation of extraction results for Ligand **L23**.

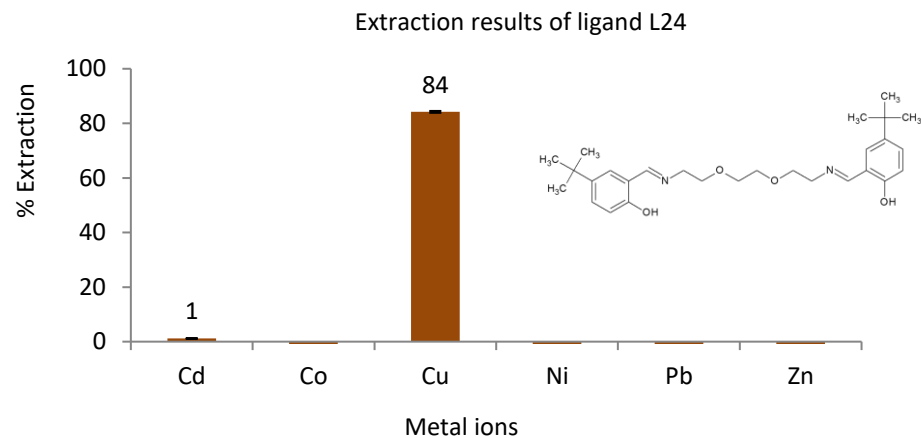


Figure 7.7 (d): Graphical representation of extraction results for Ligand **L24**.

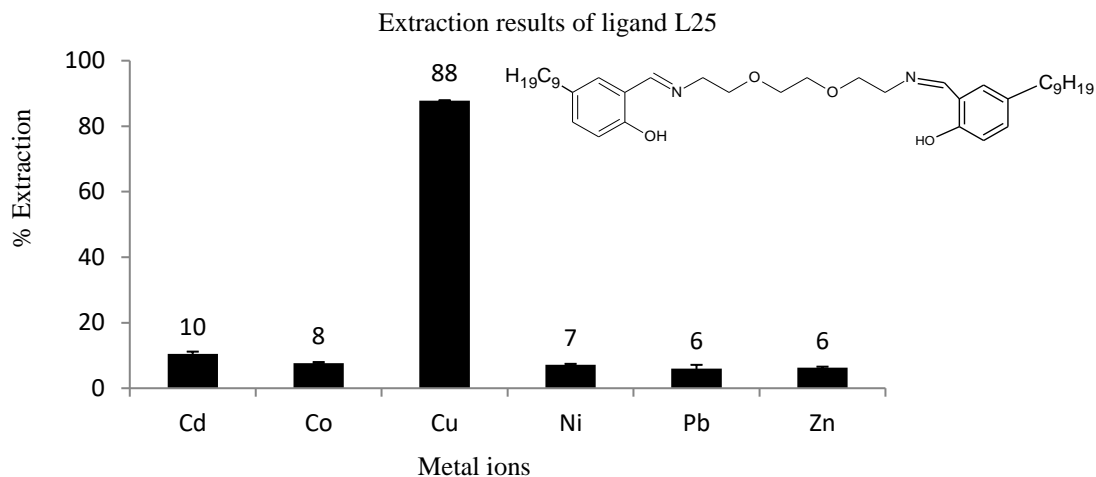


Figure 7. 6 Graphical representations of extraction results for ligand L25

### 7.5.1 Discussion of results from class E ligands

From the ICP results, it was confirmed that the ligands showed high selectivity and extraction towards  $\text{Cu}^{2+}$  ions as shown in Figure 7.7. This is in accordance with the stability of divalent metal ions as shown by the Irving-Williams series [75] as discussed for pentadentate ligand systems. The results also showed that the *tert-butyl* substituted phenyl ring had the lowest extraction which is consistent with the results obtained for the above pentadentate systems.

The order of extraction for this class E ligand series can therefore be given by the following order; naphthyl >salicylaldehyde >5-methoxysalicylaldehyde >5-nonylaldehyde>tert butyl aldehyde. In this ligand series crystal structures were not obtained. But since the extraction order for this system is relatively similar to those of the pentadentate system above, it is therefore possible to propose a similar coordination mode for these ligands to the copper ion. The general comparisons of the results of the competitive solvent extraction studies of the hexadentate system over the pentadentate system suggest similar behaviour with the hexadentate system extracting the  $\text{Cu}^{2+}$  ions slightly higher than the pentadentate system

### 7.6 Dilution studies

The high selectivity of these ligands towards copper means that the other metals are selectively not extracted in the presence of the  $\text{Cu}^{2+}$  ions. A selectivity studies test was therefore undertaken to determine if the ligands would extract another metal in the absence of the  $\text{Cu}^{2+}$  ions or in low concentration of  $\text{Cu}^{2+}$  ions achieved by dilution of the amount of the  $\text{Cu}^{2+}$  ions while the other metal ions concentration are kept constant. By undertaking this study an added

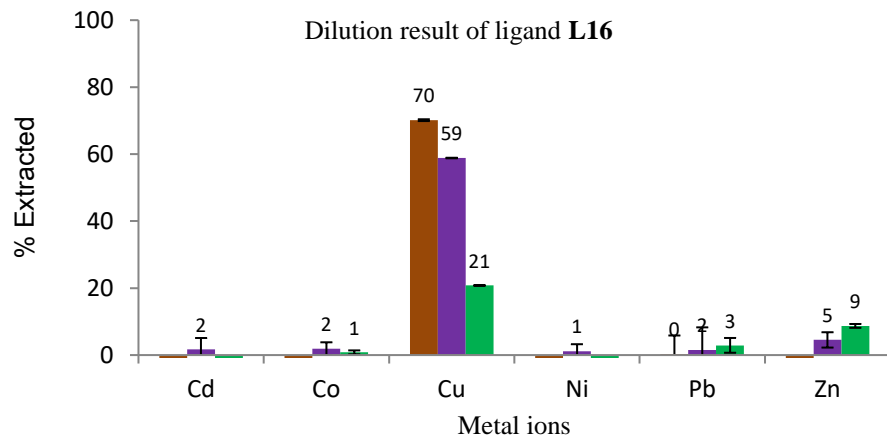


Figure 7.8 (a): Graphical representation of dilution studies of **L16**.

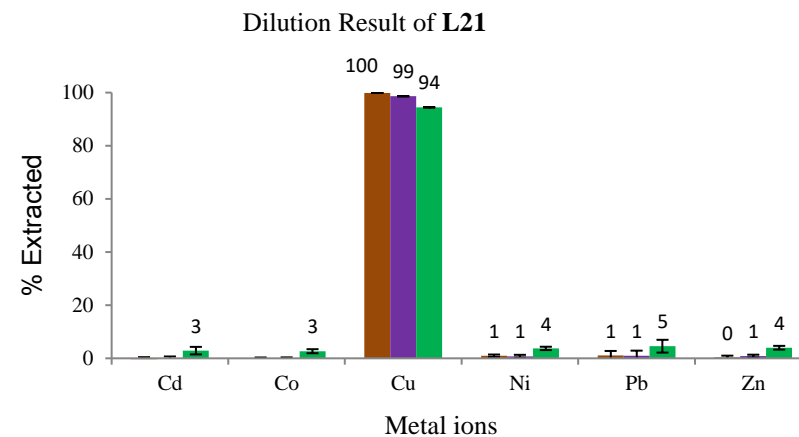


Figure 7.8 (b): Graphical representation of dilution studies of **L21**.

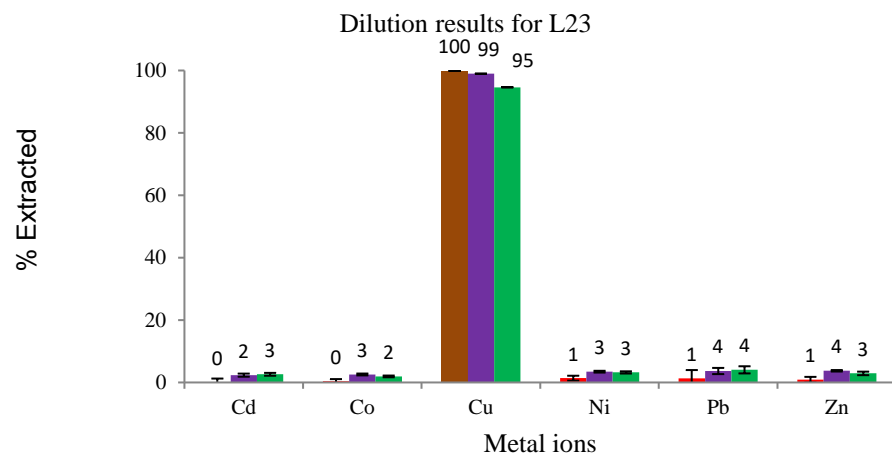


Figure 7. 7 Graphical representation of dilution studies of **L23**

Cu<sup>2+</sup> concentration to the ligands and other metals was reduced as showed in the keys

	1:1X10 <sup>-1</sup> Cu
	1:1 X 10 <sup>-2</sup> Cu
	1:1 X 10 <sup>-3</sup> Cu

-advantage is observed since the sensitivity (dilution limit) of the ligands to the  $\text{Cu}^{2+}$  ion in the competitive basis is achieved.

### 7.6.1 Procedure

The dilution studies were therefore carried out by varying  $\text{Cu}^{2+}$  ions concentration at pH 5 based on the experimental method in section 5.2. The  $\text{Cu}^{2+}$  ion concentration was reduced by a factor of 10 from  $10^{-1}$  M, to  $10^{-2}$  M and finally to  $10^{-3}$  M. Ligand **L16** and ligand **L23** were chosen to represent class D and class E respectively. These ligands were chosen on the basis of having the highest extraction in their class. A third ligand **L21** was also selected since it has a *salicylaldehyde* group similar to ligand **L16**, but it also has a hexadentate donor system which is similar to ligand **L23**. The results are discussed below.

### 7.6.2 Discussion on dilution studies

The results showed that even when the copper concentration is reduced 10-fold, 100 fold and 1000 times, the ligands preference for the  $\text{Cu}^{2+}$  ions is still very high. In the absence of the  $\text{Cu}^{2+}$  ions, the ligands have very low extraction which are within the experimental error range for no extraction of the other metals. The results show that these ligands are specifically designed to extract the  $\text{Cu}^{2+}$  ions. The reasons for this can be attributed to various factors including the chelate effect and the extraction pH which will be discussed in the subsequent section. It is however observed that for ligand **L16** with the salicylaldehyde group, the reduced amount of copper leads to reduction in extraction % of  $\text{Cu}^{2+}$ . Based on this result it is postulated that the reduction in  $\text{Cu}^{2+}$  concentration leads to excess ligands, therefore the obtained mode of coordination of the ligand has to change in the system leading to the reduction of the %  $\text{Cu}^{2+}$  extracted. It is also observed that in this particular ligand,  $\text{Zn}^{2+}$  ion is also extracted at 9 % at copper concentration of  $10^{-3}$  M as shown in the graphical representation in Figure 7.9 (a). The order of competitive metal extraction in this ligand is consistent with the Irving-Williams series [75].

### 7.7 pH studies

These ligands did not show any leaching hence the effect of pH on the extraction of these ligands was therefore studied. The purpose of this study is to determine selectivity of these ligands at different pH as well as the determination of the resistance of these ligands to the hydrolysis effect. This study is therefore based on the principle that metals such as  $\text{Ni}^{2+}$  and  $\text{Co}^{2+}$  are known to form stable complexes under relatively lower pH than  $\text{Cu}^{2+}$ . Two ligands

were therefore selected for this study: ligand **L23** due to its high extraction and ligand **L25** due to its ability to resist leaching. The results are therefore shown in Figure 7.9 and 7.10.

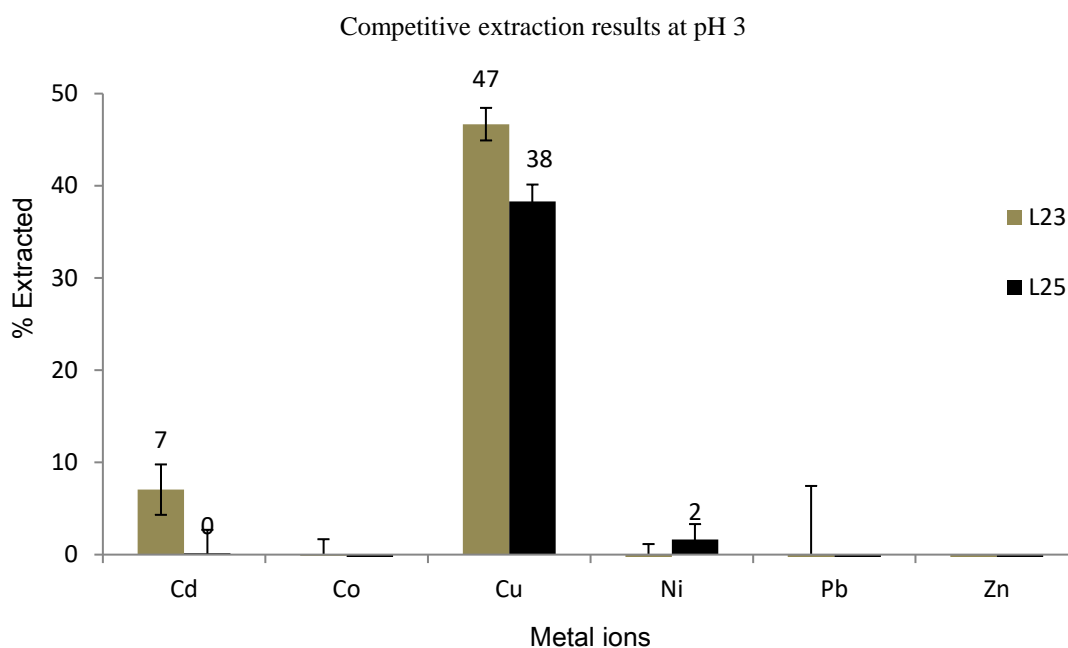


Figure 7. 8 Graphical representations of competitive solvent extraction for ligand **L23** and **L25** pH 3.

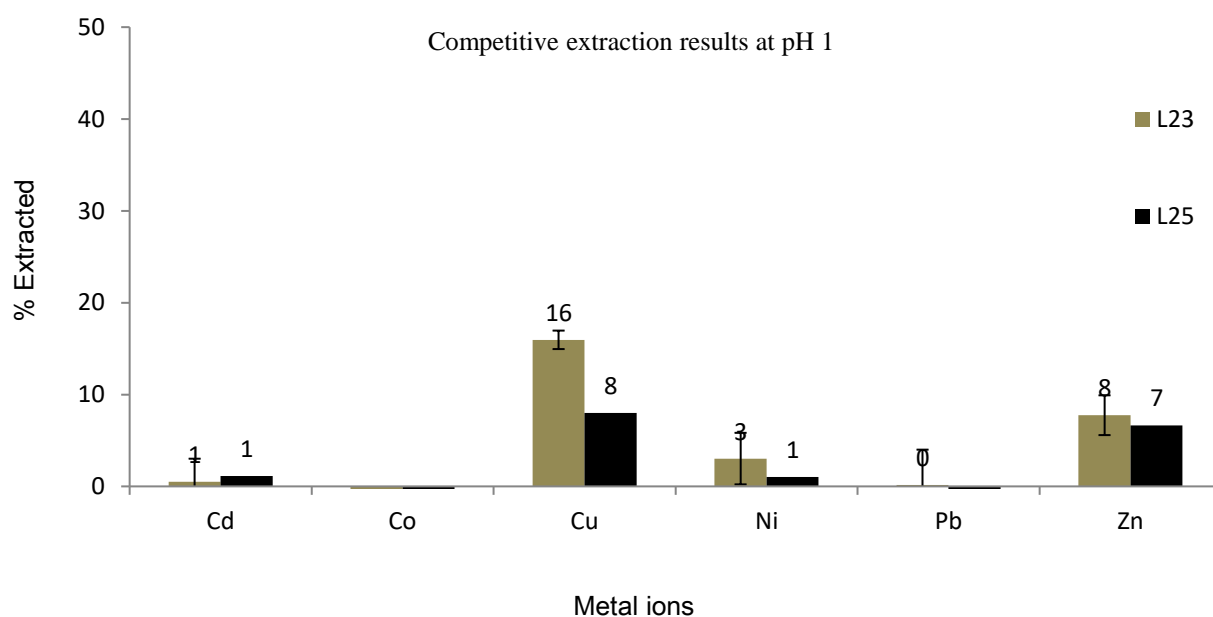


Figure 7. 9 Graphical representations of competitive solvent extraction for ligand **L23** and **L25** at pH 1

The results obtained from competitive extraction at different pH can therefore be discussed as follows. The first observation is that at different pH levels, there is extraction of  $\text{Cu}^{2+}$  with

another metal ion. For pH 3 it is observed that  $\text{Cd}^{2+}$  ions are co-extracted with the  $\text{Cu}^{2+}$  ions while at pH 1  $\text{Zn}^{2+}$  ions are extracted with  $\text{Cu}^{2+}$  ions.

The second observation from these studies show that the lowering of pH (pH 1 and pH 3) leads to reduction of extraction ability. It is observed that extraction of  $\text{Cu}^{2+}$  is much reduced at both the pH's. For pH 3 there is reduction of about 50 % for both of these ligands (**L23**, 48 % reduction, **L25**, 50 % reduction), while at pH 1 there is 80 % reduction for both of these ligands. This reduction in extraction potential was expected due to the high acidic nature of the solution. This reduction can therefore be attributed to two factors. The first is the reduced deprotonation ability of the ligand and the second is due to the hydrolysis of the imine peak of the ligand.

### 7.7.1 pH isotherms in extraction

The pH isotherms are a graphical representation showing the % metal ion extracted vs the pH as shown in Figure 7.11. The isotherms therefore shows the “strengths” of the extractants which can be compared by recording the pH values at which they are 50% loaded with metal (the “ $\text{pH}_{1/2}$  values”)[7].

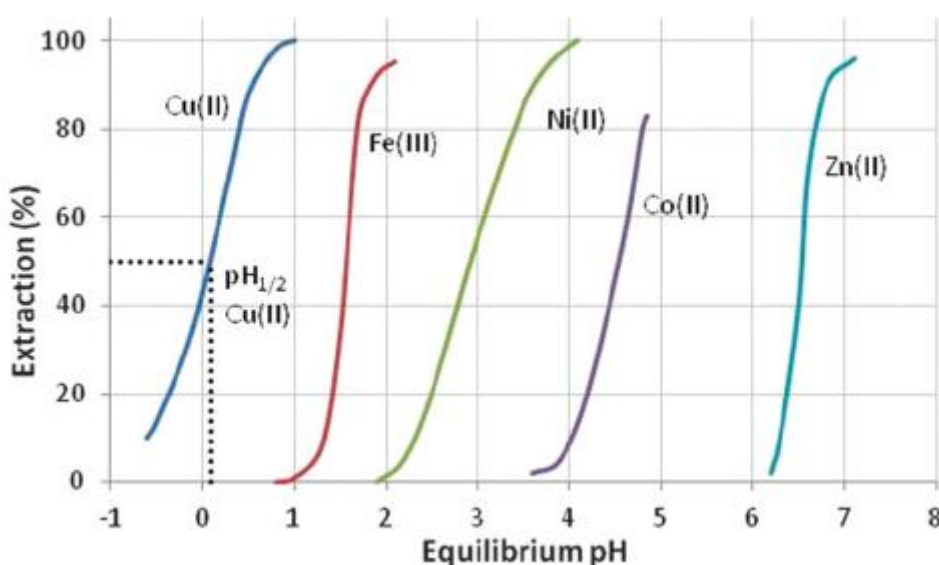


Figure 7. 10 pH isotherm of 5 metal ions for ArcogaP50 commercial extractant courtesy of Wilson et al[7].

From this isotherm a strong extractant for metal cations have low  $\text{pH}_{1/2}$  values, indicating that they are capable of recovering metals from highly acidic feed solutions. Conversely, a weak extractant for metal cations is only capable of recovering metals at high pH. Since all the ligands have a higher tendency to extract  $\text{Cu}^{2+}$  ions, the pH isotherm studies were obtained for  $\text{Cu}^{2+}$  ions at different pH for only three ligands that showed the highest % extraction, ligands

**L23, L24** and **L25**. The results obtained are shown in the graphical representation in Figure 7.12.

### 7.7.1.2 Discussion of pH isotherms

The results obtained showed that the different ligands have different extraction % at different pH. The ligand **L23** showed the highest extraction at pH less than 5 while the other ligands showed extraction of 100 % at higher pH. From this result it shows that the increase of the organic nature as substituent on the ligands pushes the equilibration point for the extraction to lower pH (increases stability in low pH).

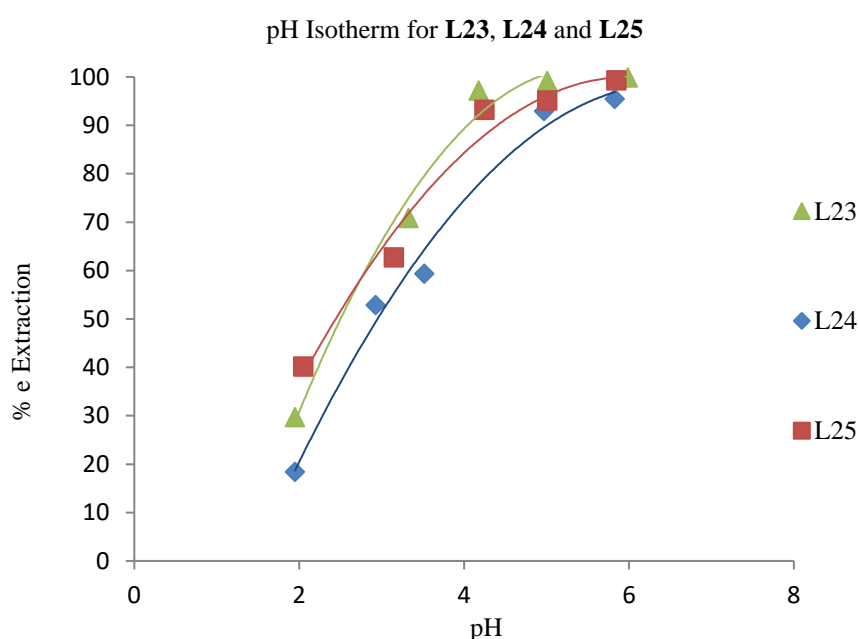


Figure 7. 11 Graphical representation of the pH isotherms for the extraction of  $\text{Cu}^{2+}$  ions under different pH (x scale in logarithmic).

## 7.8 Competitive bulk liquid transport studies

The bulk liquid transport studies for selected ligands was therefore carried out following the procedure as outlined in Chapter 5.9.4. The aim is to determine transport through the bulk liquid membrane. This study has the desired advantage of studying both the extracting capacity of the ligand and its ability to release the cation in a liquid solution of lower pH in one set up. The driving force for this process is the pH difference.

### 7.8.1 Experimental set up for transport studies for the O-donor ligands

The experimental was carried out with the Schiff base bearing the O-donor ligands as per the procedure outlined in Chapter 5.9.2. All the reagents and instrumentation used were similar to those used in Chapter 5.9.1. The experiment was carried out in a thermostated water bath at 25°C and the results are reported as follows.

### 7.8.2 Results and discussion

The following results in Figure 7.14 (a) and Figure 7.14 (b) were obtained for transport of ligand **L23** and ligand **L24**. Ligand **L23** was chosen because of its high extraction % in competitive basis while ligand **L24** was chosen as an analogous ligand in the same series with lower extraction %. The ligand **L24** was also chosen on the basis of transport results of the N-donor ligands that had shown that ligands with low extraction form good transport ligands.

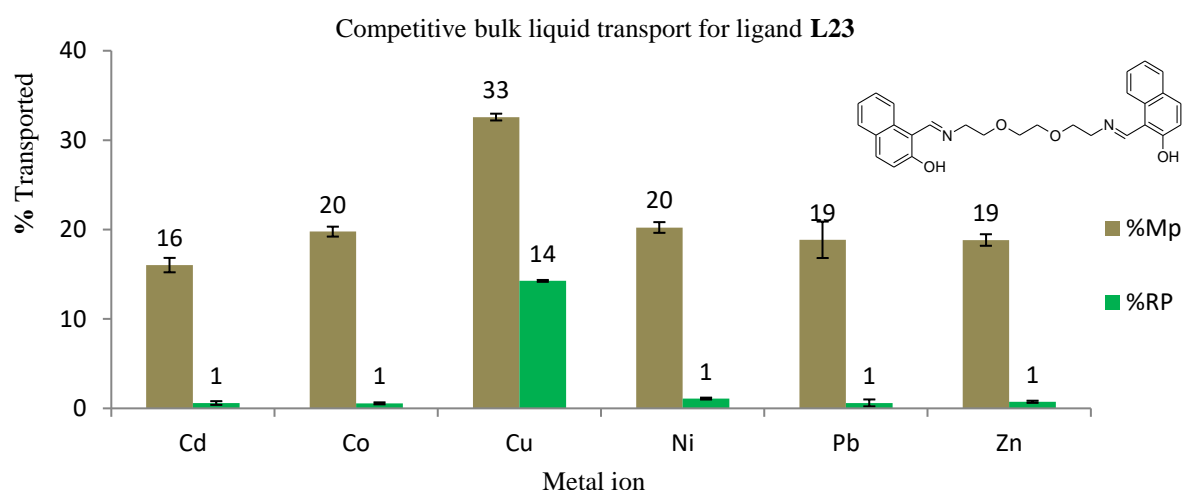


Figure 7. 12 Graphical representation of bulk liquid transport for ligand **L23**

Note %MP is equal to the control minus source phase after extraction, while the % RP is the % transported into the receiving phase.

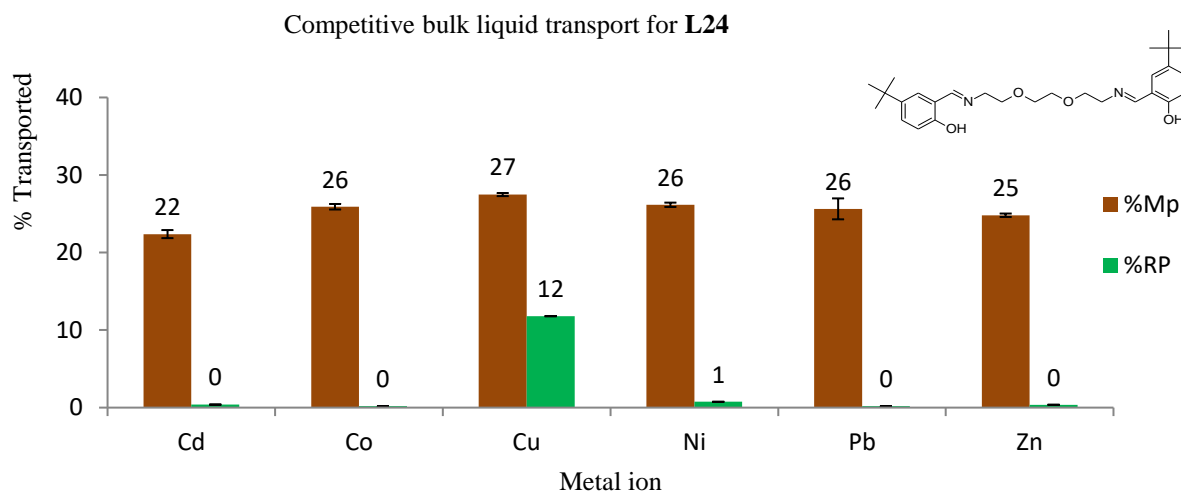


Figure 7. 13 Graphical representation of the transport results for ligand **L24** for selected base metal ions (Mp is equal to the control minus source phase after extraction, while the % RP is the % transported into the receiving phase).

### 7.8.3 Discussion of transport results

For an ion carrier to accomplish active transport (transport against the concentration gradient) across the different interfaces (interfaces between an aqueous source phase and the membrane phase and that between the aqueous receiving phase and the bulk liquid membrane phase), the ligand needs to have a high ion-binding ability at the source phase/membrane interface and a low ion-binding ability at the membrane/receiving phase interface. Meeting this contradictory requirement is often a challenge and requires an ion carrier (extractant) with a switching mechanism [212, 213]. Ligands **L23** had the highest extraction of  $\text{Cu}^{2+}$  ions in competitive basis. In the transport set up the metal ion has to diffuse from the source phase to the receiving phase. It is therefore observed that almost 1/3 (33 %) of the  $\text{Cu}^{2+}$  ions diffused through the membrane interface to the organic phase as shown by Figure 7.14, from this only 14 % of the  $\text{Cu}^{2+}$  ions are then diffused into the lower pH receiving phase. For ligand **L24** (*tert butyl* substituent) which initially extracted very minimal  $\text{Cu}^{2+}$  ion, in this case it diffuses an amount also closer to 1/3 (27 %) to the membrane phase and releases about 12 % into the receiving phase as shown by Figure 7.15.

From the above results the other metal ions are also relatively highly extracted to the membrane phase as shown by the high %MP. It is however, also observed that very little percentage of these metal ions are released to the receiving phase (low % RP). These results show that the  $\text{Cu}^{2+}$  ions are relatively easily released when they come in contact with the aqueous receiving

phase at lower pH. On the other hand, the other metal ions also in the membrane phase are quite resistance to release from the organic phase. This is due to their inability to be released into the receiving phase at lower pH. This result therefore seems to contradict the Irving-Williams series [75] since the  $\text{Cu}^{2+}$  ion forms much more stable complexes over the other metal ions. This contradiction is therefore explained by the transport mechanism discussed below.

### 7.8.3.1 Mechanism of transport

The transport process occurs when the ligand is deprotonated and diffuses to the source phase-membrane phase interface where it is deprotonated by the higher pH (pH 4.98). This allows the ligand to coordinate to the metal ions and diffuse back to the bulk of the membrane phase. Due to the agitation by stirring of the bulk organic phase the formed complex is diffused to the receiving phase-organic phase interface where the ligand is re-protonated and releases the metal ions into the receiving phase. The metal ion will then diffuse to the bulk of the receiving phase while the re-protonated ligand will diffuse back to the bulk organic phase and the process repeated over and over in the 24-hour cycle. Therefore the high transport of the other metal ions into the membrane phase/organic phase occurs due to the presence of the bulk membrane barrier created at the interface of the lipophilic organic solvent and the aqueous source phase/this barrier reduces the contact between the  $\text{Cu}^{2+}$  ions and the ligand since all the metal ions will equally have the same chance to diffuse to this interface, the protonated ligand will therefore have the ability to equally coordinate to any of these metal ions at the interface. The observed result therefore shows that at the receiving phase, phase-organic interface these ligands do not easily release the other divalent metal ions as easily as they do the  $\text{Cu}^{2+}$  ions. Therefore the  $\text{Cu}^{2+}$  ions are released to the receiving phase to a large extent than the other metal ions. The contradiction to the Irving-Williams series that gives the order of formation due to stability of the complex is therefore observed in this sense. However, this stability is restricted to metal ions and not to the ligands and therefore different ligands will have different stability with different metal ions as observed for this class of ligands.

## 7.9 Summary and conclusion

Ten different ligands containing O-donor groups were subjected to competitive solvent extraction for the selected base metal ions. The ligands did not show any leaching effect. The *pentadenate* ligands were observed to have excellent selectivity of  $\text{Cu}^{2+}$  over the other 5 other metal ions, this was in accordance with Irving-Williams series [75].

The much bulkier organic ligands were observed to have lower extraction than the unsubstituted phenyl-based groups. For the pentadentate ligands the unsubstituted **L16** was observed to show the greatest extraction of  $\text{Cu}^{2+}$ . For the hexadentate class E ligands the *naphthyl* based ligand **L23** was observed to have the highest extraction followed by the unsubstituted salicylaldehyde based group.

The lowering of the pH was also observed to have an influence in the competitive extraction of the ligands with reduction of over 60 % at pH 3 and 80 % for pH 1. The ligands were also observed to be highly selective towards  $\text{Cu}^{2+}$  ions even when the  $\text{Cu}^{2+}$  was reduced. For Ligand **L16**  $\text{Zn}^{2+}$  was co-extracted at 5 % in very low  $\text{Cu}^{2+}$  concentration of  $10^{-3}$  M and also at no copper concentration. The results from competitive transport studies also shows high transport of the  $\text{Cu}^{2+}$  ions. The pH isotherms were also carried out showing the ability of these ligands to extract various proportions of  $\text{Cu}^{2+}$  at different pH.

# CHAPTER 8

---

## GENERAL DISCUSSION, CONCLUSION AND REFERENCES

---

## 8:1 Summary

The aim of this dissertation was to study the Schiff base ligands in the hydrometallurgical solvent extraction process. The work started with the synthesis of two meta-substituted *salicylaldehydes* containing the *5-tert-butyl* and *5-nonyl-salicylaldehyde*. These two aldehydes were therefore obtained in good yield at 72 % and 84 % respectively. Three more aldehydes containing *5-methoxy* aldehyde, unsubstituted *salicylaldehyde* and *naphthylaldehyde* were purchased to have five aldehydes that were used for the synthesis of the various salen type ligands.

Schiff base ligands were therefore synthesized by the condensation method using five different diamines and the five aldehydes mentioned above to obtain a series of *bis-imine* Schiff base ligands. Because the diamine used contains various donor groups and different alkyl groups between the amine in their structures the *bis amine* was therefore used to classify these ligands into five classes.

The five classes of ligands were further divided according to which donor group is in the spacer of the *bis imine*. The different donor groups were the N-donor ligands and the O-donor ligands. The N-donor based ligands were divided into three; the *pentadentate* based N-(2-aminoethyl) ethane-1, 2-diamine which were classified as the class A ligands, the *pentadentate* N-(3-aminopropyl) propane-1,3-diamine which were classified as class B ligands or the propyl based salen type ligands, and finally the *heptadentate* N,N-bis(2-aminoethyl)ethane-1,2-diamine which were classified as class C or the *tripodal* ligands.

For the O-donor containing ligands, 2,2 aminoethoxy)ethylamine and 2,2-[ethane-1,2-dibis(oxy)diethanamine were used to synthesise the *pentadentate* O-donor ligands class D and the *hexadentate* class E ligands respectively. All the synthesized ligands were therefore obtained in good yields and were fully characterized using different analytical techniques such as FT-IR, <sup>1</sup>H NMR, <sup>13</sup>C NMR, MS and CHN analysis.

From the electronic studies on the FT-IR and NMR (<sup>1</sup>H NMR and <sup>13</sup>C NMR) it was observed that the different substituents led to different electronic effects in the ligands. The results indicated that the addition of the substituent on the phenyl group has a much greater effect on the imine shift on both the IR and the NMR studies than the effect of adding the alkyl groups between the donor atoms. The inductive effect on these ligands was therefore observed to lead to stability of the phenyl group where the N-containing ligands with the *naphthyl* group **L8**

was observed to undergo thermal induced tautomerism. This was also observed for the O-donor group ligands with the *methoxy* containing *heptadentate* ligand showing light induced tautomerism. The tautomerism effect was accompanied by the colour change in both cases. However the tautomeric effect observed for the *heptadentate* ligand **L17** was more dramatic and was the first time being reported for these types of ligands. This colour change was observed through confocal microscope and solid state UV-Vis. The results from confocal microscopy study showed that this molecule was able to fluoresce in solid state by emitting radiation over a wide band gap from 503 nm to 650 nm.

From this class, three crystal structures of class D ligands were obtained showing that the ligands are symmetrical and bent toward the phenyl group of each molecule. This result confirmed the interaction results that were obtained earlier in the electronic study of this class of ligands indicating the equivalence of the  $^1\text{H}$  NMR.

From the synthesized ligands, a few selected ligands were therefore used for the coordination studies, ligands **L1**, **L4**, **L17**, and **L18** were used to synthesise various complexes whose crystal structures were also determined. These complexes were obtained showing different coordination geometry around the metal centre. The single crystal X-ray diffraction analysis showed that two ligands from class D, ligand **L17** and ligand **L18** containing the *methoxy* substituent and *naphthyl* group have a propensity to coordinate forming metallocycles with the  $\text{Cu}^{2+}$  metal. The geometry around the  $\text{Cu}^{2+}$  metal centre was shown to be distorted square planar geometry in both complexes. For the class A ligands with N-donor, ligand **L1** was obtained as an octahedral coordinated cobalt complex with DCM solvate whereas its analogous  $\text{Cu}^{2+}$  complex was obtained as a hydrolytic product with one of the imines hydrolyzed. The ligand **L4-Cu** was also obtained as a hydrolytic product both of these hydrolytic products had a trigonal pyramidal geometry around the  $\text{Cu}^{2+}$  metal centre. Finally, the bi-metallic **Pb-Cu** complex with the **L19** ligand was discussed. This complex consisted of four metallocycles coordinated to one  $\text{Pb}^{2+}$  centre with a distorted octahedral geometry around this Pb-metal centre.

From the coordination studies, seven ligands were studied for fluorescence in the presence of the base metals. The five class E ligands that had *hexadentate* O-donor groups were observed to fluoresce with the unsubstituted *naphthyl* and *salicylaldehyde* groups showing the highest fluorescence on the fluorimeter. The study of the effect of some commonly used solvent in the fluorescence of selected ligands was also studied. The results indicated that the different

solvents have different fluorescence. Methanol was observed to have the highest fluorescence, then DMF and finally acetonitrile. Upon addition of the metal ion analytes, the fluorescence was either enhanced or quenched. Ligands containing the N-donors were observed to have high sensitivity towards  $\text{Pb}^{2+}$  ions while the O-donor ligands observed to have enhanced sensitivity towards the  $\text{Zn}^{2+}$  ions.  $\text{Cu}^{2+}$  was observed to quench the fluorescence of all the ligands.

After all the synthesis and characterization of the various ligands these ligands were subsequently studied for competitive solvent extraction for the selected divalent metal ions. The results from the ICP-OES showed varied levels of extraction based on the different class of ligands that were available.

For the N-donor ligands class A ligands and class C ligands showed very disappointing results which were characterized by high levels of leaching. However, for each of these classes of ligand the *nonyl* containing substituent was able to withstand the high bleeding effect and was able to show high selectivity of  $\text{Cu}^{2+}$  ions. The selectivity of the  $\text{Cu}^{2+}$  ions was also observed for the class B ligands that showed partial bleeding for most of the ligands in this class. For this class of ligands, the *naphthyl* containing group showed the highest selectivity while ligand **L10** having the *nonyl* group showed the highest extraction of  $\text{Cu}^{2+}$  for all the N-donor ligands.

For the ligands with O-donor in the spacer ligands class D and class E the results obtained from the ICP-OES indicated that these ligands did not leach and all showed high selectivity of  $\text{Cu}^{2+}$ . Since the ligand bleeding was not a consideration in this class it was therefore shown that the nature of coordination has an influence on the ability of these ligands to extract the metal ions. The ligands with the unsubstituted phenyl group or using the *naphthyl* group were therefore observed to have higher extraction than the ligands that have a substituent.

For the ligands that were affected by bleeding, all were used together with selected synergists to study the synergist effects in the extraction of the divalent base metals ions. Three synergists, one containing a carboxylic functional group, one containing a sulfonic acid functional group and a benzyl sulfonic functional group, with different length of alkyl chain length, were used. The results indicate that the carboxylic acid based synergist had a tendency to increase selectivity of  $\text{Pb}^{2+}$  ions over the other divalent metal ions and the addition of the synergist leads to synergistic extraction of the  $\text{Pb}^{2+}$  ions over the  $\text{Cu}^{2+}$  ions for the ligands synthesized from the unsubstituted *salicylaldehyde* and *methoxy* substituents. For the ligand with the *naphthyl* and *tert-butyl* substituents these were observed to extract  $\text{Cu}^{2+}$  over the  $\text{Pb}^{2+}$ .

The synergist composed of the straight chain alkyl sulfonate was also observed to have a preference for  $\text{Pb}^{2+}$  over the  $\text{Cu}^{2+}$ , however in the presence of the ligands the synergistic preference was for both the metal ions.

For the benzy sulfonate synergist this was observed to have preference of  $\text{Pb}^{2+}$  and  $\text{Cu}^{2+}$  however the use of this synergist in the solvent extraction leads to low selectivity of all the other divalent metals. Because of this a proposed mechanism of coordination was suggested. The carboxylic based synergistic effect was observed to occur through interaction and therefore the larger metal ions would be selectively extracted over the other metal ions. The sulfonate based synergist was observed to synergistically act by agglomerating and therefore the addition of the benzyl groups leads to lower selectivity but high agglomeration.

Finally, selected ligands were studied for transport through bulk liquid membrane transport which showed that  $\text{Cu}^{2+}$  ions were selectively transported over the other metal ions. This was due to the low stability of the  $\text{Cu}^{2+}$  complexes in the aqueous phase under low pH which allows the metal ions to be released into the receiving phase.

## 8.2 Conclusion

Fifteen multidentate salen type ligands were synthesized with N-donor in their backbone through the Schiff base condensation method and completely characterized through FT-IR,  $^1\text{H}$  NMR,  $^{13}\text{C}$  NMR, MS and CHN analytical techniques. Five of these ligands **L2**, **L3**, **L5**, **L10**, and **L15** were obtained as novel ligands.

Ten O-donor salen type ligands were also successfully synthesized and fully characterized through various analytical techniques. Seven of these ligands were obtained as novel, namely ligand **L16**, **L17**, **L18**, **L20**, **L22**, **L24** and **L25**. One of the ligands from the hexadentate class D series with the *methoxy* substituent on the phenyl ring ligand **L22** was observed to undergo reversible colour change in solid state in the presence of direct light and was studied by confocal microscope showing emission at bandwidth of between 611-503 nm.

From the novel ligands synthesized, three of the ligands were crystallized and their structures determined. Ligands **L16** and **L17** were shown to crystallize in orthorhombic crystal system. Ligand **L18** was observed to crystallize in a monoclinic crystal system. Ligand **L16** and **L17** were shown to have intramolecular H-bonding between the phenolic H and the N-atom of the

imine. For ligand **L18** the phenolic proton was observed to reside on the N-atom of the imine and the phenolic oxygen stabilized by the aromatic naphthyl group.

Six novel complexes were synthesized and characterized by FT-IR, UV-Vis and MS analytical techniques. These metal complexes were studied through single crystal X-ray diffraction and their structures determined. For the salen type ligands **L1-Co** complex this was obtained as an octahedral complex. For **L1-Cu** complex and **L4-Cu** complex these were obtained as trigonal-bipyramidal coordinated complexes. The O-donor based **L17-Cu** and **L18-Cu** were obtained as metallocycles with the  $\text{Cu}^{2+}$  metal centre coordinated in square planar geometry. The **Cu-Pb** complex of Ligand **L19** with a  $\text{Pb}^{2+}$  centre coordinated in octahedral geometry to four metallocycles complexes of  $\text{Cu}^{2+}$  similar to those of **L17-Cu** and **L18-Cu**.

Selected ligands were studied for fluorescence which showed the ligand **L21** with the hexadentate O-donor showing higher fluorescence. While ligand **L23** with the *naphthyl* group display formation of an exciplex. Upon introduction of the metals it was observed that the *hexadentate* salen type O-donor ligands have a strong fluorescence response to  $\text{Zn}^{2+}$  ions, while the *pentadentate* N-donor were observed to have a higher response towards  $\text{Pb}^{2+}$ . The ligands were also observed to quench in the presence of  $\text{Cu}^{2+}$ .

The fifteen ligands containing the N-donor were all used in solvent extraction study. All the ligands except the *nonyl* containing ligands for class A and C were shown to bleed extensively to the aqueous phase. The ligands from class B ligands **L7-L10** were shown to extract  $\text{Cu}^{2+}$  over other metal ions. However, the ligand from class B **L6** with the unsubstituted *salicylaldehyde* was shown to have partial bleeding. The other ligands in this class did not bleed into the aqueous phase. The ten O-donor ligands were also subjected to competitive solvent extraction studies. These ligands did show any sign of bleeding into the aqueous phase and therefore show high selectivity of  $\text{Cu}^{2+}$  ions over the other base metals. Two of the ligands containing the *nonyl* substituent were studied for pH effect indicating the ability of these ligands to be used in different pH's to effect extraction.

Twelve N-donor ligands were subjected to competitive synergistic extraction with three different synergists. Extraction results for *palmitic* acid and the dodecyl sulfonate showed selectivity towards  $\text{Pb}^{2+}$ . For the dodecyl benzylsulfonate synergist this was shown to have higher extraction for  $\text{Pb}^{2+}$  but with very poor selectivity towards the other metal ions. The synergistic effect with the different ligands was observed to be towards  $\text{Cu}^{2+}$  and  $\text{Pb}^{2+}$  with

dodecyl benzy sulfonate synergistic systems showed low selectivity towards the other metal ions.

Selected ligands were subjected to competitive bulk liquid transport (BML) for the N-donor ligands, the *nonyl* containing ligands **L5**, **L10** and **L15** showed high selectivity and transport of  $\text{Cu}^{2+}$  ions at 18 %, 16 % and 22 % for these ligands respectively. The transport efficiency of the system was also observed to be very high with 54 % 61 % and 95 % of the  $\text{Cu}^{2+}$  ions that were extracted into the membrane phase released into the receiving phase for the different ligands. For the O-donor ligand, *hexadentate* ligands **L23** and **L24** were used showing transport of  $\text{Cu}^{2+}$  at 14 % and 12 % respectively. In both of these O-donor ligands, both the transport amount and the efficiency were observed to have reduced at 42 % and 44 % respectively. For ligand **L24**, a relatively high amount of metal ion in the membrane phase for only  $\text{Cu}^{2+}$  was released. Ligand **L11** was also studied for synergistic effect in transport using the different synergist. The results showed that by using palmitic acid, dodecyl sulfonate and dodecyl benzy sulfonate led to 15 %, 15 % and 4 % respectively for the synergist.

### 8.3 Future work

The various ligands used in these studies showed some interesting characteristics which certainly need a full-on assault. However due to time constraints and availability of funding, these could not be fully explored. The work covered in this dissertation was also very broad encompassing ligand synthesis, photochromism, complex synthesis, crystallography, fluorescence, solvent extraction and transport studies. Because of this there are some work that requires intimate research time and resource. The future work encompasses some of these proposed works.

#### i). Photochromic effect

Study of this effect needs some comprehensive research. One of the experiments that had been suggested but could not include in this work due to time delay, includes the light induced NMR studies which was started with collaboration with the University of York (UK). This involves the structural elucidation of the ligand through NMR by passing light through the  $^1\text{H}$  NMR and observing the transition effect on the structure of the ligand.

**ii). Time dependency study**

The second study involves a time dependency computation study on the tautomeric effect. In this study, the obtained crystal structure of one of the ligands with the hydrogen atoms attached to the imine centre and not the phenolic oxygen is examined. There is ongoing research into developing the crystal structure of the same ligand but with the hydrogen atoms attached to the phenolic oxygen. This can be achieved through temperature controlled crystallization. From these results a time dependence study can be undertaken through computation calculations using the two coordinates of the tautomeric protons.

**iii). Fluorescence study**

Because of the interesting results obtained from the fluorescence study, a full study of the use of these ligand as cationic sensors is necessary.

**iv). Structural elucidation through crystallization**

More work on the structural elucidation of these types of ligands needs to be undertaken to examine the mode of coordination of the other metals with the different divalent metals and bi-metallic ions.

**v). Solvent extraction and transport studies**

Temperature effect on both solvent extraction and transport of these ligands can be undertaken using the same ligands.

**vi). The stripping study**

These ligands can also be studied for these ligands

**vii). Stability studies**

The stability study of the complexes formed can also be undertaken through potentiometric titration.

**8.4 REFERENCES**

1. A. C. Reardon, *Metallurgy for the Non-Metallurgist*, 2011 ASM International. 73-84.

2. G. Bates, W. Davidson, J. E. Forgan, R. S. Gale, P. A. Henderson, D. K. King, M. G. Light, M. E. Moore, J. Stephen, P. A. Tasker, C.C. Tong. *Supramolecular Chemistry*. 2015, **24** (2), 117-126
3. Pradhan, S. and S. Mishra, *Metall. Res. Technol.*, 2015, **112**(2), 202.
4. P. A. Tasker, P. G. Plieger, L. C. West. J. A. McCleverty, T. J. Meyer, *Comprehensive Coordination Chemistry II*. 2005, Springer, Netherlands., 124-138
5. M. J. Nicol, C. A. Fleming, J. S. Preston, G. Wilkinson, R. D. Gillard, J. A. McCleverty, *Application to extractive metallurgy*. Comprehensive Coordination Chemistry, ed. P. Oxford. 1987, London, Uk. 412-416
6. Habashi, F.A., *A Textbook of Hydrometallurgy*. 1993, Quebec, 384-396.
7. M. A. Wilson, P. J. Bailey, P. A. Tasker, J. R. Turkington, R. A. Grant, J. B. Love. *Chemical Society Reviews*, 2014. **43**, 123-134.
8. Habashi, F., *Hydrometallurgy*, 2005, **79**, 15-22.
9. E. Löfström-Engdahl, E. Aneheim, C. Ekberg, M. Foreman, G. Skarnemark, *Diluent effects in solvent extraction*, in *ACSEPT (Actinide reCycling by Separation and Transmutation)*, P.o.t.F.A.I. Workshop, Editor. 2010, Chalmers University of technology: Portugal. 31 March – 2 April.
10. C. F. Bucholz, N. *Allgem. J. der. Chemie.*, 1805, (**4**), 157.
11. M. Berthelot, J. Jungfleisch, *J. Ann. Chim.*, 1872 (26), 396.
12. W. Nernst, *phy. Chem.*, 1891(8), 110.
13. H. Morse., *Phy. Chemie.*, 1902(41), 709.
14. P. Dey. PhD Thesis department of chemistry *Allahabad University*, 2011. p 1-39
15. I. M, Kolthoff, E.B. Sandell, *J. Am. Chem. Soc.*, 1964, (**63**), 1906.
16. J. Rydberg, C. Musikas, G. R. Choppin, *Principles and Practices of Solvent Extraction*, ed. M. Dekker. 1992, 14-18.
17. W. A. Zoubi, *J. Coord. Chem*, 2013, **66** (13), 2264–2289.
18. G. A. Kordosky, *Copper recovery using leach/solvent extraction/electrowinning technology: Forty years of innovation, 2.2 million tonnes of copper annually*. in *International Solvent Extraction Conference*. 2002. Cape Town, South Africa, Mar. 17-21.
19. W. G. Davenport, *Copper extraction from the 60's into the 21st century*. In *Copper 99-Cobre 99 International Conference*, 1999, Phoenix, USA.

20. P. A. Tasker, P. G. Plieger, L. C. West, J. A. McCleverty. *Complexes for Hydrometallurgy and Extraction*. Comprehensive Coordination Chemistry II, ed. M. J.A., T. J., Eds. Vol. 9. 2004, London, Elsevier, London, 759.
21. D. A. Skoog, D. M. West, F. J. Holler, S. R. Crouch *Fundamentals of Analytical Chemistry*. 9 ed, Brooks/Cole, 2014, Belmont, CA 94002-3098, Mary Finch.
22. M. C. Jan Rydberg, C. Musikas, G. R. Choppin, *Solvent extraction principles and practice*, 2nd ed, 2004, New York.: Marcel Dekker, inc.
23. L. R. P. Reavill, *A New Platinum Metals Refinery Platinum Metals Rev.* 1984. **28** (1): 2-6.
24. T. T. Teng, Y. Yusup, L.W. Low, *Heavy Metal Ion Extraction Using Organic Solvents: An Application of the Equilibrium Slope Method in Stoichiometry and Research - The Importance of Quantity in Biomedicine*, INTECH, Editor. 2012, INTECH: Malaysia, 121-134.
25. V. S. Kislik, *Solvent Extraction. Classical and Novel Approaches*. Casali Institute of Applied Chemistry, The Hebrew University of Jerusalem, Campus Givat Ram, 2012, Jerusalem 91904, Israel: Elsevier B.v., 189-205, 73-79.
26. <http://www.mining-solutions.basf.com/ev/internet/mining-solutions/enGB/events/index>. [cited 9 september 2016]; investment portfolio].
27. J. R. Turkington, P. J. Bailey, J. B. Love, M. A. Wilson, P. A Tasker, *Chem. Commun.* 2013, **49**, 1891.
28. A. I. Okewole, N. P. Magwa, Z. R. Tshentu, *Hydrometallurgy*, 2012, **121** (124), 81-89.
29. A. E. Martell, R. D. Hancock, *Metal complexes in aqueous solutions*, Modern inorganic chemistry, ed. J. John P., Facklers, 1996, New York: Plenum, 1-87.
30. C. Reichardt, *Solvents and Solvent Effects in Organic Chemistry*. Third, Updated and Enlarged Edition. 2003, Weinheim: WILEY-VCH Verlag GmbH & Co., KGaA 417.

31. L. Fengying, L. Dagang, M. Sonakshi, P. Nana, H. Yan, L. Jiangang, *Industrial & Eng. Chem. Res.* 2014, **53** (5), 1866-1877.
32. M. C. Ogwuegbu, F. Chileshe, *Mineral Processing and Extractive Metallurgy Review*, 2000, **21**, 497-525.
33. R. A. Richardson, PhD Thesis *schiff bases as solvent extraction reagents*, in *chemistry*. 1972, The university of Auckland: Australia. 1-16.
34. N. Magwa, PhD thesis, *Chemistry*, 2015, Rhodes University, Rhodes.
35. R. B. Sudderth, G. A. Kordosky., *Chemical Reagents in the Mineral Processing Industry*, ed. M.A.R. S.M.E., 1986, Littleton Colorado.
36. A. Chatterjee, S. Basu, *J. Inorg. Nucl. Chem.*, 1991, **150**, 177.
37. A. Poskanzer, B. Foreman, *J. Inorg. Nucl. Chem.*, 1961, **16**, 323.
38. A. Maria, *Solvent Extraction and Ion Exchange*, 2009, **27**, 159.
39. R. S. Chauhan, L. R. Kakkar, *Bulletin of the Chemical Society of Japan*, 1992, **65**, 1033.
40. V. Jordanov, M. Atanassova, and I. Dukov, *Separation Science and Technology*, 2002, **37**, 3349.
41. H. Watarai and M. Endoh, *Japan Society for Analytical Chemistry*, 1991, **7**, 137.
42. B. Meng, G. X. Sun, *Journal of Radioanalytical and Nuclear Chemistry*, 1998, **231**, 203.
43. B. A. Moyer, L. H. Delmau, G. J. Lumetta, C. F. Baes, *Solvent Extraction and Ion Exchange*, 1993, **11**, 889.
44. M. H. Chhatre, V. M. Shinde, *Sep. Purif. Techn.*, 1999, **17**, 117.
45. R. G. Pearson., *Hard and Soft Acid and Bases.*, Dowden, Hutchinson and Ross, Stroudsburg, PA., 1973, 64.

46. R. Pearson, , *J. Am. Soc.*, 1968, **85**(22), 3533-3539.
47. A. Riisiö, , PhD Thesis *Syntheses, characterization and properties of cu(ii), mo(vi) and U(vi) complexes with diaminotetraphenolate ligands*, Department of Chemistry, University of Jyväskylä 2013, Finland, 93.
48. O. Andersen, *Environmental Health Perspectives*, 1984, **54**, 249-266.
49. G. Schwarzenbach, *Helv. Chim. Scand*, 1946. **29**, 1338.
50. F. Kandil, W. A. Zoubi, M. K. Chebani, *Separation Science and Technology*, 2012. **47**(12), 1754-1761
51. H. Shih-Yao, B. Wiencek, M. John, *Sep. Sci. Tech*, 2000, **35**(4), 469-481.
52. Z. Lazarova, M. Lazarova, *Solvent Extraction and Ion Exchange*, 2005, **23**(5), 695-711.
53. W. Al Zoubi, *Appl. Organometal. Chem.* 2017, **31**, 3574.
54. A. M Abu-Dief, B. M. A. Mohamed, *A review on versatile applications of transition metal complexes incorporating Schiff bases*. science direct, 2015, **4**, 119-133.
55. H. Schiff, J. Liebigs *Annalen der Chemie*, 1864, **131**, 118-119.
56. M. Nisar, M. K. Khosa, K. Rehman, S. S. Chatha, M. A. Jamal, M. Yousaf, K. M. Zia. *J. Chem. Soc. Pak.* 2011. **33**(3), 421.
57. Ilhan Salih, Temel Hamdi, Yilmaz Ismail, Sekerci Memet. *J. Organometallic Chem*, 2007, **692**(18), 3855-3865.
58. F. I. Nworie, F. I. Nwabue, N. I. Elom, S. O. Eluu, *J. Basic. Appl. Res*, 2016, **2**(3), 295-305.
59. G. J. Morgan, H. D. Drew, *J. Chem. soc. Trans.*, 1920, **17**, 1456.
60. Itrat Anis, M. Aslam, N. Afza, L. Iqbal, Z. Noreen, A. Hussain, M. Safder, *International Journal of Current Pharmaceutical Research*, 2013. **5**, 48-57.
61. M. Andrade, C.S., J. E. Borges, C. Freire., *J. Phys. Org. Chem.*, 2005, **18**, 935-940

62. F. Farnoush, G., Mohammad, D. Rassoul, N. Parviz, R. Siavash, *Sensors*, 2008, **8** (3), 1645
63. N Alizadeh, S. Ershad, H. Naeimi, H. Sharghi, M. Shamsipur, *Pol. J. Chem Rev.*, 1999, **73**, 915-925.
64. M. Shamsipur, M. Yousefi, M. Hoseini, M. R. Ganjali, H. Sharghi, H. Naeimi, *Anal. Chem.*, 2001, **73**, 2869-2874.
65. N. R. Bader, PhD thesis. *Schiff's bases complexation and solid phase extraction for improved trace element analysis*, Universität Duisburg-Essen: Duisburg. in *Vom Fachbereich Chemie*, 2009, 1-18.
66. P. G. Cozzi, *Chem. Soc. Rev.*, 2004. **33**, 410-421.
67. Z. L. You, H. L. Zhu, Z. S. W. Liu, *Anorg. Allg. Chem*, 2004, **630**, 1617-1622.
68. Z. L. You, H. L. Zhu, *Anorg. Allg. Chem*, 2004, **630**, 2754 – 2760.
69. R. B. Atkins, G. Kokot, E. Mockler, G. M. Sinn, *Inorg. Chem.*, 1985, **24**, 127.
70. Tasker, P.A., C.C. Tong, and A. N. Westra, *Coordination Chemistry Reviews*, 2007, **251**, 1868-1877.
71. W. Saban, H.F. Ogotu., R. Malgas-Enus, R. C. Luckay, *New journal of chemistry*, 2016, **5000**(2), 72.
72. H. Irving, R. J. P Williams, *Nature*, 1948, **162**, 746-747.
73. H. Irving, R. J. P Williams, *J. Chem. Soc.*, 1953, 3192-3210.
74. B. Grgas, S. Nikolija S. Paulija, N. Raos, N. Ces. *Croat. Chem. Acta.*, 1999, **72**, 885-895.
75. H. Irving, F. J. C. Rossotti, R. J. P. Williams, *J. Chem. Soc.*, 1955, 1906-1919
76. J. Stary, *The Solvent Extraction of Metal Chelates*. Pergamon, London 1964. p78
77. S. K. Singh, *Hydrometallurgy*, 2007. **87**: 190–196.

78. D. Reza, F. A. Khanramaki, M. Salimi, B. Ashtari, P.S. Mojtaba, *Journal of Radioanalytical and Nuclear Chemistry*, 2013. **298**(1): 125-132.
79. S. Tarahomi, G.H. Rounaghi, and M. Chamsaz, *Study of Competitive Transport of Some Heavy Metal Cations Across*, *Russian Journal of Applied Chemistry*, 2015, **88**(7), 1219–1228.
80. N. N. Li, *Separating hydrocarbons with liquid membranes*, U. Patent, ed, 1968, US Patent, 794.
81. G. Arslan, *Hazard. Mater*, 2009, **165**, 729.
82. M. Shamsipur, R. Davarkhah, A. R. Khanchi, *Sep. Purif. Technol.*, 2010, **71**, 63.
83. N. Alizadeh, S. Ershad, H. Naeimi, H. Sharghi, M. Shamsipur, *Sep. Purif. Technol.*, 2012, **90**, 83.
84. H. K. Alpoguz, *J. Macromol. Sci. A Pure Appl. Chem*, 2007, **44**, 17.
85. V. V. Belova, A. E. Kostanyan, Y. A. Zakhodyaeva, A. I. Kholkina, O. A. Logutenko, *hydrometallurgy*, 2014, **150**, 144-152
86. S. Ambe, K. Yashiki, H. Maeda, S. Enomoto, T. Ozaki, F. Ambe, *J. Radioanal. Nucl. Chem.*, 1998. **236**(1-2), 181–185.
87. R. A. Kumbasar, S. Kasap, *Hydrometallurgy*, 2009, **95**, 121–126.
88. J. Tian, J. Yin, K. Chen, G. Rao, M. Jiang, R. Chi, *Int. J. Miner. Process.* 2011. **98**, 125-131.
89. F. J. Alguacil, A.G. Coedo, M.T. Dorado, *Hydrometallurgy*, 2000, **57**, 51–56.
90. S. Altin, Y. Yildirim, A. Altin, *Hydrometallurgy*, 2010, **103**, 144–149.
91. G. Benzal, A. Kumar, A. Delshams, A. M. Sastre, *Hydrometallurgy*, 2004, **74**, 117-130.
92. A. Bhattacharyya, P. K. Mohapatra, V. K. Manchanda, *Sep. Purif. Technol*, 2006, **50**, 278-281.

93. H. Shabani, A. M. Dadfarnia, S. Shahbaazi, Z. Jafari, A. A. Aji, *Bull. Chem. Soc. Ethiop*, 2008, **22**, 323.
94. R. M. Izatt, K. Pawlak, J. S. Bradshaw, R. L. Bruening, *J. Am. Chem. Soc.*, 1983, **105**, 1785.
95. R. M. Izatt, K. Pawlak, J. S. Bradshaw, R. L. Bruening, *Sep. Purif. Methods*, 1986, **15**, 21.
96. D. R. Khanramaki, F. Asgari, M. Salimi, B. Ashtari, P. S. Mojtaba. *J. Rad. Nucl. Chem.*, 2012. **298**(1), 125-132.
97. G. Morgan. D.H. Drew, *J. Chem soc. Trans.*, 1920, **17**, 1456.
98. Q. Saima. N. M. Memon, A. Mallah, R. Soomro, M.Y. Khuhawar, *Curr. Analyt. Chem*, 2014, **10**, 393-417.
99. P. A. Vigato, S. Tamburini, *Coord. Chem. Rev.*, 2004, **248**, 1717-2128.
100. D. E. Metzler, M. Ikawa, E. E. Snell, *J. Am. Chem. Soc.*, 1954, **76**, 648.
101. A. E. B. stein, M. M. Shenyakin, *Biokhimiia*, 1953, **18**, 393.
102. U. Hamza, A. Uzairu, M. S. Sallau, E.S. Abechi, *Der. Chem. Sinica*, 2015, **6**(1), 25-33.
103. A. A. El-Sherif, M.S. Aljahdali, *J. Coord. inat. Chem.*, 2013, **66**(19), 3423-3468.
104. A. A. El-Sherif, M. R. Shehata, M. M. Shoukry, M. H. Barakat. *J. Spect. Acta (A)*, 2012, **96**, 889.
105. K.N. Campbell, H. Sommers, B. K. Campbell, *J. Am. Chem. Soc.*, 1944, **66**, 82.
106. Hine, J. and C.Y. Yeh, *J. Am. Chem. Soc.*, 1967, **86**, 2669.
107. H.Tazoki, K. Miyano, *J. Chem. Soc.*, 1959, 9769.
108. C. Munir, S.M. Yousaf, N. Ahmad, *J. Chem. Soc. Pak.*, 1985, **7**, 301.
109. H. L. Choudhury, T. Parvin, *Tetrahedron*, 2011, 950.

110. R. Aldred, R. Johnston, D. Levin, N. James, *J. Chem. Soc. Perk Trans*, 1, 1994(13), 1823-1831.
111. J. Matijevic-Sosa, M. Vinkovic, D. E. Vikić-Topi, *Croatica Chemica Acta*, 2006, **79**(3), 480-495.
112. R. M. Claramunt, L.C. Santa M. D. Mari'a, D. Sanz, J. Elguero, *Progress in Nuclear Magnetic Resonance Spectroscopy*, 2006, **49**, 169-206.
113. M. Abdullah, B., Krystoff, *Molecule*, 2007, **12**, 1796-1804.
114. M. Zbačnik, K. Pičuljan, J. Parlov-Vuković, Novak, A. Roodt *Crystals*, 2017, **7**(25).
115. J. W. Steed, *Coord. Chem. Rev.*, 2001, **215**(1), 171-221.
116. Pedersen, C.J., *J. Am. Chem. Soc.*, 1967, **89**, 7017.
117. M. C. Atanassova, *J. Serb. Chem. Soc.*, 2008, **73** (1): 29–39
118. P. R. Ashton, *Agwe. Chem. Int.* 1995, **34**(17), 1865-1869.
119. K.B. Chung, J. Chung, *Polym. Sci.*, 1992, **30**, 1089.
120. E. Weber, F. Vogtle. *Host Guest Complex Chemistry*, 14, 1981, New York, Springer.
121. W. Zoubi, A. L. Kandil, F. Chebani, M. Khaled *Spectr. Acta Part A, Molecular and Biomolecular Spectroscopy*, 2011, **79**(5), 1909-1914.
122. G.W. Gokel, J. E. Trafton, *Cation Binding by Macrocycles*, 253, 1990, New York.
123. P.A. Vigato, S. Tamburini, D.E. Fenton, *Coord. Chem. Rev.*, 1990, **106**(25).
124. Alekseeva, E.V.C., Irina A. Malev, Valery V. Timonov, Aleksander M. Levin, Oleg V., *Electrochimica Acta*, 2012, **225**, 378-391.
125. A. Ghaffari, M. B. M. Pooyan, H. A. Rudbari, G. Bruno, *J. Molec. Structure.*, 2014, **1063**, 1-7.
126. Z. Pouramini, A. Moradi, *Arabian Journal of Chemistry*, 2012, **5**, 99–102.

127. Z. Pouramini, A. Moradi, *Research on Chemical Intermediates*, 2012, **38**(9), 2401-2409.
128. Y. Zhi, B.W. X. Yao, *Crit Rev Biomed Eng.*, 2015, **43**(4), 297-322.
129. J. K. Sun, W. Li, C. Chen, C. X. Ren, D. M. Pan, J. Zhang., *Angew. Chem. Int. Ed.*, 2013, **52**, 6653-6657.
130. D. A. Davis, A.H., J. Yang, L. D. Cremar, D. V. Gough, S. L. Potisek, M. T. Ong, P. V. Braun, T. J. Martinez, S. R. White, J. S. Moore and N. R. Sottos, *Nature*, 2009, **459**, 68-72.
131. Qi Sui, X.-T.R., Yu-Xiang Dai, Kai Wang, Wen-Tao Li, Teng Gong, Jia-Jia Fang, Bo Zou, En-Qing Gao and Lin Wang, *Chem. Sci*, 2017. **8**. 2758-2768.
132. Z. J. Zhang, S. C. Xiang, G. C. Guo, G. Xu, M. S. Wang, J. P. Zou, S. P. Guo and J. S. Huang, *Angew. Chem. Int. Ed.*, 2008, **47**, 4149-4152.
133. J.-K. Sun, J. Zhang., *DaltonTrans*, 2015, **44**, 19041-19055.
134. S. Prashanthi. P. H. Kumar, D. Siva, S. R. Lanke, V. J. Rao, S. Basak, P. R. Bangal J. *Phys. Chem. C*, 2011, **115**, 20682-20688.
135. O. Sato, J. Tao, Y. Z. Zhang, *Angew. Chem., Int. Ed*, 2007, **46**, 2152-2187.
136. J. Harada, T.F.a.K.O., *J. Am. Chem. Soc.*, 2007, **129**, 16216-16221.
137. A. K. Padhy, A. K. Mishra, M. Mohapatra, A. K. Pati, S. Mishra, *RSC Advances*, 2014, **4**, 8044-8049.
138. F. Tjosaas, A. Fiksdahl. *Organomet. Chem.* 2007, **692**, 5429.
139. K. L. Haas, K. J. Franz, *Chem Rev.*, 2009, **109**(10), 4921-4960.
140. Mohammed Younas stephen Druon-Bocquet, J.R., Joseph Sanchez, *Separation Science and Technology*, 2015, **50**, 1523-1531.
141. D. Reinen, M. P Atanasov, Kahler, D.Babel, *Coordination Chemistry Reviews*, 2010, **254**(23), 2703-2754.

142. F.S. Ham, *J. Luminescence*, 2000, **85** (4), 193-197.
143. Murphy, B. and B. Hathaway, *Coordination Chemistry Reviews*, 2003, **243**, 237-262.
144. J. W. Roebuck, J. R. Turkington, D. M. Rogers, P. J. Bailey, V. Griffin, A. J. Fischmann, G. S. Nichol, M. Pelser, S. Parsons P. A. Tasker. *Dalton Trans*, 2016, **45**, 3734-3742.
145. Ogotu, H., MSc thesis *structural elucidation and the anticancer studies of silver phosphine complexes*, in *Department of Chemistry*. 2014, University of Johannesburg: Johannesburg.
146. V.R. Thalladi, B.S. Goud, V.J. Hoy, F.H. Allen, J. A. K. Howard, G. R. Desiraju J. *Chem. Soc.Chem. Commun*, 1996, 401.
147. G. Sheldrick, *Acta Crys. Sect A*, 2008. **64**(1), 112-122.
148. WinGX: Farrugia, L.J., *J. Appl. Cryst.*, 2012, **45**, 849-854.
149. Dolomanov, O.V.B., Luc J. Gildea, Richard J. Howard, Judith A. K. Puschmann, Horst, *J. Appl. Crystallography*, 2009, **42**(2), 339-341.
150. Roy, N., Harun A. R. Pramanik, Paul C. Pradip, Sanjoy T. Singh. , *J. Fluorescence*, 2014, **24**(4), 1099-1106.
151. M. A. Guadalupe, Quintero-Tacalez, Alcntara-Flores, J. L. Bernas, S. A. Carrasco, M. L. M. Otero, M. M.R, Yasmi Alcantara-Flores and Yasmi Reyes-Ortega, *Acta Cryst. E*, 2008, **64**(m), 631-m632.
152. P. R. Raithby, G., Shields, F. H. Allen, W. D. S. Motherwell, *Acta Cryst B*, 2000, **56**, 444-454.
153. F. B. Kaynak, D. Ulku, O. atakol S. Durmus, *Acta Cryst.* 1999, **C55**, 1784-1785.
154. S. Yang, Y. H. Chen, F. Zhang, Q. Chena X. Yua, *Acta Cryst.*, 2004, **E60**(m), 582-m584.

155. V. T. Yilmaza, I. Degirmencioglu, O. Andaca, S. Karabocek, A. M. Z. Slawinc, *Journal of Molecular Structure*, 2003, **654**, 125-129.
156. Francis Carré, J. Robert. P. Corriu, E. Lancelle-Beltran, A. Mehdi, C. Reyé, R. Guilard, J. Sýkora, A. Van der Lee, *Dalton Trans*, 2003, 3211 - 3215.
157. D. E. Fenton, G. P. Westwood, A. Bashall, M. McPartlin, I. J. Scowen, *J. Chem. Soc., Dalton Trans*, 1994, 2213.
158. X Zhou, Y. P. Cai, S. Z. Zhu, Q. Zhan, M.S. Liu, Z. Y. Zhou, L. Chen, *Crystal Growth & Design*, 2008, **8**(7), 2077-2079.
159. P. Bhattacharyya, J. Parr, A. M. Z. Slawin *Chem. Soc., Dalton Trans.*, 1998, 3263-3267.
160. Ray N, L. Hulett, R. Sheahan, B. J. Hathaway *Inorg. Nucl. Chem. Lett*, 1978, **14**, 305.
161. J. Richard, P. H. Fereday, S. Tyagi and B. J. Hathaway, *Inorg. Nucl. Chem. Letters*, 1981, **17**(No.7/8), 243-246.
162. E. Gervas, A. M Assey, B. Ray, J. Butcher, Y, Gultneh, *Acta Cryst*, 2010, **E**, **66**, m1475.
163. K. Vimal, A. P Bhardwaj, S.P. Narinder Singh, M.S. Hundal, G.Hundal, *Tetrahedron*, 2008, **64**, 5384-5391
164. N. M. Chattopadhyay, A. S. Sengupta, *J. Photochem. Photobiol, A* 2005, **177**, 55-60.
165. A. Vogler, H. Kunkely., *Coordination Chemistry Reviews*, 2004, **248**, 273-278.
166. A. E. Martel, R. M. Smith, *critical stability constants*, ed. plenum. Vol. 1, New York. 1974-1988.
167. J. Bjerrum and E. Christensen, *Ammine formation in aqueous solution: Theory of the reversible step reaction*. 1941, Copenhagen: Hasse.
168. S. Trofimenko, *J. Am. Chem. Soc*, 1967a, **89**, 3165-3170.

169. S. Trofimenko, *J. Am. Chem. Soc.*, 1967b, **89**, 6288–6294.
170. Clayden, Greeves Warren and wother *organic chemistry*. 2001, New york, Oxford University.
171. J. Heinsberg, *MSc Thesis, synthesis of salen type ligands in the extraction of selceted metals ions Chemistry and polymer science*. 2017, Stellenbosch University, Stellenbosch.
172. S. Tarahomi, G. H. Rounaghi, M. Chamsaz, *Russian Journal of Applied Chemistry*, 2015, **88** (No. 7), 1219–1228.
173. J. E. Ross, L. Anderson, L Timothy, Antonio, R. Mark, B. Alex, N. Mikael, *J. Phys Chem B*, 2013, **117**(19), 5916-5924.
174. G. Cunninghame, P. Scargill, H. M. Willis. *AERE C/M*, 1954, 215.
175. C. A. Blake, C. F. Baes, K. B. Brown, C. F. Coleman, J. C. White. *2nd Intern. Conf. Peaceful Uses At. Energy*, 1958, Geneva.
176. V. V. Ramakrishna, S. K. Patil, *Struct. Bonding*, 1984, **56**, 35–90.
177. E. F. Kassierer, A. S. Kertes, *J. Inorg. Nucl. Chem.*, 1972, **34**, 778–780.
178. Y.A. El-Nadi, *Sep. Purf. Rev.*, 2016, **00**, 1-21,
179. J. Rey, S. Dourdain, J.-F. Dufrière, L. Berthon, J. M. Muller, S. Pellet-Rostaing and T. Zemb, *Langmuir* 2016, **32**, 13095–13105.
180. V. Gasperov, K.G, Leonard, F. Lindoy, S. M. Mahinay, *Dalton. Trans*, 2004, 3829 - 3834.
181. K. Osseo-Asare, D.R. Renninger, *Hydrometallurgy*, 1984. **13**, 45-62.
182. Keith R. Barnard<sup>1</sup>, G.L.N., Mark I. Ogden<sup>2</sup>, and Brian W. Skelton, *Crystallographic Determination of Three Ni- $\alpha$ -Hydroxyoxime-Carboxylic Acid Synergist Complexes*. *Solvent Extraction and Ion Exchange*, 2010, **28**, 778-792.

183. K. R. Barnard, M.N. Tsuntsaeveva, *Solvent Extraction and Ion Exchange*, 2013, **31**, 79-94.
184. D. Barkat, Z. Derriche, *Turkish Journal of Chemistry*, 2001, **25**, 381-389.
185. J. P. Brunette, M. Taheri, G. J. Goetz-Grandmont, M. J. F. Leroy, *Solvent Extr. Ion Exch.*, 1985, **3**, 309.
186. D. Barkat, M. Kameche, *Phys. Chem. Liq.*, 2007, **45**, 289.
187. M. L. Dietz, E. P. Horwitz, S. Rhoads, R. A. Bartsh and J. Krzykawski, *Solvent Ext. Ion Exch*, 1996, **14**, 1.
188. B. A. Uzoukwu, C. I. Ukegbu, *Indian J. Chem.*, 1997, **36**, 351.
189. J. Li, H.H. Shan Zhu, F. Hu, Y. Wang, *Dalton Trans.* 2017, **46**, 1075-1082.
190. R. Golbedaghi, S. S. Hamid, R. Khavasi, A. G. Blackman, *Polyhedron*, 2014, **68**, 151-156.
191. K. Ikeda, M. Ohba, H. Okawa. *J. Chem. Soc., Dalton Trans.* 2001. 3119-3124
192. S. Zhu, H. Hu, Jiugang Hu, J. Li, F. Hu, Y. Wang, *Journal of Molecular Structure*, 2017, **1144**: 191-198.
193. J. Rey S. Dourdain, L. Berthon, J. Jestin, S. Pellet-Rostaing, T. Zemb., *Langmuir* 2015, **31**, 7006–7015.
194. P. Ekwall, P. Stenius, *International Review of Science, Physical Chemistry*, 1975. **7**(2), 215–248.
195. H. F. Eicke. *Aggregation and Micellization. Top. Curr. Chem.*, 1980, **87**, 85-145.
196. H. F. Eicke, *Pure Appl. Chem.* 1980, **52**, 1349-1357.
197. H. F. Eicke, *Pure Appl. Chem.*, 1981, **53**, 1417–1424.
198. H. F. Eicke, Z. Markovic, *J. Colloid Interface Sci*, 1981, **79**, 151–158.

199. C. Dejognat, S. Dourdain, V. Dubois, L. Berthon, S. Pellet-Rostaing, J. F. Dufreche, T. Zemb, *Phys. Chem.* 2014, **16**, 339–7349.
200. S. Dourdain, I. Hofmeister, O. Pecheur, J. F. Dufrêche, R. Turgis, A. Leydier, J. Jestin, F. Testard, S. Pellet-Rostaing, T. Zemb. *Langmuir.* 2012, **28**, 11319 – 11328.
201. T. Zemb, C. Bauer, P. Bauduin, L. Belloni, C. Dejognat, O. Diat, V. Dubois, J. F. Dufreche, S. Dourdain, M. Duvail, C. Larpent, F. Testard, S. Pellet-Rostaing, S. *Colloid Polym. Sci.*, 2015, **293**, 1–22.
202. S. Nishimura, C. H. Ke N.C Li, *J Phys Chem*, 1968, **72**, 1297.
203. D. S. Flett, *J. Chem. Technol. Biotechnol*, 1999, **74**, 99-105.
204. R. Silvio, J. R Taffarel, *Minerals Engineering*, 2010, **23**, 771-779.
205. B. H. Pearce, H. F. Ogutu, R. C. Luckay, *European Journal of Inorganic Chemistry*, 2017 (8).
206. K. R. Barnard, G. L. Nealon, M. I. Ogden, B. W. Skelton. *Solvent Extraction and Ion Exchange*, 2010, **28**, 778-792.
207. R. D. Shannon, *Acta Crystallographic. Sect. A*, 1976, **A32**, 751.
208. F. A. Cotton, G.W., *Advanced Inorganic Chemistry*. 4th ed. 1980, New York: Wiley-Interscience publication. 757-759.
209. A. I. Okewole, PhD Thesis, *Application of bidentate n,n'-donor extractants in the hydrometallurgical separation of base metals from an acidic sulfate medium, in chemistry*. 2012, Rodes university, Grahamstown, 15.
210. K. R. Barnard, D.W. Shiers, N. J. Kelly, D. Lombardo, *Solvent Extraction and Ion Exchange*, 2015, **33**, 166-182.
211. D. S. Flett, *J. Organomet. Chem*, 2005, **690**, 2426-2438.
212. T. Szabó, E. Hirsch, T. Tóth, P. Huszthy, *Tetrahedron, A symmetry*, 2014, **25**, 1443-1449.

213. Z. Chen; L. Echegoyen, *In Crown Compounds: Toward Future Applications*. VCH, S. R. Cooper, Ed;. 1992, New York. 27–39.

---

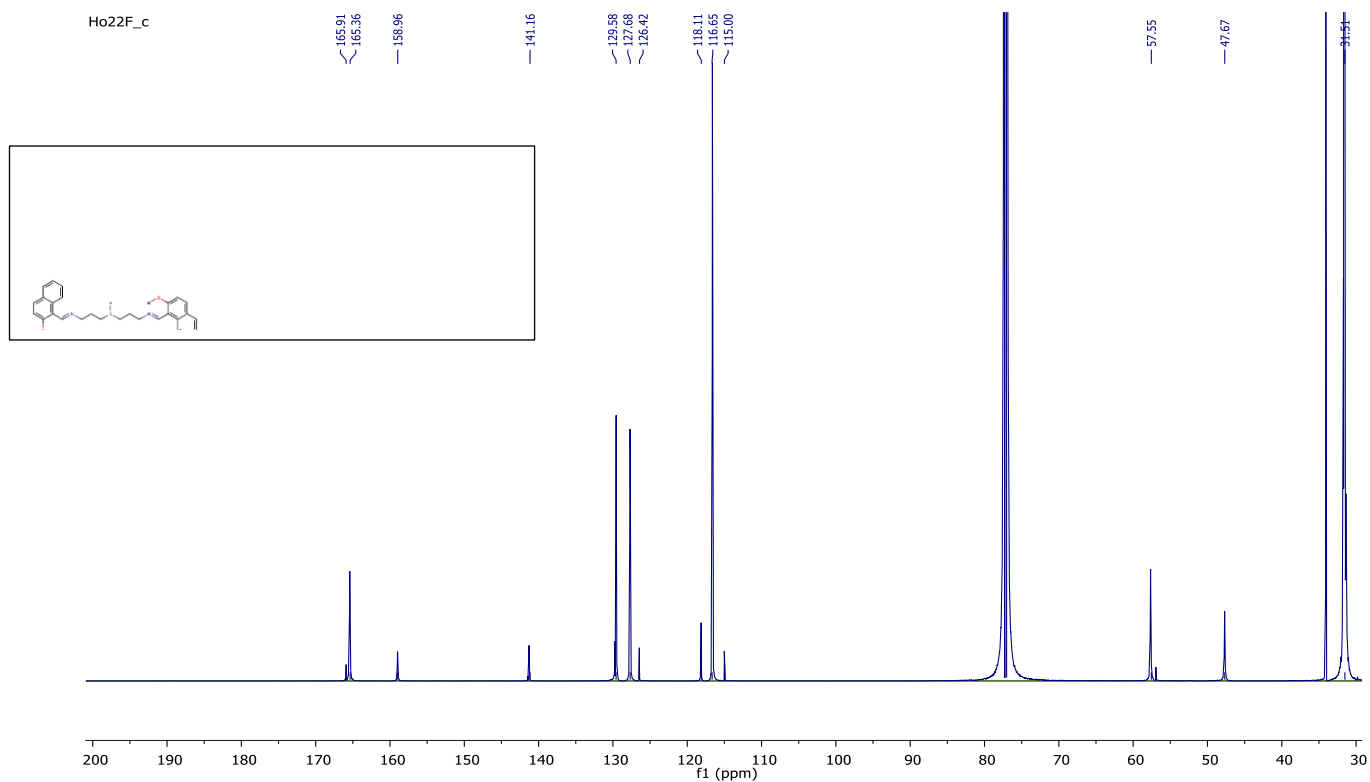
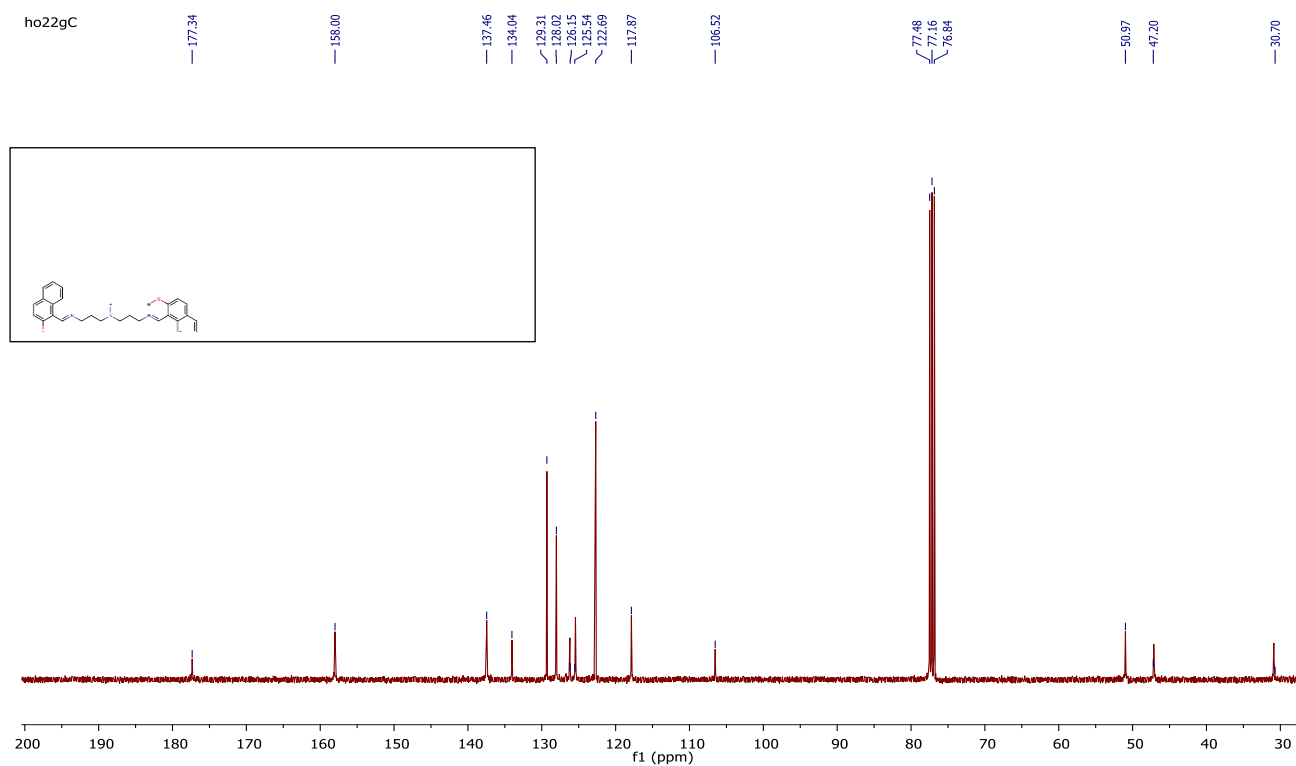
---

# APPENDICES

---

---

## Appendix 1: SELECTED NMR SPECTRA

Figure 1: Spectra of  $^{13}\text{C}$   $\{^1\text{H}\}$  NMR for ligand L8Figure 2: The  $^{13}\text{C}$   $\{^1\text{H}\}$  NMR. for Ligand L8a1 in  $\text{CDCl}_3$

## Appendix 2: SELECTED IR ANALYSIS OF CLASS A COMPLEXES

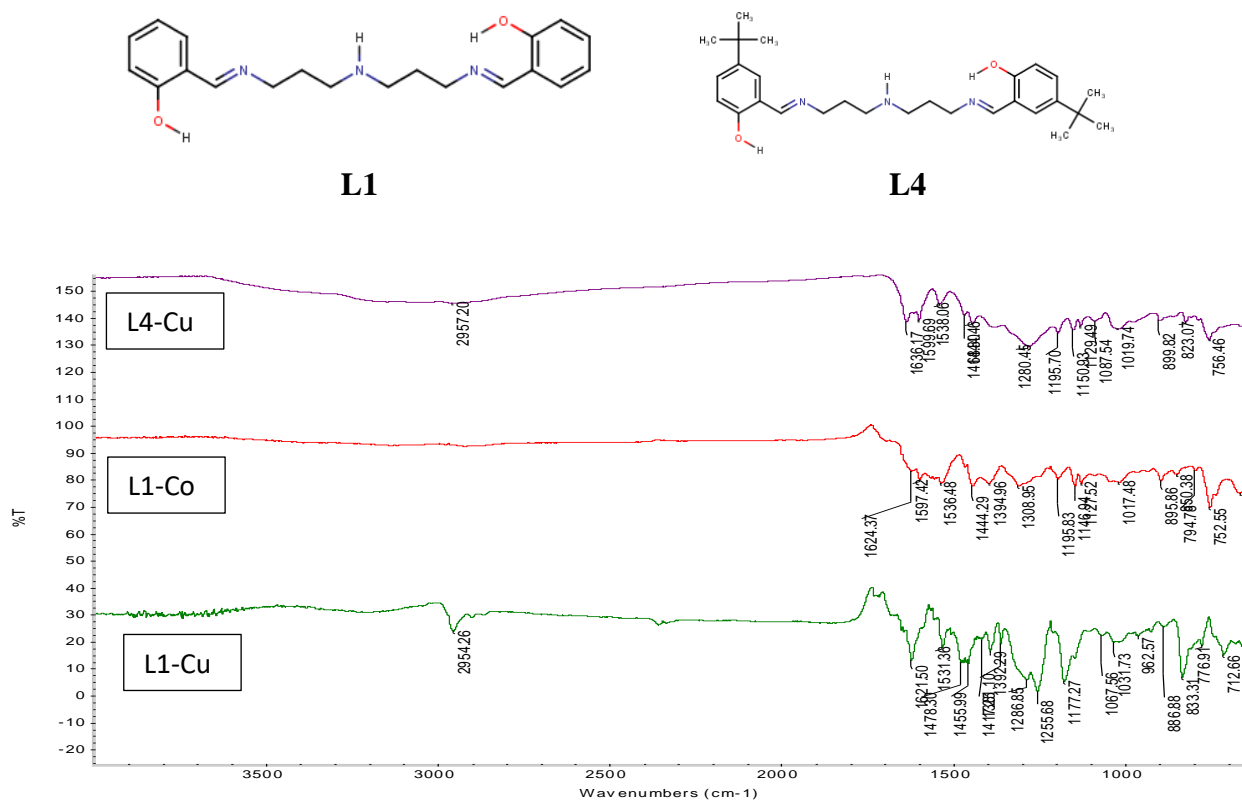


Figure 3: ATR-IR spectra of L1-Cu, L1-Co and L4\_Cu

## Appendix 3: MASS SPECTRUM OF SELECTED COMPLEXES

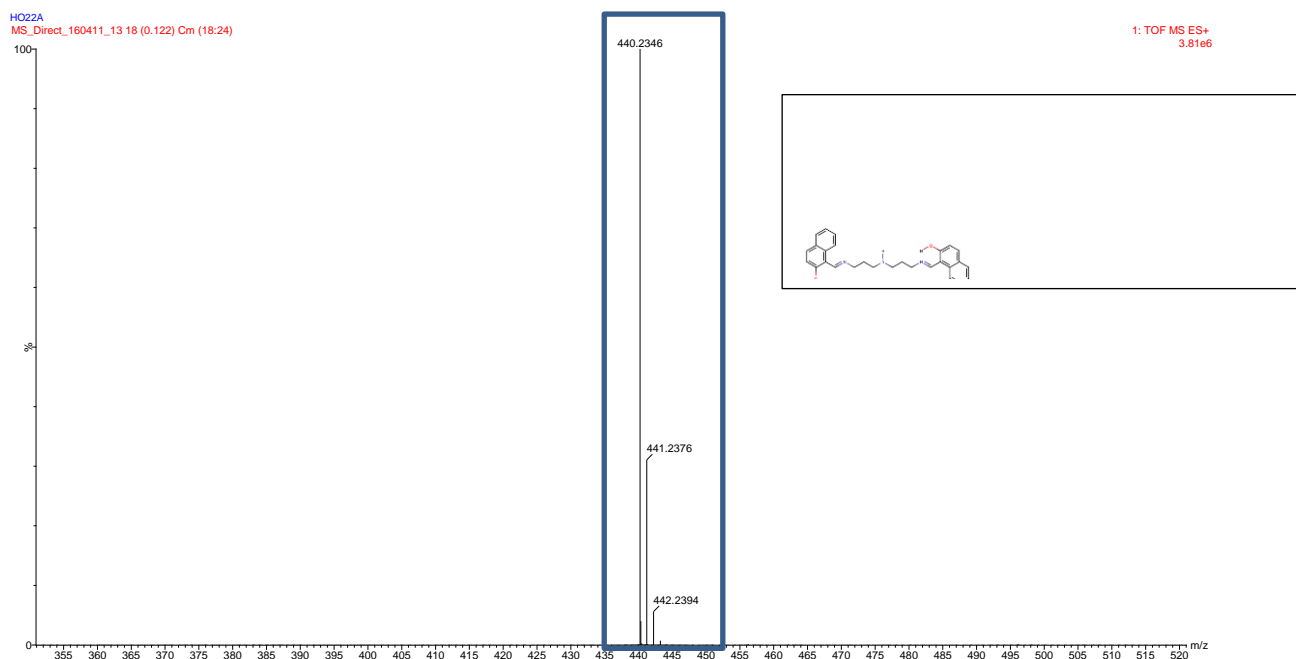


Figure 4: Mass Spectra of Ligand L8a

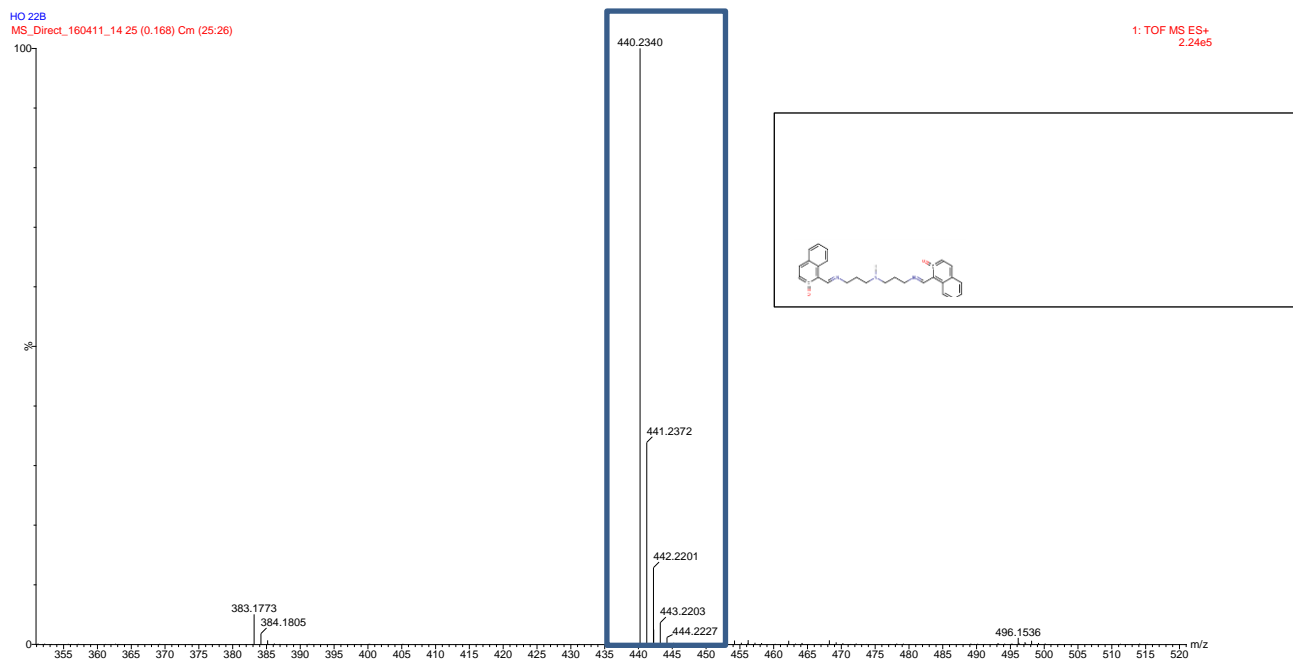


Figure 5: spectrum of Mass spec of L8b

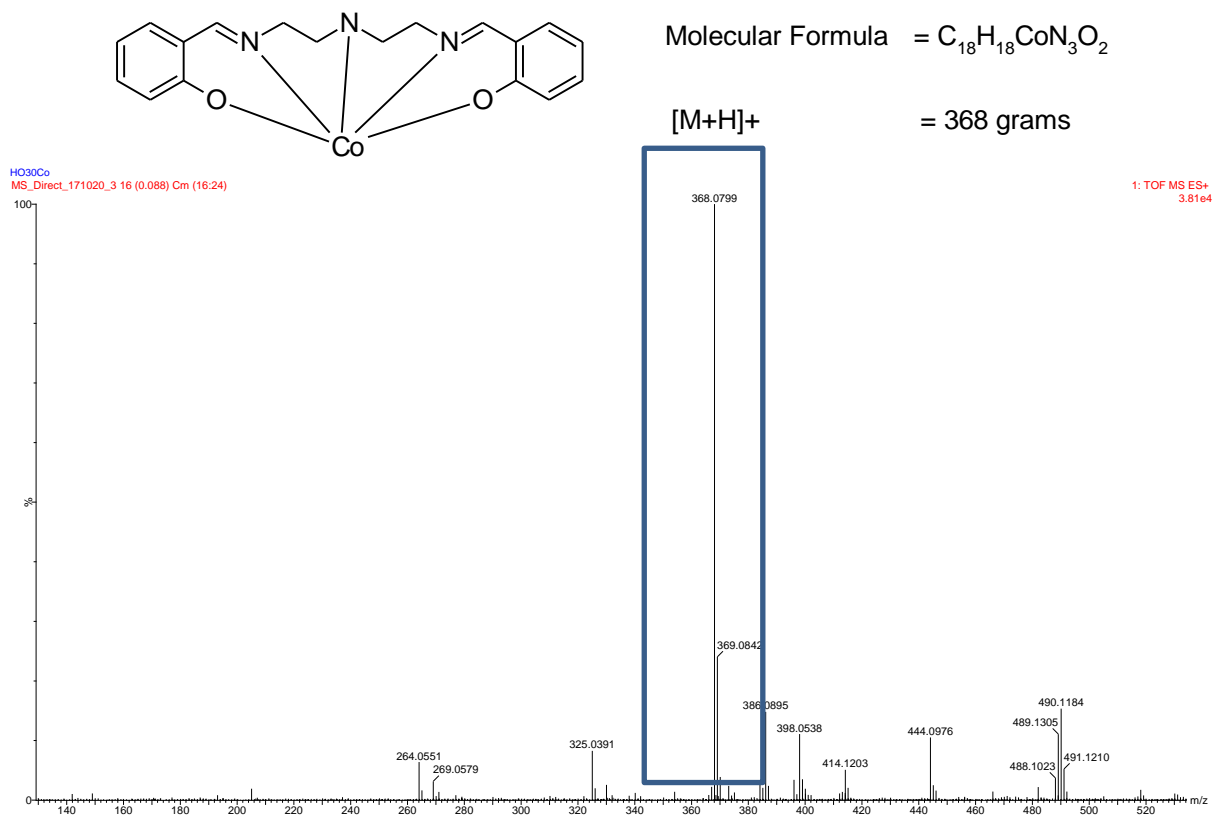
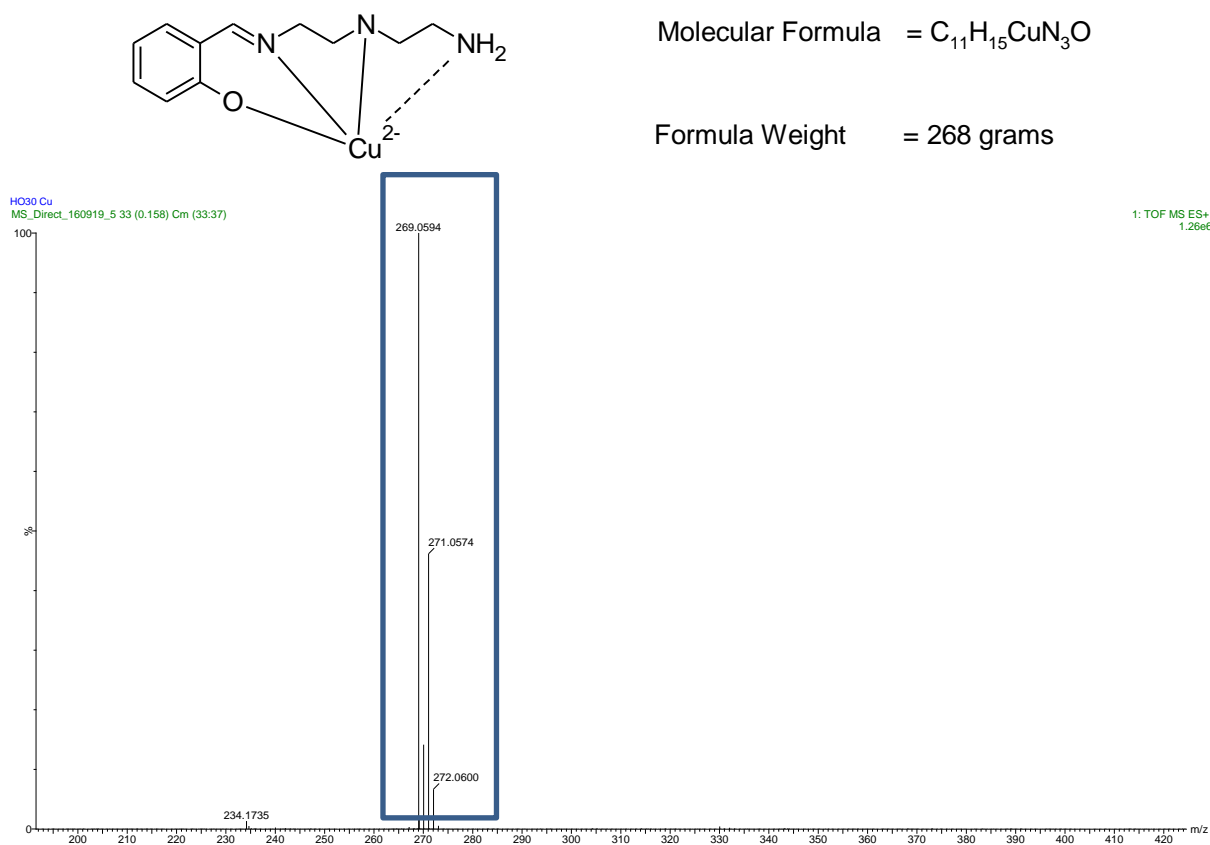
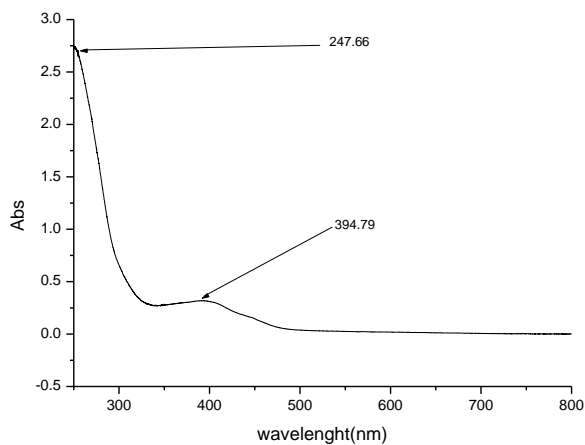


Figure 6: spectrum of Ms for L1-Co



**Figure 7: spectrum of MS for L1-Cu**

*Appendix 4: SELECTED UV ANALYSIS*



**Figure 8a: Uv vis spectrum L1-Cu**

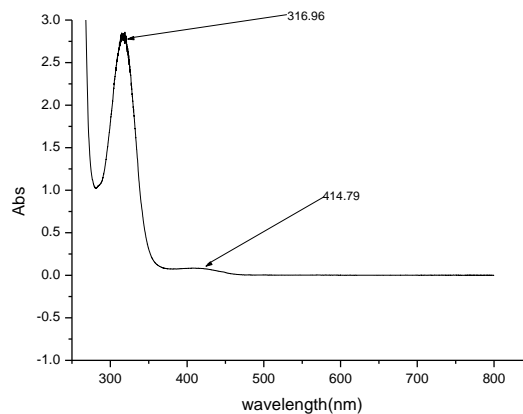


**Figure 8b: Uv vis spectrum L1-Co**

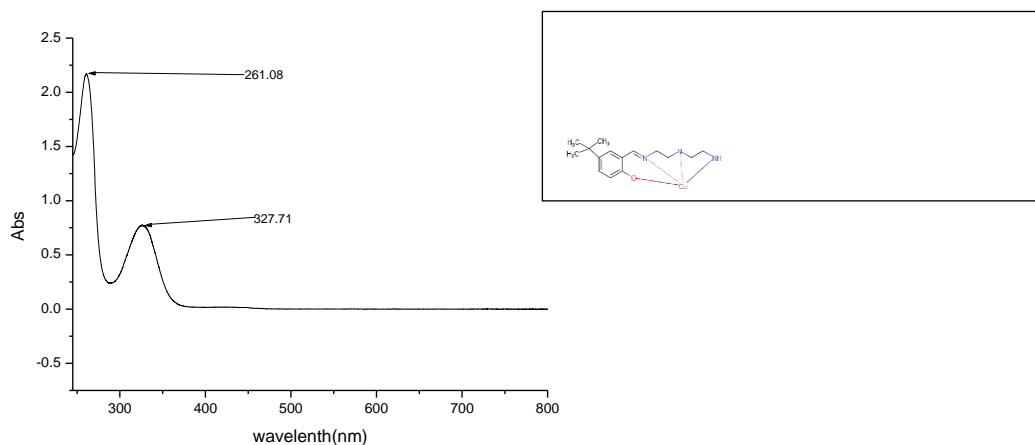


**Figure 8c: Uv vis spectrum L4-Cu**

*Appendix 5: CONTINUOUS VARIATION UNDER UV ANALYSIS FOR LIGAND L24 AND CU METAL*

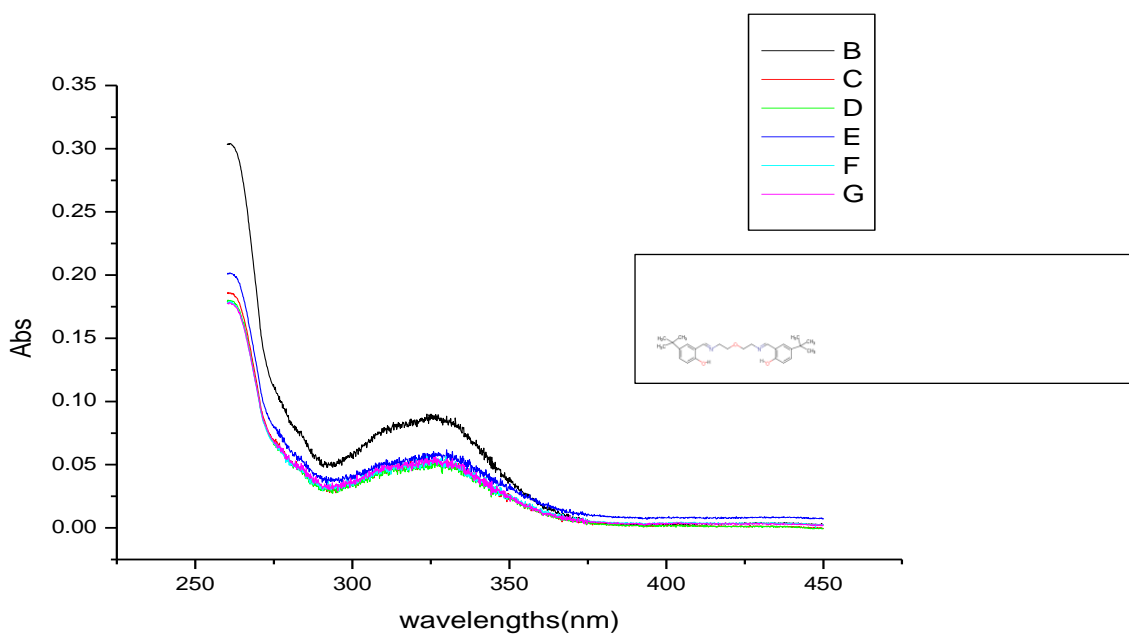


**Figure 9: Spectra of fluorescence of L4**